Dependence of sonic velocity on effective stress in fine-grained sediments

Mavatikua, Lubanzadio

Dependence of Sonic Velocity on Effective Stress in Fine-Grained Sediments

By

Lubanzadio Mavatikua

Department of Earth Sciences

University of Durham

A thesis submitted as partial fulfilment of the requirements of the University of Durham for the degree of Doctor of Philosophy
June 2005

Abstract

Overpressure estimation methods that use sonic velocity as a proxy for porosity only account for excess pressure due to disequilibrium compaction; the influence of unloading processes in generating larger excess pressure observed in most basins is ignored. Wireline log data and pore pressure measurements from wells across the Central Graben and the East Shetland Basin, North Sea, have been used to find out whether velocity is sensitive to the contribution of unloading processes to observed overpressures. The approach was to focus on fine-grained sediments, chalk and mudstones, and establish a relationship between sonic velocity and other petrophysical parameters, necessarily including porosity and vertical effective stress, when the latter variables are treated as independent.

Investigation of the Chalk in the Central Graben has shown that velocity has no detectable dependence on vertical effective stress when porosity and effective stress are treated as independent variables. The significance is that velocity in Chalk cannot be used to detect the presence of any overpressure caused by unloading. It is suggested that the absence of an observable velocity reduction in unloaded Chalk is due to cementation.

Analyses in the Lower Cretaceous and Jurassic mudstones show that gamma ray count and depth can usefully be taken as additional parameters in overpressure estimation. In both the Cromer Knoll and in the Heather formation, there is a small but significant dependence of velocity on vertical effective stress when porosity and effective stress are taken as independent variables together with gamma ray count and depth. The sensitivity factor is 21.8 m/s/MPa in the Cromer Knoll and 17.4 m/s/MPa in the Heather. The contribution of the vertical effective stress with associated independent variables (gamma-ray and depth) produced RMS errors between measured and forward-calculated values of sonic velocity of 101 m/s for the Cromer Knoll and 107 m/s for the Heather Formation. The discrepancies may be attributed to the contributions of other rock parameters that were not taken into account.

Declaration

The content of this thesis is entirely the work of the named author. Any previously published or unpublished work by other people is acknowledged by reference. No part of this thesis has previously been submitted for a degree in this or any other university.

Lubanzadio Mavatikua

Department of Earth Sciences
University of Durham
June 2005

To the memories of the *A. Mavatikuas*,
– both Ndontoni, my Dad and Kany, my big brother –,
Who both passed away during the very last stage of our journey
Towards this milestone.

Acknowledgements

First and foremost, I would like to express my gratitude to Prof. Neil Goulty and Dr. Richard Swarbrick (Dick), who set up this project. They supervised the research and provided constant support during the preparation of this work. I must confess that I am indebted to Neil for he provided - perhaps without realising it - the greener ground on which my efforts and this achievement did develop. He has always been disposed to offer guidance and has trusted me whole- heartedly, even when I was close to the "natural fracturing" caused by various stresses experienced during my times in Durham. I also wish to acknowledge my GeoPOP team mates (Jamaal Hoesni, Tom Sinclair, Martin Traugott and Adrian White) and Dr. Anthony Mallon, for the talks and expertise shared within the world of geopressure and geosciences.

The journey to this milestone has been long, and occasionally arduous. All along, I encountered many people at various levels and capacities, collaborating with many institutions and organisations. Each of these people and organisations had a wonderful ability to enhance my determination and drive towards education, knowledge, science and technology. They did give me confidence throughout and offered assistance in many ways. I hope this thesis does justice to all their efforts and invaluable inputs to the entire undertaking. Thanks.

On a more special note, I thank the Government of Japan who, through the World Bank, granted me a Joint-Japan World Bank Graduate Scholarship Program Award which led to this work. The University of Lagos, the University of Durham, the Canon Collins Educational Trust for Southern Africa (CCETSA) are all thanked for their financial support towards the end of the entire project. Enterprise Oil, today part of Shell Petroleum UK, is thanked for financial support of the research.

To the entire staff and postgraduate students, both past and present, within the Durham Earth Sciences Department; to many friends in the UK, especially the Afcab Soc-ers, the EPTs and the M'fumistes, I say we have made it together as all of you did help create the world and environment in which this piece of work has evolved over the last few years.

To my cousin Gd Samy Luyindula Kamalandua; to my elderly granny and matriarch Ndona Kauvovwa, my mum Isabel Matondo and to Becky Nitu Mpuidi, my fiancée, for all the sacrifice and un-ending love from far away in the Kongo Land of Angola and the DRC; find herewith a gift for your patience, staunch moral support and understanding in awaiting the project to completion.

Finally, many more of you deserve acknowledgement at this time. If you feel so, consider yourself acknowledged 'coz you are not missed out!

Lbd

Contents

Figures

Tables

Chapter 1

Introduction

1.1. General introduction

1.2. Velocity of compressional waves

1.3. Pressure concepts in porous media and reservoirs

1.4. Fine-grained sediments in this study

1.5. An overview of other related work

1. INTRODUCTION

1.1. General introduction

1.1.1. Scope of the study

When drilling wells in overpressured areas, it is important to have advance knowledge of the pore pressures likely to be encountered in permeable reservoir formations. The mudweight may be adjusted or a casing point chosen to avoid losing control of the well. These steps, known as well prognosis and borehole control, are achieved with the use of some attributes and well information, along with analysis of velocity information, i.e. interval velocities from seismic data and sonic velocities.

Seismic velocity has been most commonly used as a parameter for overpressure determination because of its sensitivity to porosity. A way to link overpressure with rock properties is to recognise that the seismic velocity of any rock in the subsurface is a function of its depositional and burial history. Elevated pore fluid pressure resulting from sealing of fluids during burial translates into rock porosity preservation and change in velocity within the rock – normally a decrease in P-wave velocity.

The importance of pore pressure prediction ahead of drilling cannot be over-emphasized, especially in newly emerging plays with high reserve replacement potential. Examples of newly emerging plays that are liable to be overpressured are deep water sediments on ocean margins, sub-salt reserves and high-pressure high-temperature (HPHT) environments. However, it is worth noting that overpressured basins are not only encountered in frontier exploration beyond continental margins and at greater depth. Overpressure is pressure above "normal" or hydrostatic pore pressure (Swarbrick, 2002) and there are many abnormally pressured basins around the world, e.g. North Sea, GoM (Gulf of Mexico), old sedimentary basins of Russia (Mouchet and Mitchell, 1989).

Overpressures are generated by mechanisms classified as either undercompaction or unloading (Swarbrick et al., 2002). The work presented in this dissertation is an investigation into the effect of overpressure due to unloading on seismic velocity. The term "unloading" here is used to refer to all mechanisms that reduce effective stress. Some purists insist that unloading only refers to process such as uplift and erosion, where the stresses acting on sediment are reduced. The term as used here includes fluid expansion mechanisms such as gas generation, which increase pore pressure without changing the vertical load.

1.1.2. Aims and impact of the study

The purpose of the work reported here is to assess whether sonic and density log information could be used to estimate overpressure generated by unloading mechanisms, in addition to that generated by undercompaction, in some sediments of the North Sea.

The approach is to establish a relationship between sonic velocity and other petrophysical parameters, necessarily including porosity and vertical effective stress, when the latter variables are treated as independent; and, if so, to determine the amounts of overpressure attributable to undercompaction and unloading processes. In short, the thesis investigates what additional geophysical data might be needed to estimate overpressure more accurately. The investigation focuses on fine-grained sediments, chalk and mudstones, of the North Sea located in the Central Graben and the East Shetland Basin. Fine-grained sediments are chosen because when wells are drilled overpressure needs to be estimated in the cap rocks fine-grained sediments before a permeable formation is penetrated to avoid the risk of a blow-out.

The drivers for this study are both academic and industrial. From an industrial view point, any possible method of pore pressure prediction ahead of drilling is worth investigating. Unloading takes place along a reversible path in porosity - effective stress space, as unloading is a poro-elastic process (Goulty, 1998). Should it be proved that the reduction in effective stress due to unloading has an effect on seismic velocity independent of porosity, such a result would warrant further investigation. An accurate assessment of different contributions to observed overpressures would enable pressure prediction experts to make unloading corrections when estimating

pore pressure from normal compaction curves. Unloading processes are ignored in most models used in overpressure prediction.

1.1.3. Use of velocity for overpressure prediction

Pore pressure prediction ahead of the bit during drilling hinges on shale compaction curves, which should ideally show how porosity is reduced with increasing burial depth when the pore pressure is hydrostatic. Use of such compaction curves assumes that any overpressures present are due to undercompaction, i.e. sediment is normally consolidated. Overpressure due to unloading is ignored.

According to soil mechanics theory, it is the effective stress that controls compaction, and consequently rock properties such as sonic velocity. The vertical effective stress is defined as the difference between the external vertical stress (or overburden or lithostatic stress) acting on the rock and the fluid pressure (pore pressure) (Terzaghi, 1943). Although porosity directly describes compaction state, sonic velocity is widely used as an indicator of compaction because it is strongly dependent on porosity (e.g., Wyllie et al., 1956; Raiga-Clemenceau et al., 1988) and routinely logged in wells.

Unloading processes (e.g., uplift and erosion, fluid lateral transfer, gas generation) all reduce effective stress. Our approach is to use sonic velocity and other petrophysical parameters to investigate the response to such processes. The relationship between vertical effective stress and porosity during normal compaction defines a normal compaction curve, also known as compressional curve (Chilingar et al., 2002). If the sediment is then unloaded, by reducing the effective stress acting on it, there is only a small elastic increase in porosity, although the seismic velocity decreases substantially when the effective stress is reduced to very low values. Thus, there is no unique relationship linking the seismic velocity to either effective stress or porosity (Goulty, 1998).

1.1.4. Thesis synopsis

The work herein is presented in seven chapters. Chapter 1 introduces the study, stating the main objectives and giving some background to the project. It

contains overviews on seismic and sonic velocity, pressure concepts in sedimentary basins and the importance of fine-grained sediments in overpressure estimation. It ends with an overview of previous related work. Chapter 2 is intended to provide the reader with a broader view of the area of investigation and the issues under consideration. It briefly gives the location and describes the regional geological setting, discusses overpressure generating mechanisms and presents the status of the high pressure and high temperature (HPHT) observed in the region. A note ascribing the use of fine-grained sediments in this investigation and a number of concepts on the use of pressure data in the industry relevant to this study are provided.

Chapter 3 states the theoretical basis of the data analysis, and discusses compaction in fine-grained sediments as used in this study. It also explains the limitations of porosity-based pore-pressure prediction. Chapter 4 contains the mathematical fundamentals of the investigation. It gives details of data sources and requirements, and assesses the petrophysical parameters used for the modelling with procedures for their computation. It includes details of the generalised linear inversion method and of the suite of programs written for the investigation.

Chapters 5 and 6 are the core of the thesis. They contain the analysis of well log data and the results from the Chalk of the Central Graben and from Mesozoic mudstones of the Central Graben and the East Shetland Basin. Each chapter starts with an introduction specific to the relevant fine-grained sediments, previous related work and the local geological setting, and is followed by a breakdown of the data sets used. In each chapter the data analysis method is adapted and the results of the analysis are given along with a conclusion pertaining to the associated fine-grained sediments. Results of the investigation in the Chalk, i.e. Chapter 5, have been published (Lubanzadio et al., 2002).

Chapter 7 is a summary of the overall conclusions and suggests how this study could be extended beyond the scope of the thesis. Two appendices complete the study: Appendix A has detailed computations of variables or derived properties involved in the study, and Appendix B contains the computational programs developed as "Excel Visual Basic macros" for the data analysis.

1.2. Velocity of compressional waves

1.2.1. Seismic velocity and the industry

Propagation of seismic waves is of great interest to seismologists, volcanologists, explorationists and engineers. In the oil and gas industry, propagation of seismic waves has been a centrepiece, as seismic sections and traces have been at the core of the industry which bears its name, the seismic industry. This industry is interested in seismic waves from exploration to production with seismic data acquisition, processing and interpretation plus the analysis of seismic attributes to model reservoirs of interest during appraisal.

Amongst properties which can be measured in the field, the most fundamental is seismic velocity. Understanding the factors controlling or affecting seismic velocity has been a challenge leading to extensive research carried out over decades. According to elasticity theory, seismic velocity depends on a rock's density and elastic moduli. Equations (1.1) and (1.2) are expression for the P- and S-wave velocities. For the compressional wave

$$V_P = \sqrt{\frac{k + \frac{4}{3}\mu}{\rho}} \qquad (1.1),$$

and for the shear wave

$$V_S = \sqrt{\frac{\mu}{\rho}} \qquad (1.2)$$

where k is the bulk modulus, μ the rigidity modulus and ρ the medium density. A useful account of seismic waves and their propagation through the earth, based on elasticity theory, is given by Sheriff and Geldart (1995).

1.2.2. Seismic and rock properties

In the search for oil and gas resources, recordings of compressional waves as well as shear waves along with wireline log data from wells provide information about the spatial distribution of subsurface properties (Nations, 1974; Gregory, 1977; Tatham, 1982; Robertson, 1987; Miller and Stewart, 1990). Use is made of seismic velocity and other associated properties known as seismic attributes in getting proper insights into the formation/reservoir properties and their extension. Seismic attributes

offer advantages in that they can highlight properties that were not visible to the interpreter on the seismic data alone. There are, in addition, other important petrophysical parameters or rock properties, such as lithology, porosity and saturation, which are required for a good understanding of the reservoir model. Fluid pressure within the reservoir is also of great interest for well planning, calling for the initial pressure distribution to be investigated.

Several studies in the area of rock physics are available on the effects of rock properties on P-wave velocity (e.g. Han et al., 1986; Mavko et al., 1998; Hilterman, 1998). The behaviour of the V_p/V_s has also been extensively studied. It has been demonstrated that V_p/V_s is a good indicator of lithology (Pickett, 1963; Nations, 1974; Eastwood and Castagna, 1983; Castagna et al., 1985), that V_p/V_s is sensitive to gas in most clastics sediments (Gregory, 1977; Tatham, 1982; Ensley, 1984, 1985), and that its response to gas in carbonate rocks is variable (Robertson, 1987). Influences of pressure and porosity on $V_p - V_s$ ratio in unconsolidated sands have also been studied (Zimmer et al., 2002).

1.2.3. Sonic velocity in porous media and sedimentary rocks

It has been established that seismic velocities, V_p and V_s, within sedimentary basins are affected by many factors, such as age, porosity, pore geometry and fluid content, depth of burial, effective stress, type and degree of cementation (McCormak et al., 1985; Miller and Stewart, 1990).

The effect of porosity on velocity has been analysed using various approaches, including the time average equation (Wyllie et al., 1956), the Picket (1963) empirical equation, the transit-time to porosity transform of Raymer et al. (1980), the empirical regression equation (Raiga-Clemenceau et al., 1988), the travel time differences to porosity linear equation (Mehta and Verma, 1991), the shale calibrated porosity-sonic transit time equation (Issler, 1992), and the shale compaction trend from sonic (Hansen, 1996).

The dependence of seismic velocity on pressure has been confirmed for a variety of rocks by laboratory measurements of elastic wave velocities in samples with varying pressure in fluids (e.g. Wyllie et al., 1958; Todd and Simmons, 1972;

Eberhart-Phillips et al., 1989; Prasad and Manghnani, 1997). Depths of burial and geological age have an effect. In addition, fracturing is also found to have an influence on velocity (e.g. Peacock et al., 1994a, 1994b).

For years, conventional logs (sonic, density, resistivity) have been used to detect zones of abnormal high pressure (e.g. Athy, 1930a, 1930b; Hubbert and Rubey, 1959; MacGregor, 1965; Eaton, 1972; Maucione et al., 1994). The velocity of compressional waves in rocks is a useful quantity to measure for pore pressure prediction because velocity is a function of lithology, fluid type, porosity and effective stress (Eberhart-Phillips et al., 1989; Prasad and Manghnani, 1997, Khazanehdari et al., 1998). Many laboratory investigations have also assessed the effect of pressure on velocity (Gregory, 1977; Domenico, 1984; Han et al., 1986; King et al., 1988). Other recognised factors affecting velocity are pore types and cementation (Massafero et al., 2002). Figure 1.1 gives trends of some rock properties on seismic velocity. Most of the studies reported above have been carried out on sandstones.

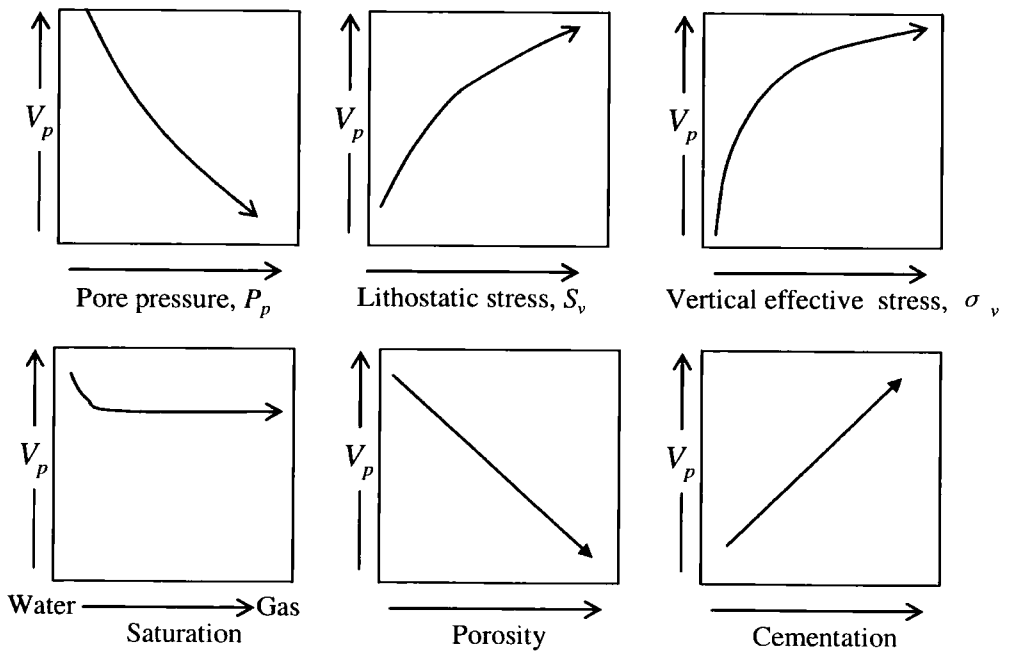

Figure 1.1. Some effects of rock properties on velocity (after Hilterman, 1998)

In a shale, it is possible to use measurements of velocity from sonic logs together with estimates of porosity from bulk density logs to arrive at an unambiguous estimate of pore pressure, as Bowers (2001) has proposed, assuming that the shale

matrix and pore fluid do not form a chemically reactive system. At the outset, it is known that it is more difficult to proceed with the same method in Chalk because of porosity variations associated with calcite precipitation. (The same difficulty would apply with respect to quartz cement in sandstones). However, due to the importance of chalk as a clastic reservoir, efforts to determine compaction curves for the chalk of the region have been made (e.g. Mallon and Swarbrick, 2002).

1.3. Pressure concepts in porous media and reservoirs

1.3.1. Formation pressure, stress and overpressure

Formation pressure, also known as pore pressure, or fluid pressure P_p, is the pressure of the fluid contained in the pore spaces of sediments or other rocks (Mouchet and Mitchell, 1989). The hydrostatic pressure at any depth z below water surface equals that exerted by a column of fluid of average fluid density at that depth, say ρ_{fluid} ;

$$P_{hydrostatic} = \rho_{fluid}\, g\, z \qquad (1.3)$$

where g is the acceleration due to gravity. This is also known as the normal pressure.

However, pore pressure under the surface in porous media is not always hydrostatic. Any value of P_p showing a discrepancy, either positive or negative, with respect to the value of corresponding hydrostatic pressure at the depth of consideration, is termed abnormal pressure. A negative pressure anomaly is termed "Underpressure", while the positive is "Overpressure" (Mouchet and Mitchell, 1989). Overpressure is defined as the amount of P_p exceeding the hydrostatic pressure (Dickinson, 1953; Gaarenstrom et al., 1993; Osborne and Swarbrick, 1997b). Over the two last decades, research has been carried out in understanding pressure regimes in sedimentary basins in terms of their history, distribution and compartmentalisation (e.g. Bradley and Powley, 1994; Ortoleva, 1994), the rate and direction of fluid flow (e.g. Swarbrick, 2004, 2005), overpressure determination (e.g. Bowers, 2002) and prediction (e.g. Huffman, 2002). A summary of abnormal pressure generating mechanisms will be given in Section 2.4.

The pore pressure P_p at a given depth z is commonly compared to the overburden stress, also known as overburden pressure, vertical stress or lithostatic stress, noted S_v. S_v is the vertical stress acting on the rock and is given by the relation:

$$S_v = \rho_b g z \qquad (1.4)$$

which is the vertical pressure produced by a column of rock with an average density ρ_b. In addition to S_v, there are two other principal stresses acting upon a unit of sediment: the maximum horizontal stress, S_H, and the minimum horizontal stress, S_h. If S_h is the minimum horizontal stress, it is also known as the fracture pressure. There are corresponding effective stresses, σ_v, σ_H and σ_h, respectively (Figure 1.2. b).

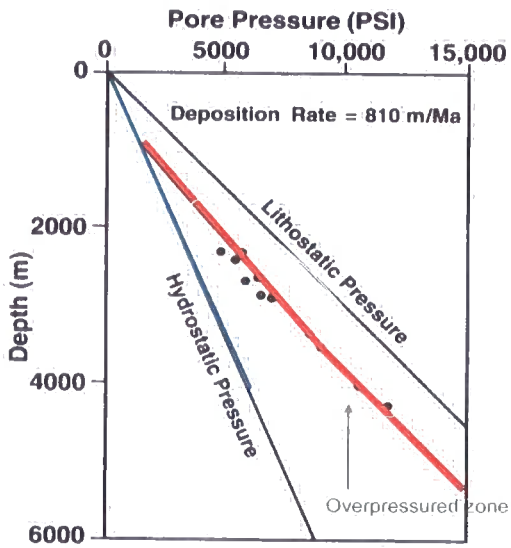

(a) Petroleum geology: Pressure – depth plot

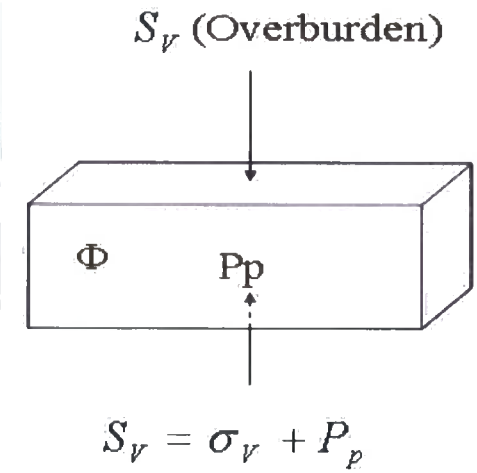

(b) Rock Mechanics: Balance of forces

Figure 1.2. Pressure concepts in sedimentary basins.

The effective stress, as well as porosity, has an effect on seismic velocity; thus these effects are of importance in many applications such as overpressure prediction from seismic data (Eaton, 1975; Dutta, 2002; Huffman, 2002; Sayers et al., 2002), and also as established recently in hydrocarbon production monitoring using time-lapse seismic measurements (Tura and Lumley, 1999; Landrø, 2001). Section 2.6 gives further details on the origin of stresses and the importance of assessing them during well prognosis, drilling and production operations. The corresponding effective stress of interest in our study is the vertical effective stress, σ_v, as introduced below.

1.3.2. The skeleton or frame or matrix pressure: vertical effective stress

The skeleton or frame pressure of a rock is the vertical effective stress (Gardner et al., 1974). It is the external vertical stress less fluid pressure. The elastic moduli of the matrix (skeleton/frame) increase with increasing effective stress, and a corresponding increase in velocity is observed. The increase in the elastic moduli is attributable to the reactions at the intergranular contacts and the closure of microcracks (e.g. Peacock et al., 1994b). Hence when both overburden pressure and formation fluid pressure are varied, only the difference between the two (the vertical effective stress) has a significant effect on velocity. A set of data given by Gardner et al. (1974) confirmed the assertion. Velocity increases with increasing vertical effective stress. Gardner et al. (1974) also established the effect – in recent basins - of the in situ cementation of sand grains in increasing the velocity compared to sand subjected to pressure in the laboratory.

1.3.3. Pressure measurements and presentation

In most fields nowadays, two dominant types of tools for pressure data collection are used: (1) high resolution tools run in open well bores prior to completion – amongst others, the modular formation dynamics tester (MDT), the formation multi-tester (FMT), the repeat formation tester (RFT) and the GeoTap pressure while drilling tool developed by Halliburton - and (2) downhole gauges (e.g. the drill stem test (DST)) that provide measurements from producing wells. The first set of tools measure pressure at known depths and are commonly used to determine fluid gradients in individual sands. By contrast, downhole gauges provide the invaluable ability to monitor pressure decline over time. Indirect pressure measurements are also used for well control. They include mudweight and borehole conditions experienced during drilling. Although the above tools have been successful, there is a drive for real time fluid pressure monitoring (mostly during directional drilling); and accordingly tests on equipment/pressure tools using optical fibres to convey data have already been carried out (Reynolds, 2004, von Flatern, 2005).

Pressure data are usually displayed on a range of plots to demonstrate the interaction between pressure, depth, stratigraphy, time and location. Plots that show pressure against depth (e.g. Figure 1.2.a) are particularly useful in illustrating fluid gradients, fluid contacts and large scale pressure differences. Datumed pressure plots,

where the effect of fluid density is removed, reveal subtle pressure variations and changes, in particular dynamic pressure gradients caused by production and static pressure gradients which are the result of variable fluid properties. Also in use are pressure-time plots. They have the ability to demonstrate excellent lateral pressure communication, in contrast to pressure depth plots and datumed pressure plots which are useful for identifying vertical pressure barriers.

1.4. Fine-grained sediments in this study

1.4.1. Interest in fine-grained sediments

Fine-grained sediments, as opposed to siliciclastic and carbonate rocks, are renowned for their low permeability. They are chalk and mudstones. Mudstones are fine-grained clastic rocks that are often described by a range of terms including clay, mud, claystone, siltstone, shale, silty mudstone, and silt rich clay (see section 2.1.3). Though their properties are difficult to assess - especially for shales – estimation of pore pressure in fine-grained sediments is important before penetrating permeable reservoir formation. Mudstones are recognised as seals as well as sometimes being hydrocarbon source rocks. Chalk is also thought to act as a regional seal in the Central North Sea (Mallon and Swarbrick, 2002; Mallon et al., 2005).

In this study, only non-reservoir sediments are considered, i.e. mudstone and chalk successions which may be described simply as overburden. Sonic and density log information are used to assess whether the presence of overpressure due to unloading processes in these fine-grained sediments can be detected and quantified. Considering the effect of gas on the P-wave velocity, it is critical to avoid sediments bearing hydrocarbons, for their presence will result in a velocity decrease that can be misinterpreted as an effect of elevated pore pressure. This suggests the choice of clean chalk and non-organic mudstone beds for the investigation (Section 3.5, Chapter 3).

1.4.2. Velocity, compaction and pore pressure in shales

Shales are recognised of being fissile and for their capacity to swell and dewater. Another property of shales is its seismic velocity anisotropy. The anisotropy in shales requires anisotropy corrections in seismic velocity analysis (e.g. Hawkins et al., 2001)

and results in overpressure prediction difficulties as observed by Domnesteanu et al., (2000) and Heppard et al. (2000). Within shale sequences, the normal increase in velocity with depth is attributed to dewatering; while higher velocities observed in sands and carbonates are primarily related to higher densities compared to shales.

Mechanical compaction during burial can only occur when the shale can dewater. As the sediments compact and the porosity reduces, so does the permeability (Mann and Mackenzie, 1990; Luo and Vasseur, 1992; Maubeuge and Lerche, 1994). It follows that pore pressure affects compaction-dependent geophysical properties, such as density, resistivity and sonic velocity. This constitutes the premise on which overpressure detection is based. Shales are then the lithology of choice as they are more responsive to processes leading to overpressure than other types of rocks (Bowers and Katsube, 2002).

As will be discussed in Section 2.5, pore prediction models are compaction curves which may vary within a basin or in between basins. Variations may be related to the lithology, grain size, rate of sedimentation, subsidence and structural history within basins. In terms of overpressure in shales, in addition to disequilibrium compaction and hydrocarbon generation within source rocks, smectite-illite transformation is also accepted as an internal overpressure generating mechanism (Osborne and Swarbrick, 1997a; Katsube et al., 1998; Lahann, 2002; Nadeau et al., 2002).

1.5. An overview of other related work

Increasingly nowadays, pore pressure determination starts with determining interval velocities from seismic data before spudding the well. Velocity information may be updated with drill-bit seismic or by acquiring sonic and VSP data during rig down-time (Dutta et al., 2002a). Many other attempts have been made to predict overpressure using interval velocities from processing seismic reflection data and velocity from sonic logs. A compiled overview on overpressure prediction from seismic data, using velocity analysis, can be found in Dutta (2002).

Hillis (1995) used sonic velocity, not for overpressure estimation, but to independently quantify apparent exhumation (height above maximum burial depth) in

the Chalk of southern North Sea. Al-Chalabi (2001) suggested interval velocity in uplift investigations, and further work reported the use of velocity-depth relationship for recognition of an uplifted unit (Al-Chalabi and Rosenkranz, 2002).

Two pieces of work are worth citing in relation with the variation of velocity with effective stress in Chalk of the North Sea. The first was carried out by Japsen (1998), who undertook a regional study of velocity depth anomalies in North Sea Chalk, and reviewed previous work by Bulat and Stoker (1987), Hillis (1995) and Sclater and Christie (1980). The second one is by Mallon and Swarbrick (2002). They determined a compaction trend for the non-reservoir Chalk in the more restricted area of the Central North Sea, using data from 59 wells. Details of their results are stated in Section 5.6, Chapter 5.

Unloading processes reduce effective stress (Goulty, 1998). As compaction is predominantly an inelastic process, only a small amount of elastic rebound occurs when the effective stress acting on a formation/sediment is reduced. The elastic rebound corresponds to an unloading curve on a plot of porosity versus effective stress (see Section 3.2). Bowers and Katsube (2002) found that transport properties (e.g. sonic velocity and resistivity) which are sensitive to pore sizes, shapes, and how pores are connected undergo more elastic rebound than bulk properties (density and porosity). They suggested that a depth interval in which resistivity and sonic velocity data appear anomalously low in comparison to bulk density is likely to be an indicator of in-situ rebound (unloading).

An interesting summary of critical challenges of pore pressure predictions is given by Huffman (2002). The seismic industry has made progress in the use of lapse-time seismic and other seismic attributes (e.g. shear-wave velocity) towards pre-drill pore pressure prediction. At the same time, prediction while drilling has made success in some areas, as it is based on the use of drilling parameters to detect deviation from a 'normal' pressure trend within the borehole. Among all methods already developed, each has its limitations. Thus, ways of fine-tuning the existing methods or building upon them are still worth exploring.

Chapter 2
The Central North Sea, fine-grained sediments and overpressure

2. THE CENTRAL NORTH SEA, FINE-GRAINED SEDIMENTS AND OVERPRESSURE

2.1. Introduction

2.1.1. Aims and outline

This chapter introduces the Central North Sea and provides the reader with a background and broader view of the area of investigation, with the purpose of putting the analysis in Chapters 5 and 6 into context. The background information covers:

- the geographical location,
- the geological history in terms of stratigraphical settings, sediment distribution, structural deformation, tectonic evolution, the burial history and reservoir stratigraphy,
- the overpressure origin and history.

This is followed by a review on a number of concepts needed to understand the origin of overpressure and the use of pressure data in the industry, pertaining to this study.

2.1.2. Central Graben and East Shetland Basin: geographical location

This investigation covers the Central Graben and the East Shetland Basin of the North Sea (Figure 2.1). The Central Graben strikes NW-SE approximately between 1°E 58°N and 4°E 56°N. The East Shetland Basin is located between 60° - 62°N and 1° - 3°E. These areas have been the subjects of many studies related to overpressure and stress investigations, due to their economic importance with several hydrocarbon-producing fields. Production comes from the normally pressured Palaeocene Forties Sandstones, the overpressured Upper Cretaceous and Danian chalks, some other plays in the Jurassic (Fulmar, Brent and Statfjord sandstones) and pre-Jurassic sandstones exhibiting high pore pressures. Figure 2.1 shows the location of the UK continental shelf and the geological area of our investigation.

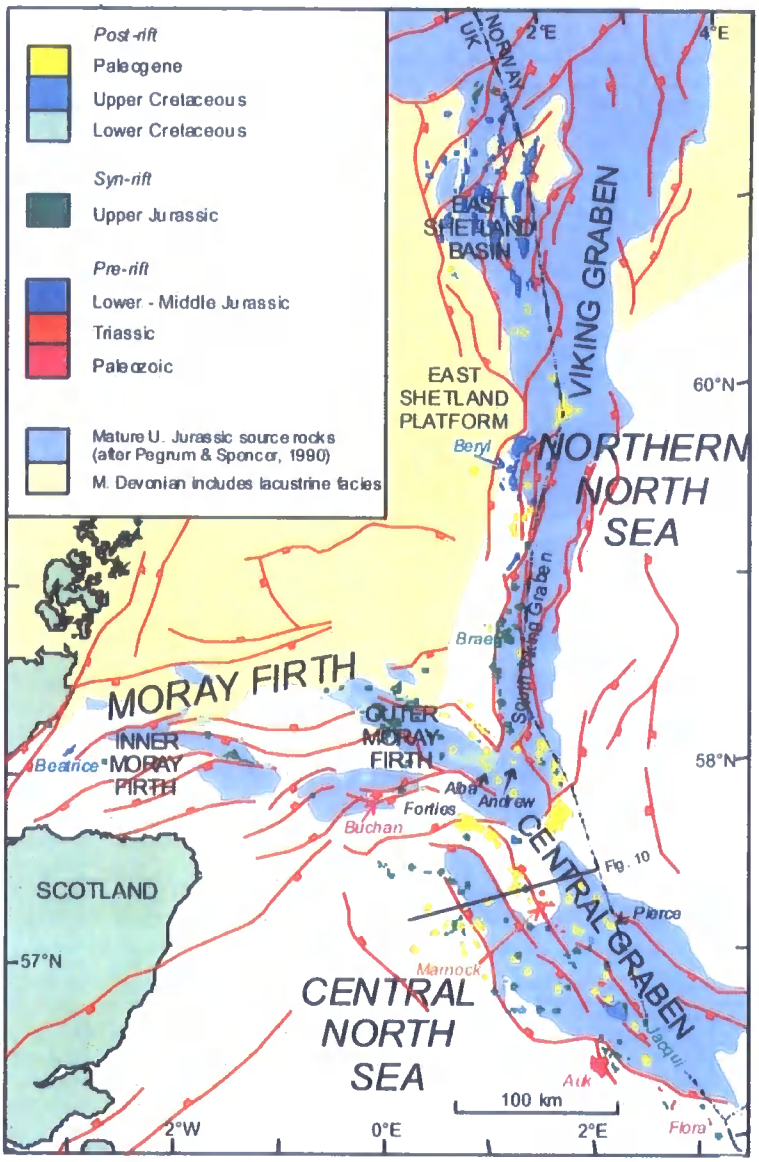

Figure 2.1. Map of the North Sea showing age of principal reservoirs and distribution of some source rocks (from DTI, 2003).

2.1.3. Fine-grained sediments: chalk and mudstones

The lithologies of the fine grained sediments considered here are chalk and mudstone; mudstones are also known as mudrocks. Chalks are fine grained sediments (micrites) composed largely of the minute skeletons of coccoliths (a nanofossil group of golden-brown algae), with only subordinate contributions of planktonic foraminifera, calcispheres and other coarser material (Scholle, 1977). Mudstones are formed by conversion of argillaceous sediments under the effects of mechanical and chemical compaction processes. According to Lapidus and Winstanley (1987), "A mudrock is a fine-grained sedimentary rock composed chiefly of particles in the silt-

clay size range. Mudrock is a general term that can be used to distinguish the finer-grained sedimentary rocks from sandstones or limestone. Mudrocks can be further identified as shale, mudstone, argillite, siltstone, claystone or marl, depending on the dominant grain-size (=texture), composition and the presence of fissility or laminations. Mudstone is a commonly used synonym for mudrock."

Claystone is a sedimentary rock of indurated clay-sized silicate materials, having the texture and composition of shale, but lacking its lamination and fissility. The particular feature about shale is that it has distinctive laminated layers and moderate to high clay content. Siltstone is principally composed of silt-graded material, which is finer than very fine sand and coarser than clay, and contains less clay than shale and lacks its fissility and fine lamination. As a detrital sedimentary rock formed by the compaction and consolidation of clay, silt, or mud, shales are vulnerable to phenomena such as swelling, shrinking, hydration, strength reduction and failure. These problems occur because shales are highly water-sensitive formations. Though they are difficult to study, mudrocks/mudstones are important rocks because they are the most abundant sedimentary rocks, making up over 65% all sedimentary rocks. In value, they are likely the source rocks for petroleum and natural gas, and are sometimes valuable ore deposits.

Across Europe, the Chalk is one of the most recognizable and conspicuous rock sequences. In the North Sea it is encountered in the Wessex Basin in southern England and in the British Isles (Evans et al., 2003b). In Southern England, the Chalk was deposited during a period of over 30 Ma (Gradstein et al., 1994, 1995; Hardenbol and Robaszynski, 1998), which is known to have been a particularly protracted highstand of sea level that followed a long-recognized major sea-level rise and marine transgression towards the end of the early Cretaceous (Suess, 1906).

Mudstones considered in the study are those of the Lower Cretaceous and the Jurassic (see section 3.5, Chapter 3). A particular characteristic of most sedimentary basins with fine-grained lithologies (such as shales) is the development of overpressure starting around depths of 2.0 km or greater below sea-bed (Swarbrick, 2004).

2.2. General geology

The general geology of the North Sea is described by Glennie (1998) and Evans et al. (2003a). The following is a short description aimed at introducing the area covered in this study and relates to the stratigraphy shown in Figure 2.2.

The Lower Jurassic is represented by the Dunlin Group and the Lias Group. These two groups overlie the Triassic strata conformally in the north and the extreme south, respectively. In the north, the Middle Jurassic comprises the Heather, which is a deposition of up to 1200 m of mudstones with occasional turbiditic sandstones, overlying the Brent Group. In the south part, the Fulmar Sandstone replaces the Heather and the West Sole Group replaces the Brent Group. The Upper Jurassic consists of the Kimmeridge Clay, which is an organic-rich mudstone deposited in low-energy intra-shelf marine environment. It is believed to act as source or seal in several fields (Doré et al., 1985; Husmo et al., 2002).

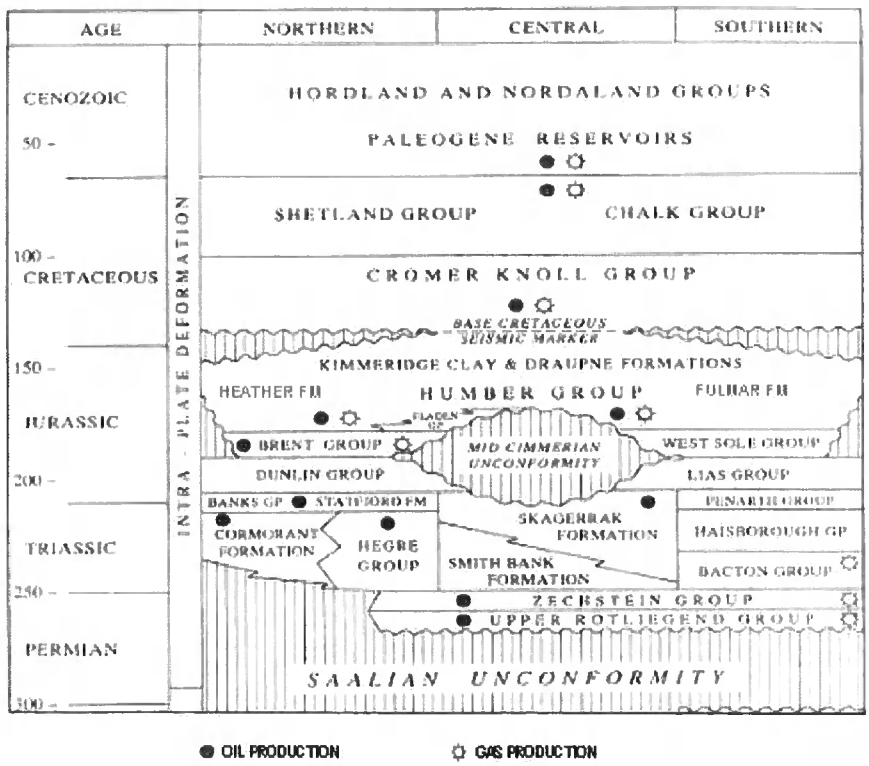

Figure 2.2. Stratigraphic column of the North Sea Basin up to the Permian. Areas with vertical hatching represent unconformities (after Brennand et al., 1998).

The Lower Cretaceous (Cromer Knoll Group) contains beds of marl, shale, claystones and limestones in the Plenus Marl, Sola and Valhall Formations. The Upper Cretaceous comprises the Chalk Group in the central and southern parts of the North Sea, with the Shetland Group in the northern part. Across the North Sea Central Graben, chalk is an important hydrocarbon reservoir, as hosted within the Upper Cretaceous and the Danian Chalk.

The post-Cretaceous in the North Sea Central Graben is made of strata which are distributed throughout the North Sea Basin. In the Central Graben and the Shetlands, the Palaeocene is made of preserved strata, which comprise siliciclastic sediments, claystones and the Danian Chalk; the latter being considered as part of the Ekofisk (Chalk Group) (Morton et al., 1993; Ahmadi et al., 2003).

Of relevance to overpressure, it is worthwhile to indicate that fine-grained sediments, chalk and mudstones, are very low permeability rocks. While shales act as seals and hydrocarbon source rocks, depending upon depositional facies and pathways, chalk can be both reservoir and seal (e.g. Scholle, 1977; Kennedy, 1980). Within much of the UK chalks, the distinction between reservoir and seal is very fine over the permeability range 0.01 to 0.5 mD. Many layers of low permeability within the Tor, Hod and Hidra Formations probably act as top seals to accumulations of hydrocarbons. In addition, the tight zone at the base of the Ekofisk and the Plenus Marl shale are known as two ubiquitous and efficient intra-Chalk seals.

In the northern part of the Central Graben, the Palaeocene consists of sheets of sandstones overlying the Chalk. The sandstones form a normally pressured aquifer overlying the Chalk Group. Consequently, the upper part of the Chalk Group is also normally pressured. However, overpressures are observed deeper in the Chalk even where it is overlain by Palaeocene sandstones. In the southern parts of the graben though, the Palaeocene sandstones are replaced by claystones which act as a seal to overpressures encountered in the Chalk Group (Holm, 1998).

2.3. Sediment compaction and diagenesis

2.3.1. Definition

Compaction and cementation, known as lithification, are part of the rock cycle. After deposition, sediments are compacted as they are buried beneath successive layers of sediment and cemented by minerals that precipitate from solution. Compaction is the physical process by which sediments are consolidated, resulting in the reduction of pore space as grains are packed closer together. Diagenesis is the physical, chemical or biological alteration of sediments into sedimentary rock at relatively low temperatures and pressures that can result in changes to the rock's original mineralogy and texture. As the loading conditions vary with time, some of sediment properties (e.g. mechanical and transport properties, such as porosity, permeability and compressibility) are affected. It follows that the pressure within the sediments is also affected. This gives rise to a variety of sedimentary rocks. Mudstones, for instance, are formed by conversion of argillaceous sediments under the effects of some mechanical compaction and chemical processes, as stated earlier.

2.3.2. Porosity reduction and oil generation/migration

Both compaction and diagenesis reduce sediment porosity. As layers of sediment accumulate, the ever increasing overburden pressure during burial causes compaction of the sediments and loss of pore fluids. It leads to the formation of rock as grains are welded or cemented together. Grains of sediment, rock fragments and fossils can be replaced by other minerals during diagenesis.

Porosity usually decreases during diagenesis, except in rare cases such as dissolution of minerals and dolomitization. Diagenesis does not include weathering processes. Hydrocarbon generation begins during diagenesis. There is not a clear, accepted distinction between diagenesis and metamorphism, although metamorphism occurs at pressures and temperatures higher than those of the outer crust, where diagenesis occurs.

The importance of compaction is enormous. Many works have revealed/confirmed that reservoir beds such as limestones and sandstones show little compaction compared to shale. Athy (1930b) published a summary on compaction in

shale as a major factor in oil migration, compared to temperature change, effect of buoyancy and capillarity. He also confirmed the role of compaction in structure development (Athy, 1930a). Figure 2.3 is an illustration contrasting shale compaction under normal conditions and rapid burial, the latter resulting in overpressured conditions, with assumed pore pressure gradients of 16.75 and 18.59 MPa/km at 3000 and 4500 m, respectively.

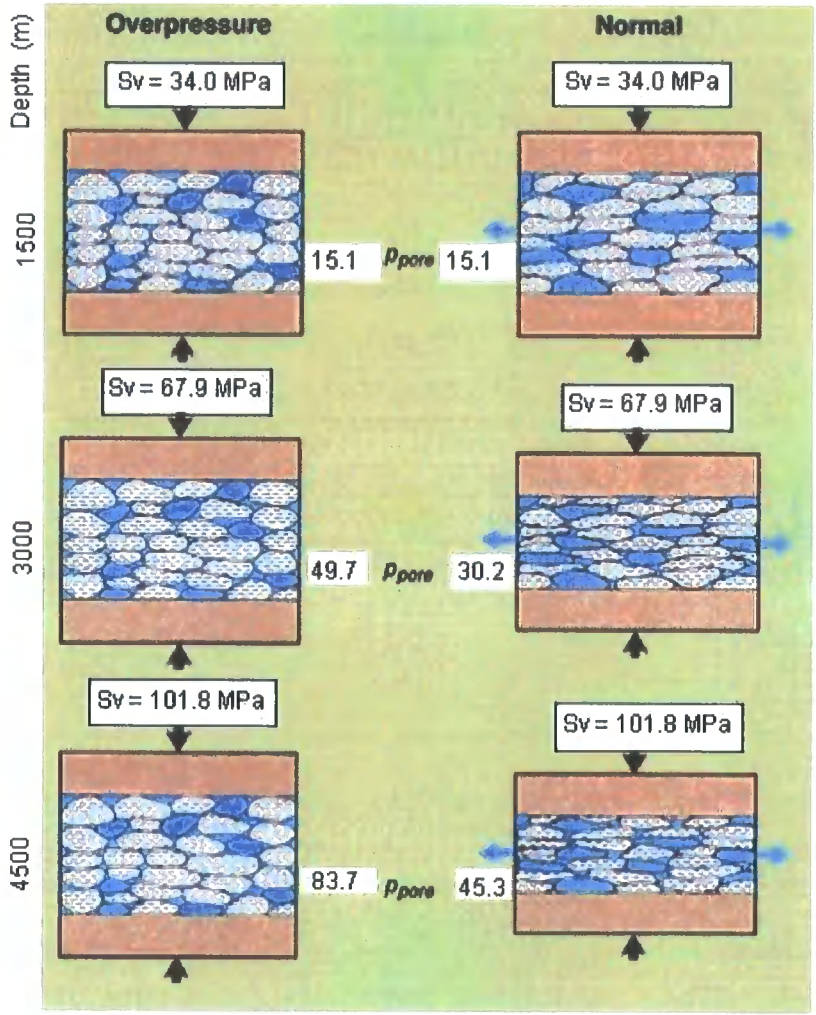

Figure 2.3. Compaction of shale in overpressured and normal conditions (modified after Schlumberger, 2004).

Further studies have revealed that compaction also exerts an important control on thermal gradients, particularly at shallower burial depths where porosity loss is most rapid. Along with compaction, bulk rock thermal conductivities show a corresponding increase with burial (Chiralli, 1975). Compaction, therefore, in addition to burial, also influences the degree and timing of source rock maturation.

Undercompaction, however, has been confirmed as the main cause of overpressure development in sedimentary basins (Swarbrick and Osborne, 1998; Huffman, 2002).

In addition to temperature, the evolution of sedimentary organic matter increases with pore pressure. The evolution of sedimentary organic matter depends also on temperature and pressure (Sajgo et al., 1986; Price and Wenger, 1992; Dalla Torre et al, 1997). As shown on Figure 2.3, overpressure increases with depth in undercompacted sequences. Where sediments are undercompacted, porosity is higher than for normal compaction, and so a greater degree of thermal maturity is expected. And it is observed that most of the world's oil and gas have been generated from overpressured source rocks (Baird, 1986; Connan, 1974; Hunt, 1990, Price and Wenger, 1992).

2.3.3. Sediment compaction and applications

Compaction in mudrocks has been studied intensively, since mudrocks are very complex materials. A number of different empirical compaction curves have been proposed to describe compaction and the changes observed in fine-grained sediments and in sandstones, as well. The first one was proposed by Athy (1930a) and is a simple exponential decay of porosity with depth. Any departure from the compaction curve can be interpreted as changes in the sediment properties (density, porosity and velocity), variation in the mixture of clay types in the shale, changes due to the thermally driven process of hydrocarbon generation or change of fluid type.

Compaction models, combined with the knowledge of the principal lithologic components in a sequence, are also used to predict density changes with depth and seismic P-wave velocity (Wiltshire and Huggard, 2000).

The normal compaction curve is derived from normally pressured sediments. However, the presence of overpressure reduces effective stress, and it is established that compaction and elastic wave propagation behaviour respond to changes in effective stress. Thus compaction curves are also used to spot the onset of overpressure (e.g. Hubbert and Rubey, 1959). Other uses of compaction curves are reported in section 2.5.1.

2.4. Overpressure

2.4.1. Generating mechanisms

In particular overpressured basins, the challenge of understanding the origin of overpressure has also received much attention during the last two decades (e.g. Osborne and Swarbrick, 1997b; Skar et al., 1998; Huffman, 2002). A re-evaluation and summary made by Swarbrick and Osborne (1998) stated that the mechanisms of abnormal pressure generation are: disequilibrium compaction, tectonic stress, reduction of load during uplift and erosion, temperature increase, water release due to mineral transformation, hydrocarbon generation, cracking of oil, osmosis, hydraulic head and buoyancy due to density contrasts. Swarbrick et al. (2002) categorised all of them into two groups: undercompaction and unloading mechanisms.

Undercompaction is generally associated with rapid burial beneath an overburden of low permeability, so that pore fluids cannot escape fast enough to maintain hydrostatic equilibrium. The pore fluids then become overpressured and the mechanical reduction in porosity with burial will be slowed. Unloading mechanisms generate overpressure by reducing the effective stress (see section 3.2, Chapter 3). They may involve fluid expansion (e.g. gas generation, lateral transfer), removal of external load (e.g. uplift and erosion) or chemical compaction (e.g. transformation of smectite to illite in shales). During chemical compaction, also known as clay diagenesis, the transformation of clay to illite is followed by dewatering (with concomitant increase in pore water volume) (Mouchet and Mitchell, 1989).

2.4.2. Overpressure in the Central North Sea

It is established that the main overpressures in the Central North Sea can be found in the Triassic, the Upper Jurassic Fulmar Sandstone and the Upper Cretaceous Chalk Group; except for the Witch Ground Graben where overpressures are not normally encountered, probably due to the shallower depth of burial of the pre-Cretaceous sediments compared to the deeper burial in the Viking and Central Graben. The Viking Graben has a similar pattern of overpressure as the Central Graben, with the maximum pre-Cretaceous overpressures found in the deepest part of the graben being similar in magnitude to the Central Graben (Holm, 1998).

Most of the Chalk within the North Sea (Norwegian, Danish and UK sectors) is generally accepted to be overpressured (Megson and Hardman, 2001, GeoPOP, 2000). In addition, in the Central Graben of the North Sea almost all Jurassic hydrocarbons fields are found in the overmature zone for the gas, while the oil fields occur in the mature zone (Cayley, 1987).

Documentation on the distribution and origin of overpressure in the Central Graben of the North Sea has been provided by Holm (1998). In his paper, he reviewed previous work on the subject across the North Sea hydrocarbon environments, evolving from models of compaction disequilibrium, aquathermal expansion and hydrocarbon generation to more complex models of episodic breaching and healing of seals (e.g. Chiarelli and Duffraud, 1980; Cayley, 1987; Burhig, 1989; Leonard, 1993; Gaarenstrom et al., 1993; Holm, 1996). A regional pressure atlas of the Central North Sea is also available from the Geosciences Project into OverPressure, and Figure 2.4 is one of the atlas maps (GeoPOP, 2000).

Compaction disequilibrium is considered to be the most important processes in the development of overpressure in the Central North Sea. In addition, oil and gas cracking - also known as hydrocarbon generation - is recognised to be of high contribution in the excessive pressure encountered in the region. Hydrocarbon generation, which is taken as an unloading mechanism, is considered to be the dominant cause of overpressure in the pre-Cretaceous of the Central Graben (~ 3000 m) (Holm, 1998).

Recent studies have shown that other unloading mechanisms are also needed to account for the amount of overpressure observed. Lateral transfer and chemical compaction - the transformation of smectite to illite - have been confirmed as part of the process of overpressure generation in the pre-Cretaceous of the Central North Sea.

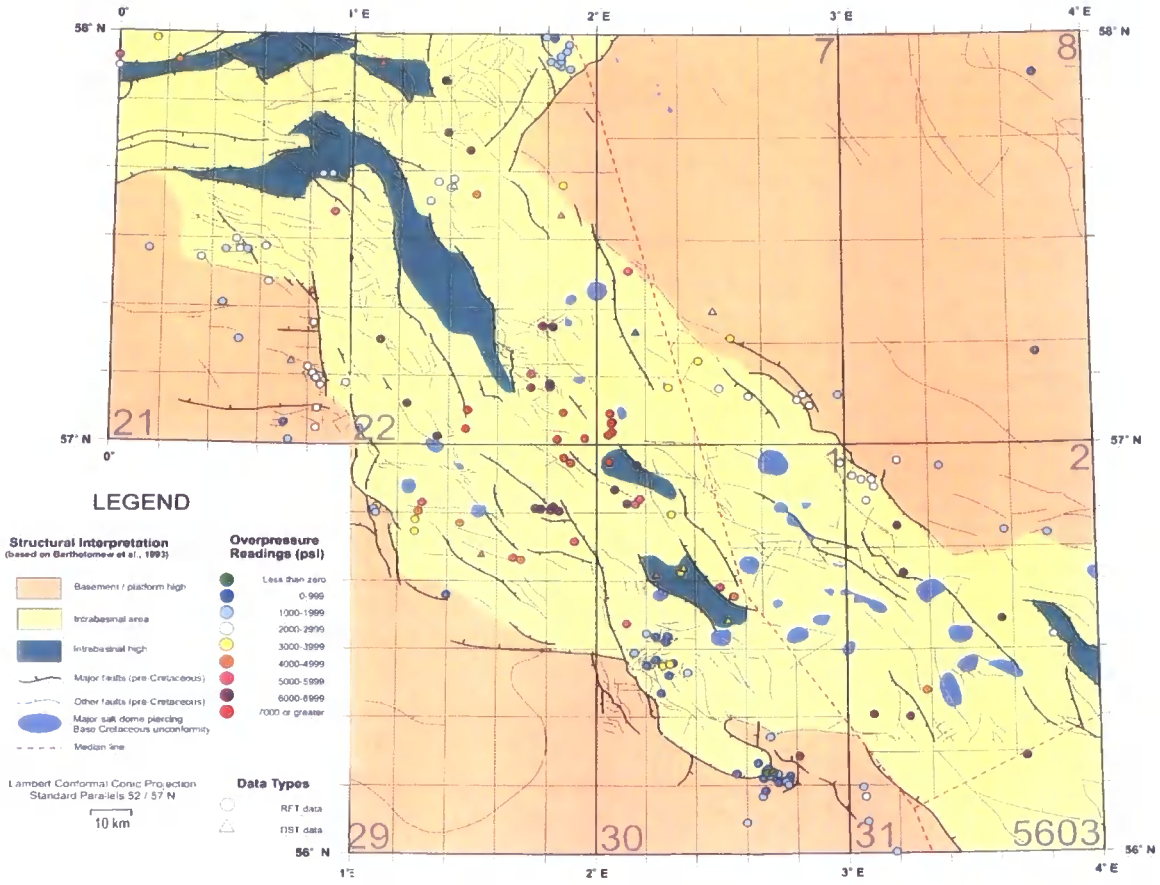

Figure 2.4. Jurassic overpressure readings in the Central North Sea (from GeoPOP, 2000).

2.5. Overpressure and the industry

2.5.1. Compaction curves and overpressure recognition

The principle of disequilibrium compaction underlies the calculation of shale overpressure; every method currently used to recognise or predict changes in pore pressure during drilling is based on formation compaction or the lack of it (Traugott, 1997; Brown et al., 1999). Shale properties have a range of behaviour in overpressured zones. Shale compaction curves describe this in terms of the rate of porosity and water loss during burial. These curves are mostly empirical curves, obtained from regional experience, sometimes with functional relationship from soil mechanics. They constitute information on porosity - depth, velocity – depth, and/or vertical effective stress – depth. When these properties are consistent with compaction disequilibrium, pore pressure can be computed using an equivalent depth-method.

Figure 2.5 outlines the use of a normal compaction curve to estimate pore pressure at a given depth, in an approach known as the Equivalent Depth Method (Eaton, 1972).

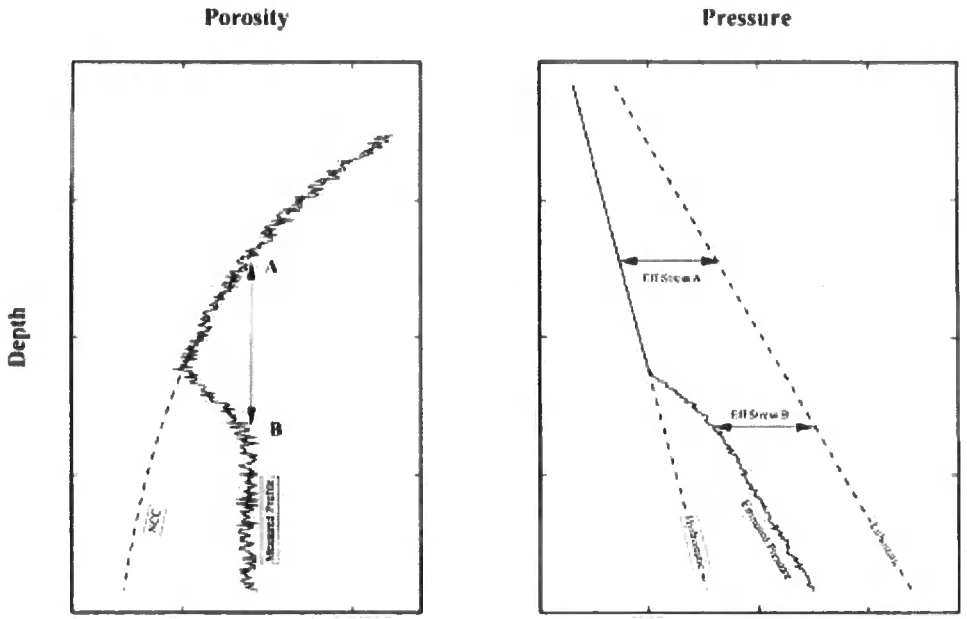

Figure 2.5. Normal compaction curve and the equivalent depth method

The upper section of the well is assumed to be normally pressured down to circa 2 km below sea bed (Swarbrick, 2004); a normal compaction curve (NCC) trend is then defined for the upper section. It is thought that sediments with equal porosities, such as those at depths A and B, have equal vertical effective stress. The effective stress can readily be estimated in the normally pressured section (e.g. at depth A), thus the pore pressure can be calculated at the overpressured zone (e.g. at depth B).

However, in some other overpressured wells the excess pressure observed is higher than the amount expected from disequilibrium compaction, which suggests that the remainder is consistent with unloading mechanisms. Lateral transfer, a mechanism whereby an inclined aquifer allows pressure communication between deep and shallower parts of a basin, has been suggested as one possible explanation (Traugott, 1977; Yardley and Swarbrick, 2000). These unloading mechanisms are the focus of this investigation (see section 3.2, Chapter 3). Figure 2.6 is a sketch portraying the response of vertical effective stress to different overpressure mechanisms.

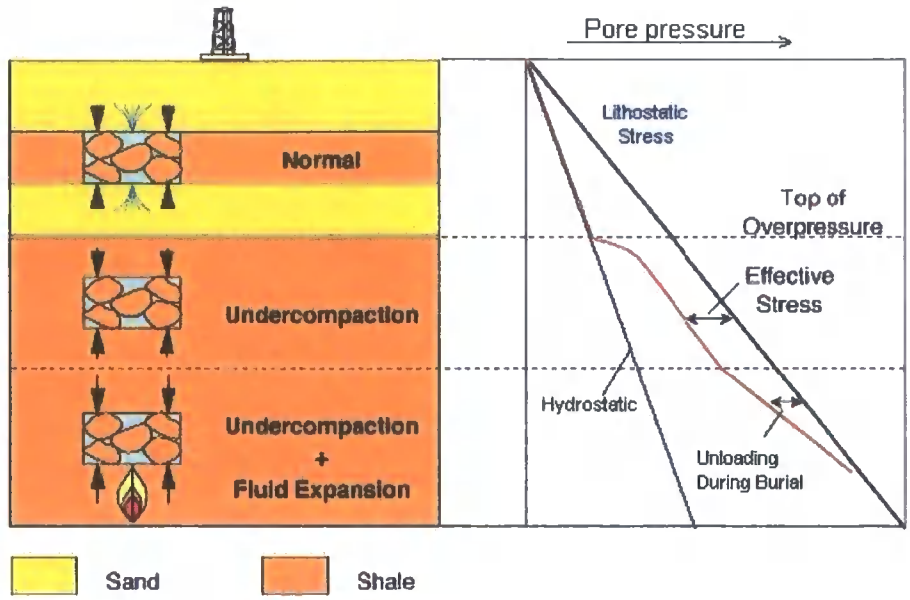

Figure 2. 6. Response of vertical effective stress to overpressure mechanisms (after Bowers, 2002)

The compaction related methods discussed above use petrophysical data. Use of seismic data in prediction of overpressured zones, based on high resolution velocity analysis of CDP data, has also been reported (e.g. Pennebaker, 1968; Reynolds, 1970; Bilgeri and Ademeno, 1982). A summary of the rock physics basis behind the seismic detection of overpressure is reported in a paper by Mukerji et al. (2002), and field applications of seismic methods are described by Dutta et al. (2002b).

2.5.2. Drilling difficulties due to HPHT

HPHT conditions are at the frontier of exploration geosciences. Although recent advances have been made in overpressure recognition and understanding (origins, mechanisms, compartmentalisation, estimation of pore pressure and its distribution), some challenges still remain to be solved, such as sealing and leaking faults in HPHT environments. However, studies on abnormal pressure have enlightened the industry and academia on a wide range of issues. These include:

- influences of abnormal pressures on petroleum systems: trap integrity, sealing capacity, reservoir quality, source rock maturation, hydrocarbon migration, fluid drive or hydrodynamics; and
- well prognosis and design in frontiers areas (Swarbrick, 2004).

Well-control problems constitute a challenge when drilling in overpressured zones. Knowledge of the state of stress in a hydrocarbon reservoir is needed for maintaining wellbore stability (drilling-induced tensile fracture and breakouts). Breakouts are brittle enlargements of the hole diameter due to the high stress concentrations around the wellbore. Hydraulic fracture may also happen due to excess pressure. The minimum horizontal stress, known as the fracture gradient, is an important indicator of how close the reservoir pore pressure is to natural hydraulic fracturing (Holm, 1998; Beekman and Skar, 2000).

2.6. Stresses, pore fluids and borehole stability

2.6.1. Sources of Earth stress and stress components

Deformation of the Earth's crust is a result of many stresses upon it by processes ranging from plate tectonic forces, crustal inhomogeneities, and other sources of stress peculiar to the dynamic earth. In the particular case of this study, stresses acting on a unit of sediment are assumed to act within a uniaxial strain model (below). The Earth's surface is considered as a free surface; that is stress must be perpendicular and parallel to this surface, which implies no shear stress.

We have then three principal stresses: vertical stress, S_v; minimum horizontal stress, S_h; and maximum horizontal stress, S_H ($S_H > S_h$). Vertical stress (S_v) is due to the weight of overlying rocks and fluids, i.e. the overburden. It is often known as the lithostatic stress. For an elastic solid, as in Equation (1.4):

$$S_v = \rho\, g\, z \qquad (2.\ 1)$$

where ρ is the density of the overlying rocks, g is the acceleration of gravity and z the depth. Horizontal stresses (S_H and S_h) are sums of tectonic and nontectonic stresses, i.e. those related to plate motions and those related to lateral confinement as overburden load is added.

2.6.2. Stress and pore fluids

Fluids present within sediments modify the effect of the total stress on the rock. The total normal stress is taken as the total force applied to or acting

perpendicularly on unit area, while the effective stress is known as that component of the total normal stress that is transmitted by grain-to-grain contact within the sediments mass. The total stress consists of the sum of the effective stress and the pore fluid pressure. In other words, the component of the total stress supported by the pore fluid is called the pore fluid pressure. In a fluid, all three principal stresses at a point are equal and this value is known as the pressure.

Following Terzaghi's principle (Terzaghi, 1943), the effective stress is equal to the total stress minus the pore pressure:

$$\begin{aligned} \sigma_v &= S_v - P_p \\ \sigma_H &= S_H - P_p \\ \sigma_h &= S_h - P_p \end{aligned} \qquad (2.2)$$

In practice, pore pressure is measured and the vertical stress computed to calculate the vertical effective stress. The vertical stress, S_v is relatively easy to estimate as the load, or weight, of the overburden (Equation 2.1). Data analysis and methodology used in this thesis are based on the above principle and the compaction regimes in fine grained sediments, as further presented in Chapter 3 (Sections 3.2 and 3.7).

However, it is worth noting at this stage that there has been a disparity in the concept of effective stress within the rock physicists' community following the Terzaghi's equation. Pores have an effect on the strength of rocks, i.e. a rock without pores is relatively stronger. Because pore space is partially supported by the fluid pressure, some authors have suggested a more general effective stress law in the form of Equation (2.3),

$$\sigma = S - \alpha P_p, \qquad (2.3)$$

introducing a constant α, known as the effective stress coefficient or Biot coefficient, with a value less than unity. In this study, it is considered that α is unity in (2.3); hence there is no distinction between (2.2) and (2.3). A clarification on the controversy about the effective stress coefficient in sandstone is given by Gurevich (2004), as summarized below.

Authors have considered $\alpha < 1$ on empirical grounds, i.e. fitting laboratory measurements/data (Prasad and Manghnani, 1997; Hermanrud et al., 1998b; Siggins and Dewhurst, 2003) supported by Biot's theory of elasticity (Biot, 1941; Geerstma, 1957). Studies suggest that no universal effective stress coefficient can be established for all rock properties, i.e. different values of α apply for different physical parameters, such as permeability, compressibility and shear modulus (Caroll and Katsube, 1983; Zimmerman, 1991; Berryman, 1992, 1995; Carcione and Tinivella, 2001).

Goulty (1998) showed that α is to be taken as unity when porosity is related to effective stress, for the Biot coefficient α appears in the expression relating the poroelastic dilatation of rocks (not the porosity) to change in mean effective stress. Zimmerman (1991) showed experimentally that for a mono-mineralic rock, the effective stress coefficient α is unity for porosity and dry elastic moduli, and equal to the Biot coefficient ($\alpha = 1 - K_0 / K_s$) for the bulk volumetric strain, where K_0 is the bulk modulus of solid matrix and K_s the bulk modulus of the solid grains, as predicted by Nur and Byerlee (1971).

In a recent study which expanded the arguments by Gardner et al. (1965), Zimmerman (1991) and Goulty (1998), Gurevich (2004) showed α to be taken as unity for a variety of rock properties of an idealized model of rock, with a margin error of 1 % effective stress. This is a theoretical approach supported by laboratory observations (Wyllie et al., 1958; Zimmerman, 1991), mostly in clean sandstones. Gurevich (2004) concludes that this is still an open subject, as the linear elasticity assumptions for the grain materials should be acceptable for quartz and calcite, but may not hold for clay minerals, some cements and bound water.

Shale and claystones are not single mineral constituent materials. Ebrom et al. (2004) concede that if the assumptions of reversibility during unloading are violated, our understanding of effective stress in mudstones and shales is not as advanced as the understanding already achieved in sandstones. Thus, since velocity prediction in mudstones and shales is part of the methodology of pore pressure prediction, they advocate more studies in quantifying P-wave and S-wave parameters in mudrock, shale and silty sand for the purpose.

2.6.3. Uniaxial strain model, borehole control and stability

2.6.3.1. The uniaxial strain model

In the uniaxial strain model, it is assumed that compaction is purely in the vertical direction with zero horizontal strain. As the model does not account for any tectonic stresses, it only applies when the basin is confined, and therefore unable to expand laterally when a vertical load is applied (Engelder, 1993). It follows that the horizontal stresses are isotropic and depend on the overburden through the Poisson's ratio. The coupling between stresses is given by the model equation

$$S_h = S_H = \left(\frac{\nu}{1-\nu}\right) S_v \qquad (2.4)$$

where ν is the Poisson's ratio of the overlying rocks.

In a poroelastic medium, relationship (2.4) applies for effective stresses, not the total stress. After observations on the effect of pore fluids on the frame of the rock, it is obvious that the difference in induced horizontal stresses depends also on whether the fluid (water/brine) can leak or drain out of the rock during burial. Clay, for instance has a low permeability so expulsion of pore fluid can be too slow to keep up with rapid burial. A material such as water or any fluid with no shear strength has a Poisson's ratio of 0.5. If a sandstone is allowed to drain (= drained sand), it has a Poisson's ratio of 0.25. In an elastic solid, the Poisson's ratio **ν** is a constant coupling elastic strains in any direction to the strains in the transverse directions.

2.6.3.2. Borehole stability and control in drilling operations

Effective stresses, $\sigma = S - P_p$, control rock failure within a well. During drilling operations, it follows from the removal of some rocks that biaxial horizontal stresses are concentrated around circular boreholes, as part of the redistribution of the previous stress prior to removal. If not controlled during mud pumping, this results in fracture and flaking off of borehole wall rock in a direction related to stress orientation. The borehole then becomes elliptic, with its long axis normal to the maximum horizontal stress. These are known as borehole failures (breakouts and hydraulic fracturing) and are reliable indicators of the orientation of maximum

horizontal stress, for they are related to horizontal stresses in the well (Zoback et al., 1985; Harper and Chambers, 2004).

The minimum horizontal component of the stress, S_h is known as the fracture pressure. It is commonly measured by a leak-off tests (LOT) after each run of casing has been set in a well (White et al., 2002).

2.7. Summary

The Central Graben and the East Shetlands basin are part of a proven hydrocarbon producing province, the Central North Sea. Its hydrocarbon plays range in age from Devonian to Early Eocene, with some of the plays in deep basins exhibiting high pressure and high temperature (HPHT). Overpressure in the region is believed to have been generated by disequilibrium compaction, unloading processes and chemical compaction. Although a great deal has already been achieved in understanding the regional stresses and overpressure distribution, further studies are still needed to account for all mechanisms contributing to the overpressure observed.

During drilling, pore pressures are estimated using methods based on compaction trends. Though compaction trends are major tools in pore pressure estimation in mudstones, regional compaction trend curves should be used with caution due to local variation in the relationship between porosity and vertical effective stress. These empirical curves are obtained from field data and tend to ignore overpressure due to other mechanisms such as unloading (see section 3.2., Chapter 3). The contributions of mechanisms other than disequilibrium compaction to the observed ovepressures are required to improve pressure prediction in HPHT fields.

Chapter 3
Fundamentals and general methodology

3. FUNDAMENTALS AND GENERAL METHODOLOGY

3.1. Introduction

In this chapter, the theoretical basis of the data analysis is set out. The choice of variables to be fitted is discussed, both in terms of geological information and significance (i.e. in line with the linear model assumptions). The other parameters used to translate the geological or physical system probed are also discussed.

Sources and types of data used in the analysis are described and the overall methodology used in the study is presented. The computational procedures, their justification and the work flow for the data analysis are presented. First, the basis of the methods used to estimate average bulk densities for shallow sediments, S_v and P_p are described; then their respective methods of computation are given. A note on data quality control concludes the chapter.

The analysis method is based on the assumption that the data fit a linear function and involves forward modelling using petrophysical data to account for overpressure due to unloading processes. It is applied to fine-grained sediments (chalk, claystone, shale), because these are very low permeability rocks in which pore pressures cannot be measured directly. The insufficiency of compaction disequilibrium as the sole cause of high pressure in North Sea sediments has been established and accepted (Kooi, 1997; Swarbrick et al., 2002). There has been a need for further understanding of other mechanisms that may be involved in generating the higher pressures observed (e.g. Norgård-Bolås et al., 2004). Interpretation of laboratory data on the variation of seismic velocity with external applied stress and pore pressure for sandstones attributed the decrease in seismic velocity with decreasing effective stress during unloading to the opening of microfractures (e.g. Gallager et al., 1974; Li et al., 2001). However, there is a lack of similar laboratory data from fine-grained rocks due to their low permeability, which makes it difficult to ensure that the pore pressure is uniform throughout the sample.

After Eberhart-Phillips et al. (1989) derived an empirical relationship between velocity and other variables in sandstones, Bowers (1994) used sonic velocity to assess overpressure mechanisms other than undercompaction in shales. Many authors have reported estimations of pore pressure in mudstones, but they are for just a single well or a few wells (e.g. Stump and Flemings, 1998; Harrold et al., 1999; Daniel, 2001). The present work considers a larger set of data (see Chapter 5 and 6), pursuing a regional approach for the Central North Sea. Pore pressure predictions using regional overpressure maps have been attempted; but so far results have not always been successful. This lack of success is attributed to varying pressure regimes across the region (Darby et al., 1996; Daniel, 2001). Work on overpressure and fluid drive may be on the verge of adding another explanation on overpressure distribution (Swarbrick, 2005).

3.2. Fundamentals of the model

3.2.1. Normal compaction and unloading in mudstones

Under the effect of increasing burial or mechanical loading, sediments change their properties from young unconsolidated sediments to lithified rocks in a process termed diagenesis, during which different physical and chemical mechanisms are involved. There are different approaches in studying the compaction behaviour and how it affects the properties of the sediments. In basin modelling, there are two fundamental relationships needed to model overpressure history: the functional relationships between porosity and effective stress and between permeability and porosity. Overpressure history in sedimentary basins has also been investigated and modelled using a pressure compartment methodology (Swarbrick, 1997; Borge, 2002).

During *normal* consolidation of sediments, increase in effective stress causes a decrease in porosity with an associated increase in seismic velocity. The reduction in porosity is mainly an irrecoverable elasto-plastic deformation, since most of the reduction in porosity is irreversible. If the sediment is then unloaded, by reducing the effective stress acting on it, there is only a small elastic increase in porosity, although the seismic velocity decreases substantially when the effective stress is reduced to

very low values. Thus, there is no unique relationship linking the seismic velocity to either effective stress or porosity. Nevertheless, many attempts have been made to predict overpressure using interval velocities from processing seismic reflection data, on the assumption that any overpressures present are exclusively due to undercompaction (i.e. sediment is normally consolidated). Overpressures caused by unloading mechanisms are ignored.

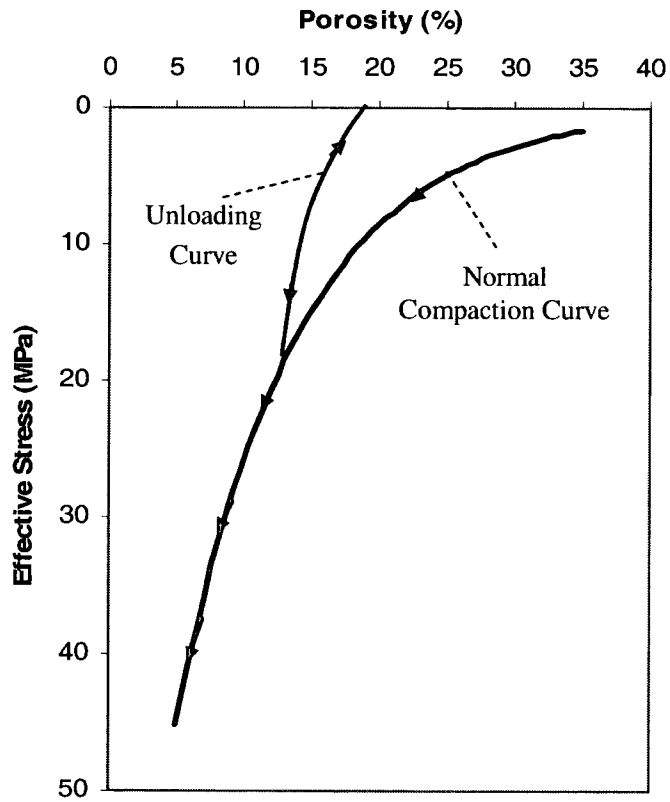

Figure 3.1. The relationship between effective stress and porosity (after Goulty, 1998; Harrold et al., 1999).

The relationship between mean effective stress and porosity (Figure 3.1) defines the compaction curve. It has a normal compaction path, which shows the inelastic process and an unloading path, portraying an elastic rebound in the velocity changes due to pressure or effective stress in accordance with the role of /dependence on burial history (Gardner et al., 1965; Goulty, 1998).

3.2.2. Approach: empirical relationship

Models are either theoretical or empirical. A theoretical model includes a set of general laws or theoretical principles. Commonly scientists resort to empirical models, which are correlations to fit field data and observations. However, such correlations generally entail some unknowns, so they are applicable only for particular

formations and environments (Gardner et al., 1974). Thus, these relations often have good response only for the data they are derived from. Empirical relations are generally some mathematical equation or expression obtained by fitting some measured observations for a particular data set, often guided by some theoretical insight. Depending on the character of the results obtained, the numerical/empirical model is classified as either deterministic or stochastic. The deterministic approach consists of generating a generic mathematical relationship from the data set based on a mechanical model (e.g. Ecclestone-Brown, 2002); while the stochastic approach considers statistical observations and probabilistic equations. This work takes a deterministic approach.

In his paper on pore pressure determination in deepwater, Traugott (1997) explained that existing pore pressure prediction models tend to fall into two categories: vertical and horizontal models. Vertical models are those for which the assumption is made that a given value of porosity determines effective stress uniquely. They are also referred to as explicit models (e.g. Alixant and Desbrandes, 1991; Rasmus and Stephens, 1991). Horizontal models, on the other hand, are those in which the effective stress is empirically related to the ratio of the measured parameter (e.g. velocity, resistivity) to the same expected value at the trend line at the same depth, for instance the Eaton relationship (Eaton, 1975). Traugott (1997) identified limitations to the two models: extrapolation of the compaction trend line to the depth of interest, assuming a straight or curved shape, for the horizontal methods; and the effects of formation temperature for the vertical ones. Temperature has been the key difference between the horizontal and vertical methods of pore pressure prediction. Thus in the analysis described here, depth has been used as a proxy for temperature in the velocity function.

Gardner et al. (1974) stated that many laboratory studies have shown that P-wave velocity in rocks is affected by pressure and fluid saturation. A change in rock lithology or composition, however, cannot be simulated very satisfactorily in the laboratory. In reality, many factors affect the seismic velocity in sediments, including lithology, grain size, porosity, pore shape, fluid type, fluid saturation, stress state, pore fluid and temperature. Some of these factors are interrelated. The scope of this investigation is limited to the main petrophysical parameters, which are believed to be

pertinent to understanding variations in velocity with overpressure. These are lithology (solid rock), porosity (rock matrix) and fluid within the pores.

3.3. The linear model assumption

3.3.1. Background

The aim is to investigate the relationships between compressional velocity, effective stress and porosity in fine-grained sediments (chalk and mudstones), with the main purpose being to determine whether unloading processes which reduce the effective stress could be detectable.

Compaction curves describe the rate of porosity loss during burial. The normal compaction curve is a continuous curve in either the porosity – vertical effective stress domain (as portrayed in Figure 3.1), or in the velocity – vertical effective stress domain. For normally compacted sediments, increase in vertical effective stress correlates with decrease in porosity, so the two variables would not be independent. However, when unloading takes place, the sediments undergo a poroelastic deformation shown as the unloading curve. In circumstances where unloading may have occurred, porosity and effective stress are independent variables.

Several compaction trends/curves have been established for the mudrocks of the North Sea (Sclater and Christie, 1980; Bulat and Stoker, 1987; Hillis, 1995; Japsen, 1998). Mallon and Swarbrick (2002) established a compaction trend in the chalk, using bulk density data. Compaction curves have been used to characterize sediments properties using sonic transit time (e.g. Issler, 1992; Hansen, 1996).

Sonic velocity and porosity are used as the primary variables in our analysis. Gamma ray count (from GR logs) is used as a simple way to account for the clay fraction and mineralogy (i.e. for lithology discrimination). In addition, resistivity is also used. The above conventional petrophysical parameters are often correlated with in situ rock strength, degree of fracturing, and the type of material occupying the pore space (Hatherly, 2001; Fullagar et al., 2004). Resistivity in particular is sensitive to many properties; among others are pore water salinity, temperature, tortuosity,

cementation factor and vertical effective stress (Wallace, 1965; MacGregor, 1965). Finally, depth is also used in the data analysis, as a proxy for temperature.

Eberhart-Phillips et al. (1989) fitted an empirical relationship between seismic velocity, effective pressure, porosity, and clay content from sandstone samples. In shales, it is possible to use measurements of velocity from sonic logs together with estimates of porosity from bulk density logs to arrive at an unambiguous estimate of pore pressure, as Bowers (2001) has proposed, assuming that the shale matrix and pore fluid do not form a chemically reactive system. Using the same approach, we assume a linear model of the general form

$$V_p = a_1 x_1 + a_2 x_2 + \ldots a_N x_N, \qquad (3.1)$$

where $x_1, x_2 \ldots x_N$ are the independent variables, and $a_1, a_2 \ldots a_N$ the coefficients.

In the course of this study, data or variables to be fitted are sonic velocity, porosity, vertical effective stress and a set of petrophysical data (resistivity, gamma ray count, depth as well). The basic linear relationship is the equation

$$V_p = V_0 + a\phi + b\sigma_v \qquad (3.2),$$

extendable with other linear terms, as applied in Chapters 5 and 6. Equation (3.2) is a simplification of the formula by Eberhart-Phillips et al. (1989) used for sandstone.

3.3.2. Bulk porosity instead of Wyllie's time average equation

A pressure analysis requires the use of rock properties, which are lithology, density, porosity, sonic velocity and resistivity. Lithology and porosity can be related empirically to velocity by the time-average equation (Wyllie et al., 1956). This equation is most reliable when the rock is under substantial pressure, is saturated with brine, and contains well-cemented grains. Wyllie's time average equation has proved inadequate for porosity estimation in carbonates and shales, with improvement being proposed and alternatives for shale porosity using transit time being developed over the years (e.g. Raymer et al., 1980; Raiga-Clemenceau, 1988; Issler, 1992; Hansen,

1996). For very low porosity rocks under large pressures, the mineral composition can be related to velocity by the theories of Voigt and Reuss. One effect of pressure variation on velocity results from the opening or closing of microcracks. Before the work of Gardner et al. (1974), existing theory did not take into account the effect of microcrack closure on the elastic behaviour of rocks under pressure or the chemical interaction between water and clay particles. In situ cracks close as the effective stress increases, and the influence of cracks lessens as a function of depth, which is one of the reasons velocity generally increases with depth. It is established that for porous sedimentary rocks, only the effective stresses (both horizontal and vertical) affect the microcrack system.

The analysis method uses the density log as a measure of bulk porosity for reasons related to the investigation. The study is interested in poroelastic deformation (unloading) within the rock. Any deformation within the rock translates into porosity and thus affects velocity because pore shapes and pore fluids influence the velocity. The rock's pore space consists of storage pores and connecting pores, with the former related to bulk properties and the latter controlling transport properties. In terms of deformations, connecting pores are more likely to undergo a poro-elastic deformation than storage pores (e.g. Bowers and Katsube, 2002). Thus velocity in a given rock sample is not solely dependent on its bulk porosity.

3.3.3. Porosity and effective stress

Some authors have included a clay term in empirical linear regression equations developed for V_p from their laboratory works on core analysis data (Tosaya and Nur, 1982; Castagna et al., 1985; Han et al., 1986; King et al., 1988; Eberhart-Phillips, 1989). The work in this thesis does not include an explicit clay content term, but gamma ray as a proxy, because it is focussed on compressional velocity, V_p , in mudrocks. It is thought that in sandstones shear velocity, V_s, is more sensitive both to porosity (Domenico, 1984) and clay (Minear, 1982) than compressional velocity, V_p. The effect is that clay tends to lower the shear modulus of the rock matrix; thus V_s decreases more than V_p. Some results suggest that dispersed clay has a negligible effect on velocity; in contrast laminated and structural shale has significant effect in reducing velocities (Minear, 1982).

In young sedimentary basins, the uppermost layers are unconsolidated. Wells in this environment will typically penetrate successive layers of sand and shale that may range in age from Holocene to Lower Eocene. For unconsolidated sediments at shallow depths, porosity varies mainly with the grain size distribution and clay content. The velocity is only slightly greater than that of sea water. However, with increasing depth the velocity increases partly because the effective stress increases and partly because cementation occurs at the grain-to-grain contacts. The increase of velocity with depth normally continues until the time-average velocity is approached. Below this depth, the layers behave like other well-consolidated rocks and the velocity depends mainly on porosity. In the shallower layers, the fluid content (i.e. water, oil or gas) has an appreciable effect on seismic velocity (Gardner et al., 1974).

The elastic moduli of the matrix (skeleton/frame) increase with increasing effective stress, and a corresponding increase in velocity is observed. The increase in the elastic moduli is attributable to the reactions at the intergranular contacts and the closure of microcracks as the effective stress increases. Hence when both overburden pressure and formation fluid pressure are varied, only the difference between the two (i.e., the vertical effective stress) has a significance on velocity. A set of data (Gardner et al., 1974) confirmed the assertion.

3.4. General procedures

A typical work flow for this study includes the following steps:

Data Collection:

- Data collection: raw data comprise composite logs, digitised log data, digital e-log data and direct measurements of pore pressure data.

Data picking or selection:

- Delineation of appropriate lithology beds (chalk, mudstones) in formations of interest (Chalk Group, Cromer Knoll, Heather).
- Reading of log values (gamma ray (GR), sonic, resistivity, depth).
- Data selection according to criteria defined.

Computation of petrophysical variables:

- Porosity, velocity.
- M parameter for mudstone.

Pore pressure, P_p, estimation:

- Pressure – depth profiles.
- Pore pressure calculation.

Overburden estimation:

- Determination of S_v.
- Estimation of vertical effective stress.

Data analysis:

- General inversion.
- Results interpretation.

Details on the selection criteria are presented in chapters 5 and 6. The final set of data needed for linear inversion is discussed in Section 4.4.3.

3.5. Lithology beds of interest and sources of data

3.5.1. Source and type of data

Data used throughout the study are wireline log data, in the form of composite and digital logs, and direct pressure measurements as RFT (Repeat Formation Tests) and FIT (Formation Integrity Tests). RFT and FIT data were read off the composite logs or extracted from GeoPOP (Geoscience Project into OverPressure) database using PressureView2.1 (Geopressure Technology, 2000). The suite of logs comprises of: caliper, natural gamma ray (GR), sonic transit time, formation density (mainly litho-density (RHOB) and formation density compensated (FDC) for few wells), neutron porosity (for some cases) and resistivity logs. The composite logs were drawn from the GeoPOP data banks. Digital log data were received from Total-Fina-Elf Exploration UK, Shell U.K. Exploration and Production and Chevron Texaco, UK. Data on the paper composite logs were digitized using the digitizing software Didger3 (Golden Software, 2001).

3.5.2. Non organic beds for data points

The fluid type in sediments significantly affects elastic properties of sediments, and gas in the pore space can be identified by a marked reduction of P-wave velocity and decrease of Poisson's ratio. A small amount of gas in sediments diminishes P-wave velocity significantly, whereas S-wave velocity is insensitive to the presence of gas (Domenico, 1976, 1977; Murphy, 1984; Lee, 2004). Thus, care has been taken to include only non-organic beds, i.e. only water-saturated beds were considered.

3.5.3. Chalk beds

Non reservoir Chalk has been considered in this study and referred to as clean chalk, as opposed to calcareous and marly chalk (see Section 5.3.1). Suitable beds were found in the Ekofisk, Hod, Tor, Hidra and Valhall Formations, i.e. both Palaeocene and Cretaceous.

3.5.4. Mudstone beds

Beds of mudstones considered are within the Lower Cretaceous and Jurassic sequences. Data points were picked only on claystone and shale beds. Marl and siltstone beds were avoided to be consistent with the lithology, as lithology is one of the important factors influencing rock velocity and density. This choice is determined by the fact that mudstones are complex mixture of fine-grained litholgical materials (Section 2.1.3, Chapter 2) and it is thought that the presence of non layered-clay components and the response of these components to increasing overburden and depth may be variable with noticeable effect on shale compaction curve (Korvin, 1984). Consequently, the Jurassic mudstone data points in this study are mainly from the Heather Formation. These are beds of claystones and shales of variable mineralogy. In places, these beds are described on the composite log as silty, calcareous, carbonaceous, glauconitic, pyritic, siliceous and anhydritic. The lithological classification in claystones and shales, for mudstone beds, and the mineralogical contents are read off the well log reports, as stated by the well site geologist. This may account as well as a source of uncertainty, though of very little impact on the results.

3.6. Calculating vertical stress in the wells

3.6.1. Formulae and methodology

The vertical or lithostatic stress, S_v, is due to the weight of overlying sediments and pore fluids. Thus, density log data have been integrated throughout the overburden to find S_v values at depths of interest. The mathematical relationship is

$$S_V = \int_{depth} \rho\, g\, dz = \sum_i \rho_i\, g\, \Delta z_i \qquad (3.3)$$

where ρ is the density of the overlying rocks, g is the acceleration of gravity and z the depth. For discrete data, the label "i" refers to the i^{th} reading on the log data (either digital or composite), and Δz_i to the depth interval accounting for the reading.

For well 22/30c-8, where digital density and sonic log data are not available, S_v was computed as:

$$S_v = (\text{depth SS} - \text{WD}) \times 0.02263 \text{ MPa/m} + \text{WD} \times 0.0098 \times 1.02 \text{ MPa/m} \quad (3.4)$$

where WD is the water depth, and depth values are in metres.

The choice of a lithostatic gradient of 0.02263 MPa/m (1 psi/ft) is dictated by trends in other wells, as will be shown below.

For computational purposes, and to reduce errors in the estimates of lithostatic stress, the overburden in the well down to the base of the Chalk Group is divided into sections as follows:

Section one: the weight of the sea water, with an average density taken as 1.02 g/cc. This section covers the water depth.

Section two: taken from the sea bed (mud line) to the top of the Tertiary. This section comprises the Quaternary glacial till.

Section three: taken from the top of the Tertiary to the top of the Chalk. As noticed within the wells under study, density logs are run above the top of the Chalk in the Danian. Thus, the section comprises Tertiary glacial till (always unlogged), shallow unlogged sediments (i.e. down to the first reliable density reading) and logged sediments. Depending on the log trend, the latter is also subdivided into two or three sub-intervals depending on the log trend responses.

Section four: from the top to the base of the Chalk Group. This section runs through the Chalk Group lithology. We distinguish between clean chalk and other type of chalk. Accordingly, the section is divided into intervals of clean chalk, herein labelled *Chalk Interval*, and other. It follows that the interval thickness of each interval of the Chalk is determined from the trend of the gamma ray (GR) log. However, where a clean chalk interval is thicker than 30.5 m (100 ft), it is divided into sub-intervals of 30.5 m each.

Given that the Tertiary above the Chalk Group comprises different formations, section three of the overburden was divided into intervals accounting for different lithology types within it, where composite logs provide lithology comments.

For each well, a table showing the calculation of the lithostatic stress was compiled. An example is shown as Table 3.4. It gives the top and bottom depths of each interval, its thickness or the thickness of sub-intervals, the corresponding average densities and interval sediments weights, and the cumulative overburden stress. Linear interpolation is used to find the S_v value for a data point within an interval.

Averages densities are converted to pressure gradient using the factor

$$1 \text{ g/cc} \equiv 0.0098 \text{ MPa/m} = 9.8 \text{ MPa/km} \qquad (3.5)$$

to find the weight or pressure exerted by sea water and underlying sediment layers. The lithostatic stress at any depth is the summation of all the pressures exerted by different intervals above that depth (Equation (3.3)). Appendix A contains tables and values of the lithostatic stress estimated for all wells in the study, and Section 3.6.3 below contains an example of a case study of lithostatic stress estimations.

3.6.2. Shallow sediments average density

At shallow depths, density logs are not usually run or give unreliable values; therefore for the Quaternary and the Tertiary above the first reliable ρ_{log} readings, average bulk densities were estimated from the density data that were available in each area. Average densities for the whole Tertiary and Quaternary interval in Quadrant 3 were estimated from the wells listed in Table 3.1. For Quadrants 21, 22 and 30 in the Central Graben, average density values for the Tertiary and Quaternary strata are calculated using average rock properties for the CNS. These average densities are obtained using the equation

$$\rho_b = (1 - \phi)\, \rho_{\text{sediment}} + \phi\, \rho_{\text{fluid}} , \qquad (3.6)$$

assuming a sediment grain density of 2.800 g/cc and average porosities of 43% and 30% for the Tertiary and glacial Quaternary claystones, respectively (Ecclestone-

Brown, 2002), as shown in Table 3.2. The shallow sediments average densities found are given in Table 3.3.

Well	Coordinates		Depth of first reading of bulk density
	Latitude	Longitude	
211/29 - 1	61° 05′ 54.301″ N	01° 41′ 28.636″ E	476 m SS
211/29 - 2	61° 03′ 12″ N	01° 42′ 27″ E	495 m SS
3/3 - 11	60° 57′ 46.15″ N	01° 32′ 26.19″ E	1299 m SS
3/15a - 5	60° 35′ 29.29″ N	01° 49′ 06.24″ E	637 m SS

Table 3.1. Wells used for average density values above the Cretaceous in Q 3.

	Grain density	Fluid density	ϕ	ρ_b	Gradient
Quaternary sediments	2.8 g/cc	1.02 g/cc	0.30	2.26 g/cc	22.15 Pa/m
Tertiary sediments	2.8 g/cc	1.02 g/cc	0.43	2.04 g/cc	19.99 Pa/m
Error estimation (one standard deviation)			±0.03	±0.05	

Values obtained by analysing petrophysical samples and data using generic methods (Ecclestone-Brown, 2002).

Table 3.2. Rock properties assumed where density logs were not available in Q21, 22 &30.

	Quaternary Glacial Till	Tertiary sediments		
		Above Palaeocene	In Palaeocene	Cretaceous
Quadrant 3: Alwyn & Ninian fields	2.15 g/cc			Q3/3: 2.461 g/cc
				Q3/9: 2.454 g/cc
				Q3/14: 2.473 g/cc
				Q3/1: 2.474 g/cc
Quadrants 21, 22 & 0: Central Graben	2.26 g/cc	2.04 g/cc	Data available	Data available

Conversion factors: 1 g/cc ≡ 0.0098 MPa/m 1 m = 3.281 ft

Table 3.3. Estimated average values of density used where density logs were not run in the wells used for this study.

3.6.3. Example: case of well 22/29 – 1S1

Three data points were selected for the study within this well. They are at depths 3308 m SS, 3339 m SS and 4336 m SS and are labelled, respectively, as data points 3, 4 and 5 (see Chapter 5).

Calculating S_v for data point 3: at 3308 m SS (3330.9 m BRT)

(a) Layer interval containing the data point:

Chalk interval: 3296.8 to 3316.9 m SS.

(b) Vertical stress acting upon the interval, due to overlying sediments:

Sv1 = 70.94 MPa at 3296.8 m depth.

(c) Vertical stress (weight of sediments) within the interval:

Sv2 = (3308 – 3296.8) x 2.464 x 0.0098 = 0.270 MPa

(d) S_v at ***3308 m SS:***

S_v = Sv1 + Sv2 = 70.94 + 0.270 = **71.2 MPa**

Calculating S_v for data point 4: at 3339 m SS (3351.9 m BRT)

(a) Layer interval containing the data point:

Chalk interval I, 3316.9 to 3346.5 m SS.

(b) Vertical stress acting upon the interval, due to overlying sediments:

Sv1 = 71.44 MPa at 3316.9 m depth.

(c) Vertical stress (weight of sediments) within the interval:

Sv2 = (3339 – 3316.9) x 2.612 x 0.0098 = 0.310 MPa

(d) S_v at ***3339 m SS:***

S_v = Sv1 + Sv2 = 71.44 + 0.310 = **71.8 MPa**

Well 22/29 - 1S1: lithostatic stress values

Bulk density readings
1st value : 2.290 g/cc @ 2666.9 m BRT
Last value: 2.551 g/cc @ 4726.7 m BRT

	Measured Depth		TVDSS		Thickness	ρ average	Vertical stress due to interval	Lithostatic stress *Sv*
	Top	Bottom	Top	Bottom	m	g/cc	MPa	(MPa)
	m BRT	m BRT	m SS	m SS				
RTE	22.9		Air gap			//////////		
Water depth	**22.9**	**118.0**	**0.0**	**95.1**	**95.1**	**1.02**	**0.95**	
Sea Bed- Tertiary Top (Glacial Till)	118.0	1755.6	95.1	1732.7	1637.6	2.26	36.27	
Tertiary Top - first RHOB reading	1755.6	2666.9	1732.7	2644.0	911.3	2.04	18.22	
Other Sediments	2666.9	3319.7	2644.0	3296.8	652.8	2.423	15.5	70.94
	3319.7	3339.8	3296.8	3316.9	20.1	2.464	0.49	71.44
	3339.8	3369.4	3316.9	3346.5	29.6	2.612	0.76	72.19
	3369.4	3390.7	3346.5	3367.8	21.3	2.595	0.54	72.73
	3390.7	3412.1	3367.8	3389.2	21.3	2.645	0.55	73.28
	3412.1	3479.4	3389.2	3456.5	67.4	2.617	1.73	75.01
	3479.4	3504.1	3456.5	3481.2	24.7	2.618	0.63	75.64
CHALK GROUP	3504.1	3580.3	3481.2	3557.4	76.2	2.633	1.97	77.61
	3580.3	3717.5	3557.4	3694.6	137.2	2.64	3.55	81.16
	3717.5	3880.5	3694.6	3857.6	163.1	2.68	4.28	85.44
	3880.5	3925.6	3857.6	3902.7	45.1	2.653	1.17	86.61
	3925.6	4024.1	3902.7	4001.2	98.4	2.639	2.55	89.16
	4024.1	4084.1	4001.2	4061.2	60	2.633	1.55	90.71
	4084.1	4128.9	4061.2	4106.0	44.8	2.624	1.15	91.86
	4128.9	4327.9	4106.0	4305.0	199	2.631	5.13	96.99
	4327.9	4367.0	4305.0	4344.1	39	2.589	0.99	97.98
	4367.0	4389.2	4344.1	4366.3	22.2	2.655	0.58	98.56
	4389.2	4431.6	4366.3	4408.7	42.4	2.648	1.1	99.66

Comments: Sea water density = 1.02 g/cc; 1 psi/ft ≡ 2.31 g/cc; 1 g/cc ≡ 0.0098 MPa/m
ρ_{av} are the averages of RHOB digital logs throughout the interval considered; S_v at the interval is the combined weight of the sea water and overlying sediments taken at the bottom of the interval.

Table 3.4. Lithostatic stress values for well 22/29 – 1S1.

Calculating S_v for data point 5: at 4336 m SS (4358.9 m BRT)

(a) Layer interval containing the data point:

Chalk interval II, 4305 to 4344.1 m SS.

(b) Vertical stress acting upon the interval, due to overlying sediments:

Sv1 = 96.99 MPa at 4305 m depth.

(c) Vertical stress (weight of sediments) within the interval:

Sv2 = (4336 – 4305) x 2.589 x 0.0098 = 0.787 MPa

(d) S_v at ***4336 m SS***:

S_v = Sv1 + Sv2 = 96.99 + 0.787 = **97.8 MPa**

3.7. Pore pressure and vertical effective stress

For each well, relevant direct pressure measurements are reported in the form of a table and a pressure-depth plot. Pressure measurements are mostly made in zones of interest, such as reservoir sandstones, and are very scarce in the Chalk of the Central North Sea. Thus, P_p values used in the study were mostly estimated from data available either in the Palaeocene for the top of Chalk, or in the Jurassic for both the mudstone and the base of Chalk data points. Just two direct pressure values were available within the Chalk.

As a general approach, estimation of P_p values for the data points are made from RFT measurements in the Jurassic and the Palaeocene, using extrapolation or interpolation. For a data point picked within a formation with direct pressure measurements (RFTs) available, interpolation is used based on the well pressure gradient of the formation, while the regional pressure trends (GeoPOP, 2000) are used for extrapolation from the well water leg, as described in the Appendix A. Available pressure measurements and production data (e.g. Drill Stem Test) are used for hydrocarbon water contact determination. Due to pressure regime differences within each of the formations under study, a note on pore pressure estimation for the data

points is given in relevant chapters (5 and 6). Details of pressure estimation within each well are given in Appendix A.

Values of the pore pressure are then used to compute the vertical effective stress. Vertical effective stress values, σ_v, are obtained from the vertical or lithostatic stress and the pore fluid pressure, using Terzaghi's relationship (Equation 2.2, Chapter 2).

3.8. Problem solving and sources of error

The sources of error in the data are diverse. The main ones are those related to the uncertainties in the wireline log readings and the extrapolated estimates of pore pressure, as few direct pore pressure measurements are available in the Chalk and the Lower Cretaceous mudstones. Though few data related to the accuracy of wireline tools readings exist in the public domain, tools are more reliable and accurate nowadays as uncertainties are reduced with new tools being developed and in use on the stream. But it is admitted that interpretation of data sets from formation evaluation can still lead to uncertainties (Woodside et al., 1998; Rourke, 2004).

The delineation of suitable lithology beds for data picking is subject to errors. Contrary to the reliable delineation of clean chalk horizons which is based on lithology log readings ($\gamma < 15$ °API) (see Section 5.3.1), the delineation for mudstone beds and their mineralogical content is bound to well site geologist observation errors, thus compounding in the data analysis. The determination of the lithostatic stress S_v is subject to error in the estimated depth of the Tertiary – Quaternary interface at the wells and to error in the estimated densities of the shallow sediments, which is ± 0.05 g/cc (Table 3.2). In the case of porosity, each bulk density value is read with an error of ± 0.005 g/cc. Thus, assuming that the densities of sea water and the matrix are constant values, error on the bulk porosity is ±0.003. Sonic velocities will be associated with a maximum error of ± 16 m/s, given a picking error in transit time readings of ± 0.5 μs/ft and taking the highest sonic velocity in Chalk of 5628 m/s (Chapter 5, Table 5.2).

Each data point contributes one equation to the system of equations in the form of equation (3.1) or equation (3.2), which defines an over-determined linear inverse problem. Various methods are available in solving this type of mathematical problem. A suitable numerical method is the general inversion method. In Chapter 4, we discuss and develop a set of Visual Basic programs in Excel ("Macro") to be used for the resolution and analysis of the problem.

3.9. Summary

With the wireline log data available, an empirical relationship is to be investigated to account for overpressure due to unloading in chalk and mudstones (see Chapters 5 and 6, respectively). The associated petrophysical data and variables are sonic velocity, bulk porosity, gamma ray count, resistivity and depth. The latter are independent variables to be fitted in a linear equation with the compressional velocity V_p, as a dependent variable. Average densities for the shallow sediments are needed for the calculation of the lithostatic stress, in the absence of log readings from the mud line down to mid-Eocene. These average densities values have been calculated and provided.

Chapter 4

Inversion method and programming

4. INVERSION METHOD AND PROGRAMMING

4.1. Introduction

The linear assumption for data fitting, introduced in Chapter 3, results in an over-determined system of linear equations, which can be solved using linear inversion. Linear analysis of geosciences data is widely used for the reasons that, although the model itself is a linear expression, the parameters or variables involved may be expressed in various forms such as squares, square roots, and logarithms, or otherwise transformed to translate the mathematical/statistical results into geophysical and geological inference of cause and effect (Krumbein and Graybill, 1965). This chapter presents the mathematical background used and sets the computational framework.

During the course of the present work, tremendous progress has been seen in numerical computation software for personal computers, with the latest packages offering map digitisation and linear inversion on a mouse click (see Section 4.3.1). However, the knowledge and mastering of the computation basics is relevant to interpreters interested in new models, for this provides understanding of the model, a control of the data (subroutines reducing input errors) and an impact in fine-tuning the visualisation of results outputs. Thus, for our data analysis a computer program, named "inversion", has been written, using Excel's Macro language (Visual Basic). In addition, some other Macro modules and spreadsheets have been developed for data selection, calculation and estimation of variables.

In this chapter, the mathematical linear model is stated. Then the algorithm and some related statistical parameters are given. Finally, the computer program is outlined.

4.2. Mathematical linear model

Suppose we have a large number of data points giving the value of Y as a function of $X_1, X_2, X_3 \ldots X_N$ ($N > 2$). Y could be considered as the dependent variable, being a function of the independent variables $X_1, X_2, X_3 \ldots X_N$, and can be written as a linear function of the form

$$Y = Y(X_1, X_2, X_3 \ldots X_N) \qquad (4.\ 1a)$$

Let us consider a single data point ($x_1, x_2, \ldots, x_N, y$), with y a value of the dependent variable Y and $x_1, x_2, \ldots, x_N$ values of respective variables $X_1, X_2, X_3 \ldots X_N$. In terms of the linear assumption, we could fit the values into an expression of the form

$$y = a_0 + a_1 x_1 + a_2 x_2 + \ldots + a_N x_N \qquad (4.1b).$$

This is a linear equation with coefficients $a_0, a_1, a_2, \ldots, a_N$.

For a set of n values of variable Y, i.e. n data points, Equation (4.1) could be written as a system of n equations:

$$\begin{aligned} y_1 &= a_0 + a_1 x_{11} + \ldots + a_N x_{1N} \\ y_2 &= a_0 + a_1 x_{21} + \ldots + a_N x_{2N} \\ &\ldots\ldots\ldots\ldots \\ y_n &= a_0 + a_1 x_{n1} + \ldots + a_N x_{nN} \end{aligned} \qquad (4.\ 2)$$

$a_0, a_1, \ldots a_N$ are real numbers and are the unknowns or parameters to be determined.

The system of equations (4.2) can be re-written in matrix form as:

$$\begin{pmatrix} y_1 \\ y_2 \\ \ldots \\ y_n \end{pmatrix} = \begin{pmatrix} 1 & x_{11} & \ldots & x_{1N} \\ 1 & x_{21} & \ldots & x_{2N} \\ \ldots & \ldots & \ldots & \ldots \\ 1 & x_{n1} & \ldots & x_{nN} \end{pmatrix} \begin{pmatrix} a_0 \\ a_1 \\ \ldots \\ a_N \end{pmatrix} \qquad (4.3a)$$

This could be solved using matrix algebra when written in the form of

$$\mathbf{Y} = \mathbf{B}\,\mathbf{Z} \qquad (4.3b)$$

with $\mathbf{B}$ being the (n x (N + 1)) matrix, and $\mathbf{Y}$ and $\mathbf{Z}$ being column vectors.

Numerically, **Y** is a vector of observed values of the dependent variable to be expressed in terms of other variables, **B** is the matrix of the values of the independent variables and **Z** is the vector of the unknown coefficients.

The above is a system of n equations, with $N + 1$ unknowns. Provided that $n > N + 1$, and that $N + 1$ equations are linearly independent, this is known as an over-determined linear inverse problem. A suitable numerical method of resolution is the general inversion method (see Section 4.3).

In the course of this study, the data or variables to be fitted are velocity, porosity, vertical effective stress, resistivity, gamma ray count and depth in various combinations with velocity as the dependent variable (Chapters 5 – 6).

4.3. Linear inversion for the over-determined case

4.3.1. Introduction

The general inversion method is a numerical method capable of solving mathematical problems with many variables of type (4.3), when variables are linearly independent. It is based on matrix algebra. Depending on the relationship between n - the number of equations and m - the number of unknowns, we have: an over-determined case for $n > m$, an under-determined case for $n < m$, and the straight-case for $n = m$.

Using matrix algebra, the over-determined system (4.3) can be solved as follows:

- Since matrix **B** is not a square matrix, its inverse $\mathbf{B}^{-1}$ cannot be found.
- Pre-multiplying **B** by its transpose, $\mathbf{B}^T$, gives a square matrix, $\mathbf{B}^T\mathbf{B}$. If $\mathbf{B}^T\mathbf{B}$ is a non-singular matrix, it has an inverse, $(\mathbf{B}^T\mathbf{B})^{-1}$.

Utilising the rules of matrix multiplication, the set of unknown coefficients in $\mathbf{Y} = \mathbf{B}\ \mathbf{Z}$ is found as

$$\mathbf{Z} = (\mathbf{B}^T\mathbf{B})^{-1}\mathbf{B}^T\mathbf{Y} \qquad (4.4)$$

The standard error for the inversion, also known as the root mean square (RMS) error for the data fitting, is calculated as:

$$\Delta Y = \sqrt{\frac{\sum_{i=1}^{n} (\Delta y_i)^2}{n-m}}, \qquad (4.5)$$

where Δy_i is the difference between the predicted value and the observed value of y_i. m is the dimension of the model or number of variables and n is the number of data points fitted.

In statistical terms, the inversion method to be used here is the multi-variable linear regression. The latest releases of graphic software and other statistical software, e.g. Minitab14 (Minitab Inc., 2003) and SigmaPlot9 (Systat Software Inc., 2004), have got functionality to perform multi-variable linear regression. The discrepancies in (4.5) correspond to the residuals, while the RMS error is the standard error in the regression statistics. The coefficients or unknowns in (4.2) are the parameter estimates of the statistical package.

4.3.2. Coefficient of determination, R^2

The coefficient of determination (or multiple correlation coefficient), R^2, is the measure of the correlation between dependent and independent variables. It is a statistic that is used to determine how well a regression fits the variables. It represents the fraction of variability in y that can be explained by the variability in x. In other words, R^2 explains how much of the variability in the y's can be explained by the fact that they are related to x.

$$R^2 = \frac{\sum_{i=1}^{n} y_i^2 - \sum_{i=1}^{n} (\Delta y_i)^2}{\sum_{i=1}^{n} y_i^2} \qquad (4.6)$$

In the case of simple linear regression, R^2 is simply the square of the correlation coefficient.

However, it is not appropriate to interpret correlation coefficients without consideration of the mechanical or physical problem. That two variables are highly correlated does not mean that one causes the other. In statistical terms, we say that correlation does not imply causation. There are many good examples of correlation which are nonsensical when interpreted in terms of causation. Henceforth, in addition to the geological and geophysical aspects to be taken into account in the course of interpretation, the significance of different variables within the linear fit is assessed.

4.3.3. Independence and significance of variables

Since petrophysical parameters are used, the assumption that these parameters are truly independent variables for the linear regression model is very difficult to satisfy, for they are part of a geological closed system. However, the correct approach is to assess whether these parameters are sufficiently independent not to invalidate results of the regression analysis (Mann, 1987). A variable may affect the response, i.e. improve the correlation and reduce the RMS error, and yet not be one of the explanatory variables. On the other hand, the input variables may be as correlated with each other as they are with the response; which means the presence of one input variable in the model may mask the effect of another input. This is one common problem in multiple regression analysis known as multicollinearity of the input variables. Thus, any outcome of the linear fitting has been assessed to make geological sense.

In addition, when the assumption of the linear model is satisfied, it is a convenient simplification to discard insignificant terms in the model, i.e. variables that do not have important explanatory effect on the response. Confidence limits and P-values serve this purpose. P-values, also known as the probability value on the hypothesis test, is the significance probability associated to the variable (see Chapter 6, Table 6.3 – 6.7).

4.4. Computation: macro module "inversion"

4.4.1. Introduction

The "inversion program" is a program designed to solve a system of equations or to fit sets of data in a linear equation for up to five linear independent variables, i.e. a system of the form (4.3) of N equations and 5 unknowns, with N up to 65000 – the maximum possible number of rows in an Excel spreadsheet. It is a Windows based program using Excel spreadsheets and the programming language is Visual Basic, i.e. the macro version of Microsoft Excel 2000.

4.4.2. Flowchart/subroutines

Start/initialise	Call initialise6D
Data input	Call takedata6D
Rearranging data/matrix	Call multiplyB tB bis6D
Matrices multiplication	Call Reduce4Gauss6D
Gauss elimination	Call GaussB tB 6D
Parameters computation	Call Parameters6D
Output	Call Finalresults
End	Sheets("sheet3").Activate
	End Sub

4.4.3. Inputting data

The program offers two options: manual input (i.e. using keyboard) and spreadsheet import for large data set. The latter is recommended to minimize error due to data recording. A spreadsheet labelled exclusively "Data" should be provided for the purpose, as the program selects it first as its launches. Blank data cells are not allowed in between the input data.

The data entry format in the input spreadsheet is of an *augmented matrix* of **B** with the column vector **Y** of equation (4.3). The only input data required are the label of the variables and observed data points (x_1, x_2, ...,x_N, y), i.e. values of independent variables X_i, i= 1,...5 or less, and those of the dependent variable Y.

Given n the number of equations or data points, and N the number of independent variables, thus the number coefficients to be determined is $m = N + 1$.

The matrix **B** is of the dimension (n x m). On the "Data" worksheet, the total number of rows and number of columns entered are then (n + 1) and (m+ 1), respectively. In a particular order: the 1st row has the labels of the variables, the 1st column is the column *unity* of **B**, i.e. values $b_{i\,1} = 1$ for any $i = 1, \ldots, n$; and the $(m + 1)^{th}$ column is that of the observable values, column vector **Y**.

SI units are used throughout and the independent variables involved are: porosity and vertical effective stress for the Chalk study (Chapter 5), with in addition gamma-ray count, resistivity, and depth for the mudstone study (Chapter 6). The dependent variable is sonic velocity; V_p. Table 4.1 is an example of "Data" spreadsheet.

The program requires three additional worksheets, which are created as the program is launched.

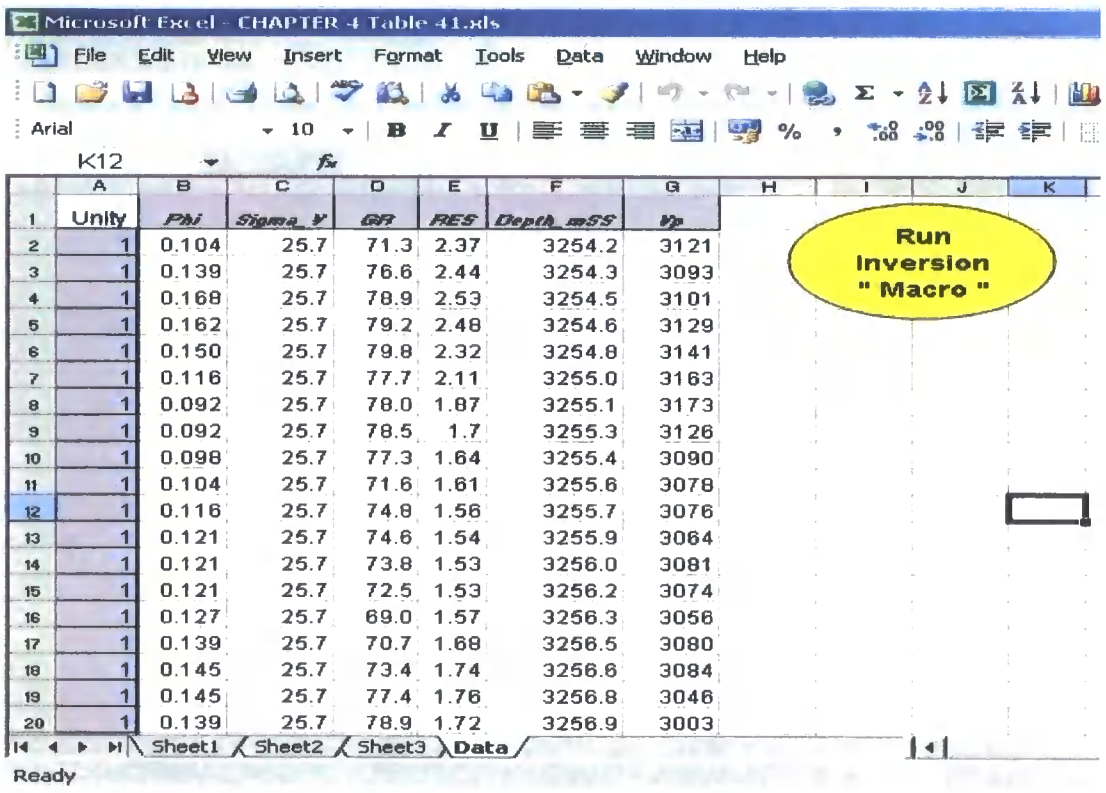

	A	B	C	D	E	F	G
1	Unity	Phi	Sigma_v	GR	RES	Depth_mSS	Vp
2	1	0.104	25.7	71.3	2.37	3254.2	3121
3	1	0.139	25.7	76.6	2.44	3254.3	3093
4	1	0.168	25.7	78.9	2.53	3254.5	3101
5	1	0.162	25.7	79.2	2.48	3254.6	3129
6	1	0.150	25.7	79.8	2.32	3254.8	3141
7	1	0.116	25.7	77.7	2.11	3255.0	3163
8	1	0.092	25.7	78.0	1.87	3255.1	3173
9	1	0.092	25.7	78.5	1.7	3255.3	3126
10	1	0.098	25.7	77.3	1.64	3255.4	3090
11	1	0.104	25.7	71.6	1.61	3255.6	3078
12	1	0.116	25.7	74.8	1.56	3255.7	3076
13	1	0.121	25.7	74.6	1.54	3255.9	3064
14	1	0.121	25.7	73.8	1.53	3256.0	3081
15	1	0.121	25.7	72.5	1.53	3256.2	3074
16	1	0.127	25.7	69.0	1.57	3256.3	3056
17	1	0.139	25.7	70.7	1.68	3256.5	3080
18	1	0.145	25.7	73.4	1.74	3256.6	3084
19	1	0.145	25.7	77.4	1.76	3256.8	3046
20	1	0.139	25.7	78.9	1.72	3256.9	3003

Table 4.1. Format for data input in "inversion program".

Note: Values of the dependent variable are inputs of the last column. It follows that the input order for the independent variables columns is not important.

4.4.4. Output

The output from the program comprises the coefficients of the independent variables in the corresponding linear equation, the predicted values of the dependent variable, i.e. velocity, the residuals and the value of the RMS error (Table 4.2).

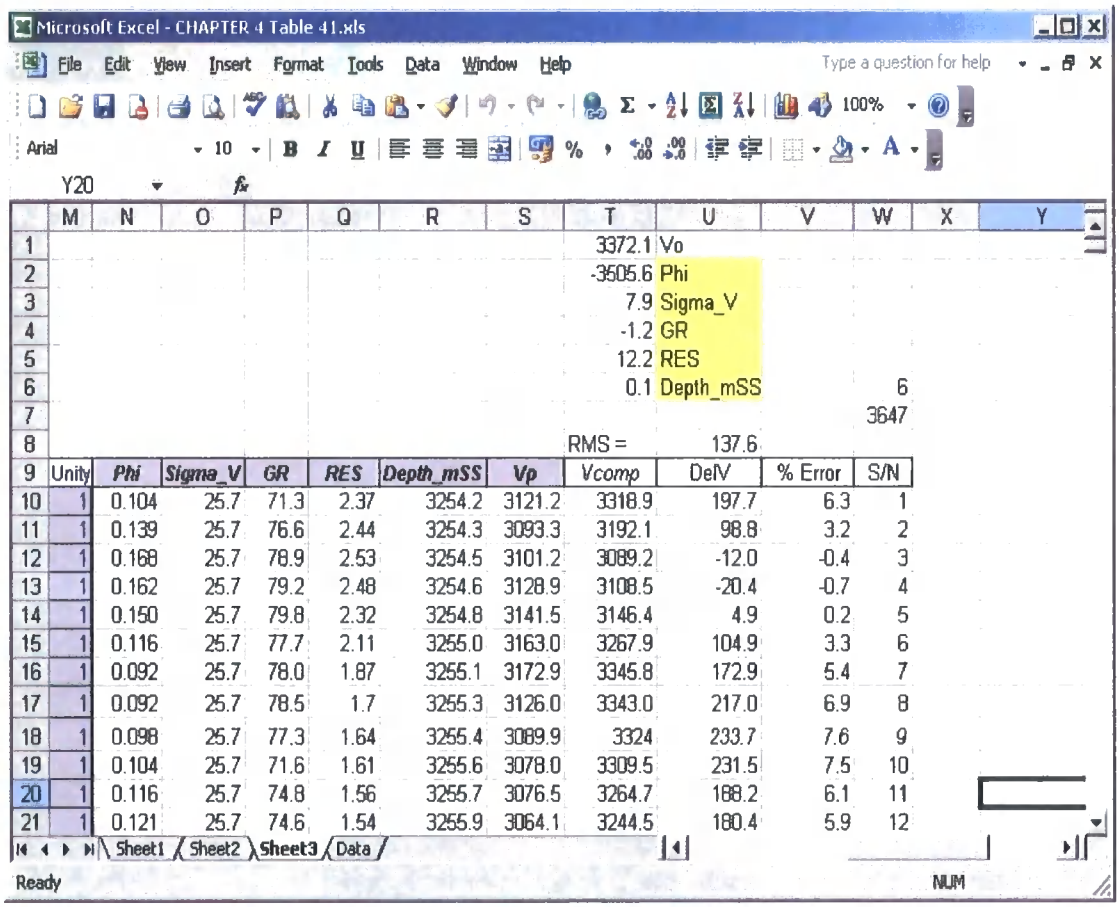

Unity	Phi	Sigma_V	GR	RES	Depth_mSS	Vp	Vcomp	DelV	% Error	S/N
1	0.104	25.7	71.3	2.37	3254.2	3121.2	3318.9	197.7	6.3	1
1	0.139	25.7	76.6	2.44	3254.3	3093.3	3192.1	98.8	3.2	2
1	0.168	25.7	78.9	2.53	3254.5	3101.2	3089.2	-12.0	-0.4	3
1	0.162	25.7	79.2	2.48	3254.6	3128.9	3108.5	-20.4	-0.7	4
1	0.150	25.7	79.8	2.32	3254.8	3141.5	3146.4	4.9	0.2	5
1	0.116	25.7	77.7	2.11	3255.0	3163.0	3267.9	104.9	3.3	6
1	0.092	25.7	78.0	1.87	3255.1	3172.9	3345.8	172.9	5.4	7
1	0.092	25.7	78.5	1.7	3255.3	3126.0	3343.0	217.0	6.9	8
1	0.098	25.7	77.3	1.64	3255.4	3089.9	3324	233.7	7.6	9
1	0.104	25.7	71.6	1.61	3255.6	3078.0	3309.5	231.5	7.5	10
1	0.116	25.7	74.8	1.56	3255.7	3076.5	3264.7	188.2	6.1	11
1	0.121	25.7	74.6	1.54	3255.9	3064.1	3244.5	180.4	5.9	12

Table 4.2. Output format of the "inversion program" results.

4.4.5. Information on data used

Table 4.3 is a summary of the data used in the "inversion program", the corresponding properties, the source of each data type and associated symbols for the study. These properties have been discussed in Chapter 3, and further details on their calculation are given in chapters 5 – 6.

Input Data		Derived from	Source data
Phi	Porosity (ϕ)	Bulk density	RHOB & FDC logs
Sigma_v	Vertical effective stress (σ_v)	Pore pressure (P_p) and lithostatic stress (S_v)	RFT & FIT and RHOB & FDC log
GR	Gamma ray count (γ)	-	Gamma ray log
Res	Resistivity (R)	-	Deep resistivity logs
Depth	Depth subsea (z)	Depth BRT and Well parameters	Wireline log reports (header and data)
Vp	Compressional or sonic velocity (V_p)	Transit time (Δt)	Sonic log

Table 4.3. Summary of sources and references on input values.

Besides the main macro module "inversion", other macros were developed for data selection (Section 6.4.1) and for S_v calculation for large set of data. Details are reported in Appendix B.

4.5. Summary

I have written and provided the computational tools/means used for data analysis, these are the "inversion program" and two other macros for data selection and variable values calculations. Though multivariate analysis software - e.g. Minitab 14 (Minitab Inc., 2003) - became available recently (close to mid-term of this study), it has been a useful experience to write the programs and the macros. Furthermore, the subroutines written to edit the data to minimise "measurement errors" (i.e. setting range of data, recognizing spurious data such as negative entries or -999 as encountered in e-logs) were directly useful. Moreover, results/outputs of the inversion using my own "inversion program" have been consistently identical with the outputs from the commercial software. This has guaranteed confidence in the geological sense of the study results. "*What could be cuter to feed a computer with wrong information but naïve expectation to obtain with precision a Napoleonic decision.* Major Alexander P. de Seversky"; quote cited in Statistics and Data Analysis in Geology (Davis, 2002).

Chapter 5
Variation of velocity with effective stress in Chalk

5.1. Introduction

5.2. Geological setting and overpressure status

5.3. Analysis method and data

5.4. Data inversion and results

5.5. Interpretation and significance of the results

5.6. Discussion and conclusions

5.7. Appendix: plots of observed and forward – calculated velocities

5. VARIATION OF VELOCITY WITH EFFECTIVE STRESS IN CHALK

5.1. Introduction

5.1.1. The Chalk in the Central North Sea

The Chalk Group of the North Sea provides the reservoir in the giant Ekofisk field, which started production in the mid-1970s. The discovery of this field was a major turning point in the exploration for petroleum in Western Europe, as it set the pace for intensive search for oil in the North Sea (Van der Bark and Thomas, 1981). The reservoir is made of Late Cretaceous and Palaeocene chalk which is the reservoir for a major complex of hydrocarbon accumulations in the Greater Ekofisk area (Norwegian Sector), as well as smaller accumulations in the Danish and British sectors of the North Sea.

The Chalk reservoir has unusually high primary porosities. The preservation of high porosity and permeability at such great burial depth is believed to be associated with overpressuring of the reservoir in combination with resedimentation and hydrocarbon saturation (Kennedy, 1987).

In this chapter, wireline log data and pore pressure measurements from eight wells are analysed to investigate how velocity in chalk of the Chalk Group of the Central Graben in the North Sea depends on vertical effective stress when porosity and vertical effective stress are treated as independent variables. The aim is to determine whether the data exhibit a reduction in velocity due to any unloading which had taken place and, if so, to establish an empirical relationship to predict pore pressure in the Chalk in this region. Results herein of this investigation have been published (Lubanzadio et al., 2002).

An overview of the related work, the local geology and the overpressure status in the chalk fields is given as Section 5.2. This is followed by the analysis method and

data set used, with details on pore pressure estimation (Section 5.3). The results of the data analysis are given in Section 5.4 and the interpretation in Section 5.5. Section 5.6 comprises some discussion and the conclusions of the investigation. Despite the high overpressures observed in some of the wells, the results show no significant reduction in velocity on unloading. Section 5.7 contains various plots of the observed data and forward-calculated velocities.

5.1.2. Related work in the area

Most of the previous work on North Sea Chalk related to this study has focused on compaction trends averaged over widely scattered data values, and much of it has used data from single hydrocarbon-bearing reservoirs or restricted geographical areas. Reservoir quality chalk, typically associated with allochthonous units, only accounts for a small fraction of the succession, and early entry of hydrocarbons has helped to maintain porosity in the reservoirs by retarding cementation (Scholle, 1977). However, the Chalk Group acts as a seal to hydrocarbons in a number of Central North Sea fields, including Fulmar and Judy, and acts as a pressure barrier to formation fluids in the underlying high pressure reservoirs.

Japsen (1998) undertook a regional study of velocity depth anomalies in North Sea Chalk, and reviewed previous work. He found positive velocity anomalies along the western and eastern margins of the North Sea basin, reflecting regional Neogene uplift and erosion, and negative anomalies in the central and southern parts of the basin, which he attributed to inhibition of compaction by the retention of overpressure. He generated velocity-depth and porosity-depth profiles for comparison of his own normal compaction trend with those previously published by Bulat and Stoker (1987), Hillis (1995), and Sclater and Christie (1980).

Mallon and Swarbrick (2002) determined a compaction trend for the non-reservoir Chalk in the more restricted area of the Central North Sea, using data from 59 wells. Their data showed a fairly abrupt decrease in the rate of porosity loss with depth at a depth of about 1500 m. They attributed this change in the rate of porosity loss to the generation of overpressure that has retarded chemical compaction in the Chalk at greater depths.

5.2. Geological setting and overpressure status

5.2.1. The Chalk Group: stratigraphy, formations and rocks

The information in this section is mainly taken from The Millennium Atlas, edited by Evans et al. (2003a).

The Chalk Group is distributed widely over the central North Sea and extends into the South Viking Graben and onto the East Shetland Platform. Stratigraphically, it includes Upper Cretaceous and Lower Palaeocene (Danian) reservoir rocks. The succession contains both carbonates and siliciclastic deposits.

Most of the Cretaceous strata in the central and southern North Sea area can be separated into two major sequences: the Lower Cretaceous Cromer Knoll Group, which is dominantly a siliciclastic succession, ranging in age from Ryazanian at the base to about the Albian-Cenomanian stage boundary; and the Upper Cretaceous Chalk. Conventionally, the Cretaceous-Tertiary Boundary is taken at the top of the chalk comprising the Tor Formation, but lithologically the Chalk Group continues well into the Early Tertiary (Danian stage) as the Ekofisk Formation, which has lithological similarity to the Upper Cretaceous (Oakman and Partington, 1998).

Upper Cretaceous and Lower Palaeocene (Danian) sediments occur widely across the North Sea and range in depth from sea bed to over 3500 m. They reach a maximum thickness of greater than 1500 m in the Central Graben, and exceed 2000 m in the northern North Sea. The Chalk and its correlative mudstone-dominated succession in the northern North Sea (the Shetland Group) were deposited over a period of 35 million years in an extensive, relatively deep, epicontinental sea during what was probably the largest transgression in the Earth's history (Surlyk et al., 2003).

The Chalk Group succession reflects the interaction of several major factors, particularly Late Cretaceous-Palaeocene regressive/transgressive history and synsedimentary tectonic activity (Kennedy, 1987). Late Cretaceous deposition in the North Sea region was preceded by an important, protracted Mid- to Late Jurassic rifting event that was followed by local oblique-slip movements during the Early

Cretaceous. However, the Late Cretaceous was a time of quiescence in the northern Europe, punctuated by important pulses of compression and inversion related to early phases of the Alpine Orogeny. These tectonic events exerted a profound influence on deposition of the Chalk in the North Sea region; some reversal of fault movement and uplift of local blocks triggered widespread mass movement of chalk that was re-deposited in slope and basinal settings.

The sediments consist of pure chalk and limestone, marly chalk, marl and calcareous chalk. Additionally, flint nodules occur at many levels. The group is subdivided into the Hidra, Blodøks, Herring, Hod, Tor and Ekofisk Formations (Surlyk et al., 2003).

The calcareous mudstones of the Blodøks and Herring Formations, and their latest equivalents, e.g. the Plenus Marl, Black Band Bed Formation, are widely distributed throughout the fields (Deegan and Scull, 1977; Surlyk et al., 2003). The alternations consist of darker and lighter units, respectively referred to as 'marls', because of the high terrigenous clay content, and 'limestones', with lower terrigenous clay content (Kennedy, 1987). In the North Sea, the Plenus Marl Formation appears to be a correlative of the younger Black Band of Yorkshire, while the Plenus Marl of onshore southern England is older. From 1993, the Plenus Marl Formation of the North Sea was re-named as the Black Band Bed by Johnson and Lott (1993) and now constitutes the basal bed of the Herring Formation.

The chalk in the Tor and Ekofisk Formations of the Norwegian sector is dominantly allochthonous, formed by the mass movement of pelagic chalk. In the north, between 58° 30' N and 60° N, the Chalk Group interfingers with the siliclastic mudstone dominated Shetland Group, with the chalk of the Hidra and Ekofisk Formations extending farthest to the north.

5.2.2. Overpressure status

The preservation of high porosity and permeability within the North Sea chalk fields is mainly associated with overpressuring, as overpressuring inhibits compaction and early entry of hydrocarbons helps maintain porosity in the reservoir by retarding associated cementation (Scholle, 1977; Hardman and Kennedy, 1980; D'Heur, 1986).

Overpressuring of the North Sea chalk fields results from rapid burial, early oil migration, buoyancy pressure of the hydrocarbon column and aquathermal pressure (Watts, 1983; Maliva and Dickson, 1992).

In the fields of interest to our study, the regional pressure of the Upper Cretaceous and Danian chalk has been mapped by Moss et al. (2003), with a distribution of pressures from water-bearing units showing strong overpressure exceeding 20 MPa (3000 psi) to the south of latitude 57° N in the Central Graben (where some of the wells in this study in Quadrants 30 and 31 are found). Direct measurements of pore pressure are mainly from porous and permeable chalk units, which tend to be found in the upper portion of the Chalk section, predominantly from re-deposited facies in which there is less cementation and high reservoir quality (Moss et al., 2003).

5.3. Analysis method and data

5.3.1. Generalities

Unloading mechanisms generate overpressure by reducing the effective stress. Only a very small fraction of the porosity lost by compaction of sediments is due to elastic deformation and recoverable on unloading. The majority of the porosity loss is due to irrecoverable, plastic deformation and chemical processes.

Porosity reduction in chalk has been studied by examining DSDP nannofossil sediments, and Garrison (1981) has reviewed the evidence of the processes involved. Mechanical compaction is significant during the first 50 m of burial, but chemical processes take over in the depth range 50–200 m. Below 200 m burial depth, dissolution and reprecipitation are the dominant processes of porosity reduction, either by stylolitization or grain-to-grain pressure solution. Precipitation of calcite cement can cause large variations in chalk porosity independent of effective stress.

Oakman and Partington (1998) produced a lithostatigraphic compilation scheme for the Cretaceous strata of the North Sea Basin. In terms of gamma ray response, neutron porosity, formation density and sonic transit time, they classified

Chalk into clean chalks (potential reservoir facies), argillaceous chalk (containing minerals) and reworked/resedimented chalk. In terms of reservoir quality and environmental setting, distinction is made between *pelagic chalks* and *re-deposited chalks*. Pelagic chalk, identified by the presence of burrows, formed by steady deposition and tends to be of poorer reservoir quality than redeposited chalk, which contains abundant clasts, formed by mass downslope movement of chalk.

In this study, chalk intervals are categorised using wireline gamma responses as follows: clean chalk with gamma ray less than 15° API, argillaceous chalk with gamma ray response above 15° API, and reworked or re-deposited chalk also with gamma ray response above 15° API but distinguished from argillaceous chalk by high neutron porosity, low formation density and low sonic velocity (Oakman and Partington, 1998).

5.3.2. Variables and data selection

Data from eight wells located between latitudes 56° N and 58° N and between longitudes 1° E and 4° E in the central North Sea (CNS) were used (Table 5.1 and Figure 5.1). The data comprise gamma ray, sonic and density logs (both in digital electronic form, except for well 22/30c-8, and composite logs) and direct pore pressure measurements made with a Repeat Formation Tester (RFT) tool.

The wells are:

UK:	22/28a - 1	22/29 – 1S1	22/30a - 2	22/30c – 8
	30/13 – 3	30/12b - 4	31/26a – 5	31/26a – 9A

Table 5.1. Wells used for the Chalk study.

Generally, the horizons used were the shallowest and deepest chalk lithologies within the Chalk that fulfilled the criterion for clean chalk. In all cases, the natural-gamma log was used to locate chalk horizons for which $\gamma < 15$ °API. Availability of suitable pore pressure measurements was also used for the selection.

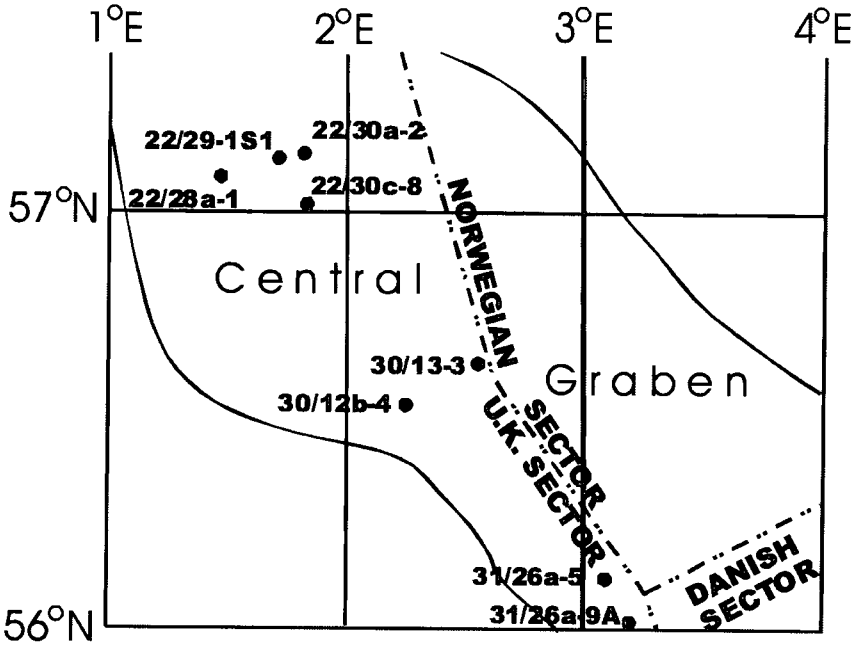

Figure 5.1. Map showing the well locations in the CNS.

Values of sonic velocity, V_p, were read off sonic logs, at clean chalk horizons that were water saturated. Corresponding porosities, ϕ, were calculated from the density log by

$$\phi = \frac{\rho_{matrix} - \rho_{\log}}{\rho_{matrix} - \rho_{fluid}} \qquad (5.1)$$

with $\rho_{\text{matrix}} = 2.71$ g/cc , $\rho_{\text{fluid}} = 1.02$ g/cc.

The vertical effective stress, σ_v is not measured directly but is calculated from the vertical or lithostatic stress and the pore fluid pressure, using Terzaghi's relation:

$$\sigma_V = S_V - P_p, \qquad (5.2)$$

where S_V is the vertical or lithostatic stress and P_p is the pore pressure. Details of vertical effective stress, σ_v, estimation in different wells and for the data points selected are given in Appendix A.

More direct pore pressure measurements, in the form of Repeat Formation Test (RFT) and Formation Integrity Test (FIT) data from these wells and neighbouring wells, and the regional pressure trend were extracted from the GeoPOP Database using *PressureView2.1* (Geopressure Technology, 2000) and the Regional Pressure Atlas of The Central North Sea (GeoPOP, 2000).

Most of the available pressure measurements are in Palaeocene and Jurassic strata. There were just three RFT measurements within the Chalk, one in well 22/30a-2 and two in 31/26a-9A, so data points (i.e., sets of values of V_p, ϕ and σ_v) were estimated at those three horizons within the Chalk.

The variation in the pore pressure within the Chalk is unknown, but the pore pressure within the Palaeocene and Jurassic strata generally follows trends parallel to the hydrostatic gradient, whereas the Chalk is thought to be the regional seal (Mallon and Swarbrick, 2002). Therefore it was decided to estimate values of V_p (sonic log), ϕ (density log) and σ_v (overburden and pore pressure) at the top and bottom of the Chalk Group in each well, where possible.

In wells 22/30c-8 and 30/13-3 there were beds of very different density near the top of the Chalk, so two data points were obtained for the top section of the Chalk in each of those wells. There were no RFT measurements in the Palaeocene for well 31/26a-5, equally no Palaeocene RFT measurement in the neighbouring wells to determine a regional pressure gradient; thus only one data point at the bottom of the Chalk was obtained from the well. And there were just three RFT measurements within the Chalk, one in well 22/30a-2 and two in 31/26a-9A, so data points (i.e., sets of values of V_p, ϕ and σ_v) were estimated at those three horizons instead of at the top of the Chalk.

Nineteen data points were picked. They are labelled as data points 1 to 19 and are identifiable by their respective related properties values, as given in Table 5.2.

Data point	Well number	Formation	Depth (ft SS)	Depth (m SS)	V_p (m/s)	ρ_{log} (g/cc)	ϕ
1	22/28a-1	Top Chalk: Ekofisk	10540	3213	4293	2.410	0.178
2		Base Chalk: Hidra	14410	4392	4800	2.610	0.059
	RTE = 130 ft						
3	22/29-1S1	Top Chalk: Ekofisk	10855	3308	4550	2.450	0.154
4		Top Chalk :Ekofisk	10955	3339	4819	2.616	0.056
5		Base Chalk: Hod	14225	4336	5414	2.640	0.041
	RTE = 75 ft						
6	22/30a-2	Chalk RFT from Tor	11263	3433	5246	2.595	0.068
7		Base Chalk: Hod	13860	4224	5038	2.580	0.077
	RTE = 130 ft						
8	22/30c-8	Top Chalk: Ekofisk	11237	3425	4354	2.400	0.183
9		Top Chalk :Ekofisk	11352	3460	4653	2.590	0.071
10		Base Chalk: Hidra	16028	4885	5210	2.620	0.053
	RTE = 39 m						
11	30/12b-4	Top Chalk: Ekofisk	10361	3158	4258	2.410	0.178
12		Base Chalk: Hod	12576	3833	5628	2.650	0.036
	RTE = 82 ft						
13	30/13-3	Top Chalk: Ekofisk	10496	3199	3833	2.360	0.207
14	RTE = 114 ft	Top Chalk: Ekofisk	10766	3281	4689	2.555	0.092
15		Base Chalk: Hod	12406	3781	5038	2.600	0.065
	31/26a-5	Top Chalk: no data					
16		Base Chalk: Hod	10258	3127	5046	2.600	0.065
	RTE = 82 ft						
17	31/26a-9A	Chalk RFT from Tor	8055	2455	3607	2.250	0.272
18		Chalk RFT from Tor	8181	2494	3586	2.244	0.276
19	RTE = 83 ft	Base Chalk: Valhall	8322	2537	4583	2.520	0.112

Table 5.2 Porosity and velocity values estimated from wireline logs.

5.3.3. Pore pressure estimation in Chalk

It is known that the CNS Chalk is overpressured, but all wells in the area are not at the same level of abnormal pressure (GeoPOP, 2000).

For each well, any relevant direct pressure measurements are given in the form of a table and a pressure-depth plot. The pore pressure values used here are either direct measurements (RFT, FIT of Very Good, Good and Fair quality) or estimates made at the top and base of the Chalk Group, at the bed of interest within each of the different wells, as described below and detailed in Appendix A.

The regional pressure gradient trend that was used (GeoPOP, 2000) is:

Hydrostatic gradient : 10.07 MPa/km (0.445 psi/ft)

Lithostatic gradient : 22.63 MPa/km (1.000 psi/ft)

[Conversion: 145 psi = 1 MPa 1 m = 3.281 ft].

For each of the nineteen data points in Table 5.2, the value of pore pressure is either a direct pressure measurement in the Chalk strata (in the case of the three data points selected at the top of the Chalk in wells 22/30a – 2 and 31/26a – 9A) or an estimate using data available within the well. Where suitable direct pressure measurements are not available, the geology and pressure regime data from neighbouring wells were used to estimate the pore pressure value. This is especially the case for wells 22/28a – 1, 22/30c - 8 and 30/12b - 4. However, others have been extrapolated vertically, either from above or below, from RFT measurements in the same well.

Estimates of pore pressure at the top of the Chalk, which mostly lies in the Early Palaeocene Ekofisk Formation, were made on the assumption that the Palaeocene sand of the CNS is normally pressured. A hydrostatic trend was taken to the depth of interest from the available measurements of pore pressure. In addition, to confirm the assumption of Palaeocene pressure status for wells 22/28a – 1, 22/30c -8 and 30/12b – 4, where neighbouring wells were used, the porosity-depth and sonic-depth plots through the Chalk section are shown (Figure 5.2), since these plots may indicate approximately the onset of overpressure (Hubbert and Rubey, 1959).

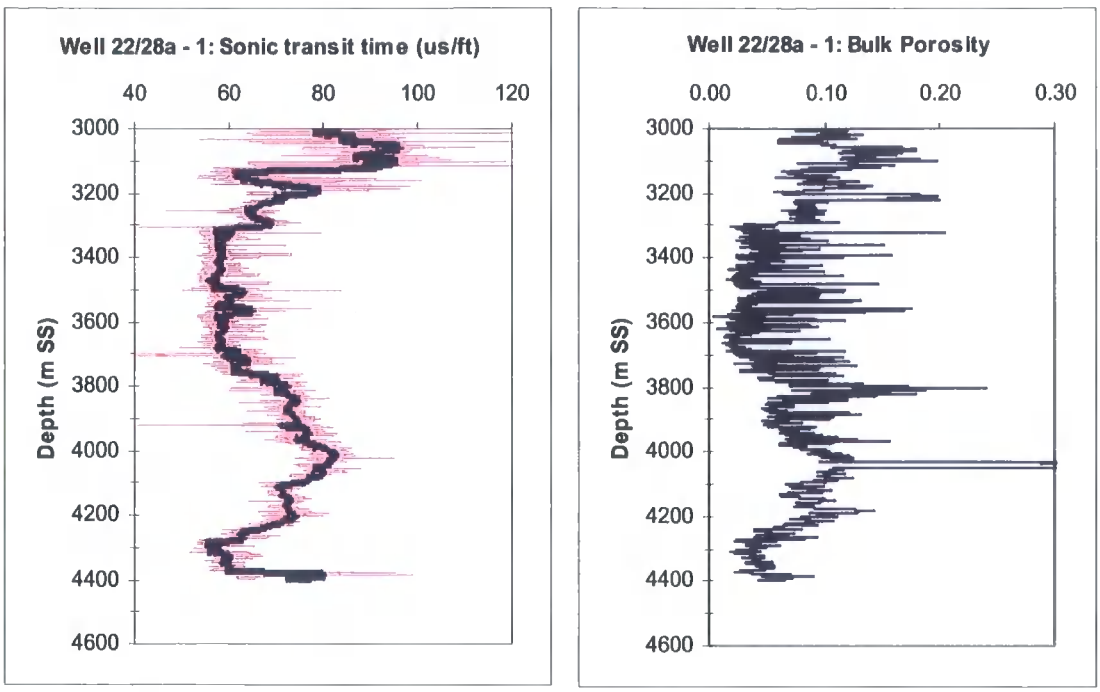

Figure 5.2. Compaction trend through the Chalk Group in Well 22/28a – 1 showing the onset of overpressure around 3750 m sub-sea.

Estimates of pore pressure at the base of the Chalk were obtained from RFT measurements in the Jurassic section as follows:

- Determine the oil-water contact (OWC) or gas-water contact (GWC) within the well, if possible using the Drill Stem Test (DST), RFT and other available log data.
- Define a pressure interval gradient trend within the immediate lithology above the GWC, OWC (if appropriate).
- Compute the equivalent pore pressure at the same depth within the water leg.
- Extrapolate along a trend parallel to hydrostatic pressure (10.07 MPa/km = 0.445 psi/ft) up to the base of the Chalk.

Values of the pore pressure were then used to compute the vertical effective stress, according to equation (5.2). The estimated values of pore pressure are given in Table 5.4 along with values of overpressure, though they are not used directly in the analysis. Section 5.3.4 is an example of pore pressure estimation.

5.3.4. Example of pore pressure estimations: well 22/29 – 1S1

RFT		Depth		Quality
psi	MPa	ft SS	m SS	
4248.70	29.30	9355.3	2851.4	Good
4310.10	29.7	9532.4	2905.3	Good
4319.70	29.8	9532.6	2905.4	Good
4337.90	29.9	9590.4	2923.0	Good
4344.50	30.0	9590.4	2923.0	Fair
4637.70	32.0	10088.5	3074.8	Good
5847.70	40.3	12006.8	3659.5	Fair
12994.50	89.6	14794.3	4509.1	Fair
13004.90	89.7	14796.3	4509.7	Good
12995.10	89.6	14798.3	4510.3	Fair
12991.40	89.6	14800.3	4510.9	Good
13024.00	89.8	14802.3	4511.5	Good
12997.90	89.6	14804.3	4512.1	Good
13069.30	90.1	15652.5	4770.6	Fair
13185.50	90.9	15762.5	4804.2	Fair
13263.90	91.5	15768.5	4806.0	Fair

Table 5.3. RFT measurements through the Palaeocene and Jurassic intervals in well 22/29 – 1S1, taken from the composite log.

This section explains how pore pressure values are estimated for the three data points selected in this well, identified as data points 3, 4 and 5 (Table 5.2).

At the top of the Chalk, the sediments are normally pressured (Figure 5.3), i.e. lying along the hydrostatic gradient of 10.07 MPa/km.

$$\therefore Pp\big|_{3308mSS} = 3308\,m \times 0.01007\,MPa/m = 33.3\,MPa \qquad (5.3)$$

$$\therefore Pp\big|_{3339mSS} = 3339\,m \times 0.01007\,MPa/m = 33.6\,MPa \qquad (5.4)$$

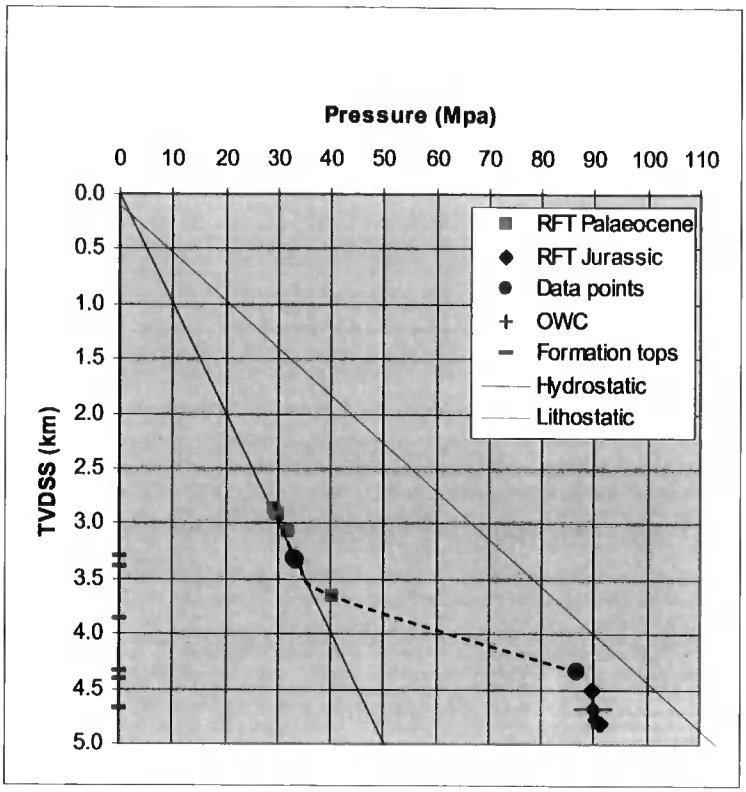

Figure 5.3. Pressure–depth plot for well 22/29 – 1S1

At the base of Chalk, the pore pressure is estimated by extrapolation from measurements in the Jurassic. Using the petrophysics data provided, the OWC is at depth 4675.4 m SS (15340 ft SS). The RFT measurements available in the water leg (Table 5.3, interval 4770.6 – 4806.0 m) suggests an overpressure value of 42.9 MPa at the OWC. Thus, extrapolating parallel to the hydrostatic gradient up to the base Chalk,

$$\therefore Pp|_{4336mSS} = 42.9 + 0.01007 \times 4336 = 86.6\ MPa \qquad (5.5)$$

With values of pore pressure and vertical stress (overburden) already estimated (see section 3.6.3, Chapter 3), Equation 5.2 gives values of the vertical effective stress. Thus,

$$\text{Data point 3: } \sigma_v|_{3308mSS} = 71.2 - 33.3 = 37.9MPa \qquad (5.6)$$

$$\text{Data point 4: } \sigma_v|_{3339mSS} = 71.8 - 33.6 = 38.2MPa \qquad (5.7)$$

$$\text{Data point 5: } \sigma_v|_{4336mSS} = 97.8 - 86.6 = 11.2\ MPa \qquad (5.8)$$

Details of pore pressure and corresponding vertical effective stress estimations for each of the 19 data points are reported in Appendix A, which also contains pressure-depth plots of the RFT measurements available for the wells. Density-depth and sonic-depth plots are also given, showing the onset of overpressure in the Chalk for some wells.

5.4. Data inversion and results

A set of nineteen data points were picked in clean chalk beds (section 5.3). The variables to be fitted by empirical equations are listed in Table 5.4. They are the estimated values of velocity, porosity, pore pressure, lithostatic stress and vertical effective stress from the eight wells used in this study. The first column of the table gives the label of each data point, as they are referred to in this chapter and Appendix A.

The total set of nineteen data points (V_p, ϕ, σ_v) were first fitted by an equation of the form

$$V_p = V_0 + a\phi + b\sigma_v \qquad (5.9)$$

using linear inversion, with V_0, a and b the parameters to be estimated.
Table 5.5 gives the column vector of observed velocity data from sonic logs and the coefficient matrix for the parameters to be determined.
The result of the inversion was

V_0 (m/s)	a (m/s)	b (m/s/MPa)
5483.8	- 7073.4	0.74

giving

$$V_p = 5484 - 7073\,\phi + 0.74\,\sigma_v \qquad (5.10)$$

with a root mean square (RMS) error of 203 m/s.

Data point	Well number	Formation	Depth ft subsea	Depth m subsea	Velocity m/s	Porosity	Pore pressure MPa	Relative depth of nearest RFT m	Overpressure MPa	Lithostatic Stress MPa	Vertical effective Stress MPa
1	22/28a-1	Ekofisk	10540	3213	4293	0.178	32.3	Other wells	0	67.6	35.3
2		Hidra	14410	4392	4800	0.059	84.5	414 below	40.3	96.3	11.8
3	22/29-1S1	Ekofisk	10855	3308	4550	0.154	33.3	233 above	0	71.2	37.9
4		Ekofisk	10955	3339	4819	0.056	33.6	264 above	0	71.8	38.2
5		Hod	14225	4336	5414	0.041	86.6	173 below	42.9	97.8	11.2
6	22/30a-2	Tor	11263	3433	5246	0.068	44.0	0	9.4	71.8	27.8
7		Hod	13860	4224	5038	0.077	84.4	133 below	41.9	92	7.6
8	22/30c-8	Ekofisk	11237	3425	4354	0.183	34.5	Other wells	0	76.9	42.4
9		Ekofisk	11352	3460	4653	0.071	34.8	Other wells	0	77.8	43.0
10		Hidra	16028	4885	5210	0.053	105.2	404 below	56.0	114.1	8.9
11	30/12b-4	Ekofisk	10361	3158	4258	0.178	50.4	Other wells	18.6	65.9	15.5
12		Hod	12576	3833	5628	0.036	44.6	68 below	6.0	83.1	38.5
13	30/13-3	Ekofisk	10496	3199	3834	0.207	50.8	221 above	18.6	67.4	16.6
14		Ekofisk	10766	3281	4689	0.092	51.7	304 above	18.7	69.4	17.7
15		Hod	12406	3781	5038	0.065	71.2	350 below	33.1	82.1	10.9
16	31/26a-5	Hod	10258	3127	5046	0.065	45.4	27 below	13.9	68.6	23.2
17	31/26a-9A	Tor	8055	2455	3607	0.272	37.9	0	13.2	52.3	14.4
18		Tor	8181	2494	3586	0.276	38.3	0	13.2	53.2	14.9
19		Valhall	8322	2537	4583	0.112	38.7	77 below	13.2	54.2	15.5

Table 5.4. Estimated values of velocity, porosity, pore pressure, lithostatic stress and vertical effective stress from the eight wells used in this study.

The differences between the measured V_p (observed values) and the forward-calculated values using Equation (5.10) (i.e., the velocity discrepancies) were found (Table 5.6), and the RMS error calculated as:

$$\Delta V = \sqrt{\frac{\sum (\Delta V_i)^2}{n-k}}, \qquad (5.11)$$

where ΔV_i is the velocity discrepancy, $i = 1....19$, n = number of data points fitted and k = dimension of the data ($k = 3$ in this case).

(Unity)	ϕ (fractional)	σ_v (MPa)	V_P (from sonic) (m/s)
1	0.178	35.3	4293
1	0.059	11.8	4800
1	0.154	37.9	4550
1	0.056	38.2	4819
1	0.041	11.2	5414
1	0.068	27.8	5246
1	0.077	7.6	5038
1	0.183	42.4	4354
1	0.071	43.0	4653
1	0.053	8.9	5210
1	0.178	15.5	4258
1	0.036	38.5	5628
1	0.207	16.6	3834
1	0.092	17.7	4689
1	0.065	10.9	5038
1	0.065	23.2	5046
1	0.272	14.4	3607
1	0.276	14.9	3586
1	0.112	15.5	4583

Table 5.5. Matrices of parameters for the inversion program.

Over the range of vertical effective stress values in the data set, 7– 43 MPa, the term $0.74\sigma_v$ in Equation (5.10) contributes a variation of only 27 m/s in the forward-calculated velocity values. This amount is not significant because it is much less than the associated RMS error. The only sensible conclusion that may be drawn is that the value of b is not significantly different from zero. In other words, the sonic velocity shows no significant dependence on vertical stress in these data, assuming that velocity depends linearly on porosity and vertical effective stress as assumed in this inversion.

In view of the finding that there is no dependence of seismic velocity on vertical stress, the simpler function

$$V_p = V_0 + a\,\phi \qquad (5.12)$$

was fitted to the nineteen points from the eight wells in the CNS. The result is

V_0 (m/s)	a (m/s)
5501.1	– 7077.2

giving

$$V_p = 5501 - 7077\ \phi, \qquad (5.13)$$

with the velocity discrepancies in the last column of Table 5.6.

S/N	Depth	ϕ	σ_v	V_P log	3 parameters		2 parameters	
					V_P calc	ΔVi	V_P calc	ΔVi
	(m SS)	(fraction)	(MPa)	(m/s)	(m/s)	(m/s)	(m/s)	(m/s)
1	3213	0.178	35.3	4293	4251.1	-41.9	4241.3	-51.7
2	4392	0.059	11.8	4800	5075.4	275.4	5083.5	283.5
3	3308	0.154	37.9	4550	4422.8	-127.2	4411.2	-138.8
4	3339	0.056	38.2	4819	5116.2	297.2	5104.7	285.7
5	4336	0.041	11.2	5414	5202.3	-211.7	5210.9	-203.1
6	3433	0.068	27.8	5246	5023.6	-222.4	5019.8	-226.2
7	4224	0.077	7.6	5038	4945.0	-93.0	4956.1	-81.9
8	3425	0.183	42.4	4354	4221.0	-133.0	4205.9	-148.1
9	3460	0.071	43.0	4653	5013.6	360.6	*4998.6*	345.6
10	4885	0.053	8.9	5210	5115.7	-94.3	5126.0	-84.0
11	3158	0.178	15.5	4258	4236.5	-21.5	4241.3	-16.7
12	3833	0.036	38.5	5628	5257.9	-370.1	5246.3	-381.7
13	3199	0.207	16.6	3834	4032.2	198.2	4036.1	202.1
14	3281	0.092	17.7	4689	4846.4	157.4	4850.0	161.0
15	3781	0.065	10.9	5038	5032.3	-5.7	5041.0	3.0
16	3127	0.065	23.2	5046	5041.4	-4.6	5041.0	-5.0
17	2455	0.272	14.4	3607	3570.8	-36.2	3576.1	-30.9
18	2494	0.276	14.9	3586	3542.9	-43.1	3547.8	-38.2
19	2537	0.112	15.5	4583	4703.3	120.3	4708.4	125.4
					RMS error	203.2	//////////	197.4

Table 5.6. Computed values of velocities using the linear equations (5.10) and (5.13) for all 19 data points.

The relationships expressed by Equations (5.10) and (5.13) are the results of the investigation into how the seismic velocity in CNS Chalk depends on porosity and

vertical effective stress, subject to the restrictions that vertical effective stress is not less than 7.6 MPa and the range of porosity values is 0.03—0.28. In the two following sections, comments are given on the data in line with other studies undertaken in this department.

5.5. Interpretation and significance of the results

5.5.1. Suitability of the data set

In total, 19 data points were obtained (Table 5.4). Composite plots of sonic velocity, porosity (determined from the density log) and pore pressure against depth are given in Figure 5.4. They may be used to infer whether some of the overpressured data points have been overpressured by disequilibrium compaction or unloading.

The burial history of the central North Sea region since the start of the Tertiary shows a total of 3000–3500 m of compacted sediments that accumulated over 65 Ma. However, rapid burial leading to 1200–1800 m of sediment, dominantly claystones, has taken place during the last 3 Ma (Swarbrick et al., 2000). This rapid burial could have led to overpressure at depth of up to 18 MPa by disequilibrium compaction, i.e. 10 MPa/km for the additional overburden. Higher overpressure in deeper fine-grained rocks may have resulted from the additional effect of earlier, slower burial, but overpressure from disequilibrium compaction is not likely to exceed 10 MPa/km of burial (Swarbrick et al., 2002).

Data points 1, 3, 4, 8 and 9, where pore pressure is hydrostatic, can be assumed to be at their maximum vertical effective stress at the present day since there has been no recent uplift. The absence of overpressure is related to drainage from the immediately overlying Palaeocene sandstone aquifer.

Data points 2, 5, 7 and 10 from the base of the Chalk exhibit overpressures in the range 40–56 MPa, too high for disequilibrium compaction alone, so it may be inferred that unloading has contributed substantially to the measured overpressures. Possible candidates for unloading mechanisms in these sediments include smectite to illite transformation, gas generation, oil to gas cracking and aquathermal pressuring, of which gas generation is the most effective (Swarbrick et al., 2002). The Kimmeridge Clay source rocks in the deeper buried regions of the study area are gas

generative (Holm, 1998). Development of high pressures in the sub-Chalk section will necessarily lead to conditions for unloading of the Chalk, especially at its base, as fluids are forced into the Chalk in an effort to reach equilibrium.

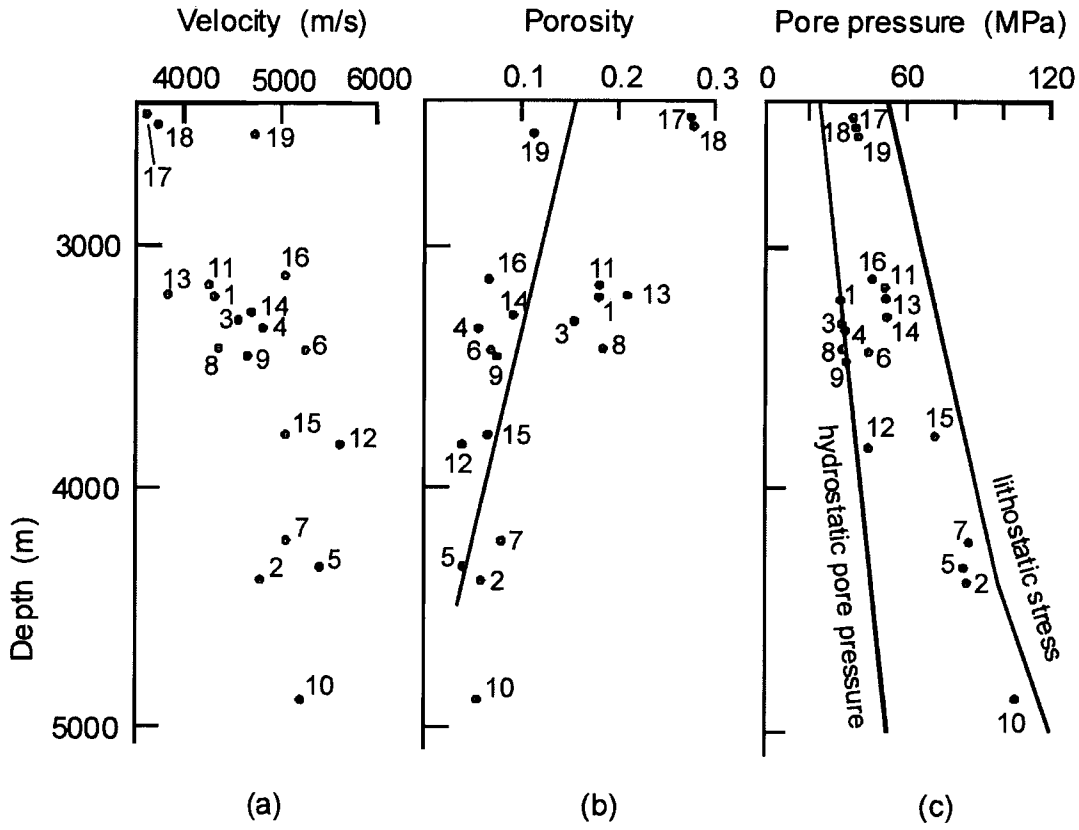

Figure 5.4. Composite depth plots of the 19 data points from the eight wells used in this study: (a) velocity from the sonic log; (b) porosity calculated from the density log; (c) pore pressure values from RFT measurements (see Appendix A). The straight line in (b) is the compaction trend for non-reservoir chalk determined by Mallon and Swarbrick (2002).

5.5.2. Data analysis

The main purpose of this investigation was to determine whether velocity depends on both porosity and effective stress as independent variables. For a normally compacted sediment, increase in vertical effective stress would be expected to correlate with decrease in porosity, so the two variables would not be independent.

In the set of 19 data points from the Chalk, analysed here, there are two reasons why the data cannot lie on a single normal compaction trend in velocity–

porosity–vertical effective stress space. Firstly, at least the five data points from the base of the Chalk with the lowest values of vertical effective stress (2, 5, 7, 10 and 15) are likely to be in an unloaded stress state. Secondly, there are three pairs of data points (3 and 4, 8 and 9, 13 and 14) where both high and low porosity chalk is present at closely spaced depths in the same wells. Some difference in calcite precipitation, possibly associated with a difference in facies, must have affected at least one data point of each pair. Accordingly, it is reasonable to treat porosity and effective stress as independent variables affecting velocity.

However, the result - Equation (5.10) – is that the sonic velocity shows no detectable dependence on the vertical effective stress in these data, assuming that velocity depends linearly on porosity and vertical stress as given in Equation (5.9).

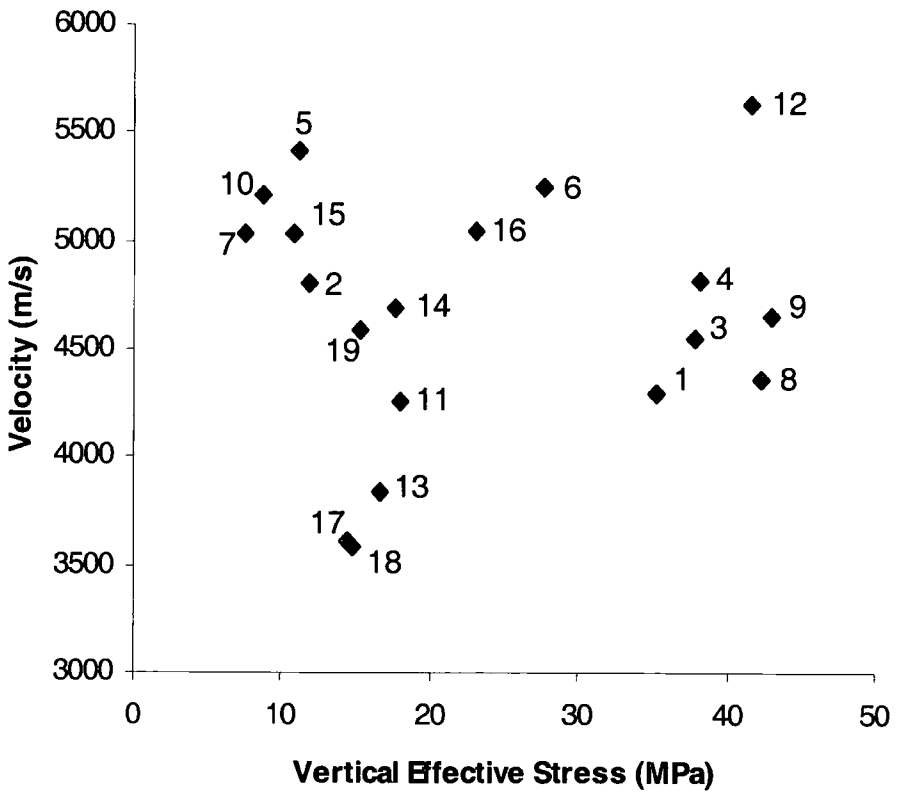

Figure 5.5. Velocity plotted against vertical effective stress

A plot of velocity against vertical effective stress (Figure 5.5) shows the lack of correlation between these two variables. The data points 2, 5, 7, 10 and 15, that are thought likely to be in an unloaded stress state, form a cluster at high velocities and

low effective stress values. Each of the three pairs of data points from the top of the Chalk (3 and 4, 8 and 9, 13 and 14), with very different porosities from comparable depths in the same wells, have different velocities at very similar values of vertical effective stress, and therefore contribute to the lack of correlation on this plot.

5.6. Discussion and conclusions

Equation (5.13), which completes the analysis of the investigation, is not an accurate velocity–porosity relationship because of the limited number of data. In order to find a more accurate relationship, a larger number of data should be used. Mallon and Swarbrick (2002) correlated porosity inferred from density logs with velocity from sonic logs using data from 59 wells passing through non-reservoir Chalk in the central North Sea. They fitted their data with a formula of the same algebraic form as the Wyllie relationship to yield

$$\phi = \frac{2066}{V_p} - 0.325 \qquad (5.14)$$

pinned at the matrix value of 6350 m/s for zero porosity. Equation (5.14) is close to the Wyllie relationship using the velocities 6400 m/s for matrix and 1615 m/s for pore fluid given by Schlumberger (1974):

$$\phi = \frac{2154}{V_p} - 0.336 \qquad (5.15)$$

The data analysed by Mallon and Swarbrick (2002) display a lot of scatter, typically over a range of 1000 m/s in velocity at constant porosity. Similar scatter is evident in the much smaller dataset used here (Figure 5.6). It is suggested that the scatter is mostly due to the response of the sonic log. It is commonly said that the sonic log in carbonates responds mainly to primary porosity, so where secondary porosity is present the velocity will appear anomalously high for the total porosity value inferred from the bulk density log (Bateman, 1985).

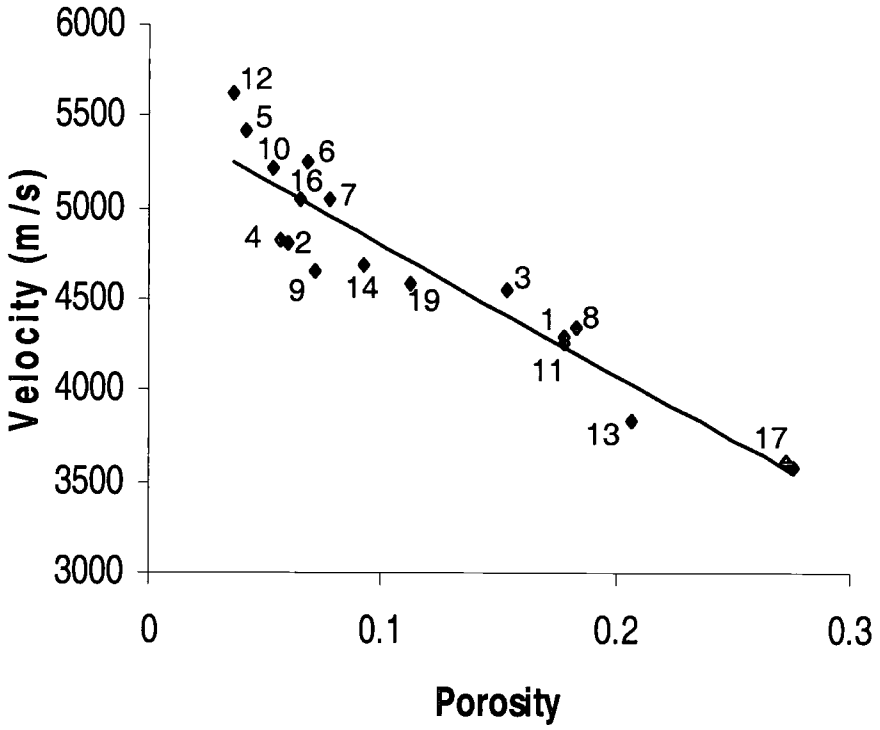

Figure 5.6. Velocity plotted against porosity with the best-fit straight line given by $V_p = 5501 - 7077\phi$

The division of porosity into primary and secondary porosity is simplistic. In fact, it has long been recognized that sonic velocity depends on 'matrix and matrix materials, grain size distribution and shape, and cementation' (Wyllie et al., 1956). That is, fabric is an important factor, and variations in fabric appear to have a strong effect on the sonic velocity in chalk. In addition, anomalously low velocity values could be due to the presence of shale or very small quantities of gas, which will both increase the sonic transit time.

Scatter in the sonic data could be masking some small dependence of velocity on vertical effective stress in the data analysed here. Nevertheless, there may be a good physical reason why velocity in the Chalk is little affected by unloading. Bowers and Katsube (2002) have proposed that the reason why the seismic velocity is reduced in unloaded shales is that connecting pores are much more compliant than storage pores. Consequently, connecting pores are likely to undergo proportionally more elastic widening on unloading, which will affect the seismic velocity and resistivity

(i.e. transport properties) but have little effect on the bulk density. Porosity reduction in the Chalk below 200 m depth takes place by precipitation of calcite, whether dissolved locally by pressure solution and stylolitization or imported by moving pore water. It is suggested, therefore, that the reason why velocity in the Chalk depends only on the porosity and not on the vertical effective stress is because of cementation.

The relationship given by Equation (5.10) is the result of this investigation into how velocity in Chalk in the Central Graben, North Sea depends on porosity and vertical effective stress, for the range of effective stress values 7–43 MPa and the range of porosity values 0.03–0.28. The main conclusion is that velocity shows no significant dependence on vertical effective stress when porosity and vertical effective stress are treated as independent variables. Consequently, it is not possible to use sonic logs and density logs in chalk to detect the presence of any overpressure caused by unloading.

A linear fit of velocity to porosity gave Equation (5.13) for porosity values in the range 0.03–0.28. However, because the number of data points used in this study is so limited, the Wyllie-type relationship of Equation (5.14) given by Mallon and Swarbrick (2002) is to be preferred for relating velocity to porosity in non-reservoir Chalk of the Central North Sea.

5.7. Appendix: Plots of observed and forward-calculated velocities values using Equation 5.10

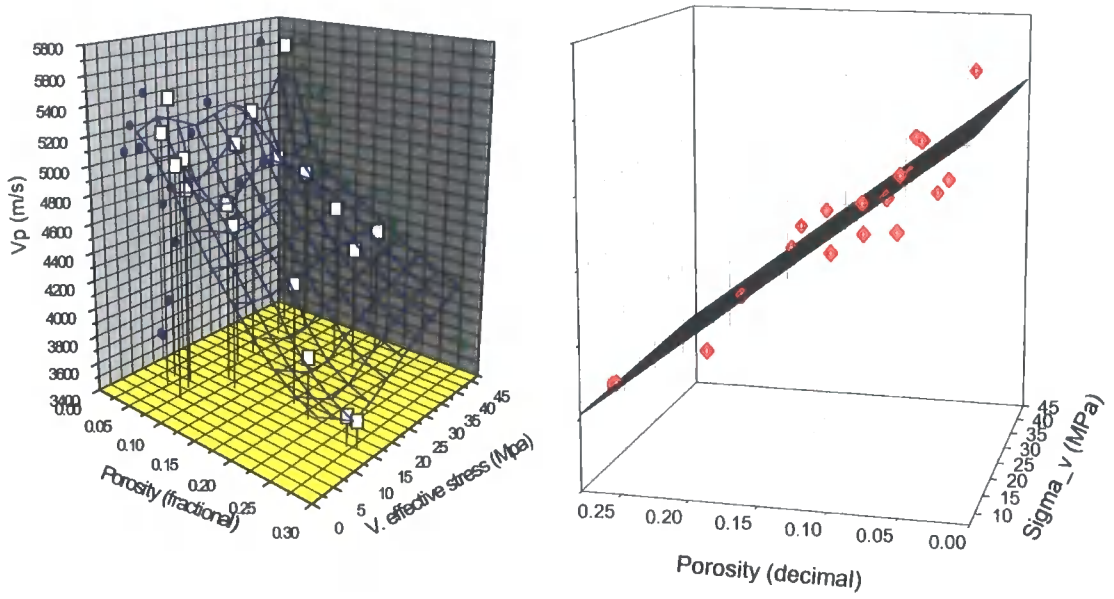

(a) 3D Mesh Plot: Observed data in velocity-porosity-vertical effective stress space.

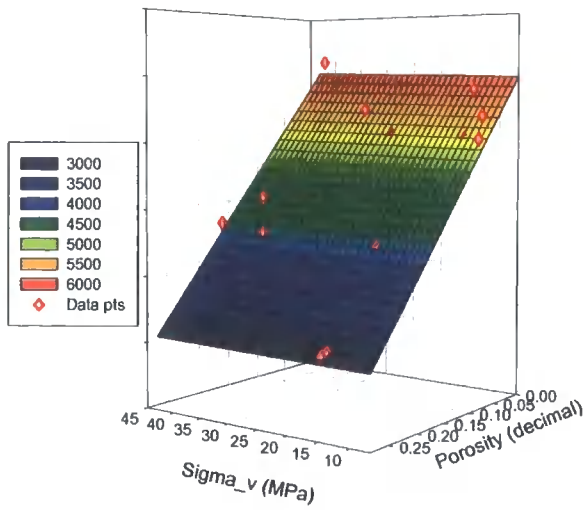

(b) view of the data above the fitted-plane surface

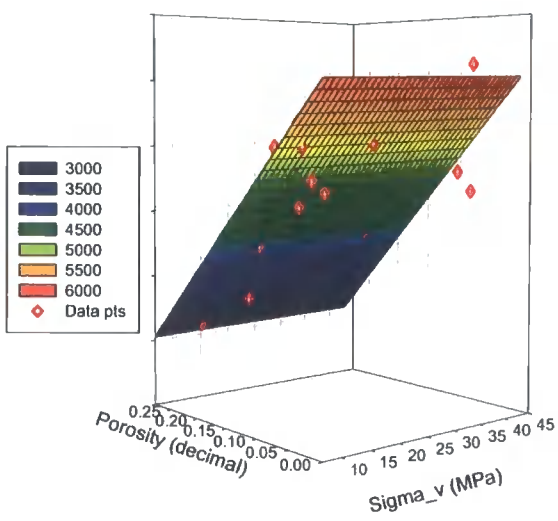

(c) View of data under the fitted-plane surface

Figure 5.7. 3D Plot of observed velocities with fitted-plane surface given by equation $V_p = 5484 - 7073\ \phi + 0.74\ \sigma_v$ (5.10).

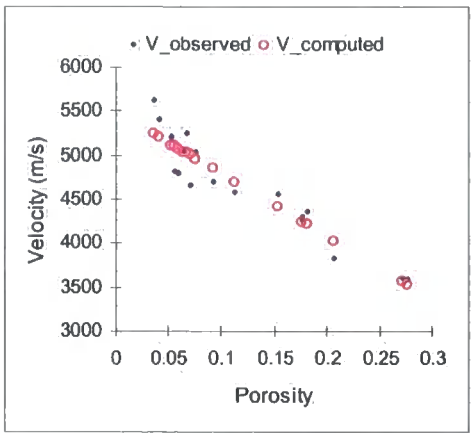

(a) Forward-calculated velocities Eq. (5.10).

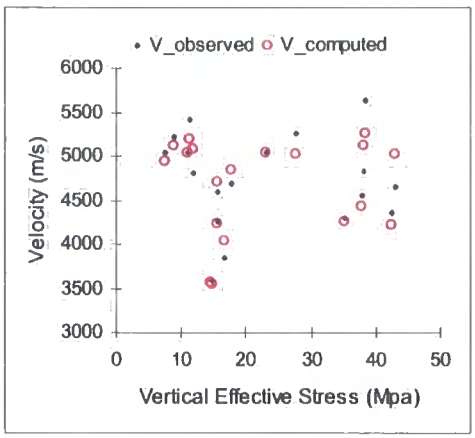

(c) Forward-calculated velocities Eq. (5.10).

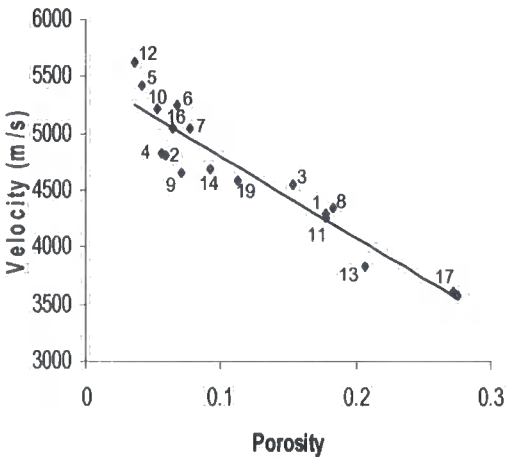

(b) Labelled data points with best-fit straight line of velocity vs. porosity given by $V_p = 5501 - 7077\phi$.

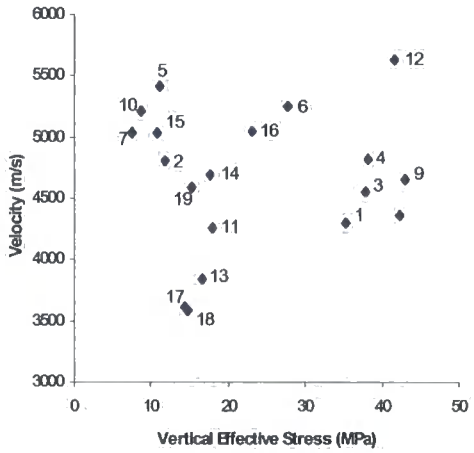

(d) Labelled data points in V_p vs. σ_v plot.

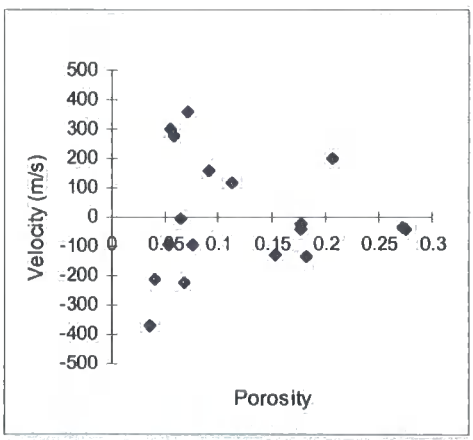

(c) Velocity discrepancies vs. porosity.

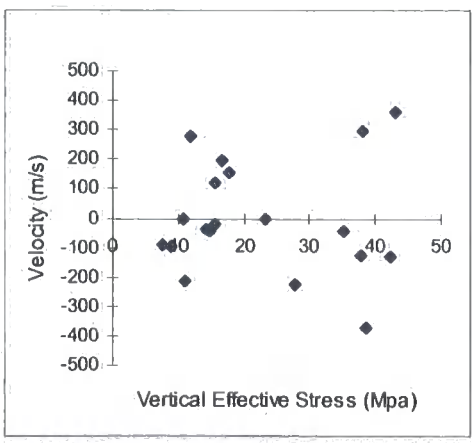

(e) Velocity discrepancies vs. vertical effective stress.

Figure 5.8. 2D Plots of observed and forward-calculated velocities Eq. (5.10).

Chapter 6
Variation of velocity with effective stress in mudstones

6. VARIATION OF VELOCITY WITH EFFECTIVE STRESS IN MUDSTONES

6.1. Introduction

Using a similar approach to that described in Chapter 5, wireline log data and pore pressure measurements have been used to investigate how sonic velocity depends on vertical effective stress in shales and claystones. The main purpose is to determine whether overpressure related to unloading processes that reduce the effective stress have a measurable effect on velocity. Unloading causes a reduction in effective stress with negligible increase in porosity; so it makes sense to treat vertical effective stress and porosity as independent variables when unloading has occurred. In the case of mudstones, porosity reduction without change in the vertical effective stress may result from chemical processes, again suggesting that porosity and vertical effective stress are independent from one another. Non-organic mudstones only have been included in the study. The data set is taken from Lower Cretaceous and Jurassic strata in the Central Graben and in the Alwyn and Ninian fields of the East Shetland Basin (Figure 6.1).

Data points were picked in various beds of undifferentiated mudstones, so the data set contains a heterogeneous mixture of silty mudstones, shales and claystones of variable mineralogy. Due to compaction and diagenesis, the properties of mudstones change as they develop from young unconsolidated sediments to fully lithified rocks. Laboratory data analysis has shown that elastic wave velocity in mudstones depends on lithology, mineralogy, porosity and pore fluid content (Jones and Wang, 1981; Anselmetti and Eberli, 1993; Nygard et al., 2004). Thus, in addition to the vertical effective stress, sonic and bulk density log readings, other variables included in the analysis were gamma-ray count and resistivity. Johnston (1987) established that velocity and resistivity in mudstones are strongly dependent on temperature compared to sandstones. Since depth is a proxy for temperature, depth was also included as an independent variable in the analysis.

For the analysis, two sets of data from the same areas, differing in the method of selection, were analysed to account for various assumptions on the linear model and the geological observations. Data points were selected from mudrock beds in wells across the Central Graben, and in the Ninian and Alwyn fields, with Set A of 209 data points and Set B of 3647 data points. Different results along the study show a dependence of the velocity on the independent variables, porosity and vertical effective stress. Two lithological variables, gamma-ray count and resistivity were introduced. Gamma-ray count reveals to have a reliable/strong response on the fit, while resistivity has demonstrated negligible contribution or undue influence to a better correlation in the relationships. In addition, testing the results across different formations for subsets of the data with different mineralogy shows no consistent effect of the variables coefficients on V_p. The overall results are given in equations of the form $V_p = 3857 - 3799\ \phi + 21.8\ \sigma_v - 9.0\ \gamma$ and $V_p = 3374 - 4345\ \phi + 17.4\ \sigma_v - 4.7\ \gamma + 0.146\ z$, respectively, for the Cromer Knoll and the Heather Formation. Hence, for the data under study, it is concluded that there is slight dependence of sonic velocity on vertical effective stress to account for unloading due to overpressure.

To present the results, the chapter is organised in nine sections. This introduction is followed by sections 6.2 and 6.3 giving some general background on the mudstones and the geological setting. Section 6.4 explains the data selection process and the analysis method, whilst sections 6.5 and 6.6 report on the results of the analysis carried out on the data sets. A preliminary discussion of the results is given in section 6.7, followed by a note concluding the chapter in section 6.8. Section 6.9 appends the chapter and contains details of properties and values on Set A of data.

6.2. Mudstones and compaction

6.2.1. Shales and claystones

Mudstone is a commonly used synonym for mudrock. It is a general term to identify shale, mudstone, argillite, siltstone, claystone or marl, depending on the dominant grain-size (= texture), composition and the presence of fissility or laminations (see section 2.3.1). Shale and claystone beds have been used for this investigation because their compaction behaviour is of interest in the prediction of

pore pressure in overpressured zones (Section 2.5.1). The recognition of any unloading process can be spotted in a velocity – porosity – vertical effective stress domain, i.e. analysing $V(\phi, \sigma_v)$, as introduced in section 3.2.

6.2.2. Compaction and properties of mudstones

Clastic sedimentary rocks are formed from detrital fragments of older rocks that have undergone erosion and weathering. After burial, they undergo compaction. Eventually, compaction is followed by cementation whereby cement-forming minerals such as quartz and calcite carried by water precipitate in the pores to bind the compacted layers together. The process is known as lithification, achieved by means of pressure and heat. During the process, the sediment undergoes a series of burial and uplift (erosion) sequences, and some diagenetic effects take place. The mechanical properties and the degree of compaction (porosity) of mudstones as a function of burial depth are known to vary greatly (Rieke and Chilingarian, 1974; Chilingarian, 1983; Baldwin and Butler, 1985; Hansen, 1996). The variation is also partly a result of differences in the rate of burial and pore fluid pressure affecting the magnitudes of the effective stress.

Under the increasing overburden pressure during burial, pore fluid is expelled from sediments. The rate of compaction is a function of the permeability of the overburden which controls the rate of water expulsion. Depending on their burial and the rate of fluid expulsion, sediments may be either normally pressured or overpressured. When the fluid cannot escape fast enough to remain in hydrostatic equilibrium during burial, the overpressure is said to be due to disequilibrium compaction. Diagenesis is a broad term which includes sediment changes due to mechanical loading, fluid flow, temperature variations and chemical reactions. Diagenetic clay dehydration is another mechanism that may cause overpressure with a reduction in effective stress, causing an unloading response by the sediments (Powers, 1967; Magara, 1975). It has been found in some experiments on Kimmeridge shale samples, which had undergone significant burial, that mechanical compaction alone cannot explain compaction, and that chemical diagenesis is a more dominant process in reducing the porosity and compressibility than mechanical compaction below 2 – 3 km depth (Nygard et al., 2004).

6.3. Geological setting

6.3.1. Lithology and stratigraphy

The time interval covered by the study is from Late Jurassic to Early Cretaceous. The Late Jurassic is known to be the most critical time interval in the evolution of the North Sea petroleum system. It was the time of deposition of the widespread Kimmeridge Clay Formation and its lateral equivalents, and its complex and diachronous tectonic history was directly responsible for the structures that have formed the vast majority of traps, not only for hydrocarbon accumulations in Upper Jurassic and Lowermost Cretaceous syn-rift reservoirs, but also in the pre- and syn-rift reservoir rocks of Devonian to Middle Jurassic age (Fraser et al., 2002).

The Upper Jurassic succession is mainly preserved within graben areas of the rift system, where it can reach a thickness of 3000 m. The top of the Upper Jurassic rocks, as estimated from the "Near Base Cretaceous" seismic reflector (Oakman and Partington, 1998), generally lies between 2500 and 5000 m below the sea bed in these graben areas. This succession belongs to the Humber Group (Richards et al., 1993) and its lateral equivalents, such as the Viking Group in the Norwegian sector (Vollset and Doré, 1984). As indicated by Richards et al. (1993), all formations of the group are diachronous lithostratigraphic formations. Mudstones of the Kimmeridge Clay Formation (Oxfordian – Ryazanian) and the Heather Formation (Callovian - Ryazanian) occupy the deeper part of the Central Graben and drape the highs (Draupne Formation). The group also contains a plethora of sandstone-dominated intervals, of which the most significant hydrocarbon-bearing intervals include the shallow-marine Fulmar and Piper Formations, the deep-marine Magnus Sandstone Member and Brae Formation, and the coastal-deltaic Sognefjord and Fensfjord Formations. The transition between the organic-rich mudstones of the Kimmeridge Clay Formation and the organic-poor mudstones of the underlying Heather Formation may be gradual. The boundary is often difficult to define in the absence of sedimentological and geochemical data; however it is generally taken at a gamma ray cut-off of 100° API (Veldkamp et al., 1996).

The Lower Cretaceous Cromer Knoll Group and the Chalk Group constitute the two major sequences of the North Sea Cretaceous. The Lower Cretaceous Cromer Knoll Group is dominantly a siliclastic succession ranging in age from Ryazanian to about the Albian–Cenomanian stage boundary. It is overlain by the Upper Cretaceous Chalk Group, which occurs throughout the southern and central areas of the North Sea, but in the north is more argillaceous where it has been assigned to the Shetland Group (Oakman and Partington, 1998). Within wells considered in the study (Table 6.2), sandstone and limestone stringers and mudstones of various diagenetic contents are found in the Lower Cretaceous Cromer Knoll Group. The group consists of the Rodby, Sola and Valhall Formations in Quadrants 21, 22 and 30, and is undivided in Quadrant 3. It becomes thinner northwards in the Shetland Group (Rawson and Riley, 1982; Copestake et al., 2003). It is absent in wells 3/9a – 2 and the Lower Cretaceous in well 3/15 – 4 is represented only by a 6 m thick interval of marl.

6.3.2. Overpressure status

Mudstone data under investigation have been taken from the Lower Cretaceous (Cromer Knoll) and the Jurassic Heather Formation. Overpressure in the Central North Sea has been discussed in Section 2.4.2. Overpressures observed in the Lower Cretaceous (Cromer Knoll) are interpreted partly as dissipation through leakage points from the Kimmeridge Clay Formation source. And those observed in the Heather as leakage from the Upper Jurassic reservoir (Gaarenstroom et al., 1993). The Kimmeridge is highy overpressured and the Upper Jurassic sandstones vary from being normally pressured with a pressure gradient of 0.01 MPa/m near the graben margins to pressure gradient in excess of 0.02 MPa/m in the centre of the graben (Holm, 1998; Moss et al., 2003).

Possible processes that control these high pressures are sedimentation rates, low permeability, kerogen transformation, oil cracking, smectite-illite transformation and aquathermal processes. These processes have contributed to higher porosity retention at depth compared to normally pressured reservoirs, within multiple, sealed pressure compartments. These processes also controlled typically complex and highly variable migration and entrapment histories of hydrocarbons throughout the Central Graben (Cayley, 1987; Moss et al., 2003).

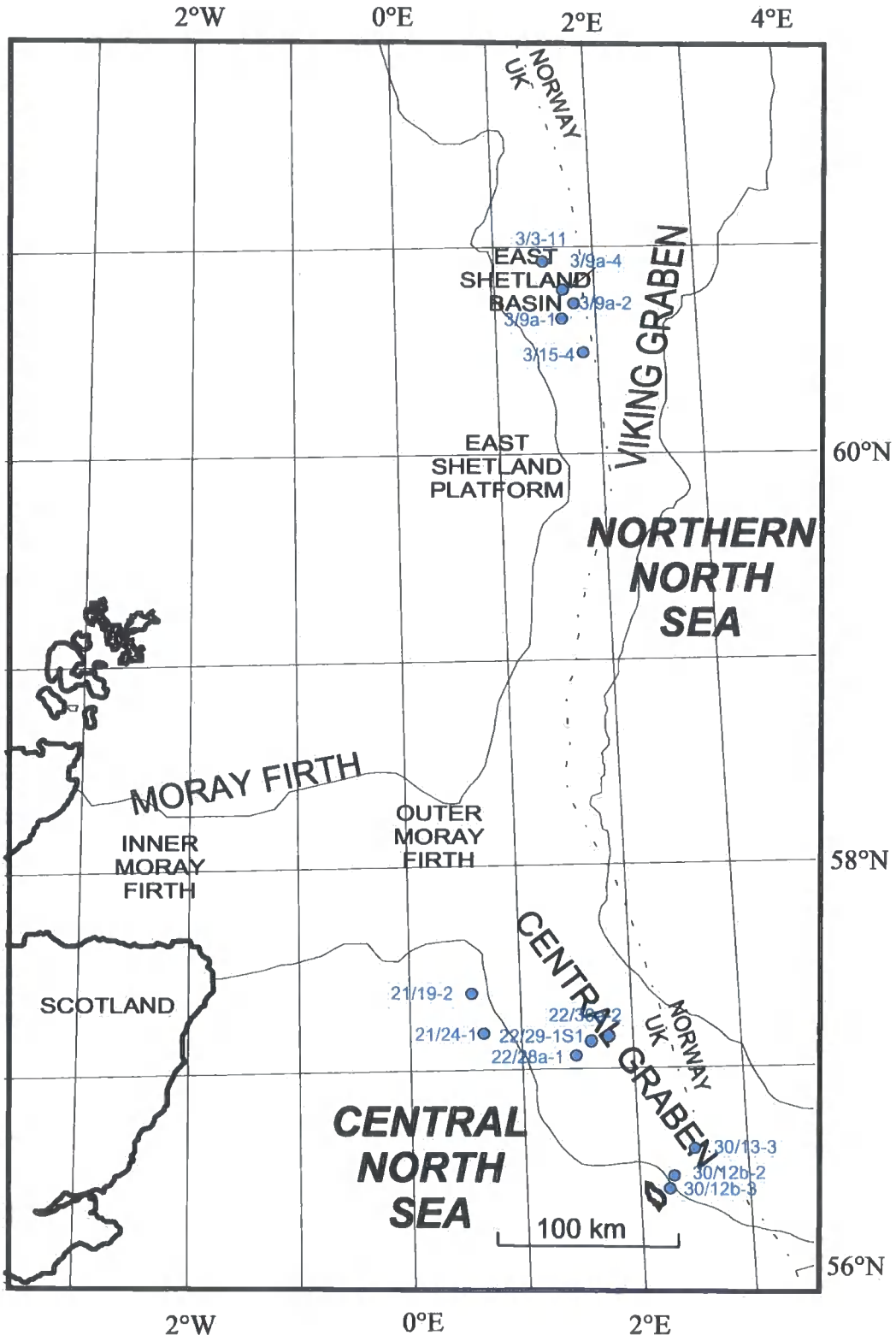

Figure 6.1. Map showing well locations in the Central Graben and the Eastern Shetland Basin.

6.4. Data selection and analysis method

6.4.1. Data selection

Data required for this analysis were sonic logs, density logs and measurements of pore pressure. The available natural gamma and resistivity logs were also used to take into account the lithology of the mudstone beds. Well data from the Lower Cretaceous (Cromer Knoll) and Jurassic (Heather) mudstones of the North Sea have been analysed. A total of eighteen wells were considered, but of them six were found to have no suitable claystones and shale data points for the study. Two of the six wells were used as neighbouring wells (22/29 -1S1 and 22/30c - 8) for pore pressure estimation in well 22/28a – 1 (see Appendix A), and the other four were used to obtain average density values above the Cretaceous in Quadrant 3 (Section 3.6.2, Chapter 3).

Beds of claystone and shale were picked in the twelve wells based on the well site geologist cuttings report/comments and lithology logs, taking $\gamma \geq 40$ °API and resistivity log values to avoid any organic-rich beds. A few data points with exceptional high resistivity were discarded, as they were outliers to the cluster of values; a threshold value of 6 Ωm was used. Furthermore, particular attention had to be paid to avoiding the inclusion of sandstones, because some Jurassic sandstone (beds and stringers) are rich in potassium feldspar which translates in high values of gamma count, i.e. $\gamma \geq 40$ API. Thus, it was decided to use the Schlumberger parameter M, which is a long established discriminant for lithological differences between shales and sandstones or limestones (Schlumberger, 1972). The parameter is defined as

$$M = \frac{\Delta t_f - \Delta t_{\log}}{\rho_{\log} - \rho_f} \times 0.01, \qquad (6.1)$$

where Δt is in μs/ft and ρ is in g/cc. For this study, Δt_f and ρ_f are taken 187 μs/ft and 1.05 g/cc, respectively.

Two different sets of data were selected for the study, namely Set A of 209 data points and Set B of 3647 data points. They are both based on individual log reading values, with an upper bound on M values of 0.65, i.e. $M \leq 0.65$. For Set A, the consistency of log data readings was assessed prior to reading selection. The digital log data are given at intervals of 0.1524 m (0.5 ft) throughout the logged interval. Intervals of 0.7 m (2.5 ft) were used to assess the consistency in lithology, i.e., intervals of 5 log values. The ranges of natural gamma log and sonic log readings over each interval are calculated as

$$dGR(M,m) = GRMax - GRmin \text{ and}$$

$$d\Delta T(M,m) = \Delta TMax - \Delta Tmin \qquad (6.2)$$

and the interval is only accepted as a data point when both $dGR(M,m) \leq 0.003$ °API and $d\Delta T(M,m) \leq 0.003$ μs/ft. This picking procedure avoids zones of lithology where the log curves were deflecting rapidly. A Visual Basic program (macro) denoted "selection" was used for data selection in each well (see Appendix B). For Set B, entire beds used for Set A were taken, i.e. claystones and shales were included if their M values were 0.65 or less.

Selected data points are from the twelve wells, located between longitudes 56° N and 62° N, and between latitudes 1° E and 4° E (Figure 6.1). The beds considered were described on the composite logs as claystones and shales, containing variable mineralogy (including the terms glauconitic, siliceous, pyritic, anhydritic). The data were classified according to the geological formation, Cromer Knoll and Heather. They were also classified in narrow ranges of M values, especially for Set B.

6.4.2. Analysis method

As in the Chalk study (Chapter 5), the initial approach was to fit V, ϕ and σ_v using a linear relationship:

$$V_p = V_o + a\,\phi + b\,\sigma_v, \qquad (6.3)$$

where V_o , a and b are parameters to be fitted. Parameters a and b are expected to be negative and positive, respectively, given that the velocity is expected to increase with

decrease in porosity and increase in vertical effective stress (e.g. Eberhart-Phillips et al., 1989).

The observed velocity was read from the sonic log. The vertical effective stress is

$$\sigma_v = S_v - P_p, \tag{6.4}$$

where S_v is the lithostatic (vertical) stress due to the overburden, and P_p is the pore pressure. And porosity was calculated from the density log by

$$\phi = \frac{\rho_{matrix} - \rho_{\log}}{\rho_{matrix} - \rho_{fluid}} \tag{6.5}$$

where $\rho_{matrix} = 2.75$ g/cc $\rho_{fluid} = 1.02$ g/cc.

In addition, two more independent variables accounting for the lithology variations have been incorporated in the inversion. These are the natural gamma ray count, γ, and the resistivity, R. Variable depth, z, was also used, but led to different outcomes (see sections 6.5 and 6.6). Equation (6.3) is extended as

$$V_p = V_o + a\,\phi + b\,\sigma_v + c\,\gamma + d\,R + e\,z \tag{6.6}$$

with c, d and e are three additional parameters to be fitted.

Pore pressure values for data points in each well were estimated from direct measurements (RFTs of Good and Fair quality). RFT data for the wells were extracted from the GeoPOP Database using PressureView2.1 or were available on the composite logs, except for well 22/28a – 1 for which RFT data from neighbouring wells were used. The regional pressure trend used is the one given in Regional Pressure Atlas of the Central North Sea (GeoPOP, 2000). Most of the available RFT measurements are in Jurassic strata. The pore pressure within the Jurassic strata generally follows trends parallel to the hydrostatic gradient, whereas the Chalk in the Central Graben is thought to be the regional seal. Therefore, values of pore pressure

in the Cromer Knoll and Heather Formations were estimated either by extrapolation from direct measurements of formation pressure available in Jurassic sands in the same wells, or by interpolation from neighbouring wells.

A regional pressure gradient trend of 10.07 MPa/km (0.445 psi/ft) was taken for the hydrostatic gradient (GeoPOP, 2000). Pore pressures in the Lower Cretaceous were estimated from RFT measurements in the Jurassic. Where these measurements were in hydrocarbon columns, the pressure in the water leg at the same depth was estimated. The latter pressures were extrapolated up to the Cromer Knoll parallel to the hydrostatic gradient (10.07 MPa/km). Data points in the Heather Formation were all in the water leg, so pressures were found by interpolating measured values. Only pressure values for well 22/28a-1 were estimated from RFT measurements in neighbouring wells, 22/29a-1S1 and 22/30c – 8. Details of the estimations are given in Appendix A.

Both sets of data were subjected to analyses as detailed in sections 6.5 and 6.6. Table 6.1 gives the overall range in values of their properties.

	Gamma ray	Bulk porosity	Sonic velocity	Resistivity	*M*
Range	40 – 112° API	0.03 – 0.34	2339 – 3674 m/s	0.17 – 5.4 Ωm	0.48 – 0.65

Table 6.1. Range values of properties for data points.

The assumption is that the data fit a linear model. A further analysis was required to interpret the parameters fitted, i.e. the results of inversion by multi-variable linear regression, and the significance of variables. A statistical test on a null hypothesis model was conducted on the parameters/coefficients. In addition to the parameter estimates, values were calculated for R^2, t-stat, P-values and the confidence interval. The t-stat values are t-statistics for the default hypothesis test that the parameter estimate is equal to 0. The P-values give the probability of observing a t-value as large or larger than the computed t-value under the null hypothesis (i.e. parameter equals 0). This P-value is needed to confirm the significance of the variable/predictor, since R^2 values are strongly influenced by violation of model assumptions, outliers and high leverage points. A P-value of 0.05 would indicate that

the parameter estimate is different from null hypothesis value at 95% confidence level. Thus, a small P-value means that the data provide evidence against the null hypothesis. A final geological interpretation is made of the statistical correlation.

6.5. Data inversion and interpretation for Set A

6.5.1. Set A of data

A total of 209 data points with values of V_p, ϕ and σ_v were obtained. They were classified according to geological formation comprising 132 in the Lower Cretaceous (Cromer Knoll) and 77 in the Jurassic (Heather Formation) (Table 6.2).

Wells	Cromer Knoll	Heather
Alwyn & Ninian Fields (Shetland Basin)		
Quadrant 3		
3/3 - 11	5	6
3/9a - 2	-	8
3/9a - 3	6	-
3/9a - 4	7	-
3/9a – N1	3	15
3/15 - 4	-	35
Central Graben		
Quadrant 21		
21/19 - 2	40	-
21/24 - 1	9	-
Quadrant 22		
22/28a - 1	58	-
22/30a - 2	2	-
Quadrant 30		
30/12b - 2	2	-
30/13 - 3	-	13
Total	132	77

Table 6.2. Wells used and number of data points picked for the shale study.

The data points, labelled from 1 to 209 (with their respective variables: porosity, velocity, overburden stress, pore pressure, vertical effective stress, etc.), are given in Section 6.9 (Table 6.10). Meanwhile, distributions of these variables across the formations/quadrants are showed in Figures 6.2 - 6.5.

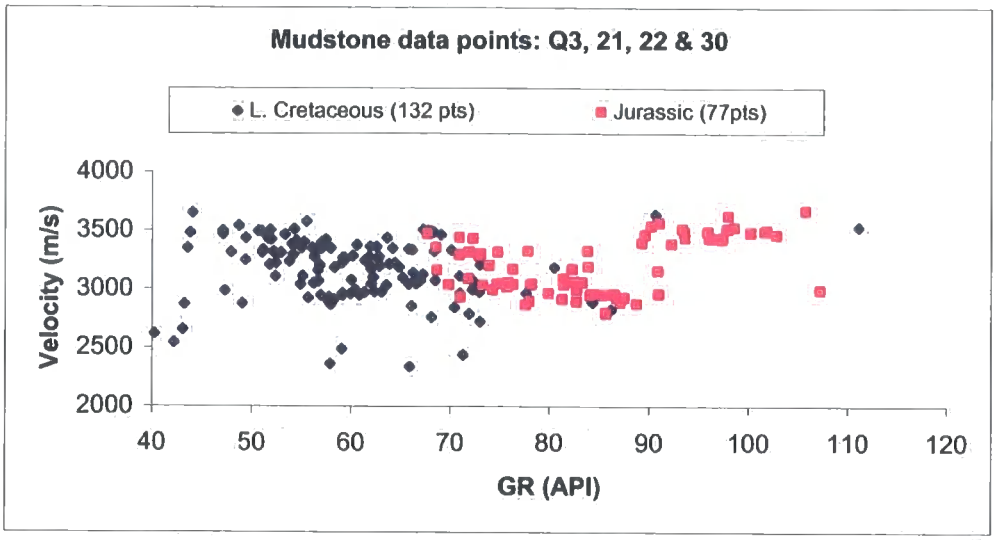

Figure 6.2. Range distribution of sonic velocity and natural gamma count for the 209 data points selected.

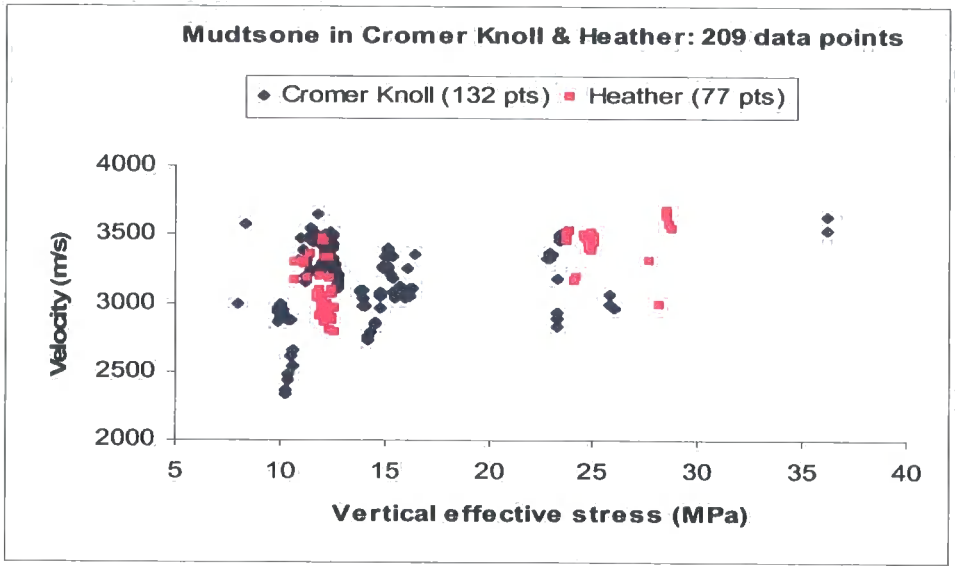

Figure 6.3. Plot of velocity vs. vertical effective stress from calculated lithostatic stress and (mostly extrapolated) pore pressures.

Figure 6.4 shows that there is a clear correlation between velocity and porosity. Estimated values of pore pressure for the 209 data points are plotted in Figure 6.5, portraying the overpressure status across quadrants and formations.

Pore pressure values for data points in each well were estimated from direct measurements (RFTs of Good and Fair quality). A regional pressure gradient trend of 10.07 MPa/km (0.445 psi/ft) was taken for the hydrostatic gradient (GeoPop, 2000).

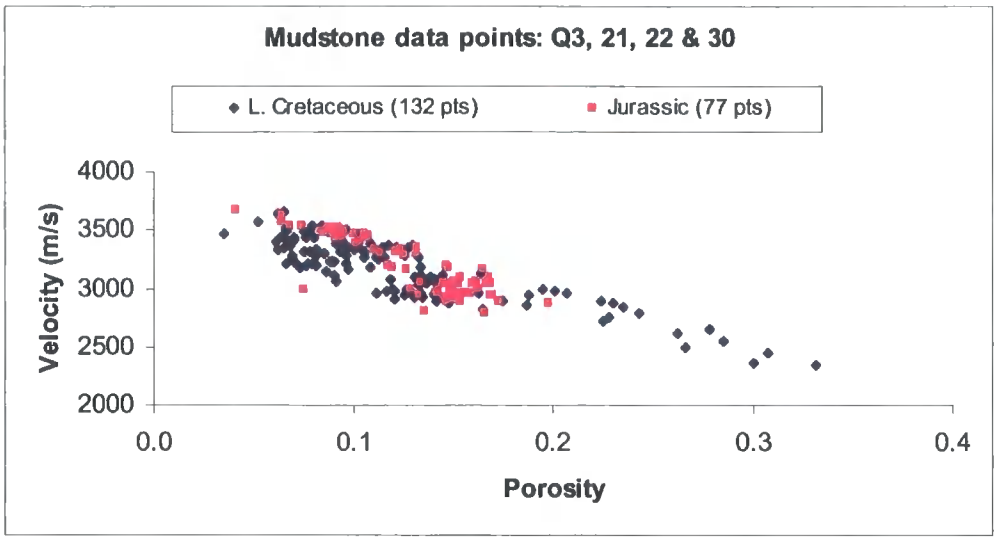

Figure 6.4. Plot of velocity vs. porosity for the 209 data points selected.

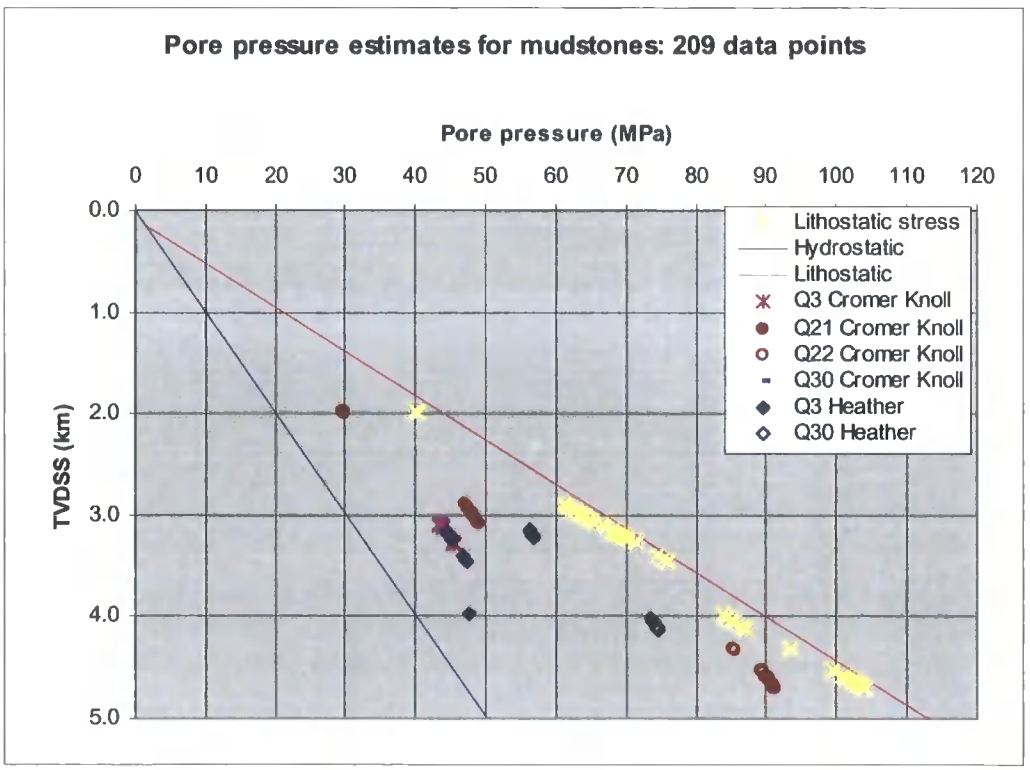

Figure 6.5. Pressure-depth plot for pore pressure estimates in Lower Cretaceous and Jurassic claystones and shale: 209 data points.

Pore pressures in the Lower Cretaceous were estimated from RFT measurements in the Jurassic. Where these measurements were in hydrocarbon columns, the pressure in the water leg at the same depth was estimated. The latter pressures were extrapolated up to the Cromer Knoll parallel to the hydrostatic gradient (10.07

MPa/km). Data points in the Heather Formation were all in the water leg, so pressures were found by interpolating measured values. Only pressure values for well 22/28a-1 were estimated from RFT measurements in a neighbouring well, 22/29a-1S1.

6.5.2. Results of the inversion

Set A comprises 132 data points in the Cromer Knoll and 77 data points in the Heather Formation. Sets of data (V_p, ϕ, σ_v, γ, R) were used to estimate parameters V_0, a, b, c and d in Equation (6.6) using linear inversion. Physical properties of mudstones, as well as mineralogy, vary with temperature (Bethke, 1985; Johnston, 1987; Dudek et al., 2002). Given that temperature increases with depth, the depth was included as an extra independent variable – denoted as z with associated parameter e - in the inversion. Inversion runs were made with values of V_p, ϕ, σ_v only, and then with values of γ, R, z added in all possible combinations. Results of the inversion along with summaries of hypothesis test and regression statistics (i.e., estimates of V_0 and parameters a, b, c, d and e; with RMS error, coefficient of determination, t-stat, P-values, etc.) are presented in Table 6.3 for the Cromer Knoll and Table 6.4 for the Heather. Depth did not yield significant improvement to the fit in the Cromer Knoll, while it did in the Heather. Figure 6.6 is a plot of the bulk porosity vs. depth.

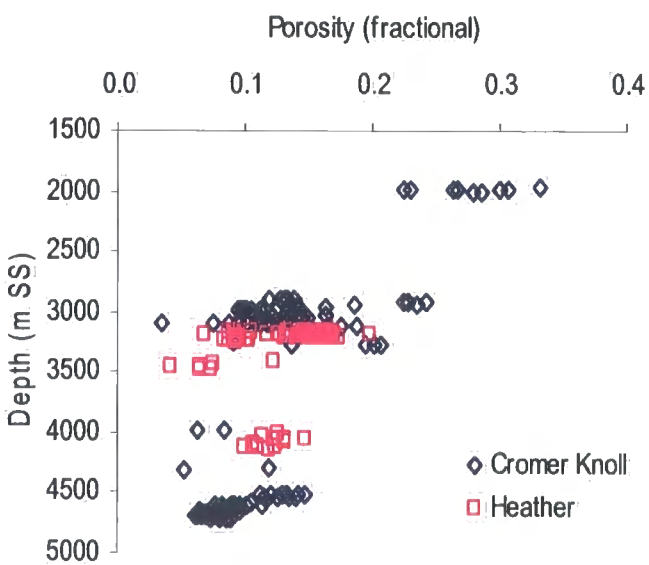

Figure 6.6. Plot of porosity vs. depth.

6.5.2.1. Cromer Knoll: 132 data points

Parameters fitted	V_0 m/s	a(Φ) m/s	b(σ_v) m/s/MPa	c(γ) m/s/°API	d(R) m/s/ Ωm	e(z) 1/s	R^2	RMS error
Data Range		*0.035 – 0.332*	*8.0 – 36.1 MPa*	*40 – 111.1 °API*	*0.43 – 3.15 Ωm*	*1976 – 4707 m SS*		
V(ϕ, σ_v, GR, R, z)	**3847**	**-3752**	**17.1**	**-8.2**	**39.5**	**-0.005**	*0.863*	*100.01*
Standard Error	104.76	256.74	3.44	1.31	19.17	0.017		
t Stat	36.72	-14.62	4.98	-6.24	2.06	-0.288		
P-value	0.00	0.00	0.00	0.00	0.04	0.774		
Lower 95%	3639.66	-4260.5	10.33	-10.78	1.56	-0.038		
Upper 95%	4054.3	-3244.4	23.9	-5.6	77.4	0.029		
V(ϕ, σ_v, GR, R)	**3822**	**-3695**	**17.6**	**-8.29**	**39.88**		*0.863*	*99.65*
Standard Error	58.8	160.78	3.09	1.25	19.06			
t Stat	65	-22.98	5.68	-6.65	2.09			
P-value	0.00	0.00	0.00	0.00	0.04			
Lower 95%	3705.67	-4012.99	11.44	-10.76	2.17			
Upper 95%	3938.38	-3376.7	23.68	-5.83	77.59			
V(ϕ, σ_v)	**3515**	**-3972**	**9.7**				*0.798*	*119.93*
Standard Error	39.36	181.9	2.01					
t Stat	89.3	-21.83	4.82					
P-value	0.00	0.00	0.00					
Lower 95%	3437.03	-4331.45	5.71					
Upper 95%	3592.78	-3611.68	13.66					
V(ϕ, σ_v, z)	**3783**	**-4470**	**6.9**			**-0.045**	*0.806*	*117.82*
Standard Error	118.99	275.34	2.3			0.019		
t Stat	31.79	-16.23	2.99			-2.378		
P-value	0.00	0.00	0.00			0.019		
Lower 95%	3547.11	-5014.61	2.33			-0.082		
Upper 95%	4018	-3924.98	11.43			-0.007		
GAMMA RAY COUNT RESPONSE IN CROMER KNOLL								
V(ϕ, σ_v, GR, z)	**3894**	**-3883**	**21.1**	**-8.8**		**-0.007**	*0.858*	*101.28*
Standard Error	103.59	251.94	2.88	1.29		0.017		
t Stat	37.59	-15.41	7.33	-6.8		-0.425		
P-value	0.00	0.00	0.00	0.00		0.671		
Lower 95%	3688.63	-4381.62	15.42	-11.36		-0.041		
Upper 95%	4098.6	-3384.52	26.82	-6.24		0.026		
V(ϕ, σ_v, GR)	**3857**	**-3799**	**21.8**	**-9.0**			*0.858*	*100.96*
Standard Error	57.12	154.92	2.36	1.22				
t Stat	67.52	-24.52	9.23	-7.35				
P-value	0.00	0.00	0.00	0.00				
Lower 95%	3743.9	-4105.31	17.14	-11.39				
Upper 95%	3969.96	-3492.24	26.49	-6.56				

RESISTIVITY RESPONSE IN CROMER KNOLL							
V(ϕ, σv, R, z)	**3717**	**-4180**	**1.8**	**66.7**	**-0.036**	*0.820*	*113.96*
Standard Error	116.98	281.9	2.74	21.27	0.018		
t Stat	31.77	-14.83	0.67	3.13	-1.973		
P-value	0.00	0.00	0.5	0	0.051		
Lower 95%	3485.47	-4738.02	-3.59	24.57	-0.072		
Upper 95%	3948.44	-3622.36	7.27	108.76	0		
V(ϕ, σv, R)	**3498**	**-3758**	**3.6**	**72.8**		*0.815*	*115.24*
Standard Error	38.13	185.6	2.63	21.28			
t Stat	91.76	-20.25	1.37	3.42			
P-value	0.00	0.00	0.17	0			
Lower 95%	3422.98	-4125.2	-1.6	30.71			
Upper 95%	3573.86	-3390.71	8.79	114.92			

Table 6.3. Estimates of parameters a, b, c, d, e in the Cromer Knoll for data points in Set A, with their P-values.

The differences between the measured V_p values and those calculated using the parameters above (i.e., the velocity discrepancies) were found, and the root mean square (RMS) error calculated as:

$$\Delta V = \sqrt{\frac{\sum (\Delta V_i)^2}{n-k}}, \qquad (6.7)$$

where ΔV_i is the velocity discrepancy, $i = 1,\ldots n$; n = number of data points fitted and k = dimension of the data.

The coefficients of determination, i.e. R^2, range from 0.798 for (V_p, ϕ, σ_v) to 0.863 for (V_p, ϕ, σ_v, γ, R). The lowest standard error (RMS error) is given by

V_0 (m/s)	a (m/s)	b (m/s/MPa)	c (m/s/API)	d (m/s/Ohmm)
3822	- 3695	17.6	- 8.3	40.0

giving

$$V_p = 3822 - 3695\ \phi + 17.6\ \sigma_v - 8.3\ \gamma + 40.0\ R \qquad (6.8)$$

with a RMS error of 100 m/s.

But resistivity, R, depends on many factors and the effect of σ_v on V_p may be masked by its inclusion as an independent variable. As we need to know how sonic velocity

depends on vertical effective stress, and the response of the natural gamma log is independent of σ_v, we suggest that the most meaningful result is given by

V_0 (m/s)	a (m/s)	b (m/s/MPa)	c (m/s/API)
3857	– 3799	21.8	- 9.0

giving

$$V_p = 3857 - 3799\,\phi + 21.8\,\sigma_v - 9.0\,\gamma \qquad (6.9)$$

with a RMS error of 101 m/s.

6.5.2.2. Heather Formation: 77 data points

Parameters fitted	V_0 m/s	a(Φ) m/s	b(σ_v) m/s/MPa	c(γ) m/s/°API	d(R) m/s/ Ωm	e(z) 1/s	R^2	RMS error
Data Range		*0.042 – 0.20*	*10.6 – 28.8 MPa*	*67.7 – 107.2 °API*	*0.17 – 5.04 Ωm*	*3151 – 4127 m SS*		
V(ϕ, σ_v, GR, R, z)	**3346**	**-4289**	**18.1**	**-5.0**	**4.53**	**0.152**	*0.817*	*107.97*
Standard Error	425.01	859.14	4.51	2.26	9.59	0.058		
t Stat	7.87	-4.99	4.01	-2.21	0.47	2.606		
P-value	0.00	0.00	0.00	0.03	0.64	0.011		
Lower 95%	2498.8	-6002.3	9.07	-9.51	-14.59	0.036		
Upper 95%	4193.7	-2576.2	27.04	-0.48	23.66	0.268		
V(ϕ, σ_v, GR, R)	**4351**	**-5836**	**12.8**	**-7.3**	**-1.37**		*0.800*	*112.23*
Standard Error	185.76	645.7	4.19	2.16	9.69			
t Stat	23.42	-9.04	3.06	-3.39	-0.14			
P-value	0.00	0.00	0.00	0.00	0.89			
Lower 95%	3980.8	-7123.1	4.45	-11.64	-20.68			
Upper 95%	4721.5	-4548.7	21.16	-3.02	17.94			
V(ϕ, σ_v)	**3878**	**-5839**	**3.8**				*0.761*	*120.92*
Standard Error	139.71	695.17	3.51					
t Stat	27.75	-8.4	1.08					
P-value	0	0	0.28					
Lower 95%	3599.1	-7224.2	-3.21					
Upper 95%	4155.9	-4453.9	10.78					
V(ϕ, σ_v, z)	**2743**	**-3740**	**14.7**			**0.204**	*0.805*	*110.08*
Standard Error	308.5	819.18	4.19			0.051		
t Stat	8.89	-4.57	3.52			4.036		
P-value	0.00	0.00	0.00			0.00		
Lower 95%	2128.3	-5372.3	6.39			0.103		
Upper 95%	3358	-2107	23.1			0.305		

GAMMA RAY COUNT RESPONSE IN HEATHER							
V(ϕ, σv, GR, z)	**3374**	**-4345**	**17.4**	**-4.73**	**0.146**	*0.817*	*107.39*
Standard Error	418.64	846.48	4.27	2.18	0.056		
t Stat	8.06	-5.13	4.08	-2.17	2.581		
P-value	0.00	0.00	0.00	0.03	0.012		
Lower 95%	2539.6	-6032.2	8.89	-9.09	0.033		
Upper 95%	4208.6	-2657.3	25.92	-0.38	0.258		
V(ϕ, σv, GR)	**4356**	**-5839**	**12.9**	**-7.5**		*0.800*	*111.47*
Standard Error	181.3	640.89	4.05	1.99			
t Stat	24.03	-9.11	3.19	-3.75			
P-value	0.00	0.00	0.00	0.00			
Lower 95%	3994.7	-7116.7	4.86	-11.41			
Upper 95%	4717.4	-4562.1	21.02	-3.49			
RESISTIVITY RESPONSE IN HEATHER							
V(ϕ, σv, R, z)	**2752**	**-3752**	**14.7**	**-0.7**	**0.203**	*0.805*	*110.84*
Standard Error	337.55	845.82	4.35	9.54	0.055		
t Stat	8.15	-4.44	3.37	-0.07	3.692		
P-value	0.00	0.00	0.00	0.95	0.00		
Lower 95%	2079.2	-5438.5	6	-19.67	0.093		
Upper 95%	3425	-2066.2	23.35	18.38	0.313		
V(ϕ, σv, R)	**3903**	**-5804**	**3.86**	**-13.8**		*0.768*	*120.04*
Standard Error	139.86	690.56	3.49	9.59			
t Stat	27.91	-8.4	1.11	-1.44			
P-value	0.00	0.00	0.27	0.15			
Lower 95%	3624.7	-7180.4	-3.08	-32.94			
Upper 95%	4182.2	-4427.8	10.81	5.27			

Table 6.4. Estimates of parameters *a*, *b*, *c*, *d*, *e* in the Heather Formation for data points in Set A, with their P-values.

In contrast to the Cromer Knoll results (Table 6.3), depth has a robust response where it is included in the inversion. However, resistivity does not have a robust P-value, so there is definitely no case for including it as an independent variable. Moreover, the lowest standard error (RMS error) of 107 m/s is achieved by

V_0 (m/s)	a (m/s)	b (m/s/MPa)	c (m/s/API)	e (1/s)
3374	- 4345	17.4	- 4.7	0.146

giving

$$V_p = 3374 - 4345\ \phi + 17.4\ \sigma_v - 4.7\ \gamma + 0.146\ z \qquad (6.10).$$

Equation (6.10) has robust probability values for all variables. Thus, it is statistically considered as the best result in Table 6.4.

6.5.3. Interpretation of the results

Figures 6.7 and 6.8 are plots of the observed variables within respective formations. They confirm that within formations there is strong correlation between velocity and porosity. Also, vertical effective stress and porosity are very weakly correlated, especially in the Cromer Knoll, and so may be considered as independent variables. A fit of velocity to porosity only gives respectively $V_p = 3363 - 4007\ \phi$ with a RMS error of 130 m/s (Figure 6.7 a) in the Cromer Knoll, and $V_p = 4016 - 6437\ \phi$ with a RMS error of 121 m/s (Figure 6.8 a) in the Heather Formation.

Furthermore, results in Table 6.3 and Table 6.4 have shown that the extra independent variable gamma ray count has a robust response (P-value) in the linear fit, and its introduction has significantly reduced the RMS error between observed and forward-calculated velocities, respectively in the range of 20 m/s in the Cromer Knoll and 10 m/s in the Heather. Also, the fitted parameter b has more than doubled. The slightly lower error obtained in introducing resistivity could not warrant its inclusion, as resistivity can be masking the effect of σ_v on V_p. Meanwhile, depth has contributed to better correlation only in the Heather. Its coefficient parameter e happens to be negative and not significant for the Cromer Knoll set of data, but is positive and significant in the Heather.

In summary, Equations (6.9) - (6.12) suggest

- that there is a strong dependence of velocity on porosity in the data set under study, both in the Cromer Knoll and in the Heather;
- that there is a slight dependence of sonic velocity on vertical effective stress when porosity and vertical effective stress are taken as independent variables;
- that lithology variation in terms of natural gamma ray count has got an impact on the relationship; and
- that dependence on depth as an independent variable is robust in the Heather Formation only.

Hence, within the limits of our data set equations (6.9) and (6.10) are the preferred to the results of the investigation at this stage.

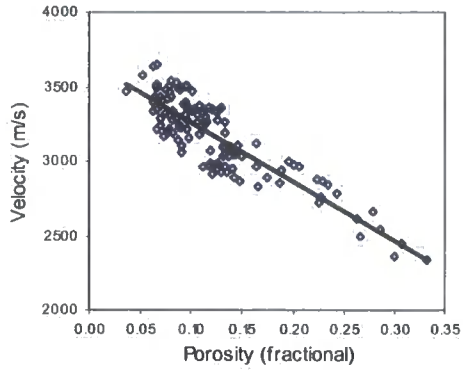

(a) Observed velocity vs. porosity, with the best-fit straight line given by $V_p = 3363 - 4007\ \phi$, $R^2 = 0.761$.

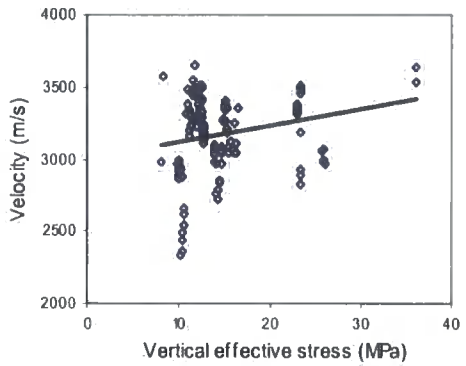

(b) Observed velocity vs. vertical effective stress.

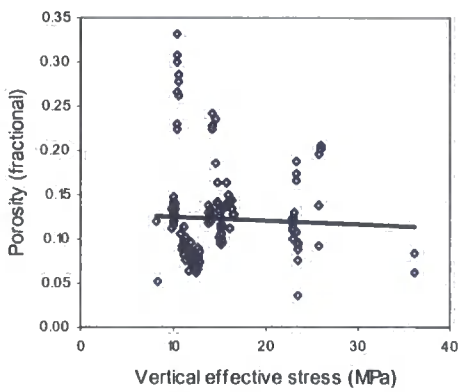

(c) Porosity vs. vertical effective stress.

Figure 6.7. Cromer Knoll data points (132).

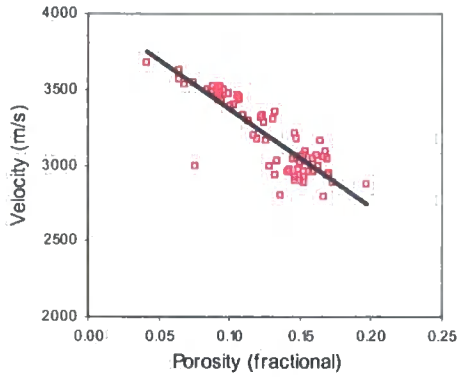

(a) Observed velocity vs. porosity, with the best-fit straight line given by $V_p = 4016 - 6437\ \phi$, $R^2 = 0.756$.

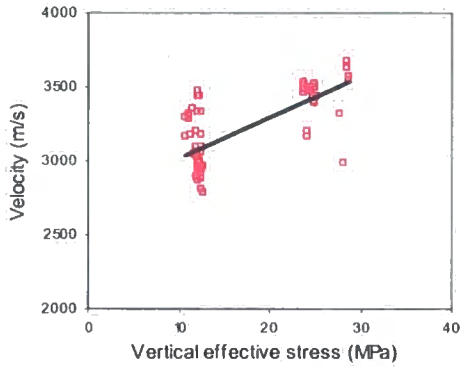

(b) Observed velocity vs. vertical effective stress.

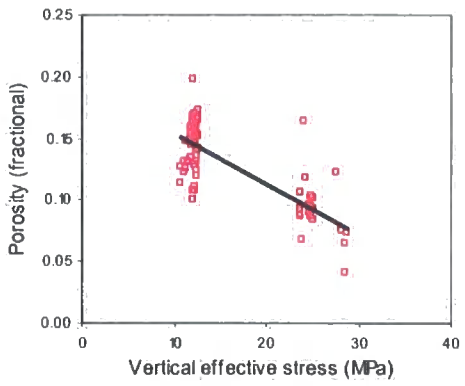

(c) Porosity vs. vertical effective stress

Figure 6.8. Heather data points (77).

The overall results suggest that variations of properties in each formation may follow different trends, which may be ascribed to differences in lithology (texture, grain size distribution and mineralogy) or chemical compaction processes. Chemical compaction processes include chemical dissolution and precipitation and become active below depth 2 – 3 km. These processes are functions of temperature and mineralogy rather than effective stress (Skempton, 1970; Bjørlykke and Høeg, 1997).

6.6. Data inversion and interpretation for Set B

6.6.1. Set B of data

When digital log data became available, it was relatively straightforward to repeat the analysis using individual data points. The only discriminant was to reject data points with $M > 0.65$. The data form set B, as defined in section 6.4.1. The first analysis fits the variables as in section 6.5, and is followed by an analysis of subsets of the data classified according to the M parameter.

Inclusion in the analysis of depth as an independent variable and the lithology variables, gamma count ray and resistivity, did not yield exactly the same response in either formation in the inversion of Set A of data (Section 6.5). In order to assess the extent of chemical diagenesis and mineralogy variation, an analysis with data selected as individual log readings from "undifferentiated" mudstone beds was carried out. Complete beds of mudstone lithology from the Heather Formation and the Cromer Knoll were used. Whilst limestone stringers and sandstones beds were carefully avoided, data selection was made with upper bound on M values of 0.65, yielding a data set of 3647 data points, Set B. Of these data points, 2308 were obtained from mudstones in the Cromer Knoll and 1339 were obtained from the Heather Formation.

Different Visual Basic programs (macros) were used to compute the variables for running the generalised linear inversion (Appendix B). Table 6.5 gives the distribution of the data across wells and formations. Respective results of the inversion are given in Tables 6.6 and 6.7.

Wells	Cromer Knoll	Heather
Alwyn & Ninian Fields (Shetland Basin)		
Quadrant 3		
3/3 - 11	130	298
3/9a - 2	-	55
3/9a - 3	33	-
3/9a - 4	44	-
3/9a – N1	32	346
3/15 - 4	-	405
Central Graben		
Quadrant 21		
21/19 - 2	769	
21/24 - 1	200	
Quadrant 22		
22/28a - 1	1027	
22/30a - 2	45	
Quadrant 30		
30/12b - 2	25	
30/13 - 3	3	235
Total	2308	1339
Total for Set B: 3647 data points		

Table 6.5. Distribution of data by well and formation (Set B).

6.6.2. Results of the inversion

The respective runs have the following outputs.

Cromer Knoll: 2308 data points

Parameters fitted	Vo m/s	a(Φ) m/s	b(σ_v) m/s/MPa	c(γ) m/s/°API	d(R) m/s/ Ωm	e(z) 1/s	*R Square*	*RMS error*
Data Range		*0.173 – 0.342 fraction*	*7.9 – 36.4 MPa*	*40 – 192 °API*	*0.40 – 0.51 Ohmm*	*1972 - 4715 m*		
V(ϕ, σ_v, GR, R, z)	**3516**	**-3261**	**12.5**	**-5.0**	**25.49**	**0.038**	*0.783*	*129.42*
Standard Error	30.54	69.51	0.87	0.32	4.45	0.005		
t Stat	115.12	-46.92	14.36	-15.45	5.73	7.592		
P-value	0.00	0.00	0.00	0.00	0.00	0.00		
Lower 95%	3456.03	-3397.59	10.78	-5.64	16.77	0.028		
Upper 95%	3575.81	-3124.99	14.19	-4.37	34.22	0.047		
V(ϕ, σ_v, GR, R)	**3716**	**-3659**	**9.4**	**-4.55**	**31.37**		*0.778*	*131.00*
Standard Error	15.56	46.23	0.78	0.32	4.44			
t Stat	238.87	-79.14	12.09	-14.12	7.07			
P-value	0.00	0.00	0.00	0.00	0.00			
Lower 95%	3685.76	-3749.67	7.9	-5.19	22.67			
Upper 95%	3746.78	-3568.34	10.96	-3.92	40.07			

$V(\phi, \sigma_v)$	**3585**	**-3865**	**3.9**			*0.753*	*138.17*
Standard Error	10.64	46.26	0.59				
t Stat	336.75	-83.55	6.66				
P-value	0.00	0.00	0.00				
Lower 95%	3563.85	-3955.93	2.78				
Upper 95%	3605.6	-3774.49	5.1				
$V(\phi, \sigma_v, z)$	**3414**	**-3554**	**5.6**		**0.029**	*0.756*	*137.23*
Standard Error	31.71	71.31	0.65		0.005		
t Stat	107.66	-49.83	8.52		5.711		
P-value	0.00	0.00	0.00		0.00		
Lower 95%	3351.8	-3693.56	4.29		0.019		
Upper 95%	3476.16	-3413.86	6.85		0.039		
GAMMA RAY COUNT RESPONSE IN CROMER KNOLL							
$V(\phi, \sigma_v, GR, z)$	**3513**	**-3276**	**14.2**	**-5.16**	**0.043**	*0.780*	*130.31*
Standard Error	30.75	69.94	0.82	0.33	0.005		
t Stat	114.25	-46.84	17.21	-15.88	8.662		
P-value	0.00	0.00	0.00	0.00	0.00		
Lower 95%	3452.57	-3413.16	12.56	-5.80	0.033		
Upper 95%	3573.16	-3138.87	15.79	-4.53	0.052		
$V(\phi, \sigma_v, GR)$	**3746**	**-3744**	**11.1**	**-4.7**		*0.773*	*132.39*
Standard Error	15.15	45.12	0.75	0.33			
t Stat	247.30	-82.98	14.69	-14.38			
P-value	0.00	0.00	0.00	0.00			
Lower 95%	3716.07	-3832.43	9.59	-5.32			
Upper 95%	3775.48	-3655.47	12.54	-4.04			
RESISTIVITY RESPONSE IN CROMER KNOLL							
$V(\phi, \sigma_v, R, z)$	**3421**	**-3525**	**3.8**	**31.3**	**0.024**	*0.761*	*135.93*
Standard Error	31.43	70.77	0.70	4.66	0.01		
t Stat	108.86	-49.82	5.47	6.73	4.60		
P-value	0.00	0.00	0.00	0.00	0.00		
Lower 95%	3359.81	-3663.95	2.45	22.20	0.01		
Upper 95%	3483.08	-3386.41	5.18	40.47	0.03		
$V(\phi, \sigma_v, R)$	**3557**	**-3767**	**2.3**	**34.8**		*0.759*	*136.53*
Standard Error	11.15	47.52	0.62	4.62			
t Stat	318.90	-79.28	3.76	7.54			
P-value	0.00	0.00	0.00	0.00			
Lower 95%	3534.89	-3860.56	1.12	25.75			
Upper 95%	3578.63	-3674.20	3.56	43.86			

Table 6.6. Estimates of parameters *a*, *b*, *c*, *d*, *e* in the Cromer Knoll for data points in Set B, with their P-values.

Heather: 1339 data points

Parameters fitted	V_0 m/s	a(Φ) m/s	b(σ_v) m/s/MPa	c(γ) m/s/°API	d(R) m/s/ Ωm	e(z) 1/s	R^2	RMS error
Data Range		*0.005 – 0.212 fraction*	*10.6 – 28.8 MPa*	*61.2 – 125.3 °API*	*0.78 – 5.83 Ohmm*	*3143 – 4128 m*		
V(ϕ, σ_v, GR, R, z)	**2662**	**-2797**	**14.1**	**-6.4**	**69.6**	**0.290**	*0.748*	*116.30*
Standard Error	82.59	147.89	0.84	0.46	4.27	0.015		
t Stat	32.23	-18.91	16.82	-13.84	16.32	19.904		
P-value	0.00	0.00	0.00	0.00	0.00	0.00		
Lower 95%	2500.23	-3086.78	12.42	-7.35	61.26	0.261		
Upper 95%	2824.29	-2506.55	15.7	-5.52	77.99	0.318		
V(ϕ, σ_v, GR, R)	**4132**	**-4386**	**7.8**	**-7.28**	**29.26**		*0.673*	*132.41*
Standard Error	42.16	141.88	0.88	0.53	4.27			
t Stat	98	-30.88	8.84	-13.81	6.85			
P-value	0.00	0.00	0.00	0.00	0.00			
Lower 95%	4049.05	-4660	6.07	-8.31	20.88			
Upper 95%	4214.46	-4103.34	9.52	-6.24	37.64			
V(ϕ, σ_v)	**3697**	**-4484**	**2.8**				*0.626*	*141.46*
Standard Error	29.9	149.32	0.78					
t Stat	123.63	-30.03	3.66					
P-value	0.00	0.00	0.00					
Lower 95%	3638.36	-4777.14	1.32					
Upper 95%	3755.69	-4191.3	4.37					
V(ϕ, σ_v, z)	**2669**	**-3118**	**10.7**			**0.210**	*0.684*	*130.00*
Standard Error	70.98	162.46	0.87			0.01		
t Stat	37.6	-19.19	12.29			15.71		
P-value	0.00	0.00	0.00			0.00		
Lower 95%	2529.77	-3436.81	9.02			0.19		
Upper 95%	2808.26	-2799.39	12.45			0.24		
GAMMA RAY COUNT RESPONSE IN HEATHER								
V(ϕ, σ_v, GR, z)	**3058**	**-3207**	**13.1**	**-3.56**		**0.177**	*0.697*	*127.35*
Standard Error	86.46	159.58	0.91	0.47		0.01		
t Stat	35.37	-20.10	14.40	-7.56		12.60		
P-value	0.00	0.00	0.00	0.00		0.00		
Lower 95%	2888.16	-3519.98	11.35	-4.49		0.15		
Upper 95%	3227.39	-2893.87	14.93	-2.64		0.20		
V(ϕ, σ_v, GR)	**4035**	**-4269**	**8.6**	**-5.54**			*0.661*	*134.67*
Standard Error	40.42	143.32	0.89	0.47				
t Stat	99.84	-29.78	9.71	-11.79				
P-value	0.00	0.00	0.00	0.00				
Lower 95%	3956.05	-4549.97	6.88	-6.46				
Upper 95%	4114.64	-3987.65	10.36	-4.62				

RESISTIVITY RESPONSE IN HEATHER							
$V(\phi, \sigma_v, R, z)$	**2188**	**-2791**	**10.0**	**47.29**	**0.308**	*0.711*	*124.33*
Standard Error	80.33	158.10	0.84	4.22	0.02		
t Stat	27.23	-17.65	11.99	11.20	19.88		
P-value	0.00	0.00	0.00	0.00	0.00		
Lower 95%	2030.12	-3101.01	8.40	39.01	0.28		
Upper 95%	2345.31	-2480.71	11.69	55.57	0.34		
$V(\phi, \sigma_v, R)$	**3697**	**-4490**	**2.8**	**0.87**		*0.626*	*141.50*
Standard Error	29.94	151.39	0.86	4.00			
t Stat	123.45	-29.66	3.22	0.22			
P-value	0.00	0.00	0.00	0.83			
Lower 95%	3637.99	-4786.58	1.08	-6.98			
Upper 95%	3755.48	-4192.59	4.45	8.72			

Table 6.7 Estimates of parameters a, b, c, d, e in the Heather Formation for data points in Set B, with their P-values.

These results (Tables 6.6 and 6.7) show the same response in terms of the significance of different variables as in Set A; but with a lesser correlation. The RMS error ranges from 116 – 142 m/s against 100 – 120 m/s for Set A results.

6.6.3. Inversion for narrow ranges of M value

Different inversion results (Table 6.3 – 6.4 for Set A, Tables 6.6 – 6.7 for Set B) show that porosity is the most significant variable or best predictor of V_p, since its P-values are consistently robust throughout with a good correlation when velocity is treated as a function of porosity and vertical effective stress. The vertical effective stress response is also a good predictor for V_p, for its associated parameter b varies a lot from one set to another, and from one formation to another. This suggests that there are systematic differences in lithologies between mudstones in the Cromer Knoll and the Heather Formation.

The M parameter, as defined in Equation 6.1, is a lithology-dependent quantity defined from porosity (sonic and density) logs. As used in the cross-plot it is defined for, its value depends on the proportions of different minerals, such as calcite, silica/quartz, anhydrite, dolomite, gypsum within the lithology (Schlumberger, 1972). The shale region is approximately between M of 0.50 and 0.65. Thus, data points of

Set B were grouped into narrow ranges of M, then inverted to assess if there is any consistent trend in the variable coefficients with M. Data distribution is given in Table 6.8 and results of the inversion in Table 6.9. The results show no trend with M values.

M ranges ▶	0.50 – 0.53	0.54 – 0.57	0.58 – 0.61	0.62 – 0.65
Cromer Knoll	73	261	804	932
Heather	7	168	309	753
Total	80	429	1113	1685

Table 6.8. Distribution of data in ranges of M values (Set B).
[The Heather set for M range values 0.50 – 0.53 is reduced to a single well].

CROMER KNOLL FORMATION									HEATHER FORMATION								
	Vo m/s	*a* m/s	*b* m/s/MPa	c m/s/° API	*d* m/s/ Ωm	*e* 1/s	Data points	RMS error		*Vo* m/s	*a* m/s	*b* m/s/MPa	c m/s/° API	*d* m/s/ Ωm	*e* 1/s	Data points	RMS error
V(ϕ, σ_v, GR, R, z)									**V(ϕ, σ_v, GR, R, z)**								
M: 0.50 – 0.53	3010	-2092	2.4	0.76	-3.05	-0.017	73	30.1	M: 0.50 – 0.53	-6438	-2655	0.0	8.21	-58.33	2.838	7	10.6
M: 0.54 – 0.57	3281	-2530	0.96	-0.44	-5.56	0.001	261	39.5	M: 0.54 – 0.57	3459	-2552	3.0	-1.76	-12.84	-0.015	168	38.1
M: 0.58 – 0.61	3525	-3117	2.80	-1.62	6.13	0.007	1003	54.4	M: 0.58 – 0.61	3422	-2914	4.7	-1.97	8.30	0.031	411	53.1
M: 0.62 – 0.65	3658	-3640	1.90	-0.47	21.14	0.015	932	59.0	M: 0.62 – 0.65	3394	-3959	-0.5	-0.11	16.890	0.552	753	55.6
V(ϕ, σ_v, GR, R)									**V(ϕ, σ_v, GR, R)**								
M: 0.50 – 0.53	2965	-1998	3.6	0.43	-19.50		73	30.1	M: 0.50 – 0.53	170	-2655	198.5	8.21	-58.33		7	10.6
M: 0.54 – 0.57	3284	-2537	0.9	-0.43	-5.37		261	39.4	M: 0.54 – 0.57	3407	-2541	2.90	-1.78	-11.25		168	38.0
M: 0.58 – 0.61	3564	-3196	2.0	-1.50	6.79		1003	54.6	M: 0.58 – 0.61	3556	-3057	4.10	-1.87	3.90		411	53.4
M: 0.62 – 0.65	3735	-3785	1.2	-0.36	21.41		932	59.3	M: 0.62 – 0.65	3864	-4209	-2.30	-0.18	10.09		753	56.3
V(ϕ, σ_v)									**V(ϕ, σ_v)**								
M: 0.50 – 0.53	2966	-1951	3.8				73	29.8	M: 0.50 – 0.53	1832	-3442	115.0				7	9.3
M: 0.54 – 0.57	3254	-2508	0.4				261	39.6	M: 0.54 – 0.57	3321	-2861	-1.1				168	39.7
M: 0.58 – 0.61	3509	-3229	0.1				1003	55.9	M: 0.58 – 0.61	3434	-3056	2.6				411	54.8
M: 0.62 – 0.65	3743	-3894	1.9				932	61.0	M: 0.62 – 0.65	3861	-4246	-1.3				753	57.0
V(ϕ, σ_v, z)									**V(ϕ, σ_v, z)**								
M: 0.50 – 0.53	3004	-2008	3.8			-0.011	73	29.9	M: 0.50 – 0.53	3005	-2008	3.8			-0.011	7	29.9
M: 0.54 – 0.57	3274	-2540	0.1			-0.003	261	39.6	M: 0.54 – 0.57	3313	-2856	-1.1			0.002	168	39.9
M: 0.58 – 0.61	3506	-3223	0.2			0.001	1003	60.0	M: 0.58 – 0.61	3321	-2924	3.1			0.027	411	54.6
M: 0.62 – 0.65	3665	-3754	2.4			0.014	932	60.5	M: 0.62 – 0.65	3807	-4199	-0.7			0.01	753	56.9

Table 6.9. (a) Results of the inversion for Set B in ranges of *M* values.
Highlighted coefficients have respective P-value ≥ 0.05; thus they are not robust, i.e. statistically not different from the null hypothesis.
It follows that the correlation/relationship fitted is not significant.

CROMER KNOLL FORMATION									HEATHER FORMATION								
	Vo m/s	*a* m/s	*b* m/s/MPa	c m/s/° API	*d* m/s/ Ωm	*e* 1/s	Data points	RMS error		*Vo* m/s	*a* m/s	*b* m/s/MPa	c m/s/° API	*d* m/s/ Ωm	*e* 1/s	Data points	RMS error
Gamma Ray count response									Gamma Ray count response								
V(ϕ, σv, GR, z)									**V(ϕ, σv, GR, z)**								
M: 0.50 – 0.53	3009	-2091	2.3	0.78		-0.017	73	29.8	M: 0.50 – 0.53	-1522	-3528	0.0	1.91		1.449	7	10.4
M: 0.54 – 0.57	3284	-2540	0.5	-0.29		-0.002	261	39.7	M: 0.54 – 0.57	3407	-2681	2.4	-1.9		0.0018	168	38.6
M: 0.58 – 0.61	3528	-3121	3.1	-1.66		0.007	1003	54.6	M: 0.58 – 0.61	3466	-2953	4.3	-1.62		0.02	411	53.3
M: 0.62 – 0.65	3673	-3736	3.2	-0.44		0.015	932	60.4	M: 0.62 – 0.65	3720	-4166	-1.1	0.73		0.02	753	56.8
V(ϕ, σv, GR)									**V(ϕ, σv, GR)**								
M: 0.50 – 0.53	2955	-1983	2.8	0.49			73	29.9	M: 0.50 – 0.53	1850	-3528	101.3	1.91			7	10.4
M: 0.54 – 0.57	3269	-2515	0.8	-0.32			261	39.6	M: 0.54 – 0.57	3413	-2685	2.4	-1.90			168	38.4
M: 0.58 – 0.61	3571	-3209	2.2	-1.53			1003	54.7	M: 0.58 – 0.61	3551	-3047	4.0	-1.69			411	53.4
M: 0.62 – 0.65	3753	-3887	2.5	-0.32			932	61.0	M: 0.62 – 0.65	3828	-4249	-1.9	0.53			753	56.9
Resistivity response									Resistivity response								
V(ϕ, σv, R, z)									**V(ϕ, σv, R, z)**								
M: 0.50 – 0.53	3013	-2029	4.7		-26.00	-0.010	73	30.1	M: 0.50 – 0.53	-2568	-3340	0.0		-5.16	1.824	7	10.7
M: 0.54 – 0.57	3267	-2532	0.2		-4.63	-0.001	261	39.5	M: 0.54 – 0.57	3382	-2690	-0.1		-14.99	-0.017	168	39.2
M: 0.58 – 0.61	3503	-3214	-0.1		8.43	0.000	1003	55.8	M: 0.58 – 0.61	3341	-2936	3.1		-2.19	0.023	411	54.7
M: 0.62 – 0.65	3649	-3660	1.06		20.98	0.014	932	59.1	M: 0.62 – 0.65	3586	-3961	-0.6		16.45	0.052	753	55.5
V(ϕ, σv, R)									**V(ϕ, σv, R)**								
M: 0.50 – 0.53	2978	-1980	4.8		-30.77		73	30.0	M: 0.50 – 0.53	1678	-3340	127.6		-5.16		7	10.7
M: 0.54 – 0.57	3263	-2525	0.3		-4.79		261	39.5	M: 0.54 – 0.57	3321	-2679	-0.2		-13.17		168	39.1
M: 0.58 – 0.61	3502	-3212	-0.1		8.42		1003	55.8	M: 0.58 – 0.61	3444	-3042	2.70		-5.07		411	54.7
M: 0.62 – 0.65	3724	-3794	0.5		21.27		932	59.6	M: 0.62 – 0.65	3854	-4213	-2.37		9.33		753	56.3

Table 6.9 (b). Results of the inversion for Set B in ranges of *M* values.
Highlighted coefficients have respective P-value ≥ 0.05; thus they are not robust, i.e. statistically not different from the null hypothesis.
It follows that the correlation/relationship fitted is not significant.

6.7. Discussion and results

From all the analysis and results (Tables 6.3 – 6.7), it is found that there are systematic differences between the Cromer Knoll and the Heather. It has also been found for the lithology variables that gamma-ray count has had a major contribution, while resistivity has been less significant and its inclusion as an independent variable is questionable. In addition, depth is a good predictor for V_p in the Heather. The classification by M parameter narrow ranges has not had any consistent effect on the variable coefficients (Table 6.9). Thus, the overall results of the study are for the full data sets from each formation.

The coefficients of determination, with lower RMS error, are better for the runs in Set A than Set B. The hypothesis test for each data set allowed us to choose the best results, in terms of the variables' significance. The preferred results for the data under study are taken from Set A and are given through each formation by Equation (6.9) for the Cromer Knoll and Equation (6.10) for the Heather.

Below are given the contributions of different independent variables taken within the analysis.

In the Cromer Knoll:

- the result (Equation 6.9) has a dependence on vertical effective stress in the term $21.8\sigma_v$, which over the range σ_v in the data set, 8 – 36.1 MPa, contributes a variation of 613 m/s in the forwarded-calculated velocity values. The dependence on gamma ray count contributes a variation of -272 m/s from the term -9.0γ over the range of gamma values 40 - 111° API.
- Without the γ variable included, the variation due to the effective stress alone would have been only of 273 m/s (Table 6.3).
- The RMS error is 101 m/s. The discrepancies between the observed velocity values and their corresponding forwarded-calculated values are in the range of -240 to 356 m/s, corresponding to percentage errors in V_p from good match (0.1%) match, up to 11.6%. Over 85% of the 132 data points have their percentage errors below 5%.

In the Heather Formation:

- The result (Equation 6.10) shows a linear dependence on vertical effective stress in the term $17.4\sigma_v$. That contributes of 317 m/s over the range of σ_v in the data set, 10.6 – 28.8 MPa. The RMS error is 107.4 m/s.
- Without the variables gamma ray and depth, the contribution of the vertical effective stress is 69.2 m/s, very small compared to the corresponding RMS error of 121 m/s.
- Within the set of predicted velocities from Equation 6.10, only a single data point comes with a discrepancy value of 542 m/s, equivalent of 18.1% of percentage error. The remaining 31 data points have discrepancies within the range of -159 to up 260 m/s, making the percentage error on V_p up to 9.3%. A total of 7 points have their respective velocity discrepancies above the RMS error.

Figure 6.9 is a plot of the observed velocities (Section 6.9, Table 6.10) and their corresponding forward-computed values using equations 6.9 and 6.10. Figures 6.10 – 6.11 are histograms showing data distribution in the respective formations, as indicated. The variable distributions satisfy the acceptable classical statistical requirements for proper use of linear fitting of these data (Mann, 1987).

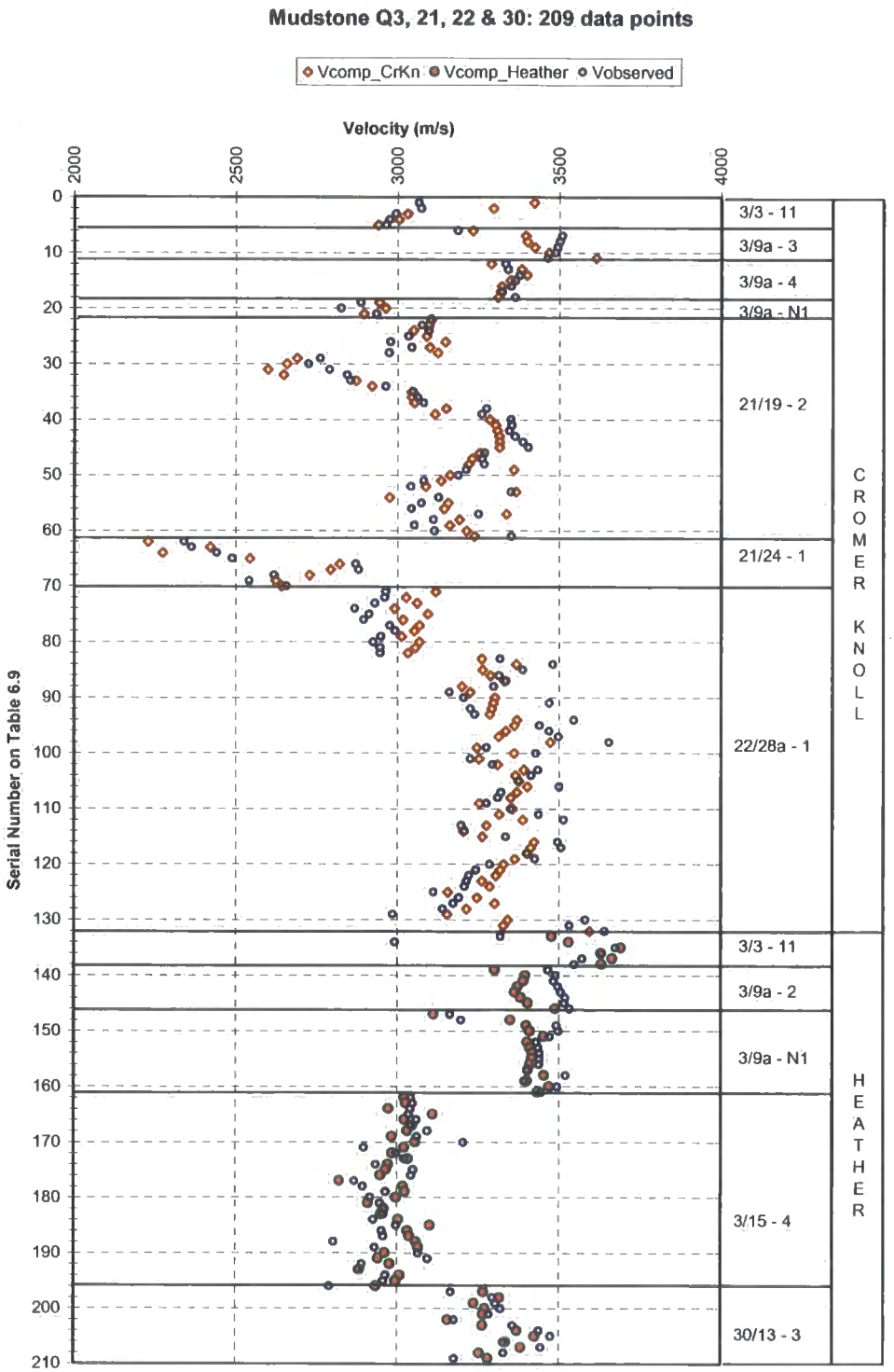

Figure 6.9. Observed values and corresponding forward-calculated values using Eqs. 6.9 and 6.11.
(Plotted by formation and wells, along Serial Number, as given in Section 6.9).

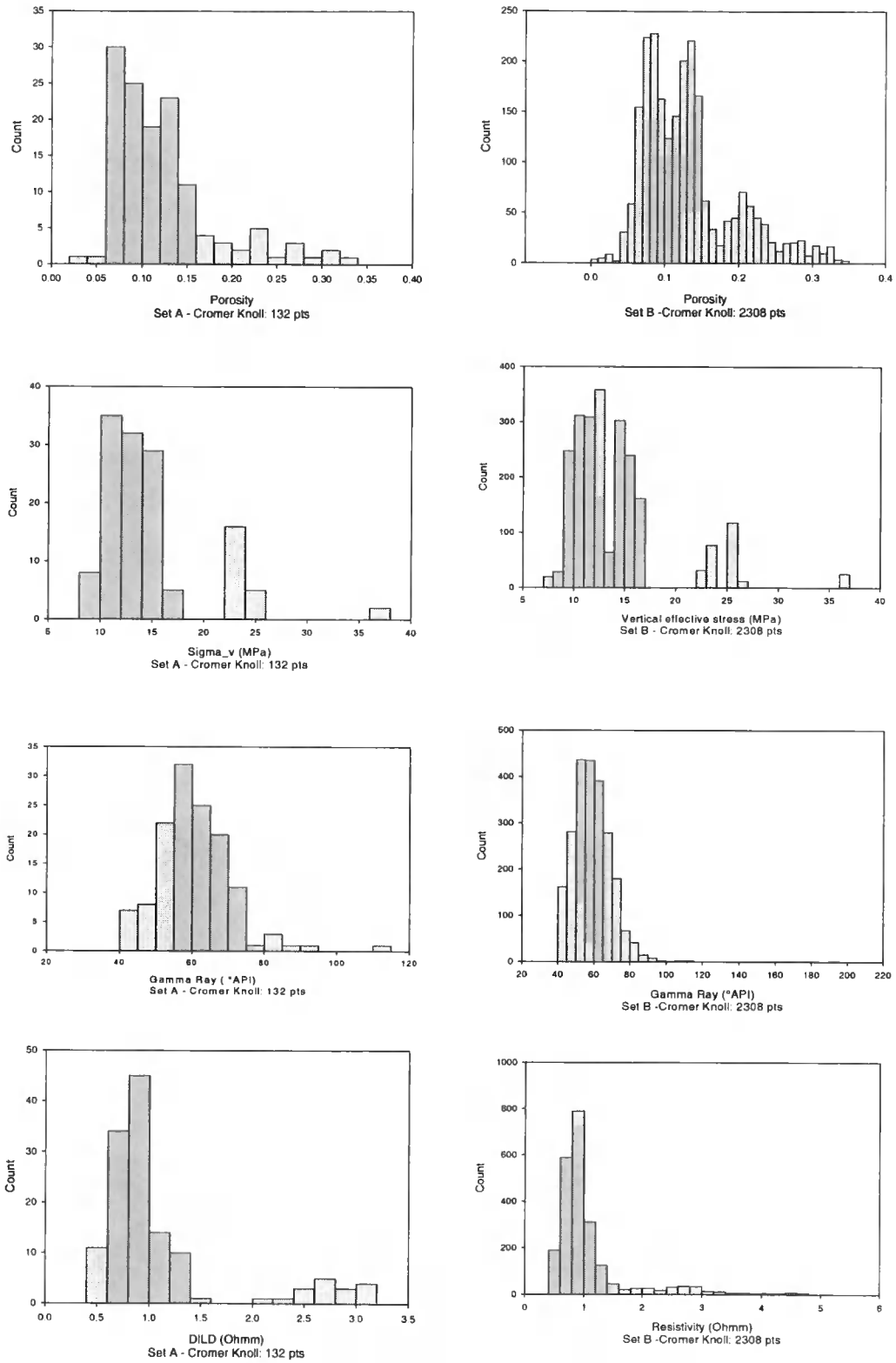

Figure 6.10. Histograms of different variables used in the inversion: Cromer Knoll Set A (132 data points) and Set B (2308 data points).

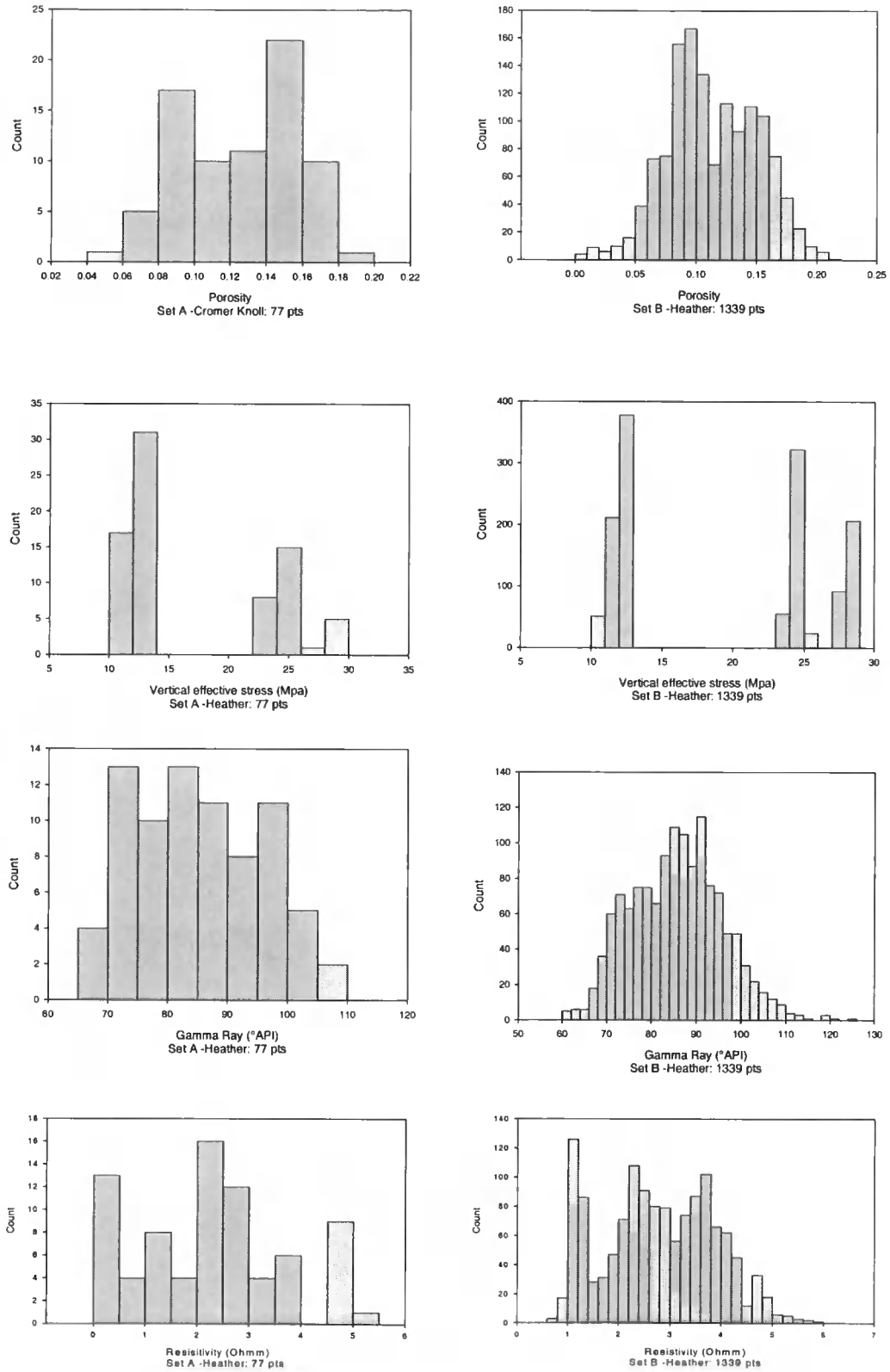

Figure 6.11. Histograms of different variables used in the inversion: Heather Set A (77 data points) and Set B (1339 data points).

6.8. Conclusion

The purpose was to investigate how sonic velocity depends on vertical effective stress in mudstones, taking porosity and vertical stress as independent variables. Due to the heterogeneous nature of mudstones, more variables to account for the lithology variations were introduced. The set of data was fitted by linear equation of the form (6.6) using a generalised inversion algorithm.

Introducing lithology variation, in terms of gamma ray count and depth as independent variables did improve the data fit. Gamma ray alone accounted for the analysis in the Cromer Knoll. The additional dependence of V_p on depth as an independent variable has proved to be robust in the Heather Formation only. The inclusion of resistivity as an independent variable could not be justified, though.

The results show that, in both the Cromer Knoll and in the Heather, there is a strong dependence of velocity on porosity and a slight dependence of sonic velocity on vertical effective stress when porosity and effective stress are taken as independent variables, along with gamma ray and depth. In the Cromer Knoll, the linear dependence of sonic velocity on vertical effective stress given by the term $21.8\sigma_v$ contributed for a variation of 613 m/s in the forwarded-calculated sonic velocity. Within the Heather data set the dependence is given by the term $17.4\sigma_v$, which makes a contribution of 317 m/s over the range vertical effective stress.

The contribution of the vertical effective stress with associated independent variables (gamma ray and depth) compared with the respective RMS errors on the results, i.e. 101.0 m/s for the Cromer Knoll and 107.4 m/s for the Heather Formation, is significant for the data fitting. However, this dependence is not enough to achieve a good match between the observed and forward-calculated velocities for individual data points (Figure 6.9).

Furthermore, discrepancies tend to be of consistent size and polarity over specific depth intervals in each well. To reduce these discrepancies variables relating to clay fraction and chemical diagenesis might be required in the analysis.

6.9. Appendix: data properties and variables values, 209 points

Data	WELL	*Pts*	DEPTH		Lithology variations				GR	Sonic	Density	Resistivity	Sv	Pp estimates	O/P	Porosity	σ_v'	*M*	Velocity
Label	Name, Fm	*S/N*	m SS	ft SS	Calc	Silt	Carb	Other	API	µs/ft	G/CC	Ohmm	MPa	MPa	MPa	Fractional	MPa		m/s
1	3/3-11 Rodby	*1*	3259.1	10693	2	2			72.4	99.48	2.592	1.31	71.1	45.3	12.5	0.091	25.7	0.57	3064
2	3/3-11 Rodby	*2*	3263.6	10708	2	2			67.0	99.20	2.512	1.27	71.2	45.4	12.5	0.138	25.8	0.60	3072
3	3/3-11 Rodby	*3*	3265.5	10714	2	2			72.2	101.77	2.412	1.19	71.2	45.4	12.5	0.195	25.8	0.63	2995
4	3/3-11 Sola	*4*	3272.3	10736.5	2				72.9	102.42	2.402	1.14	71.4	45.5	12.5	0.201	25.9	0.63	2976
5	3/3-11 Sola	*5*	3277.4	10753					77.7	102.83	2.392	1.08	71.5	45.5	12.5	0.207	26.0	0.63	2964
6	3/9a_3 CrKn	*1*	3087	10128.6		2			80.5	95.698	2.563	2.18	66.6	43.3	12.2	0.108	23.3	0.60	3185
7	3/9a_3 CrKn	*2*	3094	10151.6		2			67.3	86.858	2.583	2.90	66.8	43.4	12.2	0.097	23.4	0.65	3509
8	3/9a_3 CrKn	*3*	3094.2	10152.1		2			67.7	87.068	2.587	2.83	66.8	43.4	12.2	0.094	23.4	0.65	3501
9	3/9a_3 CrKn	*4*	3094.3	10152.6		2			68.0	87.224	2.598	2.76	66.8	43.4	12.2	0.088	23.4	0.64	3494
10	3/9a_3 CrKn	*5*	3094.5	10153.1		2			68.4	87.395	2.619	2.70	66.8	43.4	12.2	0.075	23.4	0.63	3487
11	3/9a_3 CrKn	*6*	3094.8	10154.1		2			69.1	87.988	2.689	2.62	66.8	43.4	12.2	0.035	23.4	0.60	3464
12	3/9a-4 CrKnoll	*1*	3082.9	10115.1					66.2	91.451	2.535	3.06	66.5	43.7	12.6	0.124	22.8	0.64	3333
13	3/9a-4 CrKnoll	*2*	3086.6	10127.1					65.8	91.233	2.575	2.50	66.6	43.7	12.6	0.101	22.9	0.63	3341
14	3/9a-4 CrKnoll	*3*	3088.6	10133.6					60.6	90.249	2.561	3.15	66.6	43.7	12.6	0.109	22.9	0.64	3377
15	3/9a-4 CrKnoll	*4*	3089	10135.1					62.5	90.620	2.546	3.01	66.7	43.7	12.6	0.118	22.9	0.64	3363
16	3/9a-4 CrKnoll	*5*	3089.6	10137.1					64.2	90.958	2.540	2.79	66.7	43.7	12.6	0.121	22.9	0.64	3351
17	3/9a-4 CrKnoll	*6*	3091.8	10144.1					68.4	91.736	2.556	2.96	66.7	43.7	12.6	0.112	23.0	0.63	3322
18	3/9a-4 CrKnoll	*7*	3095.9	10157.6	2	2			61.9	90.642	2.525	2.54	66.8	43.8	12.6	0.130	23.0	0.65	3363
19	3/9a-N1 CrKnoll	*1*	3115.5	10222.1					84.3	105.57	2.448	0.45	67.3	44.0	12.6	0.175	23.3	0.58	2887

20	3/9a-N1 CrKnoll	2	3116	10223.6					86.2	107.87	2.464	0.47	67.3	44.0	12.6	0.165	23.3	0.56	2825
21	3/9a-N1 CrKnoll	3	3117.2	10227.6					84.1	103.84	2.425	0.49	67.3	44.0	12.6	0.188	23.3	0.60	2935
22	21/19-2 CrKn	1	2891.2	9486	1	1			62.2	98.300	2.524	0.85	61.0	47.2	18.1	0.131	13.8	0.60	3101
23	21/19-2 CrKn	2	2893.3	9493	1	1			68.5	99.150	2.545	0.89	61.1	47.2	18.1	0.118	13.9	0.59	3074
24	21/19-2 CrKn	3	2896.5	9503.5	1	1			65.2	98.450	2.510	0.86	61.2	47.2	18.1	0.139	13.9	0.61	3096
25	21/19-2 CrKn	4	2898.2	9509	1	1			63.5	100.500	2.521	0.83	61.2	47.3	18.1	0.132	13.9	0.59	3033
26	21/19-2 CrKn	5	2900.5	9516.5	1	1			62.3	102.338	2.542	0.77	61.3	47.3	18.1	0.120	14.0	0.57	2978
27	21/19-2 CrKn	6	2901.4	9519.5	1	1			62.0	100.175	2.519	0.79	61.3	47.3	18.1	0.134	14.0	0.59	3043
28	21/19-2 CrKn	7	2904	9528	1	1			61.4	102.500	2.527	0.75	61.3	47.3	18.1	0.129	14.0	0.57	2974
29	21/19-2 CrKn	8	2913	9557.5	1	1			68.1	110.41	2.356	0.6	61.6	47.4	18.1	0.228	14.2	0.59	2760
30	21/19-2 CrKn	9	2920.3	9581.5	1	1			73.0	111.887	2.361	0.63	61.7	47.5	18.1	0.225	14.2	0.57	2724
31	21/19-2 CrKn	10	2921.5	9585.5	1	1			71.9	109.287	2.330	0.67	61.8	47.5	18.1	0.243	14.3	0.61	2789
32	21/19-2 CrKn	11	2942.2	9653.5	1	1			70.5	107.150	2.343	0.69	62.2	47.7	18.1	0.235	14.5	0.62	2844
33	21/19-2 CrKn	12	2946.8	9668.5	1	1			66.1	106.750	2.427	0.71	62.3	47.7	18.1	0.187	14.6	0.58	2855
34	21/19-2 CrKn	13	2957.3	9703	1	1			71.0	102.836	2.468	0.78	62.6	47.9	18.1	0.163	14.7	0.59	2964
35	21/19-2 CrKn	14	2960.4	9713	1	1			66.5	100.003	2.504	0.83	62.7	47.9	18.1	0.142	14.8	0.60	3048
36	21/19-2 CrKn	15	2960.5	9713.5	1	1			66.8	99.597	2.506	0.85	62.7	47.9	18.1	0.141	14.8	0.60	3060
37	21/19-2 CrKn	16	2960.7	9714	1	1			66.4	98.961	2.507	0.88	62.7	47.9	18.1	0.140	14.8	0.60	3080
38	21/19-2 CrKn	17	2968.8	9740.5	1	1			61.8	93.072	2.532	0.96	62.9	48.0	18.1	0.126	14.9	0.63	3275
39	21/19-2 CrKn	18	2968.9	9741	1	1			62.7	93.495	2.520	0.94	62.9	48.0	18.1	0.133	14.9	0.64	3260
40	21/19-2 CrKn	19	2978.5	9772.5	1	1			57.0	90.998	2.573	1.11	63.1	48.1	18.1	0.103	15.1	0.63	3349
41	21/19-2 CrKn	20	2981.4	9782	1	1			56.1	90.893	2.577	1.25	63.2	48.1	18.1	0.100	15.1	0.63	3353
42	21/19-2 CrKn	21	2981.6	9782.5	1	1			56.6	91.114	2.581	1.24	63.2	48.1	18.1	0.097	15.1	0.63	3345
43	21/19-2 CrKn	22	2981.7	9783	1	1			56.7	90.623	2.584	1.24	63.2	48.1	18.1	0.096	15.1	0.63	3363

44	21/19-2 CrKn	*23*	2981.9	9783.5	1	1			57.0	89.990	2.586	1.25	63.2	48.1	18.1	0.095	15.1	0.63	3387
45	21/19-2 CrKn	*24*	2982	9784	1	1			57.0	89.550	2.586	1.27	63.2	48.1	18.1	0.095	15.1	0.63	3404
46	21/19-2 CrKn	*25*	2987.2	9801	1	1			59.3	93.256	2.567	1.17	63.3	48.2	18.1	0.106	15.2	0.62	*3268*
47	21/19-2 CrKn	*26*	2987.4	9801.5	1	1			59.4	93.483	2.556	1.16	63.3	48.2	18.1	0.112	15.2	0.62	*3260*
48	21/19-2 CrKn	*27*	2987.5	9802	1	1			59.2	93.280	2.551	1.17	63.3	48.2	18.1	0.115	15.2	0.62	*3267*
49	21/19-2 CrKn	*28*	2994.5	9825	1	1		2	51.8	94.907	2.583	1.08	63.5	48.2	18.1	0.097	15.3	0.60	*3211*
50	21/19-2 CrKn	*29*	2999.1	9840	1	1		2	58.3	95.636	2.519	0.94	63.6	48.3	18.1	0.134	15.4	0.62	*3187*
51	21/19-2 CrKn	*30*	3003	9853	1	1		2	60.0	98.948	2.513	0.89	63.7	48.3	18.1	0.137	15.4	0.60	*3080*
52	21/19-2 CrKn	*31*	3009	9872.5	1	1		2	65.8	100.248	2.514	0.84	63.9	48.4	18.1	0.136	15.5	0.59	*3040*
53	21/19-2 CrKn	*32*	2997.1	9833.5	1	1		2	43.5	90.977	2.552	1.21	63.6	48.3	18.1	0.115	15.3	0.64	3350
54	21/19-2 CrKn	*33*	3024.1	9922	1	1		2	67.2	97.511	2.467	0.86	64.3	48.5	18.1	0.164	15.7	0.63	3126
55	21/19-2 CrKn*	*34*	3039.3	9972	1	1		2S	56.7	99.201	2.504	0.80	64.6	48.7	18.1	0.142	16.0	0.60	3072
56	21/19-2 CrKn*	*35*	3041	9977.5	1	1		2S	54.9	100.201	2.491	0.78	64.7	48.7	18.1	0.150	16.0	0.60	3042
57	21/19-2 CrKn*	*36*	3047.4	9998.5	1	1		2S	49.3	93.785	2.555	0.94	64.8	48.8	18.1	0.113	16.1	0.62	3250
58	21/19-2 CrKn*	*37*	3057.8	10032.5	1	1		2S	52.4	98.010	2.499	0.88	65.1	48.9	18.1	0.145	16.2	0.61	3110
59	21/19-2 CrKn*	*38*	3059.3	10037.5	1	1		2S	56.2	99.883	2.501	0.80	65.1	48.9	18.1	0.144	16.3	0.60	3051
60	21/19-2 CrKn*	*39*	3064.8	10055.5	1	1		2S	55.1	97.909	2.520	0.84	65.3	48.9	18.1	0.133	16.3	0.61	3113
61	21/19-2 CrKn*	*40*	3076.2	10093	1	1		2S	55.0	90.949	2.529	1.04	65.6	49.0	18.1	0.128	16.5	0.65	3351
62	21/24-1 CrKn	*1*	1976.1	6483.5	2				65.9	130.282	2.176	0.43	40.0	29.7	9.8	0.332	10.3	0.50	2339
63	21/24-1 CrKn	*2*	1978.1	6490	2				57.8	129.004	2.230	0.44	40.0	29.7	9.8	0.301	10.3	0.49	2363
64	21/24-1 CrKn	*3*	1980.8	6499	2				71.3	124.878	2.218	0.49	40.1	29.7	9.8	0.308	10.3	0.53	2441
65	21/24-1 CrKn	*4*	1982.3	6504	2				59.0	122.494	2.290	0.54	40.1	29.8	9.8	0.266	10.4	0.52	2488
66	21/24-1 CrKn	*5*	1987.2	6520	2				43.3	106.138	2.352	0.68	40.2	29.8	9.8	0.230	10.4	0.62	2872
67	21/24-1 CrKn	*6*	1989.6	6528	2				49.0	105.810	2.362	0.71	40.3	29.8	9.8	0.224	10.5	0.62	2880
68	21/24-1 CrKn	*7*	1994.2	6543	2				40.2	116.384	2.296	0.51	40.4	29.9	9.8	0.262	10.5	0.57	2619

69		*8*	1999.2	6559.5	2				42.2	119.956	2.256	0.52	40.5	29.9	9.8	0.286	10.6	0.56	2541
70	21/24-1 CrKn	*9*	2000	6562	2				43.1	114.710	2.268	0.53	40.5	29.9	9.8	0.279	10.6	0.59	2657
71	22/28a - 1Sola	*1*	4517.2	14821					59.1	102.825	2.556	0.78	99.2	89.4	0.0	0.112	9.9	0.56	2964
72	22/28a - 1Sola	*2*	4518.4	14825					59.9	102.925	2.518	0.64	99.3	89.4	0.0	0.134	9.9	0.57	2961
73	22/28a - 1Sola	*3*	4519	14827					57.8	103.975	2.525	0.68	99.3	89.4	0.0	0.130	9.9	0.56	2931
74	22/28a - 1Sola	*4*	4520.9	14833					57.9	106.250	2.494	0.85	99.3	89.4	0.0	0.148	9.9	0.56	2869
75	22/28a - 1Sola	*5*	4522.7	14839					58.2	104.625	2.541	0.73	99.4	89.4	0.0	0.121	10.0	0.55	2913
76	22/28a - 1Sola	*6*	4523.6	14842					57.7	105.225	2.504	0.64	99.4	89.4	0.0	0.142	10.0	0.56	2897
77	22/28a - 1Sola	*7*	4525.1	14847					63.0	102.400	2.549	0.78	99.4	89.4	0.0	0.116	10.0	0.56	2976
78	22/28a - 1Sola	*8*	4526.1	14850					60.4	101.850	2.531	0.81	99.5	89.4	0.0	0.127	10.0	0.58	2992
79	22/28a - 1Sola	*9*	4527.1	14853.5					59.1	103.350	2.507	0.82	99.5	89.5	0.0	0.140	10.0	0.57	2949
80	22/28a - 1Sola	*10*	4532.8	14872					55.6	104.175	2.517	2.28	99.6	89.5	0.0	0.135	10.1	0.56	2926
81	22/28a - 1Sola	*11*	4533.5	14874.5					60.9	103.425	2.533	1.47	99.6	89.5	0.0	0.126	10.1	0.56	2947
82	22/28a - 1Sola	*12*	4535.8	14882	2				56.9	103.400	2.506	2.41	99.7	89.5	0.0	0.141	10.2	0.57	2948
83	22/28a - 1Vhall	*13*	4578.5	15022	3	2P			47.9	91.875	2.567	0.84	100.8	90.0	0.0	0.106	10.8	0.63	3317
84	22/28a - 1Vhall	*14*	4591.6	15065	3	2P			43.8	87.575	2.597	1.01	101.1	90.1	0.0	0.089	11.0	0.64	3480
85	22/28a - 1Vhall	*15*	4592.8	15069	3	2P			54.0	90.000	2.591	0.85	101.2	90.1	0.0	0.092	11.0	0.63	3387
86	22/28a - 1Vhall	*16*	4601.2	15096.5	3	2P			51.0	91.975	2.588	0.78	101.4	90.2	0.0	0.093	11.2	0.62	3314
87	22/28a - 1Vhall	*17*	4602.3	15100	3	2P			51.1	91.375	2.609	0.83	101.4	90.2	0.0	0.082	11.2	0.61	3336
88	22/28a - 1Vhall	*18*	4605	15109	3	2P			52.4	92.425	2.553	0.75	101.5	90.2	0.0	0.114	11.2	0.63	3298
89	22/28a - 1Vhall	*19*	4605.9	15112	3	2P			56.6	96.450	2.582	0.67	101.5	90.3	0.0	0.097	11.2	0.59	3160
90	22/28a - 1Vhall	*20*	4606.5	15114	3	2P			56.8	95.125	2.617	0.68	101.5	90.3	0.0	0.077	11.3	0.59	3204
91	22/28a - 1Vhall	*21*	4609.4	15123.5	3	2P			47.1	87.85	2.575	0.96	101.6	90.3	0.0	0.101	11.3	0.65	3469
92	22/28a - 1Vhall	*22*	4616.9	15148	3	2P			52.4	94.500	2.593	0.84	101.8	90.4	0.0	0.091	11.4	0.60	3225

93	22/28a - 1Vhall	*23*	4620.2	15159	3	2P			53.8	94.100	2.596	0.76	101.9	90.4	0.0	0.089	11.5	0.60	3239
94	22/28a - 1Vhall	*24*	4621.9	15164.5	3	2P			48.7	85.975	2.613	1.16	101.9	90.4	0.0	0.079	11.5	0.65	3545
95	22/28a - 1Vhall	*25*	4625	15174.5	3	2P			49.4	88.625	2.612	0.93	102.0	90.4	0.0	0.080	11.5	0.63	3439
96	22/28a - 1Vhall	*26*	4632.1	15198	3	2P			53.3	87.875	2.614	0.91	102.2	90.5	0.0	0.078	11.6	0.63	3468
97	22/28a - 1Vhall	*27*	4637.9	15217	3	2P			50.6	87.150	2.593	0.93	102.3	90.6	0.0	0.091	11.7	0.65	3497
98	22/28a - 1Vhall	*28*	4641	15227	3	2P			44.1	83.425	2.638	1.19	102.4	90.6	0.0	0.065	11.8	0.65	3653
99	22/28a - 1Vhall	*29*	4648	15250	3	0			56.3	93.050	2.583	0.73	102.6	90.7	0.0	0.096	11.9	0.61	3275
100	22/28a - 1Vhall	*30*	4650.4	15258	3	0			51.9	88.925	2.618	0.87	102.6	90.7	0.0	0.076	11.9	0.63	3427
101	22/28a - 1Vhall	*31*	4653.6	15268.5	3	0			59.0	94.500	2.597	0.74	102.7	90.7	0.0	0.088	12.0	0.60	3225
102	22/28a - 1Vhall	*32*	4654.5	15271.5	3	0			54.2	92.525	2.603	0.83	102.7	90.7	0.0	0.085	12.0	0.61	3294
103	22/28a - 1Vhall	*33*	4659.7	15288.5				A	51.6	88.750	2.629	0.97	102.9	90.8	0.0	0.070	12.1	0.62	3434
104	22/28a - 1Vhall	*34*	4660.8	15292				A	54.5	89.300	2.628	0.82	102.9	90.8	0.0	0.070	12.1	0.62	3413
105	22/28a - 1Vhall	*35*	4665.5	15307.5				A	54.2	90.325	2.632	0.86	103.0	90.9	0.0	0.068	12.2	0.61	3374
106	22/28a - 1Vhall	*36*	4667.5	15314				A	47.1	87.075	2.614	0.95	103.1	90.9	0.0	0.079	12.2	0.64	3500
107	22/28a - 1Vhall	*37*	4669.3	15320				A	52.2	91.800	2.620	0.75	103.1	90.9	0.0	0.075	12.2	0.61	3320
108	22/28a - 1Vhall	*38*	4670.5	15324				A	52.9	92.075	2.614	0.86	103.1	90.9	0.0	0.079	12.2	0.61	3310
109	22/28a - 1Vhall	*39*	4673.1	15332.5				A	62.8	93.050	2.609	0.79	103.2	90.9	0.0	0.081	12.3	0.60	3275
110	22/28a - 1Vhall	*40*	4674.5	15337				A	57.9	90.975	2.636	0.81	103.3	90.9	0.0	0.066	12.3	0.61	3350
111	22/28a - 1Vhall	*41*	4676.6	15344				A	63.6	88.675	2.640	0.99	103.3	91.0	0.0	0.063	12.3	0.62	3437
112	22/28a - 1Vhall	*42*	4678	15348.5				A	54.3	86.750	2.635	1.27	103.3	91.0	0.0	0.066	12.4	0.63	3513
113	22/28a - 1Vhall	*43*	4683.8	15367.5				A	62.9	95.325	2.618	0.82	103.5	91.0	0.0	0.076	12.5	0.58	3197
114	22/28a - 1Vhall	*44*	4685.5	15373				A	73.0	95.000	2.627	0.75	103.5	91.1	0.0	0.071	12.5	0.58	3208
115	22/28a - 1Vhall	*45*	4686.4	15376				A	70.1	91.400	2.642	0.85	103.6	91.1	0.0	0.063	12.5	0.60	3335
116	22/28a - 1Vhall	*46*	4689.1	15385				A	51.0	87.200	2.636	1.05	103.6	91.1	0.0	0.066	12.5	0.63	3495

117	22/28a - 1Vhall	*47*	4690	15388				A	51.9	86.925	2.635	1.08	103.6	91.1	0.0	0.067	12.5	0.63	3506
118	22/28a - 1Vhall	*48*	4691.6	15393				A	55.3	89.625	2.643	0.90	103.7	91.1	0.0	0.062	12.6	0.61	3401
119	22/28a - 1Vhall	*49*	4692.2	15395				A	57.4	89.000	2.635	0.92	103.7	91.1	0.0	0.066	12.6	0.62	3425
120	22/28a - 1Vhall	*50*	4694	15401				A	60.2	92.775	2.630	0.90	103.8	91.1	0.0	0.069	12.6	0.60	3285
121	22/28a - 1Vhall	*51*	4696.7	15410				A	61.4	93.975	2.630	0.84	103.8	91.2	0.0	0.070	12.7	0.59	3243
122	22/28a - 1Vhall	*52*	4699.2	15418				A	64.4	94.625	2.636	0.73	103.9	91.2	0.0	0.066	12.7	0.58	3221
123	22/28a - 1Vhall	*53*	4699.8	15420				A	63.8	94.850	2.613	0.77	103.9	91.2	0.0	0.079	12.7	0.59	3213
124	22/28a - 1Vhall	*54*	4700.4	15422				A	61.9	95.025	2.616	0.85	103.9	91.2	0.0	0.077	12.7	0.59	3207
125	22/28a - 1Vhall	*55*	4703.1	15431				A	71.0	97.975	2.594	0.67	104.0	91.2	0.0	0.090	12.8	0.58	3111
126	22/28a - 1Vhall	*56*	4704.1	15434				A	64.8	95.550	2.610	0.70	104.0	91.2	0.0	0.081	12.8	0.59	3190
127	22/28a - 1Vhall	*57*	4706.2	15441				A	62.0	96.075	2.623	0.69	104.1	91.3	0.0	0.073	12.8	0.58	3172
128	22/28a - 1Vhall	*58*	4707.4	15445				A	66.2	97.100	2.600	0.67	104.1	91.3	0.0	0.086	12.8	0.58	3139
129	22/30a - 2Vh upper	*1*	4300.4	14109.5					47.3	102.050	2.544	0.88	93.3	85.3	0.0	0.119	8.0	0.57	2987
130	22/30a - 2VhLower	*2*	4318.5	14169	1	1			55.5	85.135	2.660	1.36	93.7	85.4	0.0	0.052	8.3	0.63	3580
131	30/12b-2 CrKn	*1*	3978.2	13052.5	1			1	111.1	86.307	2.604	3.14	83.8	47.7	0.0	0.084	36.1	0.65	3531
132	30/12b-2 CrKn	*2*	3979.1	13055.5	1			1	90.6	83.729	2.642	2.75	83.8	47.7	0.0	0.063	36.1	0.65	3640
133	3/3-11 Heather	*1*	3397.7	11148	2	2		Mica	71.9	91.826	2.538	1.61	74.4	46.7	12.5	0.123	27.7	0.64	3319
134	3/3-11 Heather	*2*	3432.3	11261.5		3	1		107.2	101.82	2.620	2.74	75.3	47.1	12.5	0.075	28.2	0.54	2993
135	3/3-11 Heather	*3*	3451.1	11323		3	1		105.7	82.96	2.678	2.86	75.7	47.3	12.5	0.042	28.5	0.64	3674
136	3/3-11 Heather	*4*	3456.3	11340	2	3	1		97.9	83.95	2.638	3.82	75.9	47.3	12.5	0.065	28.6	0.65	3630
137	3/3-11 Heather	*5*	3461.3	11356.5	2	3	1	Mica	91.0	85.340	2.638	4.81	76.0	47.4	12.5	0.065	28.6	0.64	3571
138	3/3-11 Heather	*6*	3467.7	11377.5	2	3	1		90.2	85.93	2.622	4.77	76.2	47.4	12.5	0.074	28.7	0.64	3547
139	3/9a-2 Heather	*1*	3166.4	10389.1	2				102.8	87.939	2.567	4.70	68.2	44.5	12.6	0.106	23.7	0.65	3466
140	3/9a-2 Heather	*2*	3167.2	10391.6					100.2	87.360	2.600	4.72	68.2	44.5	12.6	0.087	23.7	0.64	3489

141	3/9a-2 Heather	3	3167.3	10392.1					100.2	87.495	2.597	4.73	68.2	44.5	12.6	0.088	23.7	0.64	3483
142	3/9a-2 Heather	4	3168	10394.1					101.6	87.154	2.593	4.73	68.2	44.5	12.6	0.091	23.8	0.65	3497
143	3/9a-2 Heather	5	3168.1	10394.6					101.8	86.940	2.589	4.72	68.2	44.5	12.6	0.093	23.8	0.65	3506
144	3/9a-2 Heather	6	3168.9	10397.1					97.9	86.611	2.589	4.82	68.3	44.5	12.6	0.093	23.8	0.65	3519
145	3/9a-2 Heather	7	3169	10397.6					97.8	86.686	2.598	4.86	68.3	44.5	12.6	0.088	23.8	0.65	3516
146	3/9a-2 Heather	8	3172.7	10409.6	2				98.6	86.287	2.632	5.04	68.4	44.5	12.6	0.068	23.8	0.64	3532
147	3/9a-N1 Heather	1	3175.9	10420					90.9	96.375	2.466	0.85	68.7	44.6	12.6	0.164	24.1	0.64	3162
148	3/9a-N1 Heather	2	3181.4	10438.3					83.9	95.326	2.546	0.50	68.8	44.7	12.6	0.118	24.2	0.61	3197
149	3/9a-N1 Heather	3	3210.3	10533.1					95.9	87.276	2.584	0.24	69.6	44.9	12.6	0.096	24.6	0.65	3492
150	3/9a-N1 Heather	4	3210.5	10533.6					95.9	87.125	2.588	0.24	69.6	44.9	12.6	0.093	24.6	0.65	3498
151	3/9a-N1 Heather	5	3211.2	10536.1					89.6	87.826	2.593	0.24	69.6	45.0	12.6	0.091	24.7	0.64	3470
152	3/9a-N1 Heather	6	3222.2	10572.2					97.3	88.875	2.586	0.25	69.9	45.1	12.6	0.095	24.8	0.64	3429
153	3/9a-N1 Heather	7	3222.4	10572.7					97.4	88.701	2.589	0.26	69.9	45.1	12.6	0.093	24.8	0.64	3436
154	3/9a-N1 Heather	8	3222.5	10573.2					97.0	88.625	2.591	0.26	69.9	45.1	12.6	0.092	24.8	0.64	3439
155	3/9a-N1 Heather	9	3222.7	10573.7					96.4	88.625	2.590	0.27	69.9	45.1	12.6	0.093	24.8	0.64	3439
156	3/9a-N1 Heather	10	3222.8	10574.2					96.0	88.650	2.587	0.27	69.9	45.1	12.6	0.094	24.8	0.64	3438
157	3/9a-N1 Heather	11	3225.9	10584					89.3	89.575	2.571	0.24	70.0	45.1	12.6	0.104	24.9	0.64	3403
158	3/9a-N1 Heather	12	3228.9	10593.9					93.3	86.575	2.598	0.24	70.1	45.1	12.6	0.088	24.9	0.65	3520
159	3/9a-N1 Heather	13	3231.9	10603.8					92.2	89.851	2.574	0.27	70.1	45.2	12.6	0.102	25.0	0.64	3392
160	3/9a-N1 Heather	14	3236.7	10619.6					93.6	87.225	2.604	0.26	70.3	45.2	12.6	0.085	25.0	0.64	3494
161	3/9a-N1 Heather	15	3241.2	10634.5					93.6	88.475	2.588	0.17	70.4	45.3	12.6	0.093	25.1	0.64	3445
162	3 15_4 Heather	1	3151.7	10340.6					81.5	100.202	2.500	2.43	68.0	56.2	24.5	0.145	11.8	0.60	3042
163	3 15_4 Heather	2	3153	10345.1					78.3	99.978	2.495	2.32	68.0	56.2	24.5	0.147	11.8	0.60	3049
164	3 15_4 Heather	3	3153.3	10346.1					78.1	100.211	2.474	2.24	68.0	56.2	24.5	0.160	11.8	0.61	3041
165	3 15_4 Heather	4	3154.2	10349.1					73.3	100.398	2.518	2.38	68.1	56.2	24.5	0.134	11.8	0.59	3036

166	3 15_4 Heather	5	3155	10351.6					75.8	99.614	2.489	2.79	68.1	56.2	24.5	0.151	11.8	0.61	3060
167	3 15_4 Heather	6	3157	10358.1	1				69.8	100.188	2.486	2.69	68.1	56.3	24.5	0.153	11.9	0.60	3042
168	3 15_4 Heather	7	3159.1	10365.1	1				71.9	98.540	2.484	2.39	68.2	56.3	24.5	0.154	11.9	0.62	3093
169	3 15_4 Heather	8	3161.3	10372.1					83.3	99.572	2.487	2.76	68.2	56.3	24.5	0.152	11.9	0.61	3061
170	3 15_4 Heather	9	3163.4	10379.1		1			73.9	95.115	2.497	2.45	68.3	56.3	24.5	0.146	11.9	0.64	3204
171	3 15_4 Heather	10	3164.6	10383.1		1			78.0	105.155	2.491	2.21	68.3	56.3	24.5	0.150	12.0	0.57	2898
172	3 15_4 Heather	11	3169	10397.6	1	1			74.3	101.651	2.469	2.44	68.4	56.4	24.5	0.163	12.0	0.60	2998
173	3 15_4 Heather	12	3170.1	10401.1	1	1			75.7	100.828	2.490	2.74	68.4	56.4	24.5	0.150	12.0	0.60	3023
174	3 15_4 Heather	13	3171.3	10405.1		1			71.1	103.827	2.457	2.53	68.5	56.4	24.5	0.169	12.1	0.59	2935
175	3 15_4 Heather	14	3172.5	10409.1		1			74.7	99.922	2.461	2.31	68.5	56.4	24.5	0.167	12.1	0.62	3050
176	3 15_4 Heather	15	3173	10410.6		1			76.3	100.134	2.457	2.26	68.5	56.4	24.5	0.169	12.1	0.62	3044
177	3 15_4 Heather	16	3175.9	10420.1		1			77.6	106.255	2.408	1.97	68.6	56.5	24.5	0.198	12.1	0.59	2868
178	3 15_4 Heather	17	3176.6	10422.6		1			82.7	105.267	2.497	1.96	68.6	56.5	24.5	0.147	12.1	0.57	2895
179	3 15_4 Heather	18	3178	10427.1		1			79.9	102.750	2.493	2.26	68.6	56.5	24.5	0.149	12.2	0.58	2966
180	3 15_4 Heather	19	3179.4	10431.6		1			81.3	104.418	2.485	2.21	68.7	56.5	24.5	0.153	12.2	0.58	2919
181	3 15_4 Heather	20	3180.5	10435.1		1			84.1	103.369	2.455	2.56	68.7	56.5	24.5	0.170	12.2	0.60	2949
182	3 15_4 Heather	21	3183	10443.6			2	S	86.5	102.896	2.479	2.48	68.8	56.5	24.5	0.157	12.2	0.59	2962
183	3 15_4 Heather	22	3183.2	10444.1			2	S	86.0	103.006	2.475	2.26	68.8	56.5	24.5	0.159	12.2	0.59	2959
184	3 15_4 Heather	23	3185.8	10452.6			2	S	86.8	104.102	2.497	2.91	68.8	56.6	24.5	0.146	12.3	0.57	2928
185	3 15_4 Heather	24	3188.1	10460.1			2	S	82.8	101.660	2.527	2.55	68.9	56.6	24.5	0.129	12.3	0.58	2998
186	3 15_4 Heather	25	3193.4	10477.6			2	S	85.2	103.175	2.504	3.16	69.0	56.6	24.5	0.142	12.4	0.58	2954
187	3 15_4 Heather	26	3193.6	10478.1			2	S	84.6	102.994	2.505	3.16	69.0	56.6	24.5	0.142	12.4	0.58	2959
188	3 15_4 Heather	27	3195.1	10483.1			2	S	85.6	108.699	2.515	3.08	69.0	56.6	24.5	0.136	12.4	0.53	2804
189	3 15_4 Heather	28	3196.2	10486.6			2	S	87.5	103.933	2.521	2.87	69.1	56.7	24.5	0.132	12.4	0.56	2933

190	3 15_4 Heather	29	3200.1	10499.6	2	1	2	S	82.5	99.444	2.470	3.94	69.2	56.7	24.5	0.162	12.5	0.62	3065
191	3 15_4 Heather	30	3200.6	10501.1	2	1	2	S	81.4	98.511	2.460	3.92	69.2	56.7	24.5	0.168	12.5	0.63	3094
192	3 15_4 Heather	31	3203.3	10510.1		1	2	S	87.1	105.387	2.485	3.10	69.2	56.7	24.5	0.153	12.5	0.57	2892
193	3 15_4 Heather	32	3204.4	10513.6		1	2	S	88.7	105.794	2.450	3.52	69.3	56.7	24.5	0.173	12.5	0.58	2881
194	3 15_4 Heather	33	3207.6	10524.1		1	2	S	91.0	102.765	2.503	3.51	69.4	56.8	24.5	0.143	12.6	0.58	2966
195	3 15_4 Heather	34	3208.5	10527.1	2	1	2	S	84.2	102.998	2.485	3.93	69.4	56.8	24.5	0.153	12.6	0.59	2959
196	3 15_4 Heather	35	3216.4	10553.1		1	2	S	85.7	109.195	2.463	2.94	69.6	56.9	24.5	0.166	12.7	0.55	2791
197	30/13 - 3Hther	1	4010.1	13157				3	68.7	96.260	2.531	1.12	84.2	73.5	33.2	0.127	10.7	0.61	3166
198	30/13 - 3Hther	2	4015.5	13175				3	70.9	92.500	2.554	1.54	84.4	73.6	33.2	0.113	10.8	0.63	3295
199	30/13 - 3Hther	3	4036.9	13245				3	73.1	92.220	2.523	1.10	84.9	73.8	33.2	0.131	11.1	0.64	3305
200	30/13 - 3Hther	4	4042.1	13262				3	74.8	91.800	2.539	1.09	85.0	73.9	33.2	0.122	11.2	0.64	3320
201	30/13 - 3Hther	5	4042.7	13264				3	72.9	92.800	2.533	1.12	85.0	73.9	33.2	0.125	11.2	0.64	3284
202	30/13 - 3Hther	6	4053	13298				3	76.3	95.980	2.494	2.21	85.3	74.0	33.2	0.148	11.3	0.63	3176
203	30/13 - 3Hther	7	4059.4	13319				3	68.6	90.780	2.521	2.09	85.5	74.0	33.2	0.132	11.4	0.65	3357
204	30/13 - 3Hther	8	4098.6	13447.5	2		1	2	72.3	88.640	2.564	1.10	86.4	74.4	33.2	0.107	12.0	0.65	3438
205	30/13 - 3Hther	9	4103.6	13464	2				67.7	87.720	2.577	1.09	86.6	74.5	33.2	0.100	12.1	0.65	3475
206	30/13 - 3Hther	10	4107.9	13478	2		1		77.8	91.580	2.559	1.15	86.7	74.5	33.2	0.110	12.2	0.63	3328
207	30/13 - 3Hther	11	4112.3	13492.5	2				71.0	88.480	2.564	1.14	86.8	74.6	33.2	0.107	12.2	0.65	3445
208	30/13 - 3Hther	12	4124	13531	2				83.8	91.520	2.536	0.93	87.1	74.7	33.2	0.124	12.4	0.64	3330
209	30/13 - 3Hther	13	4126.8	13540	2				82.3	95.960	2.543	0.99	87.1	74.7	33.2	0.120	12.4	0.61	3176
Data	WELL	Pts	DEPTH Sub sea		Lithology variations				GR	Sonic	Density	Resistivity	Sv	Pp estimates	O/P	Bulk Porosity	Sigma _V	M	Velocity
Label	Name, Fm	S/N	m	ft	Calc	Silt	Carb	Other	API	US/FT	G/C3	Ohmm	MPa	MPa	MPa	Fractional	MPa		m/s

Legend for lithology variations: Calc: calcareous , Silt : silty, Carb: carbonaceous | Values: 1: yes, 2: slightly, 3: very, high, P: in part | Others: 1: Glauconitic, 2: Pyritic, 3: Siliceous, S: sandy, A: Anhydritic

Table 6.10. Data points for the analysis (209): properties and variables values.

Chapter 7
Summary of conclusions and suggested future work

7.1. Introduction

7.2. Summary of conclusions

7.3. Proposal for further analysis

7. SUMMARY OF CONCLUSIONS AND SUGGESTED FUTURE WORK

7.1. Introduction

This chapter constitutes a summary of the overall conclusions and gives some comments on how this study could be extended beyond the scope of the thesis.

Overpressure prediction models used in well planning are generally based on the assumption that overpressure has been generated by undercompaction. There is a clear need for models to account additionally for overpressure generated by unloading mechanisms, such as hydrocarbon generation, chemical compaction (diagenesis) and fluid flow by lateral transfer.

The ultimate objective of the research was to find an improved method of pore pressure estimation/prediction using sonic, density and other log information with pore pressure measurements in the fine-grained sediments of the Central North Sea. In order to achieve that objective, two separate studies were carried out, on the Chalk of the Central Graben and Mesozoic mudstones of the Central Graben and East Shetland Basin, to investigate how seismic velocity varies with effective stress independently of porosity.

7.2. Summary of conclusions

7.2.1. Chalk study

Investigation into the Chalk of the Central Graben has shown that velocity shows no detectable dependence on vertical effective stress when porosity and vertical effective stress are treated as independent variables. This result contrasts with the behaviour of shales, which exhibit a reduction in velocity on unloading. The significance is that sonic velocity and density in chalk cannot be used to detect the

presence of any overpressure caused by unloading. It is suggested that the absence of an observable velocity reduction in unloaded Chalk is due to cementation. The velocity–porosity relationship found in this investigation (see Equation 5.13, Chapter 5) is consistent with the work of Mallon and Swarbrick (2002) within the limits of error. They correlated porosity inferred from density logs with velocity from sonic logs using data from 59 wells passing through non-reservoir Chalk in the central North Sea., yielding a velocity – porosity relationship of the same algebraic form as the Wyllie relationship (see Equation 5.14, Chapter 5).

As in the case of the larger data set analysed by Mallon and Swarbrick (2002), the much smaller dataset used here (Figure 5.6) displays a lot of scatter. It is suggested that the scatter is mostly due to the response of the sonic log in carbonates, in that it depends on the relative proportions of variations of primary and secondary porosity (Bateman, 1985) and on variations in the fabric (grain size distribution and shape, and cementation) (Wyllie et al., 1956). In addition, anomalously low velocity values could be due to the presence of shale or very small quantities of gas, which will both increase the sonic transit time.

Scatter in the sonic data could be masking some small dependence of velocity on vertical effective stress in the data analysed here. Nevertheless, there seem to be good physical reasons why velocity in the Chalk is little affected by unloading.

7.2.2. Variation in mudstones

Other petrophysical parameters were added in the analyses for mudstones, namely gamma ray count, resistivity and depth. These were included to account for lithology heterogeneity in mudstones and temperature.

The results attest that gamma count as an independent variable does improve the data fit within the formations. The dependence on depth improved the fit between observed and forward-calculated velocities within the Heather Formation mudstones. The Cromer Knoll mudstones showed less dependence on depth. The results and concerns about independence of variables do not warrant the use of resistivity as an independent variable for sonic velocity analysis to account for unloading processes.

The overall results on mudstones suggest that vertical effective stress does have an effect on sonic velocity. For these data sets, the observed dependence of velocity on vertical effective stress contributes 613 m/s and 317 m/s to the forward - calculated sonic velocities in the Cromer Knoll Formation and the Heather Formation, respectively. This is compared to respective RMS errors of 101 m/s and 107 m/s.

7.3. Proposal for further analysis

In both investigations, i.e. chalk and mudstones, the aim was to determine how sonic velocity V_p depends on vertical effective stress σ_v. Results of data analysis in mudstones have shown that there is a slight dependence when more parameters are added to account for the lithology. A first suggestion for further work is more analyses with a larger set of data to investigate regional differences within and between basins.

Referring to the conclusion of Bowers and Katsube (2002) that transport properties (e.g. sonic and resistivity) are more likely than density to be affected by unloading, further work should concentrate to evaluate the use of wireline logs as a predictor of the vertical effective stress, and hence of pore pressure. Data will be fitted in an equation of the type $\sigma_v = \sigma_0 + A\phi + B\ V + C\ \gamma + D\ R + E\ z$. This means treating the vertical effective stress σ_v as the variable dependent on other petrophysical parameters.

Appendices

Appendix A. Variables calculations by well (Chalk study)

- Overburden or lithostatic stress, S_v
- Pore pressure, P_p
- Vertical effective stress, σ_v

Appendix B. Programs – Visual Basic macros

- Inversion program
- Data selection and variable calculations (mudstones study)
- Software and applications used in the study

Appendix A
Lithostatic stress S_v and Pore pressure P_p estimations

A.1. Well 22/28a – 1

A.2. Well 22/29 – 1S1

A.3. Well 22/30a – 2

A.4. Well 22/30c – 8

A.5. Well 30/12b – 4

A.6. Well 30/13 – 3

A.7. Well 31/26a – 5

A.8. Well 31/26a – 9A

APPENDIX A. LITHOSTATIC STRESS, S_v, AND PORE PRESSURE, *Pp*, ESTIMATIONS.

A.1. Well 22/28a – 1

A.1.1. Lithostatic stress estimation

Well 22/28a - 1 RTE: 130 ft , 39.6 m		Measured Depth		TVD	
		ft BRT	m BRT	ft SS	m SS
Lower Palaeocene	TOP Lower Palaeocene EKOFISK	10582 10625	3225.2 3238.3	10452 10495	3185.6 3198.7
Upper Cretaceous	TOR	10970	3343.5	10840	3303.9
	HOD	12212	3722.0	12082	3682.4
	PLENNUS MARL	14483	4414.2	14353	4374.6
	HIDRA FM.	14524	4426.7	14394	4387.1
Lower Cretaceous	RODBY FM.	14744	4493.8	14614	4454.1
	SOLA FM.	14930	4550.4	14800	4510.8
	VALHALL FM.	15030	4580.9	14900	4541.3
Jurassic	KIMMERIDGE CLAY HOT SHALE	15650	4769.9	15520	4730.3
	HEATER FM.	15917	4851.3	15787	4811.6
	FULMAR SAND	16359	4986.0	16229	4946.4
Permian	ZECHSTEIN ANHYDRITE	16522	5035.7	16392	4996.0

Table A.1. Formation tops for well 22/28a – 1.

Data point (m SS)	Layer interval (m SS)	Vertical stress due to interval (MPa)	Vertical stress upon interval (MPa)	Lithostatic stress S_V (MPa)
#1: 3213	3200.1 – 3221.6	Sv2 = (3213 – 3200.1) x 2.451 x 0.0098 = 0.126	Sv1= 67.49	S_V = Sv1 + Sv2 = 67.49 + 0.126 = **67.6**
#2: 4392	4387.1 – 4397.5	Sv2 = (4392 – 4387.1) x 2.618 x 0.0098 = 0.126	Sv1= 96.139	S_V = Sv1 + Sv2 = 96.139 + 0.126 = **96.3**

Table A.2. Estimates of lithostatic stress for data points 1 and 2 (well 22/28a – 1).

Comments: Sea water density = 1.02 g/cc; 1 psi/ft ≡ 2.31 g/cc; 1 g/cc ≡ 0.0098 MPa/m
ρ_{av} are the averages of RHOB digital logs throughout the interval considered; S_v at the interval is the combined weight of the sea water and overlying sediments taken at the bottom of the interval.

Well 22/28a - 1
57° 04' 58.118'' , 01° 28' 44.095''

Bulk density readings
1st value : 2.403 g/cc @ 2727.5 m BRT
Last value: 2.039 g/cc @ 5104.2 m BRT

	Measured Depth		TVDSS		Thickness	ρ average	Vertical stress due to interval	Lithostatic stress Sv
	Top	Bottom	Top	Bottom				
	m BRT	m BRT	m SS	m SS	m	g/cc	MPa	(MPa)
RTE	**39.6**		Air gap			//////////		
Water depth	**39.6**	**137.2**	**0.0**	**97.5**	**97.5**	**1.02**	0.97	
Sea Bed - Tertiary Top (Glacial Till)	137.2	1286.7	97.5	1247.1	1149.5	2.260	25.46	
Tertiary Top - first RHOB reading	1286.7	2727.5	1247.1	2687.9	1440.8	2.040	28.80	
Other Sediments	2727.5	3239.7	2687.9	3200.1	512.2	2.441	12.25	67.49
CHALK GROUP	3239.7	3261.2	3200.1	3221.6	21.5	2.451	0.52	68.01
	3261.2	3290.3	3221.6	3250.7	29.1	2.692	0.77	68.78
	3290.3	3322.2	3250.7	3282.6	31.9	2.580	0.81	69.58
	3322.2	3343.3	3282.6	3303.7	21.1	2.619	0.54	70.12
	3343.3	3374.0	3303.7	3334.4	30.7	2.615	0.79	70.91
	3374.0	3404.4	3334.4	3364.8	30.5	2.614	0.78	71.69
	3404.4	3434.9	3364.8	3395.3	30.5	2.616	0.78	72.47
	3434.9	3465.4	3395.3	3425.8	30.5	2.622	0.78	73.25
	3465.4	3495.9	3425.8	3456.3	30.5	2.623	0.78	74.04
	3495.9	3526.4	3456.3	3486.8	30.5	2.646	0.79	74.83
	3526.4	3556.8	3486.8	3517.2	30.5	2.602	0.78	75.61
	3556.8	3587.3	3517.2	3547.7	30.5	2.629	0.79	76.39
	3587.3	3617.8	3547.7	3578.2	30.5	2.602	0.78	77.17
	3617.8	3648.3	3578.2	3608.7	30.5	2.648	0.79	77.96
	3648.3	3678.8	3608.7	3639.2	30.5	2.650	0.79	78.75
	3678.8	3709.2	3639.2	3669.6	30.5	2.658	0.79	79.54
	3709.2	3739.7	3669.6	3700.1	30.5	2.640	0.79	80.33
	3739.7	3770.2	3700.1	3730.6	30.5	2.607	0.78	81.11
	3770.2	3800.7	3730.6	3761.1	30.5	2.615	0.78	81.89
	3800.7	3815.8	3761.1	3776.2	15.1	2.632	0.39	82.28
	3815.8	3841.8	3776.2	3802.2	26.0	2.527	0.64	82.93
	3841.8	3867.7	3802.2	3828.1	25.9	2.511	0.64	83.56
	3867.7	4215.0	3828.1	4175.4	347.3	2.101	7.15	90.72
	4215.0	4227.4	4175.4	4187.8	12.4	2.532	0.31	91.02
	4227.4	4312.6	4187.8	4273.0	85.2	2.594	2.16	93.19
	4312.6	4337.1	4273.0	4297.5	24.5	2.642	0.63	93.82
	4337.1	4361.5	4297.5	4321.9	24.4	2.654	0.63	94.46
	4361.5	4385.9	4321.9	4346.3	24.4	2.641	0.63	95.09
	4385.9	4414.2	4346.3	4374.6	28.3	2.641	0.73	95.82
	4414.2	4426.7	4374.6	4387.1	12.5	2.602	0.32	96.14
	4426.7	4437.1	4387.1	4397.5	10.4	2.618	0.27	96.41

Table A.3. Lithostatic stress value for well 22/28a – 1.

A.1.2. Pore pressure estimation – approach in well 22/28a - 1

RFT measurements were made in the Cretaceous and Jurassic within the interval 4156.4 to 4984.2 m SS (13637 to 16353 ft SS). All tests were unsuccessful as the permeability is reported either dry or supercharged and tight.

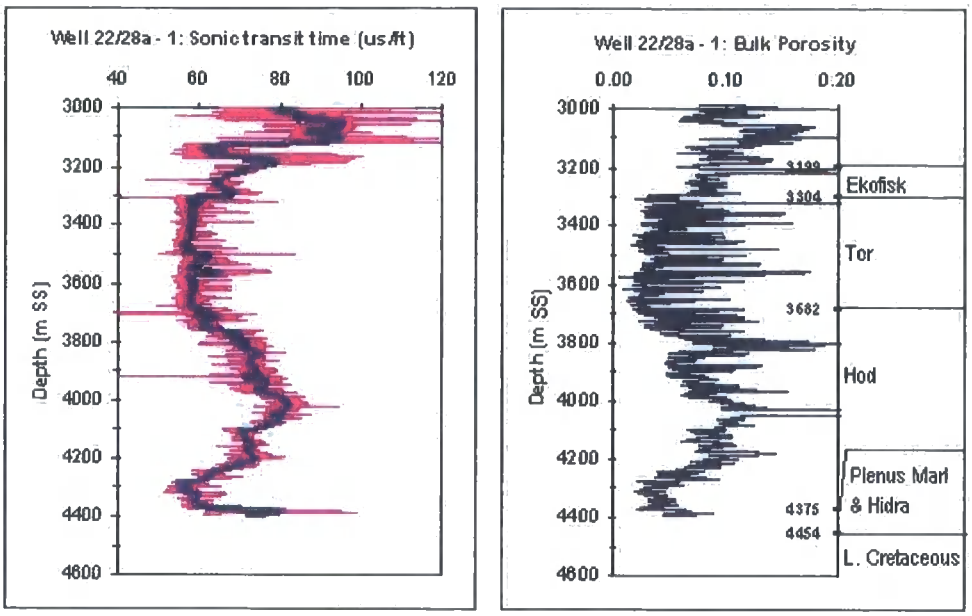

Figure A.1. Compaction trend through the Chalk Group in Well 22/28a – 1 showing the onset of overpressure around 3750 m subsea.

A Regional Study Approach

As no good quality direct pressure measurement values are available, estimation of the Pp within the chalk is made in a regional approach considering RFT data available in other wells within the quadrant and neighbouring quadrants.

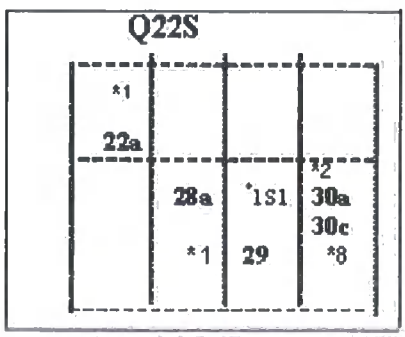

Figure A.2. Location sketch of neighbouring wells.

WELL	# DATA	QUALITY		RFT		Depth	
				psi	MPa	ft SS	m SS
22/22a-1	14	V.G & GOOD	1st reading	3930.3	27.1	8667	2641.6
	2	FAIR	last reading	4359.8	30.1	9446	2879
22/29-1S1	16	Good & Fair	1st reading	4248.7	29.3	9355	2851.3
			last reading	13263.9	91.5	15769	4806.2
22/30a-2	2	Fair		6370.7	43.9	11264	3433.1
		Poor		6440.9	44.4	11428	3482.5
22/30c-8	13	V.G & GOOD	1st reading	15949.4	110.1	17288	5269.1
	5	LOW PERM.	last reading	16091	111	17865	5445

Table A.4. RFT available in neighbouring wells.

Data point (m SS)	Formation Pressure status and approach	**Pore pressure Pp (MPa)**
#1: 3213 Ekofisk	Regional trend: The Palaeocene is known to be normally pressured with zero overpressure in Quadrants 21S, 22S of the Central North Sea (GeoPOP, 2000)	
	$\therefore\ Pp\|_{3213m} = 3213m \times 0.01007\,MPa/m = 32.3\,MPa$	
#2: 4392 Hidra	Neighbouring well: Value determined considering gradient in well 22/29-1S1 where the corresponding Jurassic overpressure is of 40.3 MPa (5846 psi).	
	$\therefore\ Pp\|_{4392m} = 4392m \times 0.01007\,MPa/m + 40.3\,MPa = 84.5\,MPa$	

Table A.5. Estimates of pore pressure for data points 1 and 2 (well 22/28a – 1).

A.2. Well 22/29 – 1S1

A.2.1. Lithostatic stress estimation

Well 22/29 – 1S1 RTE: 22.9 ft, 75 m		Measured Depth		TVD	
		ft BRT	m BRT	ft SS	m SS
Top Late Palaeocene		9604	2927.2	9529	2904.3
Early Palaeocene	EKOFISK	10892	3319.7	10817	3296.9
Late Cretaceous	TOR	11195	3412.1	11120	3389.2
	HOD	12732	3880.5	12657	3857.7
	UPPER VALHALL	14328	4367.0	14253	4344.1
	LOWER VALHALL	14401	4389.2	14326	4366.4
Jurassic	KIMMERIDGE	14540	4431.6	14465	4408.7
	HEATHER FM.	14908	4543.7	14833	4520.9
	FULMAR	15054	4588.24	14979	4565.4
	PETLAND FM.	15101	4602.6	15026	4579.7
Triassic	SKAGGERAK	15413	4697.7	15338	4674.8

Table A.6. Formation tops for well 22/29 – 1S1.

Data point (m SS)	Layer interval (m SS)	Vertical stress due to interval (MPa)	Vertical stress upon interval (MPa)	Lithostatic stress S_V (MPa)
#3: 3308	3296.8 – 3316.9	Sv2 = (3308 – 3296.8) x 2.464 x 0.0098 = 0.270	Sv1= 70.94	S_V = Sv1 + Sv2 = 70.94 + 0.270 = **71.2**
#4: 3339	3316.9 – 3346.5	Sv2 = (3339 – 3316.9) x 2.612 x 0.0098 = 0.310	Sv1= 71.44	S_V = Sv1 + Sv2 = 71.44 + 0.310 = **71.8**
#5: 4336	4305.0 – 4344.1	Sv2 = (4336 – 4305.0) x 2.589 x 0.0098 = 0.787	Sv1= 96.99	S_V = Sv1 + Sv2 = 96.99 + 0.787 = **97.8**

Table A.7. Estimates of lithostatic stress for data points 3, 4 and 5 (well 22/29 – 1S1).

Well 22/29 - 1S1
57° 08' 18.1'' ; 01° 44' 05.4''

Bulk density readings
1st value : 2.290 g/cc @ 2666.9 m BRT
Last value: 2.551 g/cc @ 4726.7 m BRT

	Measured Depth		TVDSS		Thickness	ρ average	Vertical stress due to interval	Lithostatic stress Sv
	Top	Bottom	Top	Bottom	m	g/cc	MPa	(MPa)
	m BRT	m BRT	m SS	m SS				
RTE	**22.9**		Air gap			//////////		
Water depth	**22.9**	**118.0**	**0.0**	**95.1**	**95.1**	**1.02**	**0.95**	
Seabed- Tertiary Top (Glacial Till)	118.0	1755.6	95.1	1732.7	1637.6	2.26	36.27	
Tertiary Top - first RHOB reading	1755.6	2666.9	1732.7	2644.0	911.3	2.04	18.22	
Other Sediments	2666.9	3319.7	2644.0	3296.8	652.8	2.423	15.50	70.94
CHALK GROUP	3319.7	3339.8	3296.8	3316.9	20.1	2.464	0.49	71.44
	3339.8	3369.4	3316.9	3346.5	29.6	2.612	0.76	72.19
	3369.4	3390.7	3346.5	3367.8	21.3	2.595	0.54	72.73
	3390.7	3412.1	3367.8	3389.2	21.3	2.645	0.55	73.28
	3412.1	3479.4	3389.2	3456.5	67.4	2.617	1.73	75.01
	3479.4	3504.1	3456.5	3481.2	24.7	2.618	0.63	75.64
	3504.1	3580.3	3481.2	3557.4	76.2	2.633	1.97	77.61
	3580.3	3717.5	3557.4	3694.6	137.2	2.640	3.55	81.16
	3717.5	3880.5	3694.6	3857.6	163.1	2.680	4.28	85.44
	3880.5	3925.6	3857.6	3902.7	45.1	2.653	1.17	86.61
	3925.6	4024.1	3902.7	4001.2	98.4	2.639	2.55	89.16
	4024.1	4084.1	4001.2	4061.2	60	2.633	1.55	90.71
	4084.1	4128.9	4061.2	4106.0	44.8	2.624	1.15	91.86
	4128.9	4327.9	4106.0	4305.0	199	2.631	5.13	96.99
	4327.9	4367.0	4305.0	4344.1	39	2.589	0.99	97.98
	4367.0	4389.2	4344.1	4366.3	22.2	2.655	0.58	98.56
	4389.2	4431.6	4366.3	4408.7	42.4	2.648	1.10	99.66

Comments: Sea water density = 1.02 g/cc; 1 psi/ft ≡ 2.31 g/cc; 1 g/cc ≡ 0.0098 MPa/m
ρ_{av} are the averages of RHOB digital logs throughout the interval considered; S_v at the interval is the combined weight of the sea water and overlying sediments taken at the bottom of the interval.

Table A.8. Lithostatic stress values for well 22/29 – 1S1.

A.2.2. Pore pressure estimation in well 22/29a – 1S1

	RFT		Depth		Quality
	psi	MPa	ft SS	m SS	
PALAEOCENE	4248.7	29.3	9355.3	2851.4	Good
	4310.1	29.7	9532.4	2905.3	Good
	4319.7	29.8	9532.6	2905.4	Good
	4337.9	29.9	9590.4	2923	Good
	4344.5	30.0	9590.4	2923	Fair
	4637.7	32.0	10088.5	3074.8	Good
CRETACEOUS	5847.7	40.3	12006.8	3659.5	Fair
JURASSIC	12994.5	89.6	14794.3	4509.1	Fair
	13004.9	89.7	14796.3	4509.7	Good
	12995.1	89.6	14798.3	4510.3	Fair
	12991.4	89.6	14800.3	4510.9	Good
	13024.0	89.8	14802.3	4511.5	Good
	12997.9	89.6	14804.3	4512.1	Good
TRIASSIC	13069.3	90.1	15652.5	4770.6	Fair
	13185.5	90.9	15762.5	4804.2	Fair
	13263.9	91.5	15768.5	4806	Fair

Table A.9. RFT measurements in well 22/29 – 1S1; taken from the composite log.

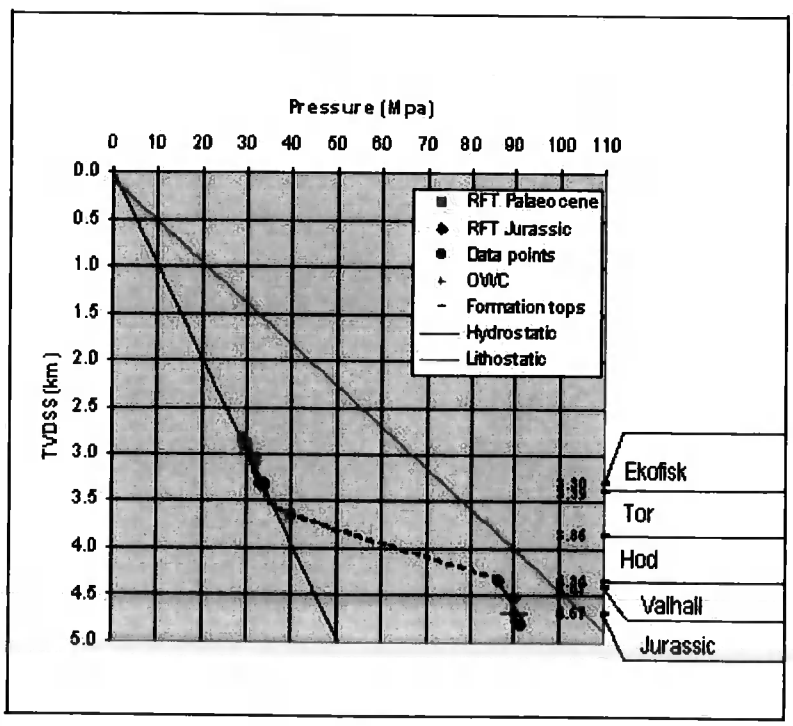

Figure A.3. Pressure – depth plot: Well 22/29 – 1S1.

The Palaeocene being normally pressured (Figure A.3), pore pressure for data points picked in the Ekofisk are estimated accordingly. For the data point at the base of the Chalk, extrapolation from the Water leg has been used.

Data point (m SS)	Formation Pressure status and approach	**Pore pressure Pp (MPa)**
#3: 3308 Ekofisk	The Palaeocene being normally pressured (Figure A.3), pore pressure for data points picked in the Ekofisk are estimated accordingly	
	$\therefore Pp\|_{3308mSS} = 3308m \times 0.01007\,MPa/m = 33.3\,MPa$	
#4: 3339 Ekofisk	As above	
	$\therefore Pp\|_{3339mSS} = 3339m \times 0.01007\,MPa/m = 33.6\,MPa$	
#5: 4336 Hod	Using the petrophysics data provided, the OWC is at depth 4675.4 m SS (15340 ft SS). The RFT measurements available in the water leg (Table A.9. i.e. interval 4770.6 – 4806.0) suggests an overpressure value of 42.9 MPa at the OWC.	
	$\therefore Pp\|_{4336mSS} = 42.9\,MPa + (0.01007\,MPa/m \times 4336m) = 86.6\,MPa$	

Table A.10. Pore pressure estimates of Data points 3, 4 and 5; in well 22/29 – 1S1.

A.3. Well 22/30a – 2

A.3.1. Lithostatic stress estimation

Well 22/30a - 2 RTE: 90 ft , 27.4 m		Measured Depth		TVD	
		ft BRT	m BRT	ft SS	m SS
Lower Palaeocene	EKOFISK	10995	3351.1	10905	3323.7
Upper Cretaceous	TOR	11348	3458.7	11258	3431.3
	HOD	13026	3970.1	12936	3942.7
Lower Cretaceous	UPPER VALHALL	14020	4273.1	13930	4245.7
(Unconformity)	LOWER VALHALL	14207	4330.1	14117	4302.7
Jurassic	HEATER FM.	14280	4352.3	14190	4324.9
(Unconformity)	FLADEN GP – PENTLAND FM.	14328	4367.0	14238	4339.5
Triassic	SKAGERRAK	14435	4399.6	14345	4372.1

Table A.11. Formation tops in well 22/30a – 2.

Well 22/30a - 2
57° 08' 52.7" ; 0° 48' 52.7"

Bulk density readings
1st value : 1.942 g/cc @ 2740.6 m BRT
Last value: 2.345 g/cc @ 4421.0 m BRT

	Measured Depth		TVDSS		Thickness	ρ average	Vertical stress due to interval	Lithostatic stress Sv
	Top	Bottom	Top	Bottom				
	m BRT	m BRT	m SS	m SS	m	g/cc	MPa	(MPa)
RTE	27.4		Air gap			//////////		
Water depth	27.4	119.5	0.0	92.1	92.1	1.020	0.92	
Seabed- Tertiary Top (Glacial Till)	119.5	789.4	92.1	762.0	669.9	2.26	14.84	
Tertiary Top - first RHOB reading	789.4	2740.6	762.0	2713.2	1951.2	2.04	39.01	
	2740.6	3351.1	2713.2	3323.7	610.5	2.376	14.34	68.98
	3351.1	3370.9	3323.7	3343.5	19.8	2.468	0.48	69.46
	3370.9	3444.1	3343.5	3416.7	73.2	2.612	1.87	71.33
	3444.1	3474.6	3416.7	3447.2	30.5	2.57	0.77	72.10
	3474.6	3505.0	3447.2	3477.6	30.4	2.575	0.77	72.87
	3505.0	3535.5	3477.6	3508.1	30.5	2.543	0.76	73.63
	3535.5	3566.0	3508.1	3538.6	30.5	2.593	0.78	74.40
Chalk Group	3566.0	3596.5	3538.6	3569.1	30.5	2.566	0.77	75.17
	3596.5	3626.9	3569.1	3599.5	30.4	2.594	0.77	75.94
	3626.9	3657.4	3599.5	3630.0	30.5	2.608	0.78	76.72
	3657.4	3687.9	3630.0	3660.5	30.5	2.611	0.78	77.50
	3687.9	3718.4	3660.5	3691.0	30.5	2.595	0.78	78.28
	3718.4	3748.9	3691.0	3721.5	30.5	2.598	0.78	79.06
	3748.9	3779.3	3721.5	3751.9	30.4	2.64	0.79	79.84
	3779.3	3809.8	3751.9	3782.4	30.5	2.639	0.79	80.63
	3809.8	3815.9	3782.4	3788.5	6.1	2.668	0.16	80.79
	3815.9	3892.1	3788.5	3864.7	76.2	2.645	1.98	82.77
	3892.1	3901.2	3864.7	3873.8	9.1	2.657	0.24	83.00
	3901.2	3928.7	3873.8	3901.3	27.5	2.623	0.71	83.71
	3928.7	3951.5	3901.3	3924.1	22.8	2.608	0.58	84.29
	3951.5	4245.7	3924.1	4218.3	294.2	2.618	7.55	91.84
	4245.7	4267.0	4218.3	4239.6	21.3	2.576	0.54	92.38
to base Chalk	4267.0	4285.3	4239.6	4257.9	18.3	2.625	0.47	92.85

Comments: Sea water density = 1.02 g/cc; 1 psi/ft ≡ 2.31 g/cc; 1 g/cc ≡ 0.0098 MPa/m
ρ_{av} are the averages of RHOB digital logs throughout the interval considered; S_v at the interval is the combined weight of the sea water and overlying sediments taken at the bottom of the interval.

Table A.12. Lithostatic stress values for well 22/30a – 2.

Data point (m SS)	Layer interval (m SS)	Vertical stress due to interval (MPa)	Vertical stress upon interval (MPa)	Lithostatic stress S_V (MPa)
#6: 3433	3416.7 – 3447.2	Sv2 = (3433 – 3416.7) x 2.570 x 0.0098 = 0.486	Sv1= 71.33	S_V = Sv1 + Sv2 = 71.33 + 0.486 = **71.8**
#7: 4224	4218.3 – 4239.6	Sv2 = (4224 – 4218.3) x 2.576 x 0.0098 = 0.144	Sv1= 91.84	S_V = Sv1 + Sv2 = 91.84 + 0.144 = **92.0**

Table A.13. Estimates of lithostatic stress for data points 6 and 7 (well 22/30a – 2).

A.3.2. Pore pressure estimation in well 22/30a – 2

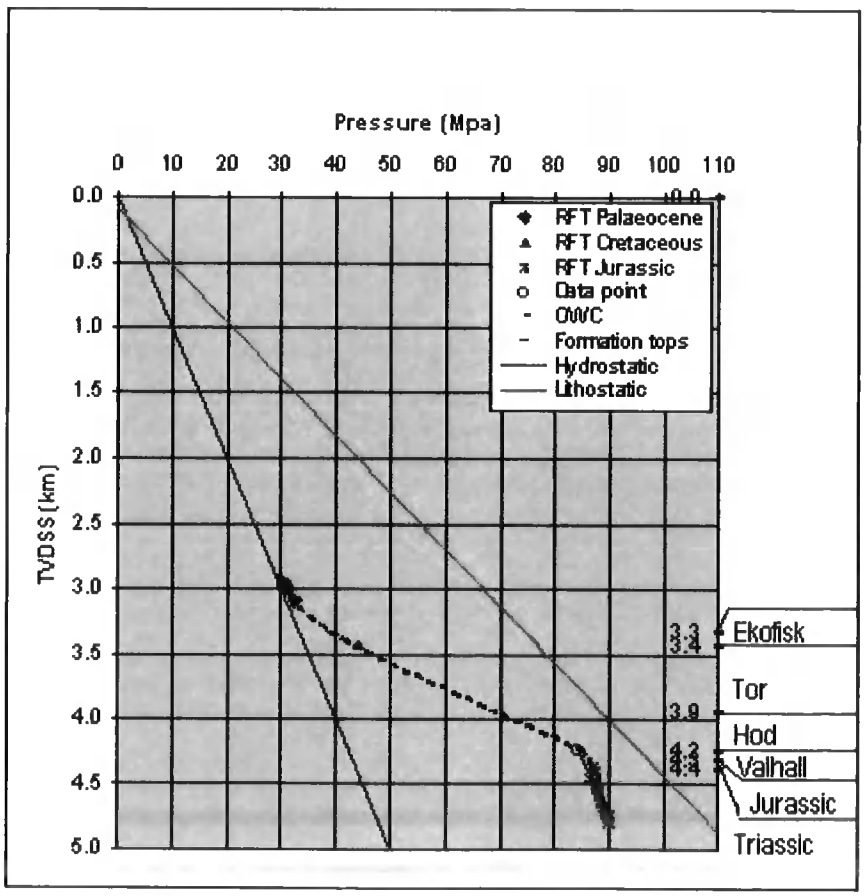

Table A.14. Pressure-depth plot for well 22/30a – 8.

	RFT		Depth		Quality
	psi	MPa	ft SS	m SS	
PALAEOCENE	4382	30.2	9687	2952.6	Fair
	4507	31.1	9744	2969.9	Fair
	4529	31.2	9861	3005.6	Good
	4704	32.4	10147	3092.7	Fair
CRETACEOUS	6385	44.0	11263	3432.9	Fair
JURASSIC	12653	87.3	14297	4357.5	Good
	12671	87.4	14324	4365.7	Good
TRIASSIC	12672	87.4	14407	4390.9	Good
	12675	87.4	14427	4397	Good
	12521	86.4	14589	4446.6	Good
	12726	87.8	14681	4474.6	Good
	12749	87.9	14770	4501.6	Good
	12756	88	14796	4509.5	Good
	12770	88.1	14842	4523.5	Good
	12780	88.1	14895	4539.9	Good
	12790	88.2	14939	4553.3	Good
	12803	88.3	14965	4561.2	Fair
	12817	88.4	15012	4575.4	Fair
	12826	88.5	15050	4587	Fair
	12839	88.5	15123	4609.2	Good
	12842	88.6	15142	4614.9	Good
	12864	88.7	15224	4640.1	Good
	12872	88.8	15254	4649.3	Good
	12912	89	15356	4680.2	Good
	12935	89.2	15404	4694.8	Good
	12978	89.5	15468	4714.6	Good
	12979	89.5	15468	4714.6	Good
	13078	90.2	15513	4728.2	Fair
	13028	89.9	15613	4758.6	Good
	13064	90.1	15717	4790.2	Good

Table A.15. Well 22/30a - 2 RFT measurements through the Palaeocene, Cretaceous Chalk and the Jurassic (Source: composite log).

Data point (m SS)	Formation Pressure status and approach	**Pore pressure Pp (MPa)**
#6: 3433 Tor	Direct pressure measurement, RFT: *44.0 MPa*	
#7: 4224 Hod	Using the petrophysics data available, the Oil Water Contact (OWC) is at depth 4661.1 m SS (15293 ft SS). The pressure gradient within water leg is $\left.\frac{\Delta P}{\Delta D}\right\|_{Water\,leg} = \frac{90.1-89.0}{4790.2-4680.2} = 0.010\,MPa/m$ And the pressure at the OWC is $\therefore\ Pp\|_{OWC:4661.1\,mSS} = 90.1+0.010\times(4661.1-4790.2) = 88.81\ MPa$ accounting for an overpressure of: O/P = 88.81 – (4661.1 x 0.01007) = 41.87 MPa	
	Extrapolating the hydrostatic parallel from the water leg, $\therefore\ Pp\|_{4224\,m} = 4224m\times 0.01007MPa/m + 41.87\,MPa = 84.4\ MPa$	

Table A.16. Pore pressure estimates of Data points 6 and 7; in well 22/30a – 2.

A.4. Well 22/30c – 8

A.4.1. Lithostatic stress estimations

Well 22/30c - 8 RTE: 130 ft, 39.6 m		Measured Depth		TVD	
		ft BRT	m BRT	ft BRT	m SS
Lower Palaeocene	EKOFISK	11296	3443	11169	3404
Upper Cretaceous	TOR	11628	3544	11500	3505
	HOD	13324	4061	13196	4022
	HERRING FM.	15749	4800	15621	4761
	PLENUS MARL	16231	4947	16103	4908
	HIDRA FM.	16313	4972	16185	4933
Lower Cretaceous	RODBY FM.	16556	5046	16428	5007
	SOLA FM.	16704	5091	16576	5052
	VALHALL FM.	16802	5121	16674	5082
Jurassic	KIMMERIDGE CLAY HOT SHALE	16815	5125	16687	5086
	HEATHER FM.	17406	5305	17278	5266

Table A.17. Formation tops for well 22/30c – 8.

Data point (m SS)	Layer interval (m SS)	Vertical stress due to interval (MPa)	Vertical stress upon interval (MPa)	Lithostatic stress S_V (MPa)
#8: 3425	3404 - 5007	Sv2 = (3425 – 3404) x 2.600 x 0.0098 = 0.535	Sv1= 76.34	S_V = Sv1 + Sv2 = 76.34 + 0.535 = **76.88**
#9: 3460	3404 - 5007	Sv2 = (3460 – 3404) x 2.600 x 0.0098 = 1.426	Sv1= 76.34	S_V = Sv1 + Sv2 = 76.34 + 1.426 = **77.77**
#10: 4885	3404 - 5007	Sv2 = (4885 – 3404) x 2.600 x 0.0098 = 37.736	Sv1= 76.34	S_V = Sv1 + Sv2 = 76.34 + 37.74 = **114.08**

Table A.18. Estimates of lithostatic stress for data points 8, 9 and 10 (well 22/30c – 8).

Well 22/30c - 8
57° 00' 43.99" ; 01° 50' 24.00"

Bulk density readings
Density gradient and lithology averages are used (i.e. No RHOB e-log available)

	Measured Depth		TVDSS		Thickness	ρ	Vertical	Lithostatic
	Top	Bottom	Top	Bottom		average	stress due	stress Sv
	m BRT	m BRT	m SS	m SS	m	g/cc	to interval MPa	MPa
RTE	39		Air Gap			//////////	//////////	
Water depth	39	131	0	92	92	1.02	0.92	
Seabed- Tertiary Top (Quaternary Glacial Till)	131	220	92	181	89	2.26	1.97	
Tertiary sediments	220	1545	181	1506	1325	2.04	26.49	29.38
Claystone to shale, limestone, sand	1545	2791	1506	2752	1246	2.55	31.14	60.52
Claystone, Limestone, dolomite	2791	3040	2752	3001	249	2.65	6.47	66.98
Limestone, Claystone	3040	3443	3001	3404	403	2.37	9.36	76.34
Top Chalk	3443	5046	3404	5007	1603	2.60	40.84	117.19
Base Chalk	5046		5007					

Comments: Sea water density = 1.02 g/cc; 1 psi/ft ≡ 2.31 g/cc; 1 g/cc ≡ 0.0098 MPa/m

ρ_{av} are the averages of RHOB digital logs throughout the interval considered; S_v at the interval is the combined weight of the sea water and overlying sediments taken at the bottom of the interval.

Table A.19. Lithostatic stress value for well 22/30c – 8.

A.4.2. Pore pressure estimation in well 22/30c - 8

Some RFT measurements available in the Jurassic, still a regional approach is being used for the top of Chalk data points.

RFT		Depth		Quality
psi	MPa	ft SS	m SS	
15964	110.1	17355	5289.5	Good
15972	110.2	17389	5299.9	Good
15976	110.2	17411	5306.6	Good
16008	110.4	17553	5349.9	Good
16015	110.4	17583	5359.0	Good
16019	110.5	17600	5364.2	Good
16026	110.5	17632	5374.0	Good
16030	110.6	17647	5378.5	Good
16046	110.7	17721	5401.1	Good
16052	110.7	17747	5409.0	Good
16057	110.7	17772	5416.6	Good
16067	110.8	17814	5429.4	Good
16072	110.8	17838	5436.8	Good

Table A.20. RFT measurements in the Jurassic. Well 22/30c – 8.

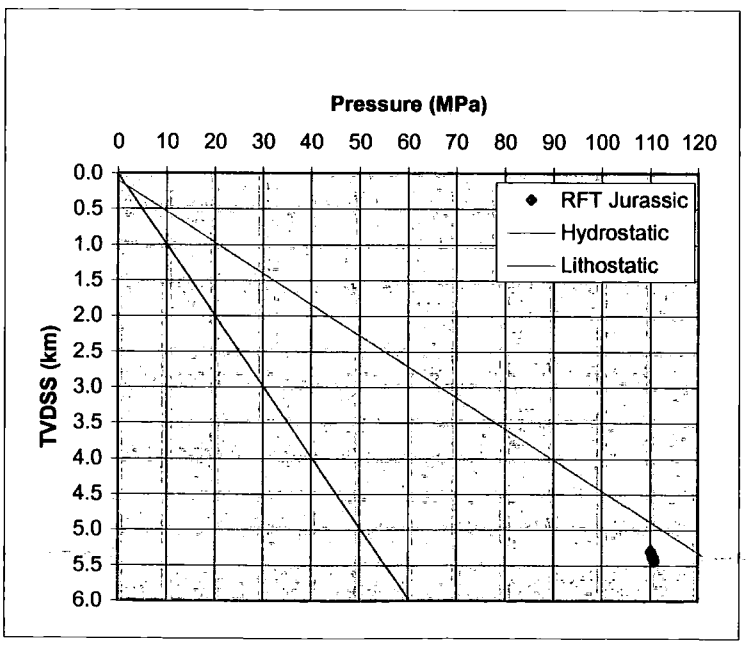

Figure A.4. Pressure – depth Plot. Well 22/30c – 8.

Field	Depth (m)	Pressure (MPa)	Overpressure (MPa)
Palaeocene			
22/30a	2908	27.6 – 34.5	0 – 3.4
22/30b & c	2940	27.6 – 34.5	Less than zero
Cretaceous			
22/30a	3433	41.4 – 48.2	6.9 – 13.8

Table A.21. Regional pressure trends suggesting that the Palaeocene is normally pressured, thus the top of Chalk (Source: GeoPOP, 2000).

Data point (m SS)	Formation Pressure status and approach	**Pore pressure Pp (MPa)**
#8: 3425 Ekofisk	$\therefore\ Pp\|_{3425m} = 3425\,m \times 0.01007\,MPa/m = 34.5\ MPa$	
#9: 3460 Ekofisk	$\therefore\ Pp\|_{3460m} = 3460\,m \times 0.01007\,MPa/m = 34.8\ MPa$	
#10: 4885 Hidra	Using the petrophysics data available, the Gas Water Contact (GWC) is at depth 5462 m SS. With Pp given in MPa and depth in meters, the RFT trend line in the Jurassic from data available (Table A.20) in the Jurassic is given by: $P_p\|_{depth} = 0.00508 \times depth + 83.2$ $\therefore\ Pp\|_{GWC:5462m} = 5462\,m \times 0.00508\,MPa/m + 83.2 = 110.9\,MPa$ Value determined considering gradient in well 22/29-1S1 where the corresponding Jurassic overpressure is of 40.3 MPa (5846 psi). Based on the hydrostatic gradient parallel in the Jurassic, we have $\therefore\ Pp\|_{4392m} = 4392m \times 0.01007 MPa/m + 40.3\,MPa = 84.5\ MPa$ Accounting for an overpressure of $O/P\|_{GWC:5462m} = 110.9 - 0.01007 \times 5462 = 56.0\,MPa$	
	And the Pore pressure estimation at the Base Chalk data point is: $Pp\|_{4885m} = 56.0 + 0.01007 \times 4885 = 105.2\,MPa$	

Table A.22. Estimates of pore pressure for data points 8, 9 and 10 (well 22/30c – 8).

A.5. Well 30/12b – 4

A.5.1. Lithostatic stress estimation

Well 30/12b - 4
56° 31' 45.97" ; 02° 14' 12.36"

Bulk density readings
1st value : 1.979 g/cc @ 1737.3 m BRT
Last value: 2.568 g/cc @ 4570.3 m BRT

	Measured Depth		TVDSS			ρ		
	Top	Bottom	Top	Bottom	Thickness	average		
	m BRT	m BRT	m SS	m SS	m	g/cc	MPa	Sv (MPa)
RTE	**25.0**		Air gap			//////////		
Water depth	79.5		0.0	79.5	79.5	1.02	0.79	
Seabed-	104.5	307.8	79.5	282.8	203.3	2.26	4.50	
Tertiary Top	307.8	1737.2	282.8	1712.2	1429.4	2.040	28.58	
Other Tertiary	1737.2	3155.1	1712.2	3130.1	1417.9	2.255	31.33	
	3155.1	3178.3	3130.1	3153.3	23.2	2.545	0.58	65.79
	3178.3	3201.5	3153.3	3176.5	23.2	2.417	0.55	66.34
	3201.5	3254.5	3176.5	3229.5	53.0	2.560	1.33	67.67
	3254.5	3400.2	3229.5	3375.2	145.7	2.512	3.59	71.25
	3400.2	3613.9	3375.2	3588.9	213.7	2.689	5.63	76.88
	3613.9	3642.2	3588.9	3617.2	28.3	2.603	0.72	77.61
Chalk Group	3642.2	3672.7	3617.2	3647.7	30.5	2.616	0.78	78.39
	3672.7	3703.1	3647.7	3678.1	30.5	2.630	0.79	79.17
	3703.1	3733.6	3678.1	3708.6	30.5	2.628	0.79	79.96
	3733.6	3764.1	3708.6	3739.1	30.5	2.568	0.77	80.73
	3764.1	3778.7	3739.1	3753.7	14.6	2.594	0.37	81.10
	3778.7	3839.7	3753.7	3814.7	61.0	2.609	1.56	82.66
	3839.7	3852.5	3814.7	3827.5	12.8	2.617	0.33	82.99
	3852.5	3868.6	3827.5	3843.6	16.2	2.650	0.42	83.41
to base Chalk	3868.6	3908.9	3843.6	3883.9	40.2	2.613	1.03	84.44

Sea water density = 1.02 g/cc; 1 psi/ft ≡ 2.31 g/cc; 1 g/cc ≡ 0.0098 MPa/m

ρ_{av} are the averages of RHOB digital logs throughout the interval considered; S_v at the interval is the combined weight of the sea water and overlying sediments taken at the bottom of the interval.

Table A.23. Lithostatic stress values for well 30/12b – 4.

Well 30/12b - 4 RTE: 82 ft , 25.0 m		Measured Depth		TVD	
		ft BRT	m BRT	ft SS	m SS
Lower Palaeocene	EKOFISK	10352	3155.1	10270	3130.1
Upper Cretaceous	TOR	10677	3254.2	10595	3229.2
	HOD	11857	3613.8	11775	3588.8
Lower Cretaceous	VALHALL	12825	3908.9	12743	3883.9
Jurassic	KIMMERIDGE	12836	3912.2	12754	3887.2
	FULMAR SAND	12879	3925.3	12797	3900.3
Triassic	SMITH BANK FM.	13288	4050.0	13206	4025.0

Table A.24. Formation tops for well 22/30c – 8.

Data point (m SS)	Layer interval (m SS)	Vertical stress due to interval (MPa)	Vertical stress upon interval (MPa)	Lithostatic stress S_V (MPa)
#11: 3158	3153.3 – 3176.5	Sv2 = (3158 – 3153.3) x 2.417 x 0.0098 = 0.111	Sv1= 65.79	S_V = Sv1 + Sv2 = 65.79 + 0.111 = **65.90**
#12: 3833	3827.5 – 3843.6	Sv2 = (3833 – 3827.5) x 2.650 x 0.0098 = 0.143	Sv1= 82.99	S_V = Sv1 + Sv2 = 82.99 + 0.143 = **83.13**

Table A.25. Estimates of lithostatic stress for data points 11 and 12 (well 30/12b – 4).

A.5.2. Pore pressure estimation in well 30/12b - 4

Only Jurassic RFT data are available in this well. For there is no Palaeocene pressure direct measurement in 30/12b -4, data from surrounding wells in block 30/7 are used to find the pore pressure for data point #11 (Top of the Chalk).

From the Regional Pressure Atlas of the Central North Sea (GeoPOP, 2000), the value of *Pp* for the Top of the Chalk is expected to be within the range of RFT values in the Palaeocene (excluding Ekofisk Formation) as given in Table A.26.

Interval depths	**2895.5 – 3200.2 m** 9500 – 10500 ft
RFT readings	**39.3 – 53.8 MPa** (5700-7800 psi)
	Q30

Table A.26. Q 30 Regional Pressure in Palaeocene, excluding Ekofisk
(Source: Regional Pressure Atlas of the CNS, GeoPOP, 2000 Plots 3.2 and 3.6).

RFT		Depth		Quality
psi	MPa	ft SS	m SS	
6593	45.5	12798	3900.6	V Good
6595	45.5	12803	3902.2	V Good
6601	45.5	12806	3903.1	V Good
6600	45.5	12820	3907.3	V Good
6601	45.5	12824	3908.6	V Good
6602	45.5	12829	3910.1	V Good
6605	45.6	12834	3911.6	V Good
6608	45.6	12841	3913.7	V Good
6594	*45.5*	*12849*	*3916.2*	*Good*
6581	*45.4*	*12869*	*3922.3*	*Good*
6592	*45.5*	*12885*	*3927.2*	*Good*
8365	57.7	13577	4138.1	Good
8484	58.5	13751	4191.1	Fair
8920	61.5	14496	4418.2	Fair

Table A. 27. Well 30/12b - 4 RFT measurements through the Jurassic
(Source: composite log).

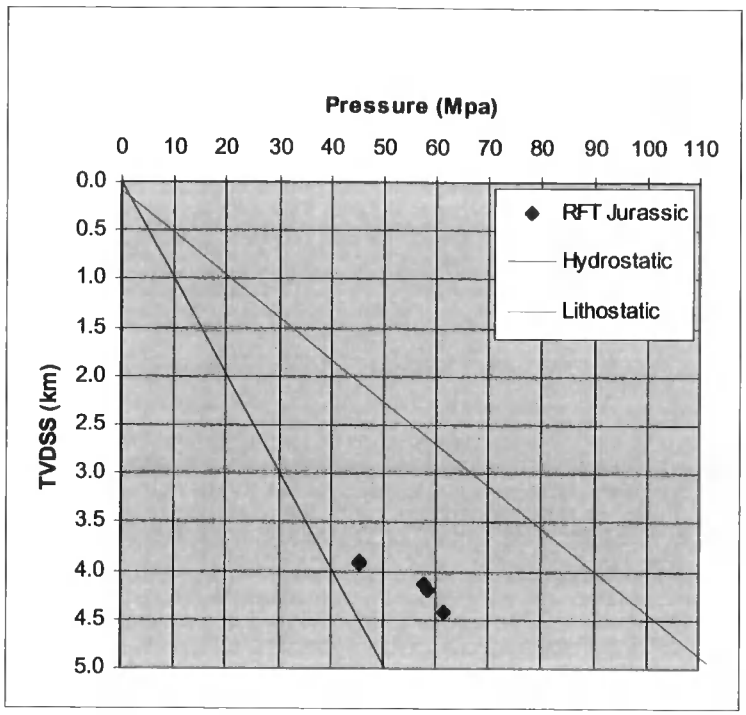

Figure A.5. Pressure – depth plot: well 30/12b – 4.

Data point (m SS)	Formation Pressure status and approach	**Pore pressure Pp (MPa)**
#11: 3158 Ekofisk	The Palaeocene in Q30 N being hydrostatic pressured, $\therefore\ Pp\|_{3158m} = 48.6\,MPa + (3158 - 2977.8\,m) \times 0.01007\,MPa/m = 50.4\ MP$	
#12: 3833 Hod	Using the petrophysics data available, the Oil Water Contact (OWC) is at depth 3986.0 m SS (13078 ft SS). The pressure gradient within the water leg is $\left.\frac{\Delta P}{\Delta D}\right\|_{Oil\ leg} = \frac{45.57 - 45.47}{3913.7 - 3900.6} = 0.00763\,MPa/m$ And the pressure at the OWC is $\therefore\ Pp\|_{OWC:3986.0\,mSS} = 45.57 + 0.00763 \times (3986.0 - 3913.6) = 46.1\ MPa$, accounting for an overpressure of: O/P = 46.1 – (3986 x 0.01007) = 5.98 MPa	
	Extrapolating the hydrostatic parallel from the water leg, pressure at the data point #12 is estimated: $\therefore\ Pp\|_{3986\,m} = 3833m \times 0.01007MPa/m + 5.98\,MPa = 44.6\ MPa$	

Table A.28. Estimates of pore pressure for data points 11 and 12 (well 30/12b - 4).

A.6. Well 30/13 – 3

A.6.1. Lithostatic stress estimation

Well 30/13 - 3
56° 37' 41.293'' N 02° 33' 09.754'' E

Bulk density readings
1st value : 2.307 g/cc @ 2897.1 m BRT
Last value: 2.518 g/cc @ 5135.0 m BRT

	Measured Depth		TVDSS		Thickness	ρ	Vertical stress due to interval	Sv
	Top	Bottom	Top	Bottom		average		
	m BRT	m BRT	m SS	m SS	m	g/cc	MPa	(MPa)
RTE	**34.7**		Air gap			//////////		
Water depth	34.7	106	0	71.3	71.3	1.02	0.71	
Seabed- Tertiary Top (Glacial Till)	106.1	1500.0	71.4	1465.3	1393.9	2.26	30.87	
Tertiary Top - first RHOB reading	1500.0	2897.9	1465.3	2863.2	1397.9	2.04	27.95	
	2897.9	3224.5	2863.2	3189.8	326.6	2.406	7.70	67.23
	3224.5	3252.1	3189.8	3217.4	27.6	2.357	0.64	67.87
	3252.1	3303.9	3217.4	3269.2	51.8	2.505	1.27	69.14
	3303.9	3334.3	3269.2	3299.6	30.5	2.54	0.76	69.90
	3334.3	3364.8	3299.6	3330.1	30.5	2.546	0.76	70.66
	3364.8	3395.3	3330.1	3360.6	30.5	2.528	0.76	71.42
	3395.3	3425.8	3360.6	3391.1	30.5	2.561	0.77	72.18
	3425.8	3456.3	3391.1	3421.6	30.5	2.59	0.77	72.96
CHALK GROUP	3456.3	3489.8	3421.6	3455.1	33.5	2.608	0.86	73.81
	3489.8	3587.2	3455.1	3552.5	97.4	2.76	2.63	76.45
	3593.4	3598	3558.7	3563.3	4.6	2.616	0.12	76.57
	3598.0	3748.9	3563.3	3714.2	150.9	2.57	3.80	80.37
	3748.9	3779.3	3714.2	3744.6	30.5	2.578	0.77	81.14
	3779.3	3809.8	3744.6	3775.1	30.5	2.608	0.78	81.92
To Base Chalk Group	3809.8	3845.8	3775.1	3811.1	36.0	2.545	0.90	82.81

Sea water density = 1.02 g/cc; 1 psi/ft ≡ 2.31 g/cc; 1 g/cc ≡ 0.0098 MPa/m

ρ_{av} are the averages of RHOB digital logs throughout the interval considered; S_v at the interval is the combined weight of the sea water and overlying sediments taken at the bottom of the interval.

Table A.29. Lithostatic stress values for well 30/13 – 3.

Well 30/13 - 3 RTE: 114 ft , 34.7 m		Measured Depth		TVD	
		ft BRT	m BRT	ft SS	m SS
Lower Palaeocene	EKOFISK	10521	3206.6	10407	3171.9
Upper Cretaceous	TOR	10820	3297.8	10706	3263.0
	HOD	11451	3490.1	11337	3455.3
Lower Palaeocene	VALHALL FM.	12618	3845.8	12504	3811.0
Upper Jurassic	KIMMERIDGE	12711	3874.1	12597	3839.4
	HEATER FM.	13262	4042.1	13148	4007.3
	JACQUI SANDSTONE	13668	4165.8	13554	4131.1
	L. HEATHER SHALE	13874	4228.6	13760	4193.8
Middle Jurassic	BRYNE FM.	14178	4321.2	14064	4286.5
Triassic	SKAGERRAK	14624	4457.2	14510	4422.4

Table A.30. Formation tops for well 30/13 – 3.

Data point (m SS)	Layer interval (m SS)	Vertical stress due to interval (MPa)	Vertical stress upon interval (MPa)	Lithostatic stress S_V (MPa)
#13: 3199 Ekofisk	3189.4 – 3217.4	Sv2 = (3199 – 3189.8) x 2.357 x 0.0098 = 0.213	Sv1= 67.23	S_V = Sv1 + Sv2 = 67.23 + 0.213 = **67.44**
#14: 3281 Ekofisk	3269.2 – 3299.6	Sv2 = (3281 – 3269.2) x 2.540x 0.0098 = 0.294	Sv1= 69.14	S_V = Sv1 + Sv2 = 69.14 + 0.294 = **69.43**
#15: 3781 Hod	3775.1 – 3811.1	Sv2 = (3781 – 3775.1) x 2.545x 0.0098 = 0.147	Sv1= 81.92	S_V = Sv1 + Sv2 = 81.92 + 0.147 = **82.06**

Table A.31. Estimates of lithostatic stress for data points 13, 14 and 15 (well 30/13 – 3).

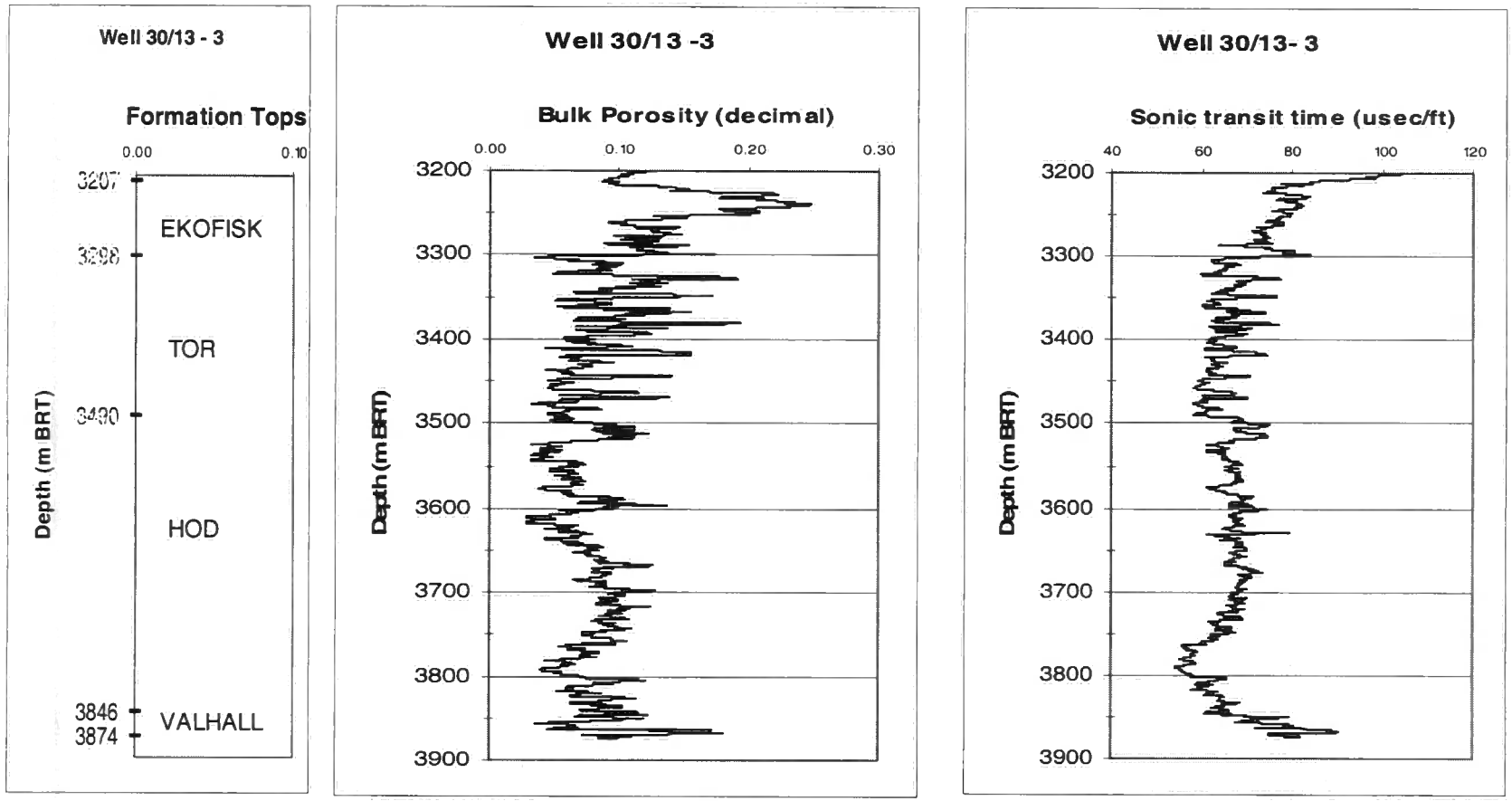

Figure A.6. Compaction trend through the Chalk Group in Well 30/13 – 3 showing the onset of overpressure (Equivalent depth method Hubbert and Rubey, 1959).

A.6.2. Pore pressure estimation

There is no pressure direct measurement within the Palaeocene in well 30/13-3. However, good quality RFT data are available in the Jurassic, as given below:

RFT		DEPTH		Quality
Psi	MPa	ft SS	m SS	
10651.0	73.5	13553	4130.8	GOOD
10652.1	73.5	13556	4131.7	GOOD
10785.4	74.4	13573	4136.8	FAIR
10786.3	74.4	13578	4138.4	GOOD
10788.5	74.4	13585	4140.5	FAIR
10790.0	74.4	13591	4142.3	GOOD
10782.1	74.4	13605	4146.6	GOOD
10784.6	74.4	13613	4149.0	FAIR
10847.0	74.8	13659	4163.1	GOOD
10901.7	75.2	13715	4180.1	FAIR
10918.3	75.3	13731	4185.0	GOOD
10933.9	75.4	13739	4187.4	FAIR-GOOD
10935.5	75.4	13743	4188.7	GOOD
10887.0	75.1	14071	4288.6	FAIR-GOOD

Table A.32. Well 30/13 – 3 RFT data in the Jurassic.

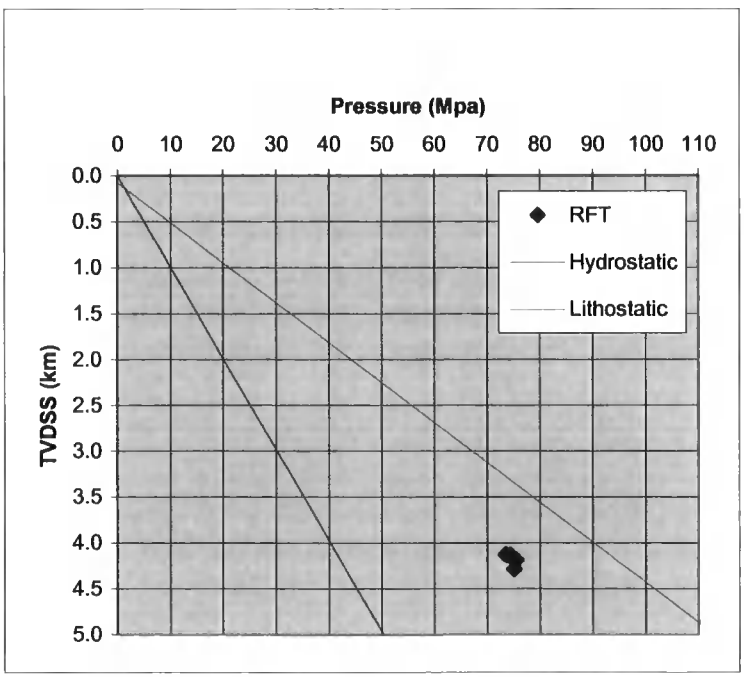

Figure A.7. Pressure – depth plot Well 30/13 – 3.

Data point (m SS)	Formation Pressure status and approach	**Pore pressure Pp (MPa)**
#13: 3199 Ekofisk (High porosity)	The Palaeocene in Q30 N being hydrostatic pressured, $\therefore\ Pp\|_{3199m} = 48.6\,MPa + (3199 - 2977.8\,m) \times 0.01007\,MPa/m = 50.8\ MPa$	
#14: 3281 Ekofisk (Low porosity)	The Palaeocene in Q30 N being hydrostatic pressured, $\therefore\ Pp\|_{3281m} = 48.6\,MPa + (3281 - 2977.8\,m) \times 0.01007\,MPa/m = 51.7\ MPa$	
#15: 3781 Hod	From the well Jurassic RFT and DST, the oil leg depth is at 4180.1 m SS (13715 ft SS), with an average RFT of 75.2 MPa (10901.7 psi).	
	Extrapolating the oil leg pressure hydrostatic parallel up to the base of chalk $\therefore\ Pp\|_{3781.2m} = 75.2\,MPa + (3781 - 4180.1\,m) \times 0.01007\,MPa/m = 71.2\ MPa$	

Table A.33. Estimates of pore pressure for data points 13, 14 and 15 (well 30/13 - 3)

Referring to Table A.26 and pressure increasing with depth, the Base Palaeocene at 3171.9 m (10407 feet TVDSS) will be of the range 48.3 – 55.2 MPa (7000-7999 psi), as confirmed by the Cretaceous Pressure Readings in block 30/13 (Vol.II Map 4.2). Figure A.8 is map showing the neighbouring wells used in the regional approach.

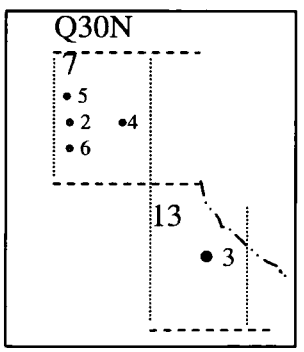

Figure A.8. Map of the neighbouring wells considered.

A.7. Well 31/26a – 5

A.7.1. Lithostatic stress estimation

Well 31/26a - 5
56° 08' 14.426" N 03° 04' 00.667" E

Bulk density readings:
1st value : 1.889 g/cc @ 1616.3 m
Last value: 2.594 g/cc @ 3510.4 m

	Measured Depth		TVDSS		Thickness	ρ average	Vertical	Sv
	Top	Bottom	Top	Bottom			MPa	
	m BRT	m BRT	m SS	m SS	m	g/cc		(MPa)
RTE	25.0		Air gap			//////////		
Water depth	25.0	97.2	0	72.2	72.2	1.020	0.72	
Sea Bed – Tertiary	97.2	1500	72.2	1475	1402.8	2.260	31.07	
Tertiary to first reading	1500.0	1616.3	1475	1591.3	116.3	2.040	2.33	
sediments	1616.3	2840.6	1591.3	2815.6	1224.3	2.234	26.80	60.92
	2840.6	2865	2815.6	2840	24.4	2.424	0.58	61.50
	2865.1	2865.9	2840.1	2840.9	0.8	2.510	0.02	61.52
	2865.9	2895.5	2840.9	2870.5	29.6	2.506	0.73	62.25
	2895.5	2919.8	2870.5	2894.8	24.3	2.506	0.60	62.84
	2920.0	2928.8	2895	2903.8	8.8	2.514	0.22	63.06
	2929.0	2942.7	2904	2917.7	13.7	2.555	0.34	63.40
	2942.9	2944.2	2917.9	2919.2	1.3	2.555	0.03	63.44
	2944.2	2974.7	2919.2	2949.7	30.5	2.457	0.73	64.17
Chalk	2974.7	3005.2	2949.7	2980.2	30.5	2.478	0.74	64.91
	3005.2	3035.7	2980.2	3010.7	30.5	2.520	0.75	65.66
	3035.7	3066.1	3010.7	3041.1	30.4	2.589	0.77	66.43
	3066.1	3096.6	3041.1	3071.6	30.5	2.608	0.78	67.21
	3096.6	3127.1	3071.6	3102.1	30.5	2.584	0.77	67.99
	3127.1	3140.5	3102.1	3115.5	13.4	2.612	0.34	68.33
	3140.7	3141.9	3115.7	3116.9	1.2	2.565	0.03	68.36
	3142.0	3159.7	3117	3134.7	17.7	2.599	0.45	68.81
	3159.9	3161.1	3134.9	3136.1	1.2	2.589	0.03	68.84
	3161.2	3164.3	3136.2	3139.3	3.1	2.587	0.08	68.92
To base Chalk	3164.3	3177.1	3139.3	3152.1	12.8	2.575	0.32	69.24

Sea water density = 1.02 g/cc; 1 psi/ft ≡ 2.31 g/cc; 1 g/cc ≡ 0.0098 MPa/m

ρ_{av} are the averages of RHOB digital logs throughout the interval considered; S_v at the interval is the combined weight of the sea water and overlying sediments taken at the bottom of the interval.

Table A.34. Lithostatic stress values for well 31/26a – 5.

Well 31/26a - 5		Measured Depth		TVD	
RTE: 82 ft , 25 m		ft BRT	m BRT	ft SS	m SS
Top Late Palaeocene		9013	2747.0	8931	2722.0
Early Palaeocene	Ekofisk	9300	2834.5	9218	2809.5
Late Cretaceous	TOR	9630	2935.1	9548	2910.1
	HOD	10308	3141.7	10226	3116.7
Jurassic	Undifferentiated Sandstone Unit	10424	3177.1	10342	3152.1
Triassic	Smith Bank Formation	10788	3288.0	10706	3263.0
Permiam	Zechstein Group	11124	3390.4	11042	3365.4
	Rotliengends Group	11432	3484.3	11350	3459.3

Table A.35. Formation tops for well 31/26a – 5.

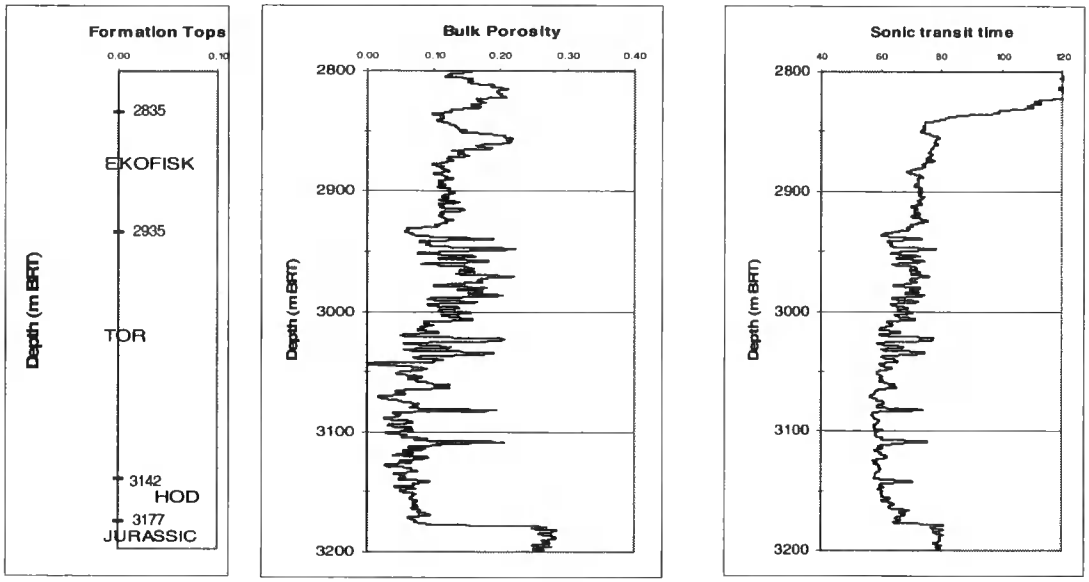

Figure A.9. Compaction trend through the Chalk Group in Well 31/26a – 5 showing the onset of overpressure (Equivalent depth method Hubbert and Rubey, 1959).

Data point (m SS)	Layer interval (m SS)	Vertical stress due to interval (MPa)	Vertical stress upon interval (MPa)	Lithostatic stress S_V (MPa)
#16: 3127 Hod	3117 – 3134.7	Sv2 = (3127 – 3117) x 2.599 x 0.0098 = 0.255	Sv1= 68.36	S_V = Sv1 + Sv2 = 68.36 + 0.255 = **68.61**

Table A.36. Estimates of lithostatic stress for data point 16 (well 31/26a - 5).

A.7.2. Pore pressure estimation

RFT		Depth		Quality
psi	MPa	ft SS	m SS	
6674	46.0	10345	3153.0	PERMEABLE
6631	45.7	10349	3154.2	PERMEABLE
6639	45.8	10364	3158.8	PERMEABLE
6646	45.8	10376	3162.5	PERMEABLE
6653	45.9	10388	3166.1	PERMEABLE
6659	45.9	10400	3169.8	PERMEABLE
6666	46.0	10413	3173.7	PERMEABLE
6671	46.0	10422	3176.5	PERMEABLE
6694	46.2	10468	3190.5	PERMEABLE
6717	46.3	10518	3205.7	PERMEABLE
6741	46.5	10568	3221.0	PERMEABLE
7056	48.7	11364	3463.6	PERMEABLE
7077	48.8	11392	3472.1	PERMEABLE
7083	48.8	11418	3480.0	PERMEABLE

Table A.37. Well 31/26a – 5 RFT data in the Jurassic (Source: composite log).

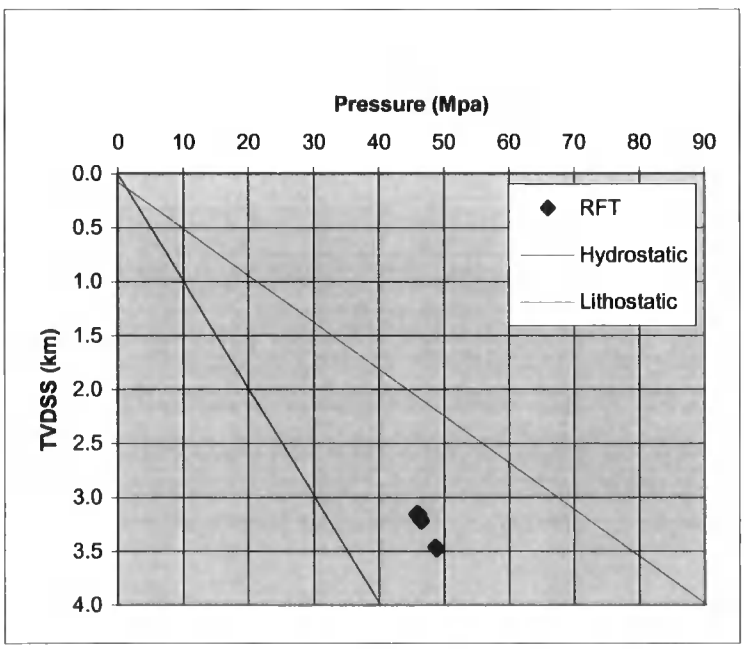

Figure A.10. Pressure –depth plot Well 31/26a – 5.

Using the RFT data available, we have

$$\left.\frac{\Delta P}{\Delta D}\right|_{Jurassic} = \frac{46.5-45.7}{3221.0-3154.2} = 0.01198\,Mpa/m$$

$$\therefore Pp|_{3127\,mSS} = 45.7 + 0.01198 \times (3127 - 3154.2) = 45.4\ Mpa$$

A.8. Well 31/26a – 9A

A.8.1. Lithostatic stress estimation

Well 31/26a – 9A

56° 00' 10.67" N 03° 11' 06.30" E

Bulk density readings:

1st value : 1.889 g/cc @ 1677.2 m

Last value: 2.536 g/cc @ 3451.7 m

	Measured Depth		TVDSS			ρ	Vertical	
	Top	Bottom	Top	Bottom	Thickness	average	MPa	Sv
	m BRT	m BRT	m SS	m SS	m	g/cc		(MPa)
RTE	25.3		Air gap			//////////		
Water depth	25.3	95.7	0	70.4	70.4	1.02	0.70	
Sea Bed – Top Tertiary	95.7	1388.6	70.4	1363.3	1292.9	2.26	28.64	
Tertiary to First reading	1388.6	1677.2	1363.3	1651.9	288.6	2.04	5.77	35.11
Chalk	1677.2	2411.2	1651.9	2385.9	734.0	2.169	15.60	50.71
	2411.2	2441.6	2385.9	2416.3	30.4	2.322	0.69	51.40
	2441.6	2472.1	2416.3	2446.8	30.5	2.326	0.70	52.10
	2472.1	2502.6	2446.8	2477.3	30.5	2.329	0.70	52.79
	2502.6	2533.1	2477.3	2507.8	30.5	2.327	0.70	53.49
	2533.1	2566.3	2507.8	2541.0	33.2	2.311	0.75	54.24
	2566.3	2568.1	2541.0	2542.8	1.8	2.266	0.04	54.28

Sea water density = 1.02 g/cc; 1 psi/ft ≡ 2.31 g/cc; 1 g/cc ≡ 0.0098 MPa/m

ρ_{av} are the averages of RHOB digital logs throughout the interval considered; S_v at the interval is the combined weight of the sea water and overlying sediments taken at the bottom of the interval.

Table A.38. Lithostatic stress values for well 31/26a – 9A.

Well 31/26a - 9A RTE: 83 ft , 25.3 m		Measured Depth		TVD	
		ft BRT	m BRT	ft SS	m SS
Top Late Palaeocene		7720	2352.9	7637	2327.6
Early Palaeocene	Ekofisk	7909	2410.5	7826	2385.2
Late Cretaceous	TOR	8109	2471.5	8026	2446.2
	HOD	8300	2529.7	8217	2504.4
	VALHALL	8412	2563.9	8329	2538.6
Jurassic	KIMMERIDGE	8426	2568.1	8343	2542.8
	FULMAR	8455	2577.0	8372	2551.7
Triassic	Smith Bank Formation	8918	2718.1	8835	2692.8
Permiam	Zechstein Group	9263	2823.2	9180	2797.9
	Rotliengends Group	9537	2906.7	9454	2881.4

Table A.39. Formation tops for well 31/26a – 9A.

Data point (m SS)	Layer interval (m SS)	Vertical stress due to interval (MPa)	Vertical stress upon interval (MPa)	Lithostatic stress S_V (MPa)
#17: 2455 Tor	2446.8 – 2477.3	Sv2 = (2455 – 2446.8) x 2.357 x 0.0098 = 0.189	Sv1= 52.10	S_V = Sv1 + Sv2 = 52.10 + 0.189 = **52.30**
#18: 2494 Tor	2477.3 – 2507.8	Sv2 = (2494 – 2477.3) x 2.327 x 0.0098 = 0.381	Sv1= 52.79	S_V = Sv1 + Sv2 = 52.79 + 0.381 = **53.17**
#19: 2537 Valhall	2507.8 - 2541	Sv2 = (2537 – 2507.8) x 2.311 x 0.0098 = 0.661	Sv1= 53.49	S_V = Sv1 + Sv2 = 53.49 + 0.661 = **54.15**

Table A.40. Estimates of lithostatic stress for data points 17, 18 and 19 (well 31/26a – 9A).

A.8.2. Pore pressure estimation

Pressure direct measurements, RFT are available within the Cretaceous and the Jurassic. RFT in the Cretaceous are of poor quality (supercharged), except two of them. This prompted the picking of two of the three well data points within the Cretaceous Chalk for accurate pressure value. For the data point at the base of the Chalk, extrapolation of the pressure gradient within the Chalk has been used.

RFT		Depth		Quality
psi	MPa	ft SS	m SS	
5499.3	**37.9**	**8055**	**2455**	**FAIR**
5557.5	**38.3**	**8181**	**2493.4**	**FAIR**
5611.2	38.7	8373	2552.0	GOOD
5617.3	38.7	8387	2556.2	FAIR
5618.9	38.8	8397	2559.3	VERY GOOD
5622.4	38.8	8407	2562.3	VERY GOOD
5633.6	38.9	8439	2572.1	GOOD
5646.6	38.9	8467	2580.6	FAIR
5668.5	39.1	8501	2591.0	FAIR
5655.8	39.0	8501.5	2591.1	VERY GOOD
5671.0	39.1	8537.5	2602.1	GOOD
5674.9	39.1	8546	2604.7	VERY GOOD
5730.8	39.5	8670	2642.5	GOOD
5774.8	39.8	8775	2674.5	GOOD
5790.0	39.9	8807	2684.2	GOOD
5791.5	39.9	8808	2684.5	FAIR
5799.3	40.0	8829	2690.9	GOOD

Table A.41. Well 31/26a – 9A RFT measurements through the Cretaceous Chalk and the Jurassic (Source: composite log).

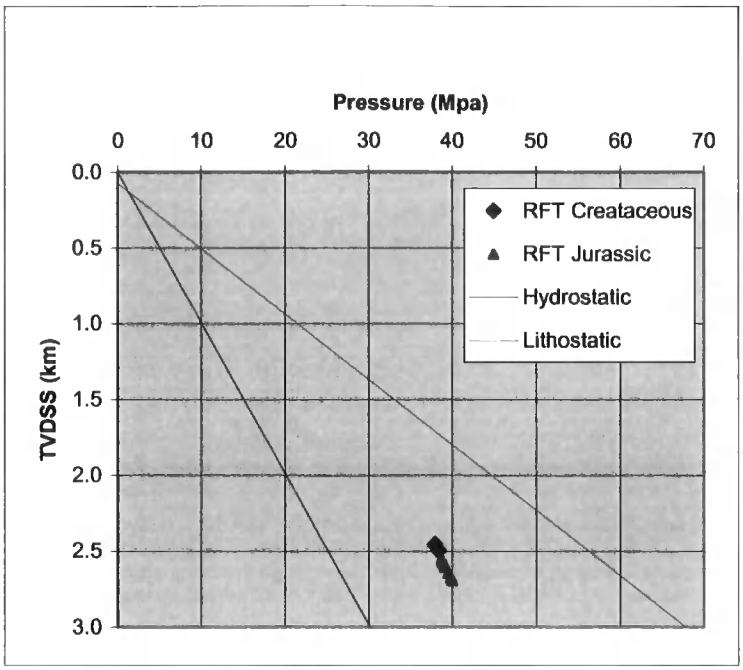

Figure A.11. Pressure –depth plot Well 31/26a – 9A.

Data point (m SS)	Formation Pressure status and approach	**Pore pressure Pp (MPa)**
#17: 2455 Tor	Direct pressure measurement, RFT: 37.9 MPa	
#18: 2494 Tor	Direct pressure measurement, RFT: 38.3 MPa	
#19: 2537 Valhall	Using the RFT data available, we have $\left.\frac{\Delta P}{\Delta D}\right\|_{Jurassic} = \frac{38.3-37.9}{2494.0-2455.0} = 0.01026\,MPa/m$	
	Thus, extrapolating the pressure gradient up to the Chalk $\therefore Pp\|_{2537mSS} = 38.3 + 0.01026 \times (2537-2494) = 38.7\ MPa$	

Table A.42. Estimates of pore pressure for data points 17, 18 and 19 (well 31/26a – 9A).

Appendix B
Programs – Visual Basic Macros

B.1. Flow charts of the programs/macros

B.2. List of software and applications used in this study

B.3. Programs in Visual Basic: Macros

APPENDIX B. Programs – Visual Basic Macros

B.1. Flow charts of the programs/macros

B.1.1. "inversion" flow chart

Note: as introduced in section 4.4.

Storage File/File to run the macro: CHAPTER Appendix A Inversion Macro.xls

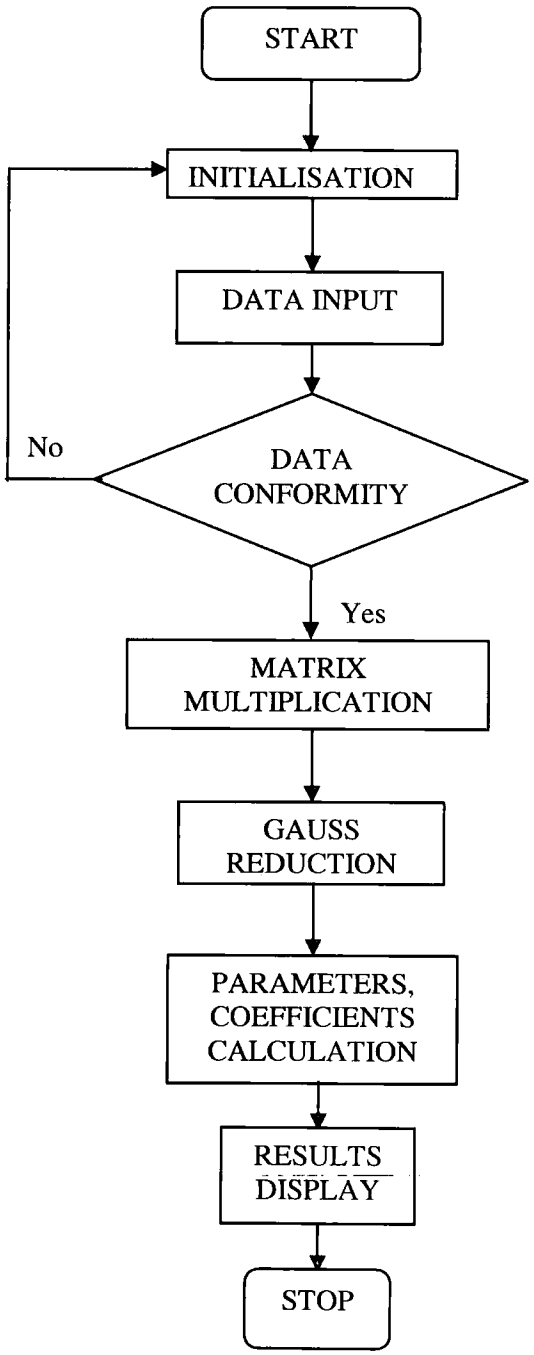

B.1.2. S_v calculation flow chart

Note: used in mudstones study, Chapter 6.

Storage File/File to run the macro: CHAPTER Appendix A Sv Macro.xls

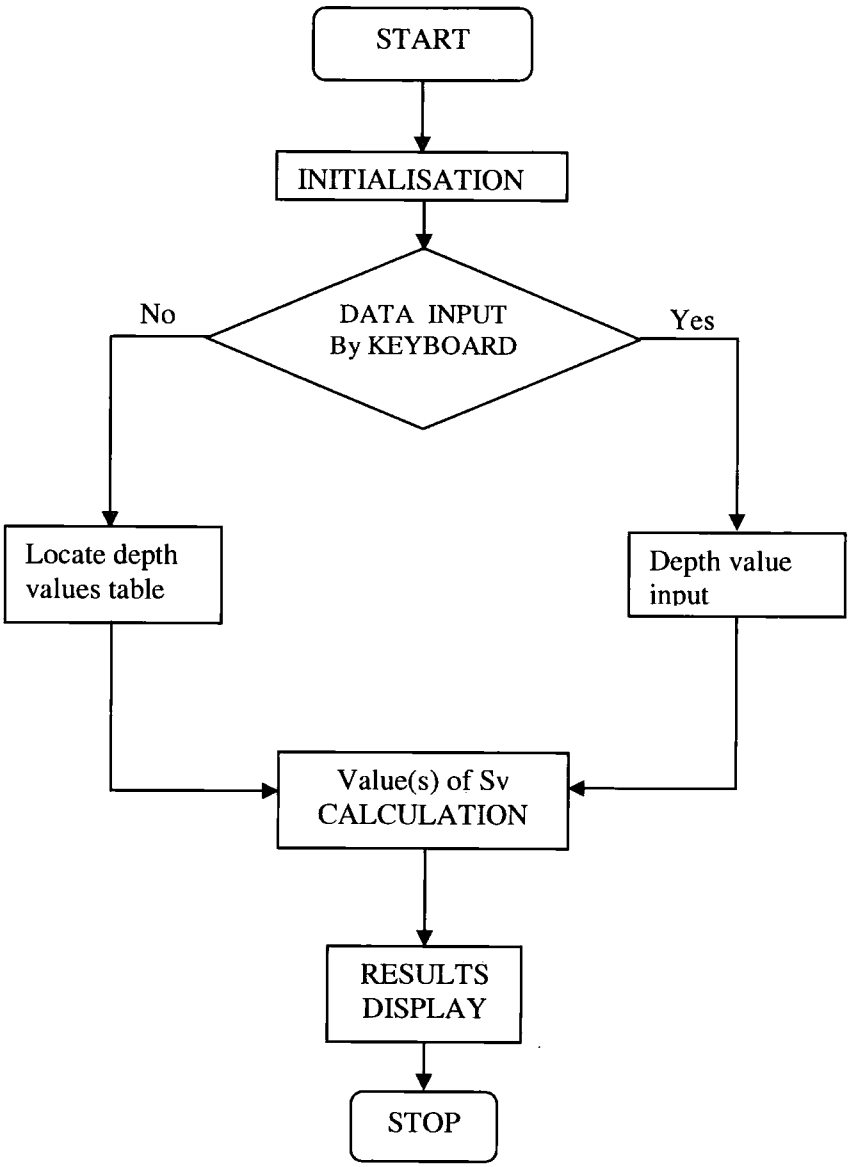

B.1.3. "Selection" algorithm

Note: as described in section 6.4.2.

Storage File/File to run the macro:

CHAPTER APPENDIXA SelectionMacroAPR05.xls

Data input:

INPUT					OUTPUT		
Depth	GR	ΔT	RHOB	ILD	dGR(M,m)	dΔT(M,m)	Status
ft	API	uS/ft	g/cc	Ohmm			

Selection basis:

Intervals of 0.7 m (2.5 ft) were used to assess the consistency in lithology, i.e., intervals of 5 log values. The ranges of natural gamma log and sonic log readings over each interval are calculated as (Equation 6.2)

$$dGR(M,m) = GRMax - GRmin \text{ and}$$

$$d\Delta T(M,m) = \Delta TMax - \Delta Tmin \qquad \text{(B.1)}$$

and the interval is only accepted as a data point when both $dGR(M,m) \leq 0.003$ °API and $d\Delta T(M,m) \leq 0.003$ μs/ft.

B.2. List of software and applications used in this study

The thesis contains figures, plots, tables, maps. All these materials were created using mainly Microsoft Office Applications; where any is from other sources and authors, references have been provided. Other packages used are CorelDraw 9, Origin 6.0, Sigma Plot 9. Other professional software used for data collection and selection include Didger 3.0, Presgraf and PressureView2.1. These packages were run on a PC (Personal Computer); with a higher graphic specification required.

B.3. Programs in Visual Basic: Macro

B.3.1. Macro for "inversion"

```
Dim m, n, v, r
Sub takedata6D()
' This module offers the data analyst the option to visually check the
' conformity of the data already keyed on sheets:="Data"

begin:
Sheets("sheet1").Select
   Sheets("Data").Activate

Range("A2").Select
ActiveCell.End(xlToRight).Select
   q = ActiveCell.Column
   n = q - 1
Reply = MsgBox("Sheet named -Data- correctly entered", vbYesNo, "A11 in cell[2-1],
with v1 in cell[2-" & n & "]")
If Reply = vbNo Then
   Call terminate
Else
   GoTo dataentered
End If

dataentered:
Sheets("Data").Activate
' Getting the number of data points, m; and number of independent variables, n
Range("A2").Select
If ActiveCell < 1 Or ActiveCell > 1 Then End
   ActiveCell.End(xlDown).Select
   k = ActiveCell.Row
   m = k - 1

Range("A2").Select
ActiveCell.End(xlToRight).Select
   q = ActiveCell.Column
   n = q - 1

MsgBox "Number of data points = " & m

' Checking conformity of an overdetermined problem
If m < n Then GoTo enterdata:
If n > 6 Then GoTo enterdata:

' Entering the (transpose of A(m x n)) "in sheet1"
Range(Cells(2, 1), Cells(m + 1, n + 1)).Select
Selection.Copy
Sheets("sheet1").Select
```

```
Range("A1").Select
Selection.PasteSpecial Paste:=xlValues, Operation:=xlNone, SkipBlanks:= _
    False, Transpose:=False

Cells(m, 1).Select
MsgBox "Number of  rows = " & m

trans = MsgBox("Are A and Vi correctly entered?", vbYesNo, "A11 in cells (1,1), v1
in cells(1,(n+1))")
If trans = vbYes Then GoTo continue
Call terminate

enterdata:
'Check that number of independent variables and equations
Sheets("Data").Activate
MsgBox "This macro is valid for overdetermined problems only, and n < 6"
Call terminate

continue:
MsgBox " Wait, while multiplying At with A"
End Sub

Sub multiplyAtA6D()
'This submodule multiply a matrix A with its transpose: (ATranspose)* A
' STEP 1: SELECTING THE STORED DATA
Sheets("sheet1").Select
Range("A1").Select
ActiveCell.End(xlDown).Select
m = ActiveCell.Row

'STEP 2: MULTIPLYING (A TRANSPOSE) BY A _ATN: NON
COMMUTATIVITY OF MATRIX MULTIPLICATION
'Multiplication of (A transpose) with A
Sheets("sheet1").Select
For i = 1 To n
  For j = 1 To n
    Sum = 0
    For k = 1 To m
    Sum = Sum + Cells(k, i) * Cells(k, j)
    Next k
  Cells(i + m + 2, j).Value = Sum
  Next j
Next i
End Sub

Sub Reduce4Gauss6D()
' PREPARING DATA FOR SYSTEM OF EQUATIONS RESOULTION BY GAUSS
REDUCTION
Sheets("Sheet1").Select
' Dubbing the Dim n, the number of columns of A
```

```
' to a new variable r ; as reference to cells (m + n + 2, n) is not responding
   Cells(2540, 254) = n
   Nombre = Cells(2540, 254)
   r = Val(Nombre)
' Preparing data on calculation sheet: "sheet2"
   Range(Cells(m + 3, 1), Cells(m + n + 2, r)).Select
   Selection.Copy
Sheets("Sheet2").Select
   Range("A1").Select
   Selection.PasteSpecial Paste:=xlValues, Operation:=xlNone, SkipBlanks:= _
      False, Transpose:=False
Sheets("Sheet1").Select
   Range(Cells(1, 1), Cells(m, r)).Select
   Application.CutCopyMode = False
   Selection.Copy
Sheets("Sheet2").Select
   Cells(1, n + 1).Select
Selection.PasteSpecial Paste:=xlValues, Operation:=xlNone, SkipBlanks:= _
      False, Transpose:=False
   Range("A1").Select
End Sub

Sub GaussAtA6D()
'This subroutine gives us the final matrix, say F
'matrix F being [(the inverse of AtA)* At], At=transpose of A
'the matrix on "sheets2" is I(unit matrix) beside F
' F is to be multiplied by vector matrix v to get the parameters
' the unknown parameters Vo, a, b, c, d, e of the linear equation.

'STEP 1: VISUAL CHECK OF THE LINEAR EQUATION CONFORMITY(i.e.
augmented matrix)
Sheets("sheet2").Activate
' MUTED CHECK
'Reply = MsgBox("Is the Augmented Matrix [with Transpose] correct?", vbYesNo,
"Checking")
'If Reply = vbNo Then Exit Sub

'STEP 2: Gauss Reduction procedure: reducing element a11 to unity
Sheets("sheet2").Activate
For k = 1 To n - 1
   Cells(k, k).Select
   pivot = Cells(k, k)
   P = Val(pivot)
   If P = 0 Then GoTo indefini

      For j = k To n
      Cells(k, j) = Cells(k, j) / P
      Next j
      For j = 1 To m
      Cells(j, n + k) = Cells(j, n + k) / P
```

```
    Next j

  'Getting zeros in all the target rows below the pivot a11
  'k should varie up to n, instead of m, coz we have a square matrix
  For i = k + 1 To n
    d = Cells(i, k)
    For j = 1 To n
      Cells(i, j).Activate
      Cells(i, j) = Cells(i, j) - d * Cells(k, j)
    Next j
    ' the broken part accounting for the transpose
    For j = 1 To m
      Cells(j, n + i).Activate
      Cells(j, n + i) = Cells(j, n + i) - d * Cells(j, n + k)
    Next j

  Next i

Next k

unknowns = MsgBox("Do you have " & n & " unknowns for the inversion?",
vbYesNo, "i.e. column C is not made of zeros")
If unknowns = vbNo Then GoTo Proceed
  P = Cells(r, r)
  If P = 0 Then GoTo indefini2
  Cells(n, n) = Cells(n, n) / P
  For j = 1 To m
  Cells(j, n + n).Select
  Cells(j, n + n) = Cells(j, n + n) / P
  Next j

Proceed:
'Getting other zeros in the  immediate upper row
' MsgBox "Getting Unit matrix"
Sheets("sheet2").Activate

Row = 2
d = Cells(1, 2) / Cells(2, 2)
  For j = 2 To n
    Cells(1, j) = Cells(1, j) - d * Cells(2, j)
  Next j
  For j = 1 To m
    Cells(j, n + 1) = Cells(j, n + 1) - d * Cells(j, n + 2)
  Next j
' MsgBox "coulmn 2"

Row = 3
If Cells(3, 3) = 0 Then Exit Sub
d = Cells(1, 3) / Cells(3, 3)
  For j = 2 To n
```

```
    Cells(1, j) = Cells(1, j) - d * Cells(3, j)
  Next j
  For j = 1 To m
    Cells(j, n + 1) = Cells(j, n + 1) - d * Cells(j, n + 3)
  Next j

d = Cells(2, 3) / Cells(3, 3)
  For j = 3 To n
    Cells(2, j) = Cells(2, j) - d * Cells(3, j)
  Next j
  For j = 1 To m
    Cells(j, n + 2) = Cells(j, n + 2) - d * Cells(j, n + 3)
  Next j
' MsgBox "coulmn 3"
If n = 3 Then Exit Sub

Row = 4
If Cells(4, 4) = 0 Then Exit Sub
d = Cells(1, 4) / Cells(4, 4)
  For j = 2 To n
    Cells(1, j) = Cells(1, j) - d * Cells(4, j)
  Next j
  For j = 1 To m
    Cells(j, n + 1) = Cells(j, n + 1) - d * Cells(j, n + 4)
  Next j

d = Cells(2, 4) / Cells(4, 4)
  For j = 3 To n
    Cells(2, j) = Cells(2, j) - d * Cells(4, j)
  Next j
  For j = 1 To m
    Cells(j, n + 2) = Cells(j, n + 2) - d * Cells(j, n + 4)
  Next j

d = Cells(3, 4) / Cells(4, 4)
  For j = 4 To n
    Cells(3, j) = Cells(3, j) - d * Cells(4, j)
  Next j
  For j = 1 To m
    Cells(j, n + 3) = Cells(j, n + 3) - d * Cells(j, n + 4)
  Next j
' MsgBox "coulmn 4"
If n = 4 Then Exit Sub

Row = 5
If Cells(5, 5) = 0 Then Exit Sub
d = Cells(1, 5) / Cells(5, 5)
  For j = 2 To n
    Cells(1, j) = Cells(1, j) - d * Cells(5, j)
  Next j
```

```
    For j = 1 To m
      Cells(j, n + 1) = Cells(j, n + 1) - d * Cells(j, n + 5)
    Next j

d = Cells(2, 5) / Cells(5, 5)
    For j = 3 To n
      Cells(2, j) = Cells(2, j) - d * Cells(5, j)
    Next j
    For j = 1 To m
      Cells(j, n + 2) = Cells(j, n + 2) - d * Cells(j, n + 5)
    Next j

d = Cells(3, 5) / Cells(5, 5)
   For j = 4 To n
     Cells(3, j) = Cells(3, j) - d * Cells(5, j)
  Next j
  For j = 1 To m
      Cells(j, n + 3) = Cells(j, n + 3) - d * Cells(j, n + 5)
    Next j

d = Cells(4, 5) / Cells(5, 5)
    For j = 5 To n
      Cells(4, j) = Cells(4, j) - d * Cells(5, j)
    Next j
    For j = 1 To m
      Cells(j, n + 4) = Cells(j, n + 4) - d * Cells(j, n + 5)
    Next j
' MsgBox "coulmn 5"
If n = 5 Then Exit Sub

Row = 6
If Cells(6, 6) = 0 Then Exit Sub
d = Cells(1, 6) / Cells(6, 6)
    For j = 2 To n
      Cells(1, j) = Cells(1, j) - d * Cells(6, j)
    Next j
    For j = 1 To m
      Cells(j, n + 1) = Cells(j, n + 1) - d * Cells(j, n + 6)
    Next j

d = Cells(2, 6) / Cells(6, 6)
    For j = 3 To n
      Cells(2, j) = Cells(2, j) - d * Cells(6, j)
    Next j
    For j = 1 To m
      Cells(j, n + 2) = Cells(j, n + 2) - d * Cells(j, n + 6)
    Next j

d = Cells(3, 6) / Cells(6, 6)
    For j = 4 To n
```

```
      Cells(3,j) = Cells(3,j) - d * Cells(6,j)
Next j
   For j = 1 To m
      Cells(j, n + 3) = Cells(j, n + 3) - d * Cells(j, n + 6)
   Next j

d = Cells(4, 6) / Cells(6, 6)
   For j = 5 To n
      Cells(4, j) = Cells(4, j) - d * Cells(6, j)
   Next j
   For j = 1 To m
      Cells(j, n + 4) = Cells(j, n + 4) - d * Cells(j, n + 6)
   Next j

d = Cells(5, 6) / Cells(6, 6)
   For j = 6 To n
      Cells(5, j) = Cells(5, j) - d * Cells(6, j)
   Next j
   For j = 1 To m
      Cells(j, n + 5) = Cells(j, n + 5) - d * Cells(j, n + 6)
   Next j
' MsgBox "coulmn 6"

Sheets("sheet2").Activate
Exit Sub

Check:
If Cells(n, n) <> 0 Then GoTo check2D
GoTo Proceed

check2D:
MsgBox " You cliked NOT A " & n & " UNKNOWNS, but this might be! As
Cells(3,3)< > 0."
Sheets("sheet2").Activate
MsgBox "The Macro is stopped. Back to your spreadsheets"
Sheets("Data").Activate
End

indefini:
MsgBox "Try to rearrange the rows and colums, pivot = 0"
Sheets("sheet2").Activate
Call terminate

indefini2:
MsgBox " Surprise! Cells(n,n) = 0. This might not be a n unknowns inversion."
Sheets("sheet2").Activate
Call terminate

End Sub
```

```
Sub Parameters6D()
' This macro prepares the matrices F (from sheet 2) and Vi (from sheet 1)
' in the working "sheet 3" for the final result.
' STEP 1: COPYING & PASTING MATRIX F
   Sheets("Sheet2").Activate

   Range(Cells(1, n + 1), Cells(m, n + n)).Select
   Selection.Copy
   Sheets("Sheet3").Activate
   Range("A1").Select

   Selection.PasteSpecial Paste:=xlValues, Operation:=xlNone, SkipBlanks:= _
         False, Transpose:=False

' STEP 2: COPYING AND PASTING UNIT VECTOR Vi (OF OBSERVED
VELOCITIES)
   Sheets("Sheet1").Activate
   Range(Cells(1, n + 1), Cells(m, n + 1)).Select
   Selection.Copy
   Sheets("Sheet3").Activate
   Cells(1, n + 2).Select
   Selection.PasteSpecial Paste:=xlValues, Operation:=xlNone, SkipBlanks:= _
      False, Transpose:=False

' STEP 3: MULTIPLICATION

MultiplyBC:
'Multiplication of B(n x m) and C(m x l)
'C (say c11,) being entered 2 colums besides B (say, elements b1m)
Sheets("sheet3").Activate
Range("A1").Select
ActiveCell.End(xlDown).Select
m = ActiveCell.Row

ActiveCell.End(xlToRight).Select
n = ActiveCell.Column

For i = 1 To n
      Sum = 0
      For k = 1 To m
      Sum = Sum + Cells(k, i) * Cells(k, n + 2)
      Next k
   Cells(i + n + 2, 10).Value = Sum
   Cells(i + n + 2, 10).Activate
Next i

' [accordingly, column 2 here below becomes 10 + 1 = 11

Cells(n + 3, 11).Value = " = V_0 [m/s]"
```

```
Cells(n + 4, 11).Value = " = a [m/s]"
If n = 2 Then Exit Sub
Cells(n + 5, 11).Value = " = b [m/s/Mpa]"
If n = 3 Then Exit Sub
Cells(n + 6, 11).Value = " = c [m/s/API]"
If n = 4 Then Exit Sub
Cells(n + 7, 11).Value = " = d [m/s/Ohmm]"
If n = 5 Then Exit Sub
Cells(n + 8, 11).Value = " = e [m/s]"

Cells(n + 2, 11).Select
End Sub

Sub terminate()
' This subroutine stops the Macro running whenever the condition
' is not satisfied in any of the VISUAL CHECKS dialog boxes
Sheets("Data").Activate
Range("A1").Select
MsgBox "Sorry, try again: check and re-enter data sheet"
MsgBox "The Macro is stopped. Back to your spreadsheets"
Sheets("Data").Activate
End

End Sub

Sub Finalresults()
' Finalresult Macro
' This macro computes V from the inversion coefficients,
' evaluates the respective discrepancies (DeltaV), percentage error, and the RMS

   Sheets("Sheet3").Select
   Range("A1:A9").Select
   Selection.EntireRow.Insert

' Copying the data set in sheet3 for calculation
   Sheets("Data").Select
   Range(Cells(1, 1), Cells(m + 1, n)).Select
   Selection.Copy
   Sheets("Sheet3").Select
   Range("M9").Select
   ActiveSheet.Paste

   Sheets("Data").Select
   Range(Cells(1, n + 1), Cells(m + 1, n + 1)).Select
   Selection.Copy
   Sheets("Sheet3").Select
   Range("S9").Select
   ActiveSheet.Paste

' Copy and past the coeff Vo, a, b, c, d, e of the inversion
```

```
' immediately above the data set.
' We should remember that the results are always pasted at column 10
' But rows depend on number of unknown n.
'   Range("J18:J23").Select
    Range(Cells(12 + n, 10), Cells(11 + n + n, 10)).Select
    Selection.Copy
    Range("M8").Select
    Selection.PasteSpecial Paste:=xlPasteValuesAndNumberFormats, Operation:= _
        xlNone, SkipBlanks:=False, Transpose:=True

    Range("T1").Select
    Selection.PasteSpecial Paste:=xlPasteValuesAndNumberFormats, Operation:= _
        xlNone, SkipBlanks:=False, Transpose:=False

' Calculating Vcomp
    For i = 10 To m + 9
        Cells(i, 20) = Cells(8, 13) + Cells(8, 14) * Cells(i, 14) + Cells(8, 15) * Cells(i, 15)
+ Cells(8, 16) * Cells(i, 16) + Cells(8, 17) * Cells(i, 17) + Cells(8, 18) * Cells(i, 18)
        Cells(i, 21) = Cells(i, 20) - Cells(i, 19)
        Cells(i, 22) = (Cells(i, 21) / Cells(i, 19)) * 100
    Next i

' Calculating the RMS
    Sum2 = 0
    For i = 10 To m + 9
        Cells(i, 23) = (Cells(i, 21)) ^ 2
        Sum2 = Sum2 + (Cells(i, 21)) ^ 2
    Next i
    Cells(8, 23).Value = Sum2
    Cells(7, 23).Value = m
    Cells(6, 23).Value = n

    Cells(8, 21).Select
    ActiveCell.FormulaR1C1 = "=SQRT(RC[2]/(R[-1]C[2] - R[-2]C[2]))"

' Indexing the data point in S/N  column
    For i = 10 To m + 9
        Cells(i, 23) = i - 9
    Next i

    Range("U9").Select
    With Selection.Interior
        .ColorIndex = 15
        .Pattern = xlSolid
        .PatternColorIndex = xlAutomatic
    End With

    Range("N9:R9").Select
    Selection.Copy
    Range("U2").Select
```

```
    Selection.PasteSpecial Paste:=xlPasteValuesAndNumberFormats, Operation:= _
        xlNone, SkipBlanks:=False, Transpose:=True
    With Selection.Interior
        .ColorIndex = 36
        .Pattern = xlSolid
    End With

    Range("S:V").Select
    Selection.NumberFormat = "0.0"
    Range("W:W").Select
    Selection.NumberFormat = "0"

    Range("T9").Value = "Vcomp"
    Range("t8").Value = "RMS = "
    Range("u9").Value = "DelV"
    Range("v9").Value = "Perc Error"
    Range("W9").Value = "S/N"

    Range("T9:V9").Select
    Application.CutCopyMode = False
    With Selection.Interior
        .ColorIndex = 15
        .Pattern = xlSolid
        .PatternColorIndex = xlAutomatic
    End With
    With ActiveCell.Characters(Start:=1, Length:=5).Font
        .Name = "Arial"
        .FontStyle = "Italic"
        .Size = 8
        .Strikethrough = False
        .Superscript = False
        .Subscript = False
        .OutlineFont = False
        .Shadow = False
        .Underline = xlUnderlineStyleNone
        .ColorIndex = xlAutomatic
    End With

    Columns("M:M").ColumnWidth = 3.57
    Columns("N:N").ColumnWidth = 6.11
    Columns("O:R").ColumnWidth = 4.29
    Columns("S:S").ColumnWidth = 6.29

    Range("W4").Select
End Sub

Sub initialise6D()
' This subroutine re-initialise the macro module for another run
' i.e. it clears the all contents on calculations sheets 1, 2 and 3 to avoid mis-calculation
```

```
Sheets("Sheet1").Select
   Cells.Select
   Selection.ClearContents
   Range("A1").Select
Sheets("Sheet2").Select
   Cells.Select
   Selection.ClearContents
   Range("A1").Select
Sheets("Sheet3").Select
   Cells.Select
   Selection.ClearContents
   Range("A1").Select
End Sub

Sub Done6D()
Dim n, m, r
Call initialise6D
Call takedata6D
Call multiplyAtA6D
Call Reduce4Gauss6D
Call GaussAtA6D
Call Parameters6D
Call Finalresults
Sheets("sheet3").Activate
Range("W4").Select
End Sub
```

B.3.2. Macro for "S_v Calculation"

```
Dim depth, numberdata, Sv, k, p, q, w, CopySv
Sub Sv_values()
' This macro computes the value of Sv (in psi)
' for a given depth (in ft BRT) keyed when prompted or
' for eventually a set of data points from a datasheets

Commence:
Sheets(2).Select
' CopySv is just a variable to allow us copy the computed Sv in the datasheet
' as used further below in copydata:

' Clearing content:these cells are given for prompt reading of Sv computed
' CopySv is just a variable to allow us copy the computed Sv in the datasheet
' as used further below in copydata:

CopySv = 0
Range("a2", "b3").ClearContents
Myanswer = MsgBox("Depth value by keyboard", vbYesNo, "ft BRT")
If Myanswer = vbYes Then
   CopySv = 1
```

```
   GoTo EnterDepth:
Else
' we have to pick the depth values from a Datapoints sheet
' we make sure that the Datapoints sheet is the first sheet of the workbook
   Sheets(1).Activate
   Call Depthpick
End If

EnterDepth:
'  Entering the depth in ft BRT for Sv calculation
   MsgBox "Give depth (ft BRT) for Sv calculation"
      depth = InputBox("Depth: ", "ft BRT")
   Cells(2, 1).Value = depth
   MsgBox " Sv for " & depth & " ft BRT"

IntervalLocation:
   ' Searching for the appropriate interval

   ' We take p as the value of the counter
   p = 9
   For M = 10 To 65
    If Cells(M, 2) > Cells(2, 1) Then GoTo Calculate:
    Cells(M, 2).Select
   MsgBox " Do you think it is OK?"
    p = p + 1
   Next M
' Controlling out of range depth
Myanswer2 = MsgBox("Sorry, check the Formations Sv Sheet ", vbOKCancel, "Try
Again!")
If Myanswer2 = vbOK Then End
If Myanswer2 = vbCancel Then End

Calculate:
Range(Cells(p, 2), Cells(p, 3)).Select
MsgBox " Sure, [depth " & depth & " ft BRT] is within this Fm interval?"
q = p - 1
Cells(2, 2) = Cells(q, 8) + 0.5 * Cells(q, 7) + (depth - Cells(q + 1, 2)) * 0.4335 *
Cells(q + 1, 5)
Cells(3, 1).Value = "ft BRT"
Cells(3, 2).Value = "Sv psi"
Cells(3, 2).Select
Selection.NumberFormat = "0.0"
Range("a2", "b3").Select
Selection.Font.Bold = True
Selection.Font.ColorIndex = 3
End

End Sub
Sub Depthpick()
Dim depth, numberdata, Sv, k, p, q, w, CopySv
```

```
' we have to pick the depth values from a Datapoints sheet
' we make sure that the Datapoints sheet is the first sheet of the workbook
Sheets(1).Activate
' Clearing the content of values of previous Sv computed
Columns("M:M").Select
Selection.ClearContents

' finding the total numbers of datapoints
'  avoiding overflow, as the macro does not run with one single data
'  for one single data, use the keyboard to enter depth (data)
If Range("B7") = 0 Then GoTo singlepoint:
'  Total number of data points
Range("B6").Select
ActiveCell.End(xlDown).Select
v = ActiveCell.Row
numberdata = v - 5
MsgBox "Number of datapoints = " & numberdata

Range("M3").Value = "Sv"
Range("M4").Value = "psi"


w = 0
Do While w < numberdata
   w = w + 1
   Sheets(1).Activate
   Cells(w + 5, 3).Select
      Application.CutCopyMode = False
      Selection.Copy
      Cells(w + 5, 16).Select
      ActiveSheet.Paste

      Sheets(2).Select
      Cells(2, 1).Select
      ActiveSheet.Paste


   ' Searching for the appropriate interval

   ' We take p as the value of the counter
   p = 9
   For M = 10 To 65
    If Cells(M, 2) > Cells(2, 1) Then GoTo Calculate2:
    Cells(M, 2).Select
'  MsgBox " Do you think it is OK?"
    p = p + 1
   Next M

Calculate2:
```

```
Cells(p, 2).Select

' MsgBox " Is it the depth" & depth & " within this interval?"

q = p - 1

Cells(2, 2) = Cells(q, 8) + 0.5 * Cells(q, 7) + (Cells(2, 1) - Cells(q + 1, 2)) * 0.4335 *
Cells(q + 1, 5)
Cells(3, 1).Value = "ft BRT"
Cells(3, 2).Value = "Sv psi"
Cells(3, 2).Select
Selection.NumberFormat = "0.0"
Range("a2", "b3").Select
Selection.Font.Bold = True
Selection.Font.ColorIndex = 3

' MsgBox "is the Sv value correct?"

' If CopySv = 1 Then

' Copying the value of calculated Sv to the datapicks sheet "sheets(1)"

   Sheets(2).Select
   Cells(2, 2).Select
   Application.CutCopyMode = False
   Selection.Copy

   Sheets(1).Select
   Cells(w + 5, 13).Select
   ActiveSheet.Paste

   Sheets(2).Activate
   Range("a2", "b2").Select
   Selection.ClearContents

   Sheets(1).Select
   Cells(w + 5, 13).Select

' MsgBox "is the Sv value copied?"


Loop
' Befeiting Sv values columns
 Columns("M:M").Select
   With Selection
      .HorizontalAlignment = xlCenter
      .VerticalAlignment = xlBottom
      .WrapText = False
      .Orientation = 0
      .AddIndent = False
```

```
    .IndentLevel = -1
    .ShrinkToFit = False
    .ReadingOrder = xlContext
    .MergeCells = False
  End With

End
singlepoint:
Sheets(1).Activate
Myanswer3 = MsgBox("Sorry, use 'KEYBOARD OPTION' to enter depth value",
vbOKCancel, "One single data only!")
End
End Sub
```

B.3.3. Macro for "Selection"

```
Dim m, n, ligne
Sub Datapick()
' This module tries to pick the data points within well lithologies
' Selection is based on log data: GR (gamma ray), DT(Sonic) and RHOB

' Macro recorded 06/02/2004 by Lbd
' Modified 2 July, 2004 to take all claystones GR > = 60 API in Heather
' and GR > = 40 in Cromer Knoll

worksheetprepare:
' Preparing the worksheet on which the data points pick
' is to be performed
' Case of well 30 13-3
  Sheets(1).Select
  trans = MsgBox("Any worksheets already named 'datapicks' or datapoints'?",
vbYesNo, "in this workbook")
  If trans = vbNo Then GoTo sheetcopy:

datasheetsdelete:
' We delete the previous "datapicks" and "datapoints" sheets
' so as there is no error when naming the new added sheet
Sheets("datapicks").Delete
Sheets("datapoints").Delete

sheetcopy:
' Copies and moves the selected worksheet at the end of all sheets
' This means the datapick sheet comes as the 2nd in the series
' i.e Copy After:=Sheets(1)
' This is to make sure that there is no "error msg"
  Sheets(1).Name = "mudstone"
  Sheets(1).Copy After:=Sheets(1)
' The working sheet is being renamed "datapicks"
```

```
' And organising the worksheet
   Sheets("mudstone (2)").Select
   Sheets("mudstone (2)").Name = "datapicks"

' Deleting column B of Depth TVDS, as we still use Depth BRT
   Columns("B:B").Select
   Selection.Delete
' Cleaning all other areas of worksheet
   Columns("F:AZ").Select
   Selection.Delete
MsgBox ("Is the new sheet still ok?")

Range("a3").Select
ActiveCell.End(xlDown).Select

k = ActiveCell.Row
n = k + 1
Range(Cells(1, 1), Cells(n, 1)).Select
Selection.EntireRow.Delete
    '
clearing:

   Range("F1").Select
   ActiveCell.FormulaR1C1 = "dGR(M,m)"
   Range("G1").Select
   ActiveCell.FormulaR1C1 = "dDT(M,m)"
   Range("I1").Select
   ActiveCell.FormulaR1C1 = "dRHOB(M,m)"
   Cells.Select
   With Selection.Font
      .Name = "Arial"
      .Size = 8
      .Strikethrough = False
      .Superscript = False
      .Subscript = False
      .OutlineFont = False
      .Shadow = False
      .Underline = xlUnderlineStyleNone
      .ColorIndex = xlAutomatic
   End With

trans1 = MsgBox("Hope this is ok, now?", vbYesNo, "with rows and columns")
   If trans1 = vbNo Then Call terminate
End Sub
Sub terminate()
MsgBox ("sorry, the conditions provided may not work. Try again")
' For the Sheets("mudstone (2)").Name = "datapicks" has been already been created
' We need to delete it to prevent error in the next macro run.
Sheets("datapicks").Delete
' We need to go back to the raw data sheet
```

```
Sheets(1).Select
Range("a1").Activate
End
End Sub
Sub CALCULONS2()
' !!!! on 30th June 04, this is modified to take dGR < 5 and dDT < 5, instead
'     of what we had earlieron (as stated below)
' This macro proceeds to the calculation of the test values
' dGR, dDT, dRHOB within a range of 5 data points (steps of data= 0.5 ft)
' Then gets a logical test to get the suitable data: dGR < 3 and dDT < 3
' At the end computes the average values of the picked data point
Dim n, m, ligne
start:
' we need to get a counter to locate the row:
' instead of the ILD column4, we could just take the depth column1
' as we need to trim the raw data sheet according to depths of interests before
proceeding
Cells(10, 4).Select
ActiveCell.End(xlDown).Select
m = ActiveCell.Row
n = m + 1

For j = 15 To n
' counter for pasting the data picked

'test de fin de calculations, basee sur la colonne E de ILD

'calcul of dGR (in column F), dDT (in column G), dRHOB (in column I)
   Cells(j, 6).Select
   Selection.NumberFormat = "0.000"
   Selection.Font.ColorIndex = 5
   ActiveCell.FormulaR1C1 = "=MAX(R[-4]C[-4]:RC[-4])-MIN(R[-4]C[-4]:RC[-4])"
   Cells(j, 7).Select
   Selection.NumberFormat = "0.000"
   Selection.Font.ColorIndex = 5
   ActiveCell.FormulaR1C1 = "=MAX(R[-4]C[-4]:RC[-4])-MIN(R[-4]C[-4]:RC[-4])"
   Cells(j, 9).Select
   Selection.NumberFormat = "0.000"
   Selection.Font.ColorIndex = 5
   ActiveCell.FormulaR1C1 = "=MAX(R[-4]C[-5]:RC[-5])-MIN(R[-4]C[-5]:RC[-5])"
   If Cells(j, 9) > 0.013 Then Selection.Font.ColorIndex = 3
   If Cells(j, 9) > 0.039 Then Selection.Font.ColorIndex = 8
' (Column H) : data pick selection test: dGR < 3 and dDT < 3
   Cells(j, 8).Select
      ActiveCell.FormulaR1C1 = _
      "=IF(RC[-2]<5,IF(RC[-1]<5,""OK"",""DISCARD""),""DISCARD"")"
Next j
End Sub

Sub selectons()
```

```
Dim m, p, q, r

' we need to get a counter to locate the row: that's p
' q is a dummy counter just to support the else statment
Cells(10, 5).Select
ActiveCell.End(xlDown).Select
m = ActiveCell.Row
n = m
p = 5
q = 0
For j = 15 To n


' Coulouring the value to be picked
If Cells(j, 8) = "OK" Then

   Range(Cells(j, 1), Cells(j, 5)).Select
   Selection.Interior.ColorIndex = 15
   Cells(j - 2, 1).Select
   Selection.Interior.ColorIndex = 6

   Range(Cells(j - 4, 1), Cells(j, 9)).Select
   Selection.Copy

   Cells(j - 4, 11).Select
   Selection.PasteSpecial Paste:=xlPasteValuesAndNumberFormats, Operation:= _
      xlNone, SkipBlanks:=False, Transpose:=False

   Cells(j - 2, 11).Select
   Selection.Interior.ColorIndex = 6

' Computing data picked properties (averages values): DEPTH, GR, DT, RHOB, ILD
   Cells(j + 1, 11).Select
   Application.CutCopyMode = False
   ActiveCell.FormulaR1C1 = "=AVERAGE(R[-5]C:R[-1]C)"

   Cells(j + 1, 12).Select
   Selection.NumberFormat = "0.0"
   ActiveCell.FormulaR1C1 = "=AVERAGE(R[-5]C:R[-1]C)"

   Cells(j + 1, 13).Select
   ActiveCell.FormulaR1C1 = "=AVERAGE(R[-5]C:R[-1]C)"
   Selection.NumberFormat = "0.000"

   Cells(j + 1, 14).Select
   ActiveCell.FormulaR1C1 = "=AVERAGE(R[-5]C:R[-1]C)"
   Selection.NumberFormat = "0.000"

   Cells(j + 1, 15).Select
   ActiveCell.FormulaR1C1 = "=AVERAGE(R[-5]C:R[-1]C)"
```

```
    Selection.NumberFormat = "0.00"

    Range(Cells(j, 16), Cells(j, 19)).Select
    Selection.Copy
    Cells((j + 1), 16).Select
    ActiveSheet.Paste
    Selection.PasteSpecial Paste:=xlPasteValuesAndNumberFormats, Operation:= _
      xlNone, SkipBlanks:=False, Transpose:=False

    Range(Cells(j + 1, 11), Cells(j + 1, 19)).Select
    Application.CutCopyMode = False
    Selection.Copy
    Cells(p, 21).Select
    Selection.PasteSpecial Paste:=xlPasteValuesAndNumberFormats, Operation:= _
      xlNone, SkipBlanks:=False, Transpose:=False

    Cells(p, 29).Select
    If Cells(p, 29) > 0.013 Then Selection.Font.ColorIndex = 3
    If Cells(p, 29) > 0.04 Then Selection.Font.ColorIndex = 8

p = p + 2
Else
q = q + 1
End If
Next j
' Stressing the results
Range("A1:I2").Select
Selection.Copy
Range("U1").Select
ActiveSheet.Paste
Selection.PasteSpecial Paste:=xlPasteValuesAndNumberFormats, Operation:= _
      xlNone, SkipBlanks:=False, Transpose:=False
Columns("Z:AC").Select
Selection.Font.ColorIndex = 5
Range("U1").Select

datapoint:
' This subroutine puts the picked data points (only) in a new sheets
' named "datapoints"
Range(Cells(1, 21), Cells(p + 2, 29)).Select
Selection.Copy
Sheets("datapicks").Select
Sheets.Add.Name = "datapoints"
    Sheets("datapicks").Select
    Selection.Copy

Sheets("datapoints").Select
    Range("A5").Select
    ActiveSheet.Paste
' Sorting data picked in RHOB variations  dRHOB(M,m) within range selection
```

```
l = 2 * p
Cells(9, 9).Select
For j = 9 To l
Cells(j, 9).Select
   If Cells(j, 9) > 0.013 Then Selection.Font.ColorIndex = 3
   If Cells(j, 9) > 0.04 Then Selection.Font.ColorIndex = 8
Next j

' Countouring cells with lines
   Columns("A:E").ColumnWidth = 6.5
   Columns("B:E").ColumnWidth = 5.15
   Columns("F:G").ColumnWidth = 7
   Columns("H:H").ColumnWidth = 3.8
   Columns("I:I").ColumnWidth = 7
' column for lithology type (calcareous, silty, carbonaceous, other)
   Columns("J:M").ColumnWidth = 3.1
   Columns("N:N").ColumnWidth = 10
   Range(Cells(5, 1), Cells(p + 3, 13)).Select
   Selection.Borders(xlDiagonalDown).LineStyle = xlNone
   Selection.Borders(xlDiagonalUp).LineStyle = xlNone
   With Selection.Borders(xlEdgeLeft)
      .LineStyle = xlContinuous
      .Weight = xlThin
      .ColorIndex = xlAutomatic
   End With
   With Selection.Borders(xlEdgeTop)
      .LineStyle = xlContinuous
      .Weight = xlThin
      .ColorIndex = xlAutomatic
   End With
   With Selection.Borders(xlEdgeBottom)
      .LineStyle = xlContinuous
      .Weight = xlThin
      .ColorIndex = xlAutomatic
   End With
   With Selection.Borders(xlEdgeRight)
      .LineStyle = xlContinuous
      .Weight = xlThin
      .ColorIndex = xlAutomatic
   End With
   With Selection.Borders(xlInsideVertical)
      .LineStyle = xlContinuous
      .Weight = xlThin
      .ColorIndex = xlAutomatic
   End With
   With Selection.Borders(xlInsideHorizontal)
      .LineStyle = xlContinuous
      .Weight = xlThin
      .ColorIndex = xlAutomatic
   End With
```

```
' Finding number of data points picked
' p was the counter for the datapick with label "OK"
' Note that all data picks are not suitable, as:
' * some of the consecutive 5 data points picked OK could be within the same bed
' * moreover there is no provision to enter from keyboard
' the boundaries of the interesting formation. Among them is the Kimmeridge clays
picked
' Thus, suitability of any data points need to be confirmed manually with the
composite-log.
r = (p - 7) / 2 + 1

Comments:
   Range("A1").Value = "WELL:"
   Application.CutCopyMode = False
   Range("A2").Value = "COMMENTS:"
   Range("C2").Value = r
   Range("D2").Value = " = Number of data points picked"
   Range("A3").Value = "DATE:"
   Range("A1").Activate

' italicising the columns of dGR, dDT and DRHOB
' for print out easy reading.
   Columns("F:I").Select
   Selection.Font.Italic = True
   Range("A1").Select

End
End Sub

Sub PicknowAll()
Dim n, m, ligne
Call Datapick
Call CALCULONS2
Call selectons
End Sub
```

References

Ahmadi, Z.M., Sawyers, M., Kenyon-Roberts, S., Stanworth, C.W, Kugler, K.A., Kristensen, J. and Fugelli, E.M.G. 2003. Paleocene. In: D. Evans, C. Graham, A. Armour and P. Bathurst (Eds. and co-ordinators), The Millennium Atlas: Petroleum Geology of the Central and Northern North Sea. The Geological Society, London, pp. 235 – 259.

Al-Chalabi, M. 2001. The use of instantaneous velocity in uplift investigations. Geophysical Prospecting, 49, 645 – 655.

Al-Chalabi, M. and Rosenkranz, P.L. 2002. Velocity-depth and time-depth relationships for a decompacted uplifted unit. Geophysical Prospecting, 50, 661 – 664.

Alixant, J. and Desbrandes, R. 1991. Explicit pore pressure evaluation concept and application. In: SPE Drilling Engineering, September 1991, pp. 182 - 188.

Anselmetti, F.S. and Eberli, G.P. 1993. Controls on sonic velocity in carbonates. Pure Appl. Geophys., 141, 287 -323.

Aplin, A. C., Yang Y. and Hansen, S. 1995. Assessment of β, the compression coefficient of mudstones and its relationship with detailed lithology. Marine and Petroleum Geology, 12, 955 – 963.

Athy, L.F. 1930a. Density, Porosity and Compaction of Sedimentary Rocks. AAPG Bulletin, 14, 1 – 22.

Athy, L.F. 1930b. Compaction and oil migration. AAPG Bulletin, 14, 25 – 35.

Audet, D.M. 1995. Compaction and overpressuring in Pleistocene sediments on the Louisiana shelf, Gulf of Mexico. Marine and Petroleum Geology, 13, 467 – 474.

Baird, R.A. 1986. Maturation and Source Rock Evaluation of Kimmeridge Clay, Norwegian North Sea. AAPG Bulletin, 70, 1 – 11.

Baldwin, B. and Butler, C. 0. 1985. Compaction curves. AAPG Bulletin, 69, 622 – 626.

Bateman, R. A. 1985. Open-hole log analysis and formation evaluation. Reidel Publishing Co., Dordrecht.

Beekman, F. and Skar, T. 2000. Tectonic stresses facilitating natural fracturing in overpressured reservoirs - inferences from numerical modelling. AAPG Bulletin, 84, 1402 - 1403.

Berryman, J. 1992. Single-scattering approximations for coefficients in Biot's equations for poroelasticity. J. Acoustic Soc. Am., 91, 551 – 571.

Berryman, J. G. 1995. Mixture theories for rock properties. In: T. J. Ahrens (Ed.), American Geophysical Union Handbook of Physical Constants. AGU, New York, pp. 205 - 228.

Bethke, C.M. 1985. A numerical model of compaction-driven groundwater flow and heat transfer and its application to the paleohydrology of intracratonic sedimentary basins. Journal of Geophysical Research 90, 6817 – 28.

Bilgeri, D. and Ademeno, E. B. 1982. Predicting abnormal pressure in sedimentary Rocks. Geophysical Prospecting, 30, 608 – 621.

Biot, M.A. 1941. General theory of three-dimensional consolidation. Journal of Applied Physics, 12, 155 – 164.

Biot, M. 1956, Theory of propagation of elastic waves in a fluid saturated porous solid. I. Low frequency range and II. Higher-frequency range: J. Acoust. Soc. Am., 28, 168 – 191.

Bjørlykke, K. and Høeg, K. 1997. Effect of burial diagenesis on stresses, compaction and fluid flow in sedimentary basins. Marine and Petroleum Geology, 14, 267 – 276.

Borge, H. 2002. Modelling generation of dissipation of overpressure sedimentary basins; an example from the Halten Terrace, offshore Norway.

Bowers, G.L. 1994. Pore pressure estimation form velocity data: accounting for overpressure mechanisms besides undercompaction. In: Proceeding of the 1994 IADC/SPE drilling Conference, 27488, pp. 515 – 530.

Bowers, G.L. 1999. Pore pressure estimation form velocity data: accounting for overpressure mechanisms beside undercompaction. SPE Reprint Series, 49, pp. 78 - 84.

Bowers, G.L. 2001. Determining an Appropriate Pore-Pressure Estimation Strategy. Offshore Technology Conference held in Houston, Texas, 30 April–3 May 2001, OTC Paper 13042.

Bowers, G.L. 2002. Detecting high pressure. The Leading Edge, 21, 174 – 177.

Bowers, G. L. and Katsube, T. J. 2002. The role of shale pore structure on the sensitivity of wire-line logs to overpressure. In A. Huffman and G.Bowers (Eds.), Pressure regimes in sedimentary basins and their prediction. AAPG Memoir 76, pp. 43 – 60.

Bradley J.S. and Powley D.E. 1994. Pressure compartments in sedimentary basins: a review. In: J.P. Ortoleva (Ed.), Basin compartments and seals. AAPG Memoir 61, pp. 3 - 26.

Brasher, J. E. and Vagle, K. R. 1996. Influence of lithofacies and diagenesis on Norwegian North Sea Chalk reservoirs. AAPG Bulletin, 80, 746 – 769.

Brennand, T.P., Van Hoorn, B., James, K.H., Glennie, K.W. 1998. Historical review of North Sea exploration. In: K.W. Glennie (Ed.), Petroleum Geology of the North Sea: Basic Concepts and Recent Advances. Blackwell, Oxford, pp. 1 – 41.

Brewster, J., Dangerfield, J.A. and Farell, H. 1986. The geology and geophysics of the Ekofisk field waterflood. Marine and Petroleum Geology, 3, 139 - 169.

Brown, P., Swarbrick, R.E. and Aplin, A.C. 1999. Estimation of pore pressure in shales: how useful are shale compaction curves? (Abstract). AAPG Bulletin, 83, 1302.

Bulat, J. and Stoker, S.J. 1987. Uplift determination from interval velocity studies, UK, southern North Sea. In J. Brooks and K.W. Glennie (Eds.), Petroleum geology of the north west Europe. Graham & Trotman, London, pp. 293 – 305.

Burhig, C. 1989. Geopressured Jurassic reservoirs in the Viking Graben: modelling a geological significance. Marine and Petroleum Geology, 6, 31 – 48.

Burland, J. B. 1990. On the compressibility and shear strength of natural clays. Geotechnique, 40, 329 - 378.

Burrus, J., Osadetz, K., Wolf, S., Doligez, B., Visser, K. and Dearborn, D. 1996. A two-dimensional regional basin model of Williston basin hydrocarbon systems. AAPG Bulletin, 80, 265 – 291.

Carcione, J. M. and Tinivella, U. 2001. The seismic response to overpressure: a modelling study based on laboratory, well and seismic data. Geophysical Prospecting, 49, 523 - 539.

Caroll, M.M. and Katsube, N. 1983. The role of Terzaghi effective stress in linearly elastic deformation. ASME Journal of Energy Resources and Technology, 105, 509 – 511.

Castagna, J.P., Batzle, M.L. and Eastwood, R.L. 1985. Relationships between compressional-wave and shear-wave velocities in clastic silicate rocks. Geophysics, 50, 571 - 581.

Cayley, G.T. 1987. Hydrocarbon migration in the Central North Sea. In: J. Brooks and K.W. Glennie (Eds.), Petroleum Geology of North West Europe. Graham & Trotman, London, pp. 549 – 555.

Chatfield, C. and Collins, A.J. 1980. Introduction to Multivariate Analysis. Chapman & Hall, London.

Chatterjee, S. and Price, B. 1977. Regression Analysis by Example. Wiley, New York.

Chiarelli, A. and Duffraud, F. 1980. Pressure origin and distribution in Jurassic of Viking Graben (United Kingdom – Norway). AAPG Bulletin, 64, 1245 – 1266.

Chilingarian, G.V. 1983. Compaction diagenesis. In: A. Parker and B.W. Sellwood (Eds.), Sediment Diagenesis. NATO Advanced Study Institute. Reidel Publishing Co., Dordrecht, pp. 57 – 167.

Chilingar, G. V., Serebryakov, V.A. and Robertson, J.O. 2002. Origin and prediction of abnormal formation pressures. Elsevier Science, Oxford.

Chiralli, A. 1975. Use of compaction profiles to predict abnormal pressures. World Oil, 180 (6), 101 – 110.

Connan, J. 1974. Time – temperature relation in Oil Genesis. AAPG Bulletin, 58, 2516 – 2521.

Copestake, P., Sims, A.P., Crittenden, S., Hamar, G.P., Ineson, J.R. and Rose, P.T. 2003. Lower Cretaceous. In: D. Evans, C. Graham, A. Armousand P. Bathurst (Editors and co-ordinators), The Millennium Atlas: Petroleum Geology of The Central and Northern North Sea. The Geological Society, London, pp. 191 – 211.

D'Heur, M. 1986. The Norwegian chalk fields. In: A.M. Spencer (Ed.), Habitat of hydrocarbons on the Norwegian continental shelf. Proceedings of international conference, Norwegian Petroleum Society. Graham & Trotman, pp. 77 - 79.

Dalla Torre, M., Mahlmann, R. F. and Ernst, W. G. 1997. Experimental study on the pressure dependence of vitrinite maturation. Geochimica et Cosmochimica Acta, 61, 14, 2921 -2928.

Daniel, R.B. 2001. Pressure prediction for a Central Graben wildcat well, UK North Sea. Marine and Petroleum Geology, 18, 235 – 250.

Darby, D., Haszeldine, R. S. and Couples, G. D. 1996. Pressure cells and pressure seals in the UK Central Graben. Marine and Petroleum Geology, 13, 865 - 878.

Davis, J.C. 2002. Statistics and Data Analysis in Geology, 3rd Edition. John Wiley & Sons, New York.

Deegan, C.E. and Scull, B. J. 1977. A proposed standard lithostratigraphic nomenclature for the Central and Northern North Sea. Report of the Institute of Geological Sciences, No 77/25; Bulletin of the Norwegian Petroleum Directorate, No. 1.

Den Hartog Jager, D., Giles, M.R. and Griffiths, G.R. 1993. Evolution of Paleogene submarine fans of the North Sea in space and time. In: J.R. Parker (Ed.), Petroleum Geology of the Northwest Europe: Proceedings of the 4th conference. The Geological Society. London, pp. 59 – 71.

Dickinson, G. 1953. Geological aspect of abnormal reservoir pressures in Gulf Coast Louisiana. AAPG Bulletin, 37, 410 – 432.

Domenico, S. N. 1976. Effect of brine-gas-mixture on velocity in an unconsolidated sand reservoir. Geophysics, 41, 882 – 894.

Domenico, S. N. 1977. Elastic properties of unconsolidated porous sand reservoirs. Geophysics, 42, 1339–1368.

Domenico, S.N. 1984. Rock lithology and porosity determination from shear and compressional wave velocity. Geophysics, 49, 1188 - 1195.

Domnesteanu, P.R., McCann, C., Sothcott, J. and Astin, T.R. 2000. Shale Seismic anisotropy in overpressured conditions, Technical Proceedings of the 62nd Annual Meeting of the European Association of Geoscientists and Engineers, 28th May – 2nd June, Glasgow, Paper C-8.

Doré, A.G., Vollset, J. and Hamar, G.P. 1985. Correlation of the offshore sequences referred to the Kimmeridge Clay Formation – relevance to the Norwegian sector. In B.M. Thomas, A.G. Doré, S.S. Eggen, P.C. Home and R. Mange Larsen (Eds.), Petroleum Geochemistry in Exploration of the Norwegian Shelf. Graham & Trotman, London, pp. 27 – 37.

DTI. 2003. Petroleum prospectivity of the principal sedimentary basins on the United Kingdom continental shelf. Department of Trade and Industry – UK, London. http://www.og.dti.gov.uk/UKpromote/summary_UKCS_2003.pdf (accessed 15 March, 2005).

Dudek, T., Srodon J., Eberl D.D., Elsass, F. and Uhlik, P. 2002. Thickness distribution of illite crystals in shales. 1: x-ray diffraction vs. high-resolution transmission electron microscopy measurements. Clays and clay minerals, 50, 562 - 577.

Dutta, N. C. 2002. Geopressure prediction using seismic data: Current status and the road ahead. Geophysics, 67, 2012 – 2041.

Dutta, N.C., Borland, W.H., Leaney, W.S., Meehan, R. and Nutt, W.L. 2002a. Pore pressure ahead of the bit: an integrated approach. In: A. Huffman, G. Bowers (Eds.), AAPG Memoir 76, pp. 165 – 169.

Dutta, N., Mukerji. T., Prasad, M. and Dvorkin, J. 2002b. Seismic detection and estimation of overpressures: field applications. CSEG (Canadian Society of Exploration Geophysicists) Recorder, September 2002, 27, 59 – 73.

Eastwood, R.L. and Castagna, J.P. 1983. Basis for interpretation of Vp/Vs ratios in complex lithology. Trans. 24th Ann. Logging Symposium. SPWLA, paper G, 1 – 17.

Eaton, B.A. 1972. Graphical method predicts geopressure worldwide. World Oil, June 1972, pp. 51 – 56.

Eaton ,B.A. 1975. The equation for geopressure prediction from well logs. Society of Petroleum Engineers of AIME, Paper No. SPE 5544.

Eberhart-Phillips, D., Han, D-H. and Zoback, M.D. 1989. Empirical relationship among seismic velocity, effective pressure, porosity and clay content in sandstone. Geophysics, 54, 82 – 89.

Ebrom, D., Heppard, P., Thomsen, L., Mueller, M., Harrold, T. and Watson, P. 2004. Effective stress and minimum velocity trends.

Ecclestone-Brown, P. 2002. Mudstone porosity and clay fraction in overpressured basins. Ph.D. Thesis. University of Durham, Durham.

Engelder, T. 1993. Stress Regimes in the Lithosphere. Princeton University Press, Princeton.

Engelder, T. and Fischer, M.P. 1994. Influence of poroelastic behaviour on the magnitude of minimum horizontal stress, S_h, in overpressured parts of sedimentary basins. Geology, 22, 949 - 952.

Ensley, R.A. 1984. Comparison of P- and S-wave seismic data: a new method for detecting gas reservoirs. Geophysics, 49, 1420 - 1431.

Ensley, R.A. 1985. Evaluation of direct hydrocarbon indicators through comparison of compressional- and shear-wave seismic data: a case study of the Myrnam gas field, Alberta. Geophysics, 50, 37 - 48.

Evans, D., Graham, C., Armour, A. and Bathrust, P (Editors and co-ordinators), 2003a. The Millennium Atlas: petroleum geology of the Central and Northern North Sea. The Geological Society, London.

Evans, D.J., Hopson, P.M., Kirby, G.A. and Bristow, C.R. 2003b. The development and seismic expression of synsedimentary features within the Chalk of southern England. Journal of the Geological Society London, 160, 797 – 813.

Feazel, C.T. and Farell H.E.. 1988. Chalk from the Ekofisk area, North Sea: nannofossils + micropores = giant fields. In: A.J. Lomando and P.M. Harris (Eds.), Giant oil and gas fields. A core workshop: SEPM Core Workshop 12, pp. 155 - 178.

Feazel, C.T. and Schatzinger, R.A. 1985, Prevention of carbonate cementation in petroleum reservoirs, In: N. Schneirdmann and P.M. Harris (Eds.), Carbonate cements. SEPM Special Publication 36, pp. 97 - 106.

Frazer, S.I., Robinson, A.M., Johnson, H.D., Underwill, J.R., Kadolosky, D.G.A., Connell, R., Johannessen, P. and Ravnås, R. 2002. Upper Jurassic. In: D. Evans, C. Graham, A. Armous and P. Bathurst (Editors and co-ordinators), The Millennium Atlas: Petroleum Geology of The Central and Northern North Sea, The Geological Society, London, pp. 157 – 189.

Fullagar, P.K., Zou, B. and Biggs, M. 2004. Stratigraphically consistent auto-interpretation of borehole data. Journal of Applied Geophysics, 55, 91 – 104.

Gaarenstrom, L., Tromp, R.A.J., De Jong, M.C. and Brandenburg, A.M. 1993. Overpressure in the Central North Sea: implications for trap integrity and drilling safety. In: J.R. Parker (Ed.), Petroleum Geology of North West Europe: Proceedings of the 4th conference, The Geological Society, London, pp. 1305 – 1313.

Gallagher J.J., Friedman M., Handin J. and Sowers G.M. 1974. Experimental studies relating to microfracture in sandstone. Tectonophysics, 21, 203 - 247.

Gardner, G. H. F., Wyllie, M. R. J. and Droschak, D. M. 1965. Hysteresis in the velocity-pressure characteristics of rocks. Geophysics, 30, 111 – 116.

Gardner, G.H.F., Gardner, L.W. and Gregory, A.R. 1974. Formation velocity and density – the diagnostics basics for stratigraphic traps. Geophysics, 39, 770 - 780.

Garrison, R. E. 1981. Diagenesis of oceanic carbonate sediments: a review of the DSDP perspective. In: J. E. Warme, R. G. Douglas and E. L. Winterer (Eds.), The Deep Sea Drilling Project; a decade of progress. Society of Economic Palaeontologists and Mineralogists Special Publication, 32, pp. 181 – 207.

Geertsma, J. 1957. The effect of fluid pressure decline on volumetric changes of porous rocks. Trans. AIME, 210, 331 - 340.

Geerstma, J. and Smit, D.C. 1961. Some aspects of elastic wave propagation in fluid - saturated porous solids. Geophysics, 26, 169 - 181.

GeoPOP. 2000. Regional Pressure Atlas of the Central North Sea. Vol. I and Vol. II. Geoscience Project into OverPressure. University of Durham, Durham.

Geopressure Technology, 2000. PressureView 2.1 - pressure database and interpretation software. Geopressure Technology Ltd, Durham.

Glennie, K.W. 1998. Petroleum Geology of the North Sea: Basic concepts and recent advances. Blackwell Science, London.

Golden Software. 2001. Didger version 3.0. Golden Software, Inc. Golden, Colorado

Goulty, N.R. 1998. Relationship between porosity and effective stress in shales. First Break, 16, 413 – 419.

Goulty, N.R. 2004. Mechanical compaction behaviour of natural clays and implication for pressure prediction. Petroleum Geoscience, 10, 5523 – 5530.

Gradstein, F.M. Agterberg, F.P., Ogg, J.G., Hardenbol, J., Van Veen, P., Thierry, J. and Huang, Z. 1994. A Mesozoic timescale. Journal of Geophysical Research, 99 (B12), 24051 - 24074.

Gradstein, F.M., Agterberg, F.P., Ogg, J.G., Hardenbol, J., Van Veen, P., Thierry, J., Huang, Z. 1995. A Triassic, Jurassic and Cretaceous timescale. In: W.A. Berggren, D.V. Kent, M.-P. Aubry and J. Hardenol (Eds.), Geochronology, Time scales and Global stratigraphic correlation. SEPM Special Publications, 54, pp. 95 – 126.

Grauls, D., Dunand, J.P. and Beaufort, D. 1995. Predicting abnormal pressure from 2-D seismic velocity modelling. Proceedings of OTC Conference, Houston, May 1995.

Gregory, A.R. 1977. Aspects of rock physics from laboratory and log data that are important to seismic interpretation. In: Payton, C.E. (Ed.), Seismic stratigraphy – applications to hydrocarbon exploration. AAPG Memoir 26, pp. 15 – 45.

Groombridge, J. 2000. Relating overpressure to seismic velocity in the Chalk of the Central North Sea. MSc Thesis, University of Durham, Durham.

Gurevich, B. 2004. A simple derivation of the effective stress coefficient for seismic velocities in porous rocks. Geophysics, 69, 393 – 397.

Han, D., Nur, A. and Morgan, D. 1986. Effects of porosity and clay content on wave velocities in sandstones. Geophysics, 51, 2093 – 2107.

Hansen, S.J. 1996. A compaction trend for Cretaceous and Tertiary shales on the Norwegian Shelf based on sonic transit times. Petroleum Geoscience, 2, 159 – 166.

Hardenbol, J. and Robaszynski, F. 1998. Introduction to the Upper Cretaceous. In: P.C. De Graciansky, J. Hardenbol, T. Jacquin and P.R. Vail (Eds.), Mesozoic and Cenozoic Sequence Stratigraphy of European Basins. SEPM Special Publications, 60, pp. 329 – 332.

Hardman, R.P.F. and Kennedy, W.J. 1980. Chalk reservoirs of the Hod field. In: Sedimentation of the North Sea reservoir rocks, Geilo 11-14 May 1980 Norsk Petroleum forening. Elsevier, Amsterdam, Paper 11.

Harrold, T.W.D., Swarbrick, R.E. and Goulty, N. R. 1999. Pore pressure estimation from mudrock porosities in tertiary basins, Southeast Asia. AAPG Bulletin, 83, 1057 – 1067.

Harper, T.R. and Chambers, J.L. 2004. Stress state and its influence on drilling performance in the Brighton Marine field, Trinidad. Marine and Petroleum Geology, 21, 947 – 963.

Hatherly, P.J. 2001. Geophysical logging for rock mass assessment. Australian Society of Exploration Geophysicists Preview, 91, 31 – 33.

Hawkins, K., Leggott, R. and Williams, G. 2001. Addressing anisotropy in 3-D Prestack depth migration: A case study from the Southern North Sea. The Leading Edge, 20, 528 - 535.

Heppard, P.D, Albertin, L.M., Wagner, E.B., Bettencourtt, J.D. 2000. Difficulties in pressure prediction using Seismic velocities due to anisotropy, velocity insensitivity and inadequate geologic prediction (Abstract). AAPG Bulletin, 84.

Hermanrud. C., Teige, G.M.G., Vik, E., Wensaas, L. and Norgård-Bolås, H.M. 1998a. Overpressure in shales – Do we know what they are and why they are there? In: A. Mitchell and D. Grauls (Eds.). Overpressures in Petroleum Exploration. Proceedings of the workshop, 7th – 8th April 1998. Bull. Centre Rech. Elf Explor. Prod., Pau, France, pp. 43 - 48.

Hermanrud. C., Wensaas, L. Teige, G.M.G., Vik, E.and Norgård-Bolås, H.M. 1998b. Shale porosities from well logs from Haltenbanken (offshore mid-Norway) show no influence of overpressuring. In: B.E. Law, G.F. Ulmishek, V.I. Slavin (Eds.), Abnormal Pressure in Hydrocarbons Environments, AAPG Memoir, 70, pp. 65 – 85.

Hillis, R. R. 1995. Quantification of Tertiary exhumation in the United Kingdom southern North Sea using sonic velocity data. AAPG Bulletin, 79, 130 – 152.

Hilterman, F. 1998. Rock property framework for comprehending deep-water seismic response. Proceedings GSH, 1998 spring aa symposium, Ann. SEG Gulf Coast Tech. Mtg. Society of Exploration Geophysics.

Holm, G..M. 1996. The Central Graben: A dynamic overpressure system. In: K.W. Glennie and A. Hurst (Eds.), Ad 1995: NW Europe's hydrocarbon industry. The Geological Society, London, pp. 107 – 122.

Holm, G. M. 1998. Distribution and origin of overpressure in the Central Graben of the North Sea. In: B. E. Law, G. F. Ulmishek and V. I. Slavin (Eds.), Abnormal pressures in hydrocarbon environments. AAPG Memoir 70, pp. 123 – 144.

Hubbert, M.K. and Rubey, W.W. 1959. Role of fluid pressure in mechanics of overthrust faulting. Geological Society of America Bulletin, 70, 115 – 166.

Huffman, A.R. 2002. The future of pore pressure prediction using geophysical methods. In: A. Huffman and G. Bowers (Eds.), Pressure regimes in sedimentary basins and their prediction. AAPG memoir 76, pp. 217 – 233.

Hunt, J.M. 1990. Generation and migration of petroleum from abnormally pressured fluid compartments. AAPG Bulletin, 74, 1 – 12.

Husmo, T., Hamar, G.P., Høiland, O., Johannessen, E.P. Romuld, A., Spencer, A.M. and Titterton, R. 2002. Lower and Middle Jurassic. In: D. Evans, C. Graham, A. Armour and P. Bathurst (Editors and co-ordinators), The Millennium Atlas: Petroleum Geology of the Central and Northern North Sea. The Geological Society, London, pp. 129 – 155.

Issler, D.R. 1992. A new approach to shale compaction and stratigraphic restoration. Beaufort-Mackenzie Basin and Mackenzie Corridor, Northern Canada. AAPG Bulletin, 76, 1170 – 1189.

Japsen, P. 1998. Regional velocity-depth anomalies, North Sea Chalk: a record of overpressure and Neogene uplift and erosion. AAPG Bulletin, 82, 2031 – 2074.

Johnson, H. and Lott, G.K. 1993. Cretaceous of the Central and Northern North Sea. In: R W O'B. Knox and W.C. Cordley (Eds.), Lithostatigraphic nomenclature of the UK North Sea, Vol. 2. British Geological Survey, Nottingham.

Johnston, D.H. 1987. Physical properties of shales at temperature and pressure. Geophysics 52, 1391 – 1401.

Jones, L.E.A. and Wang, H.F. 1981. Ultrasonic sonic velocities in Cretaceous shales from the Williston Basin. Geophysics, 46, 288 – 297.

Katsube, T. J., Bloch, J. and Wayne, C.C. 1998. The effect of diagenetic alteration on shale pore-structure and its implication for abnormal pressures and geophysical signatures. In: A. Mitchell and D. Grauls (Eds.), Overpressures in Petroleum Exploration. Proceedings of the workshop, 7th – 8th April 1998. Bull. Centre Rech. Elf Explor. Prod., Pau, France, pp. 49 - 54.

Kennedy, W.J. 1980. Aspects of chalk sedimentation in the southern Norwegian offshore. In: The Sedimentation of the North Sea reservoir rocks, Geilo, 11 – 14 May, 1980. Norwegian Petroleum Society, Oslo, pp. 29.

Kennedy, W.J. 1987. Sedimentology of Late Cretaceous-Palaeocene Chalk reservoirs, North Sea Central Graben. In: J. Brooks and K. Glennie (Eds.), Petroleum Geology of North West Europe. Graham & Trotman, London, pp. 469 - 481.

Khazanehdari, J., McCann, C., Sothcott, J. and Astin, T.R. 1998. The inter-relationships between velocity, stress, pore-fluid and permeability in clean sandstones. Technical Proceedings of the 60th Annual meeting of the EAGE, Liepzig. Paper No 10 – 28, 358 – 359.

King, M.S., Stauffer, M.R., Yang, H.J.P. and Hajnal, Z. 1988. Elastic-wave and related properties of clastic rocks from the Athabasca Basin, Western Canada. Canadian Journal of Exploration Geophysics, 24, 2, 110 - 116

Kooi, H. 1997. Insufficience of compaction disequilibrium as the sole cause of high pore fluid pressures in pre-Cenozoic sediments. Basin Research, 9, 227 – 241.

Korvin, G. 1984. Shale compaction and statistical physics. Geophys. Journ. of the Royal Astronomical Society, 78, 35 - 50.

Krumbein, W.C., Graybill, F. A. 1965. An introduction to Statistical Models in Geology. McGraw-Hill, London.

Lahann, R. 2002. Impact of smectite diagenesis on compaction modeling and compaction equilibrium. In: A.R. Huffman and G.L. Bowers (Eds.), Pressure regimes in sedimentary basins and their prediction. AAPG Memoir 66, pp. 61 – 72.

Landrø, M. 2001. Discrimination between pressure and fluid saturation changes from time lapse seismic data. Geophysics, 66, 836 - 844.

Lapidus, D.F. and Winstanley, I. 1987. Collins Dictionary of Geology. HarperCollins Publishers, London.

Lee, M.W. 2004. Elastic velocities of partially gas-saturated unconsolidated sediments. Marine and Petroleum Geology, 21, 641 – 650.

Leonard, R.C. 1993. Distribution of sub-surface pressure in the Norwegian Central Graben and application for exploration. In: J.R. Parker (Ed.), Petroleum Geology of North West Europe: Proceedings of the 4th conference, The Geological Society of London, London, pp. 295 – 303.

Lerche, I. 1990. Basin analysis: Quantitative methods. Academic Press, SanDiego, California

Li, Y.G., Chester, F.M. and Vidale, J.E. 2001. Shallow seismic profiling at the Punchbowl fault zone, Southern California. Bulletin of the Seismological Society of America, 91, 1820 - 1830.

Lubanzadio, M., Goulty N.R. and Swarbrick, R.E. 2002. Variation of velocity with effective stress in chalk: null result from North Sea well data. Marine and Petroleum Geology, 19, 921 – 927.

Luo, X. and Vasseur. G. 1992. Contributions of compaction and aquathermal pressuring to geopressure and the influence of environmental conditions. AAPG Bulletin, 76, 1550 – 1559.

Luo, X. and Vasseur, G. 1996. Geopressuring mechanism of organic matter cracking: numerical modelling. AAPG Bulletin, 80, 856 – 874.

MacGregor, J.R. 1965. Quantitative determination of reservoir pressures from conductivity log. AAPG Bulletin, 49, 1502 – 1511.

Magara, K. 1975. Re-evaluation of montmorillonite dehydratation as cause of abnormal pressure and hydrocarbon migration. AAPG Bulletin 59, 292 - 302.

Maliva, R. G. and Dickson, J.A.D. 1992. Microfacies and diagenetic controls of porosity in Cretaceous/Tertiary Chalks, Eldfisk Field, Norwegian North Sea. AAPG Bulletin, 76, 1825 - 1838.

Mallon, A. and Swarbrick, R.E. 2002. A compaction trend for non-reservoir North Sea Chalk. Marine and Petroleum Geology, 19, 527 – 539.

Mallon, J. A., Swarbrick, R.E. and Katsube, T.J. 2005. Permeability of fine-grained rocks: New evidence from chalks. Geology, 33, 1, 21 - 24.

Mann, C.J. 1987. Misuses of linear regression in Earth Sciences. In: W. B. Size (Ed.), Use and Abuse of Statistical Methods in the Earth Sciences. International Association for Mathematical Geology. Oxford University Press, Oxford.

Mann, D. M. and Mackenzie, A.S. 1990. Prediction of pore fluid pressures in sedimentary basins: Marine and Petroleum Geology, 7, 55 – 65.

Massaferro, J.L., Anselmetti, F.S., Eberli, G.P., Baechle, G.T., Bracco-Gartner, G. and Sun, Y.-F. 2002. Effects of pore types on velocity and permeability in carbonates. Shell Exploration and Production Newsletter (EPNL), Special Issue "Seismic Petrophysics", Nov 2002.

Maubeuge, F. and Lerche, I. 1994. Geopressure evolution and hydrocarbon generation in a North Indonesian Basin – Two-Dimensional Quantitative Modeling. Marine and Petroleum Geology, 11, 104 - 115.

Maucione, D., Serebryakov, V., Valasek, P., Wang, Y., Smithson, S. 1994. A sonic log study of abnormally pressured zones in the Powder River Basin of Wyoming. In: J.P. Ortoleva (Ed.), Basin compartments and seals. AAPG Memoir 61, pp. 333 – 348.

Mavko, G., Mukerji, T. and Dvorkin, J. 1998. Rock physics handbook: tools for seismic analysis in porous media. Cambridge University Press, Cambridge.

McCormack, M.D., Dunbar, J.A. and Sharp, W.W., 1985, A stratigraphic interpretation of shear and compressional wave seismic data for the Pennsylvanian Morrow formation of southeastern New Mexico. In: O. R. Berg and D. G. Woolverton (Eds.), Seismic Stratigraphy II: an integrated approach to hydrocarbon exploration. AAPG Memoir 39, pp. 225 - 239.

Megson, J. and Hardman, R. 2001. Hydrocarbons in the Chalk of the North Sea. Petroleum Geosciences, 7, 3 – 12.

Mehta, C.H. and Verma, B.H. 1991. Porosity interpretation through seismics. Geoexploration, 28, 91 – 106.

Miller, S.L.M. and Stewart, R.R. 1990. Effects of lithology, porosity and shaliness on P and

S-wave velocities from sonic logs. Can. J. Expl. Geophys., 26, 94 - 103.

Minear, J.W. 1982. Clay models and acoustic velocities. 57th Annual Fall Technical Conference and Exhibition of the Soc. Petr. Eng., New Orleans, Sept. 26-29, Paper SPE 11031.

Minitab Inc. 2003. Minitab Release 14 for Windows. Addison-Wesley, Pennsylvania State College.

Moos, D. 1999. Predicting Pore Pressure from Porosity and Velocity: Abstract. AAPG Bulletin, 83, 1329 - 1330.

Morton, A.C., Hallsworth, C.R. and Wilkinson, G.C. 1993. Stratigraphic evolution and provenance during Paleocene deposition in the Northern North Sea. In: J.R. Parker (Ed.) Petroleum Geology of the Northwest Europe: Proceedings of the 4th Conference. The Geological Society, London, pp. 73 – 74.

Moss, B., Barson, D., Rakbit, K., Denis, H. and Swarbrick, R. 2003. Formation pore pressures. In: D. Evans, C. Graham, A. Armous and P. Bathurst (Editors and co-ordinators), The Millennium Atlas: Petroleum Geology of the Central and Northern North Sea. The Geological Society, London, pp. 317 - 329.

Mouchet, J.P., Mitchell, A. 1989. Abnormal pressures while drilling. Elf Aquitaine. Edition. Boussens, France.

Mukerji. T., Dutta, N., Prasad, M. and Dvorkin, J. 2002. Seismic detection and estimation of overpressures: the Rock Physics Basis. CSEG Recorder, September 2002, 27, 36 – 57.

Murphy, W. F. 1984. Acoustic measures of partial gas saturation in tight sandstones. Journal Geophysical Research, 89, 11549 – 11559.

Nadeau, H.P., Peacor, R.D., Yan, J. and Hillier, S. 2002. I-S precipitation in pore space as the cause of geopressuring in Mesozoic mudstones, Egersund Basin, Norwegian continental shelf. American Mineralogist, 87, 1580 – 1589.

Nations, J.F. 1974. Lithology and porosity from acoustic shear and compressional wave transit time relationships. 15th Ann. Symp. Soc. Prof. Well Log Analysts, McAllen, Texas.

Norgård Bolås, H.M., Hermanrud, C. and Teige, G.M.G. 2004. Origin of overpressures in shales: constraints from basin modelling. AAPG Bulletin, 88, 193 – 211.

Nur, A. and Byerlee, J.D. 1971. An effective stress law for elastic deformation of rocks with fluids. J. Geophys. Res., 76, 6414 – 6419.

Nygard, R., Gutierrez, M., Gautan, R. and Hoeg, K. 2004. Compaction behaviour of argillaceous sediments as function of diagenesis. Marine and Petroleum Geology 21, 349 - 362.

Oakman, C.D. and Partington, M.A. 1998. Chap 9. Cretaceous. In: K.W. Glennie (Ed.), Petroleum Geology of the North Sea: Basic Concepts and Recent Advances. Blackwell, Oxford, pp. 294 - 349.

Ortoleva, P. J. 1994. Basin compartmentation: definitions and mechanisms. In: J.P. Ortoleva (Ed.), Basin compartments and seals. AAPG Memoir 61, pp. 39 – 51.

Osborne, M.J. and Swarbrick, R.E. 1997a. How overpressure and diagenesis interact in sedimentary basins - consequences for porosity preservation in HPHT reservoir sandstones. Proceedings of Indonesian Petroleum Association.

Osborne, M.J. and Swarbrick, R.E. 1997b. Mechanisms for generating overpressure in sedimentary basins: a re-evaluation. AAPG Bulletin, 81, 1023 - 1041.

Peacock, S., McCann, C., Sothcott, J. and Astin, T. R. 1994a. Seismic velocities in fractured rocks: An experimental verification of Hudson's theory. Geophysical Prospecting, 42, 27 - 80.

Peacock, S., McCann, C., Sothcott, J. and Astin, T.R. 1994b. Experimental measurements of seismic attenuation in microfractured sedimentary rock. Geophysics, 59, 1342 - 1351.

Pennebaker, E. S. 1968. Seismic data indicate depth, magnitude of abnormal pressure. World Oil, 166 (7), 73 - 78.

Pickett, G.R. 1963. Acoustic character logs and their applications in formation evaluation: 1. Can. Petr. Tech. 15, 659 - 667.

Powers, M.C. 1967. Fluid-release mechanisms in compacting marine mudrocks and their importance in oil exploration. AAPG Bulletin 51, 1240 - 1245.

Prasad, M., Manghnani, M.H. 1997. Effect of pore and differential pressure on compressional wave velocity and quality factor in Berea and Michigan sandstones. Geophysics, 62, 4, 1163 – 1176.

Price, L.C. and Wenger, L.M. 1992. The influence of pressure on petroleum generation and maturation as suggested by aqueous pyrolysis. Organic Geochemistry 19, 141 – 159.

Raiga-Clemenceau, J., Martin, J.P., Nicoletis, S. 1988. The concept of acoustic factor for more porosity determination from transit time data. The Log Analyst, 29, No. 1, 54 – 60.

Rasmus, J.C. and Stephens, D.M.R. 1991. Real-Time Pore Pressure Evaluation from MWD/LWD Measurements and Drilling-Derived Formation Strength. SPE Drilling Engineering, December 1991, pp. 264 - 272.

Rawson, P.F. and Riley, L.A. 1982. Latest Jurassic – Early Cretaceous events and the "late Cimmerian Unconformity" in North Sea area. AAPG Bulletin 66, 2628 – 2648.

Raymer, L. L., Hunt, E. R. and Gardner, J. S. 1980. An improved sonic transit time to porosity transform. 21st Annual Logging Symposium, Transaction of the Soc. Prof. Well Log Analysts, pp. P1 – P13.

Reynolds, E.B. 1970. Predicting overpressured zones with seismic data. World Oil, 171, 78 - 82.

Reynolds, T. 2004. Pressure Data in the development of a Giant Oilfield: ACG Azerbaijan. 2004 – 5 AAPG Distinguished Lecture. http://www.aapg.org/education/dist_lect/download/reynolds.pdf (accessed 15 March, 2005).

Richards, P.C., Lott, G.K., Johnson, H.D., Knox, R.W. O'B. and Riding, J.B. 1993. Jurassic of the Central and Northern North Sea. In: R.W. O'B. Knox and W.G. Cordley (Eds.), Lithostratigraphic Nomenclature of the U.K. North Sea, Vol. 3. British Geological Survey, Nottingham.

Rieke, H.H. and Chilingarian, G.V. 1974. Compaction of argillaceous sediments. In: Developments in Sedimentology, No 16. Elsevier, Amsterdam.

Robertson, J.D. 1987. Carbonate porosity from S/P travel time ratios. Geophysics, 52, 346 – 1354.

Rourke, M. 2004. Downhole formation fluid identification in complex multi-layer reservoirs. OilOnline. http://www.oilonline.com/news/features/aog/20040201.Downhole.13562.asp

(accessed 15 April, 2005)

Rowan, E.L., Hayba, D. O., Nelson, P. H., Burns, W. M. and Houseknecht, D. W. Sandstone and shale compaction curves derived from sonic and gamma ray logs in Offshore Wells, North Slope, Alaska—Parameters for basin modeling. U.S. Geological Survey, Open-File Report 03-329. http://geology.wr.usgs.gov/open-file/of03-329/ (accessed 15 March, 2005).

Sajgo C., McEvoy J., Wolff G. A. and Horvath Z. A. 1986. Influence of temperature and pressure on maturation processes-I. Preliminary report. Organic Geochemistry, 10, 33 1 - 337.

Sayers, C. M., Johnson, G. M. and Denyer, G. 2002. Predrill pore pressure prediction using seismic data. Geophysics, 67, 1286 – 1292.

Schlumberger. 1972. Log Interpretation Volume 1 – Principles. Schlumberger Ltd, New York.

Schlumberger. 1974. Log interpretation Volume 2 – Applications. Schlumberger Ltd., New York.

Schlumberger, 2004. Oil field glossary (on-line). Schlumberger Ltd. http://www.glossary.oilfield.slb.com/ (accessed 15 March, 2005).

Scholle, P.A. 1977. Chalk diagenesis and its relation to petroleum exploration: oil from chalks, a modern miracle? AAPG Bulletin, 61, 982 – 1009.

Sclater, J. G. and Christie, P. A. F. 1980. Continental stretching: an explanation of the post-mid-Cretaceous subsidence of the central North Sea basin. Journal of Geophysical Research, 85, 3711 – 3739.

Sheriff, R. E. and Geldart, L.P. 1995. Exploration seismology, 2nd edition. Cambridge University Press, Cambridge.

Siggins, A.F. and Dewhurst, D. N. 2003. Saturation, pore pressure and effective stress from sandstone acoustic properties. Geophys. Res. Lett. 30, 2, 1089.

Skar, T., Van Balen, R., Hansen, S. 1998. Overpressuring in Cretaceous shale on the Halten Terrace, offshore Mid-Norway: nature and causes. In: A. Mitchell, D. Grauls (Eds.), Overpressure in petroleum exploration: Proc. Workshop, Pau, 1998. Bull. Centre Rech. Elf Explor. Prod., Mémoire 22, pp. 69 – 75.

Skar, T., Van Balen, R.T., Arnesen, L., Cloetingh, S. 1999. Origin of overpressures on the Halten Terrace, offshore of Mid-Norway: the potential role of mechanical compaction, pressure transfer and stress. In: A.C. Aplin, A.J. Fleet and J.H.S. Macquaker (Eds.), Muds and mudstones: physical and fluid flow properties. Geological Society of London, Special publication, 158, pp. 137 - 156.

Skempton, A.W. 1970. The consolidation of clays by gravitational compaction. Quarterly Journal of the Geological Society of London, 125, 373 – 411.

Stewart R.R., Huddleston P.D. and Kan T.K. 1984. Seismic versus sonic velocities. Geophysics 49, 1153 - 1168.

Stump, B.B., Flemings, P.B. 1998. Predicting overpressure from shale porosity in Eugene Island 330, offshore Louisiana (Abstract). AAPG Bulletin, 82.

Stump, B.B., Flemings, P.B. 2000. Overpressure and fluid flow in dipping structures of the offshore Gulf of Mexico (Eugene Island 330 field). Journal of Geochemical Exploration, 69 – 70, 23 - 28.

Suess, E. 1906. The face of the Earth (English translation of Das Antlitz der Erde), Vol. 2. Clarendon Press, Oxford.

Surlyk, F., Dons, T., Clausen, K., Higman, J. 2003. Upper Cretaceous. In Evans, D., Graham, C., Armour, A. and Bathrust, P. (Editors and co-ordinators), The Millennium Atlas: petroleum geology of the Central and Northern North Sea. The Geological, London, pp. 213 – 233.

Swarbrick, R.E. 1997. Pressure compartments and their interdependence on overpressure mechanisms; example from the North Sea (Abstract). AAPG Bulletin, 81, 1415.

Swarbrick, R.E. 2002. Challenges of porosity-based pore pressure prediction. CSEG Recorder, September 2002, 27, 74 – 77.

Swarbrick, R.E. 2004. Pressures and overpressure in the subsurface. Training Course. Geopressure UK Ltd, Durham. http://www.geopressure.co.uk (accessed 15 March, 2005).

Swarbrick, R.E. 2005. Overpressure and fluid drive in sedimentary basins. 2004 -5 AAPG Distinguished Lecture, March 2005. University of Durham, Durham. www.aapg.org/education/dist_lect/download/swarbrick.pdf (accessed 15 March, 2005).

Swarbrick, R.E. and Osborne, M.J. 1998. Mechanisms that generate abnormal pressures: an overview. In: B.E. Law, G.F. Ulmishek, G.F. and V.I. Slavin (Eds.), Abnormal pressures in Hydrocarbon Environments. AAPG Memoir 70, pp. 111 – 116.

Swarbrick, R. E., Osborne, M. J., Grunberger, D., Yardley, G. S., Macleod, G., Aplin, A. C., Larter, S. R., Knight, I. and Auld, H. 2000. Integrated study of the Judy Field (Block 30/7a)—an overpressured Central North Sea oil/gas field. Marine and Petroleum Geology, 17, 993 – 1010.

Swarbrick, R. E., Osborne, M. J. and Yardley, G. S. 2002. Comparison of overpressure magnitude resulting from the main generating mechanisms. In: A. Huffman and G. Bowers (Eds.), Pressure regimes in sedimentary basins and their prediction. AAPG Memoir 76, pp. 1 – 12.

Systat Software Inc. 2004. SigmaPlot 2004 for Windows, version 2004. Systat, California

Takahashi, I. 2000. Quantifying information and uncertainty of rock property estimation from seismic data. Stanford University. PhD Thesis.

Tatham, R.T. 1982. Vp/Vs and lithology. Geophysics, 47. 336 – 344.

Teige, G.M.G., Hermanrud, C., Wensass, L., Nordgård-Bolas, H.M. 1999. The lack of relationship between overpressure and porosity in North Sea and Haltenbanken shales. Marine and Petroleum Geology, 16, 321 – 335.

Terzaghi, K. 1943. Theoretical soil mechanics. Wiley, New York.

Todd, T. and Simmons, G. 1972. Effect of pore pressure on the velocity of compressional waves in low porosity rocks. Journal of Geophysical Research, 77, 3731 – 3743.

Tosaya, C. and Nur, A. 1982. Effects of diagenesis and clays on compressional velocities in rocks. Geophys. Res. Lett., 9, 5 – 8.

Traugott, M.O. 1997. Pore pressure and fracture determinations in deepwater. Deepwater Technology, Supplement to World Oil, August 1997, 218 (8), 68 – 70.

Tura, A. and Lumley, D. 1999. Estimating pressure and saturation changes from time-lapse AVO data. 69th Annual International Meetings, SEG, Expanded Abstracts, 1655 – 1658.

Ungerer, P., J. Burrus, B. Doligez, P. Y. Chenet and F. Bessis, 1990, Basin evaluation by integrated two-dimensional modelling of heat transfer, fluid flow, hydrocarbon generation and migration. AAPG Bulletin, 74, 309 – 335.

Van der Bark, E. and Thomas, O.D. 1981. Ekofisk: First of the giant oil fields in Western Europe. AAPG Bulletin, 65, 2341 – 2363.

Veldkamp, J.J., Gaillard, M.G., Jonkers, H.A. and Levell, B.K. 1996. A Kimmeridgian time-slice through the Humber Group of the central North sea: a test of sequence stratigraphic methods. In: A. Hurst, H.D. Johnson, S.D. Burley, A.C. Canham and D.S. Mackertich (Eds.), Geology of the Humber Group: central Graben and Moray Firth, UKCS. Special Publication No. 114, The Geological Society, London, pp. 1 – 28.

Vollset, J. and Doré, A.G. (Eds.) 1984. A revised Triassic and Jurassic lithostratigraphic nomenclature for the Norwegian North Sea. Bulletin of the Norwegian Petroleum Directorate, No. 3.

Von Flatern, R. 2005. Scope of things to come. Offshore Engineer. March 2005, pp. 33 – 36.

Wallace, W.E. Jr. 1965. Will induction log yield pressure data? Oil & Gas Journal. Sept 1965, pp. 124 – 126.

Wang, C.Y, Xie, X.N. 1998. Hydrofracturing and episodic fluid flow in shale-rich basins: a numerical study. AAPG Bulletin, 82, 1857 - 1869.

Watts, L. 1983. Microfractures in chalks of Albuskjell field, Norwegian sector, North Sea: possible origin and distribution. AAPG Bulletin, 67, 207 – 234.

Welte, D. H. and M. A. Yukler, 1981, Petroleum origin and accumulation in basin evolution; A quantitative model. AAPG Bulletin, 65, 1387 – 1396.

White, A.J. 2001. Minimum stress and prore fluid pressure in sedimentary basins. Ph.D. Thesis, University of Durham, Durham.

White, A.J., Traugott, M.O. and Swarbrick, R.E. 2002. The use of leak-off tests as means of predicting minimum in-situ stress. Petroleum Geoscience, 8, 189 – 193.

Wiltshire, M.J. and Huggard, L.M. 2000. The 3-C acoustic process – A new approach to predicting acoustic wave performance in sediments. APPEA (Australian Petroleum Production & Exploration Association) Journal, 40, part 1, 367 – 378.

Woodside, J.M., Kenter, J.A.M. and Köhnen, A. 1998. Acoustic properties from logs and discrete measurements (sites 966 and 967) on Erastosthenes Seamount: controls and ground truth. In: A.H.F. Robertson, K.-C. Emeis, C. Richter and A. Camerlenghi (Eds.), Proceedings of the Ocean Drilling program, Scientific Results, ODP College Station, Texas, Vol. 160, Paper 42.

Wyllie, M. R. J., Gregory, A. R. and Gardener, L. W. 1956. Elastic wave velocities in heterogeneous and porous media. Geophysics, 21, 41 – 70.

Wyllie, M. R. J., Gregory, A. R. and Gardner, G. H. F. 1958. An experimental investigation of factors affecting elastic wave velocities in porous media. Geophysics, 23, 459 – 493.

Wyllie, M.R.J, Gardner, G.H.F. and Gregory, A.R. 1962. Studies of elastic wave attenuation in porous media. Geophysics, 27, 569 - 589.

Yardley, G. and Swarbrick, R.E. 2000. Lateral transfer: a source of additional overpressure? Marine and Petroleum Geology, 17, 523 – 537.

Zimmer, M., Prasad M. and Mavko, G. 2002. Pressure and porosity influences on Vp – Vs ratio in unconsolidated sands. The Leading Edge, 21, 178 – 183.

Zimmerman, R. W. 1991. Compressibility of sandstones. Elsevier, New York.

Zoback, M.D., Moos, D., Mastin, L. and Anderson, R.N. 1985. Well bore breakouts and in situ stress. Journal of Geophysical Research, 90 (B7), 5523 - 5530.